

ANALYSIS OF THE HETEROGENEITY SCALE EFFECTS ON PUMP AND
TREAT AQUIFER REMEDIATION DESIGN

A THESIS SUBMITTED TO
THE GRADUATE SCHOOL OF NATURAL AND APPLIED SCIENCES
OF
MIDDLE EAST TECHNICAL UNIVERSITY

BY

GAMZE GÜNGÖR DEMİRCİ

IN PARTIAL FULFILLMENT OF THE REQUIREMENTS
FOR
THE DEGREE OF DOCTOR OF PHILOSOPHY
IN
ENVIRONMENTAL ENGINEERING

MAY 2009

Approval of the thesis:

**ANALYSIS OF THE HETEROGENEITY SCALE EFFECTS ON PUMP
AND TREAT AQUIFER REMEDIATION DESIGN**

submitted by **GAMZE GÜNGÖR DEMİRCİ** in partial fulfillment of the
requirements for the degree of **Doctor of Philosophy in Environmental
Engineering Department, Middle East Technical University** by,

Prof. Dr. Canan Özgen
Dean, Graduate School of **Natural and Applied Sciences** _____

Prof. Dr. Göksel N. Demirer
Head of Department, **Environmental Engineering** _____

Assoc. Prof. Dr. Ayşegül Aksoy
Supervisor, **Environmental Engineering Dept., METU** _____

Examining Committee Members

Prof. Dr. Kahraman Ünlü
Environmental Engineering Dept., METU _____

Assoc. Prof. Dr. Ayşegül Aksoy
Environmental Engineering Dept., METU _____

Assoc. Prof. Dr. Ertan Durmuşoğlu
Environmental Engineering Dept., Kocaeli University _____

Dr. Emre Alp
Environmental Engineering Dept., METU _____

Dr. Elçin Kentel
Civil Engineering Dept., METU _____

Date: _____ **08.05.2009**

I hereby declare that all information in this document has been obtained and presented in accordance with academic rules and ethical conduct. I also declare that, as required by these rules and conduct, I have fully cited and referenced all material and results that are not original to this work.

Name, Last Name : GAMZE GÜNGÖR DEMİRCİ

Signature :

ABSTRACT

ANALYSIS OF THE HETEROGENEITY SCALE EFFECTS ON PUMP AND TREAT AQUIFER REMEDIATION DESIGN

Güngör Demirci, Gamze

Ph.D., Department of Environmental Engineering

Supervisor: Assoc. Prof. Dr. Ayşegül Aksoy

May 2009, 272 pages

The effect of heterogeneity correlation scale (λ) of hydraulic conductivity (K), equilibrium distribution coefficient (K_d) and mass transfer rate (α) on the design and cost of the P&T remediation system for different heterogeneity levels (defined by the variance ($\sigma^2_{\ln K}$)) and parameter distributions under the rate-limited sorption conditions was evaluated in this study. In addition, the impacts of initial amount of contaminant mass and plume configuration on the remediation design and cost were explored. The effects of different K heterogeneity and remediation design conditions on the length of remediation period, the influence of λ anisotropy of K , correlation between K and K_d , and K_d and α , and the fraction of equilibrium sorption sites (f) on the pump-and-treat (P&T) design and cost were the other studied subjects. In this study, simulation-optimization approach, in which a groundwater flow and contaminant transport simulation model was linked with a genetic algorithm (GA) library, was used. Results showed that not only the amount of PCE mass initially present in the aquifer was important in terms of P&T design, cost and remediation time, but also the location and size of the high and low K

regions defined by $\lambda_{\ln K}$ as well as the magnitudes of K represented by geometric mean and $\sigma^2_{\ln K}$ were influential. It was also found that P&T designs utilizing higher numbers of wells with lower pumping rates may be more robust predicting the time-to-compliance compared to a single well with higher pumping rate for aquifers heterogeneous in K . Homogenous K_d assumption might cause serious error in both the design and the cost of remediation. The magnitude of this error may change depending on the spatial distribution of K and K_d , $\lambda_{\ln K_d}$, $\sigma^2_{\ln K_d}$ and $\sigma^2_{\ln K}$. The effect of heterogeneity in α on the design and cost of remediation may or may not be significant depending on K , K_d and α distributions, $\lambda_{\ln \alpha}$ and $\sigma^2_{\ln \alpha}$. Increased amount of kinetically sorbed mass defined by decreased f value resulted in more costly remediation.

Keywords: Groundwater, Pump-and-treat Remediation, Heterogeneity, Correlation Scale, Simulation-optimization

ÖZ

HETEROJENLİK BOYUTUNUN POMPAJİ TAKİP EDEN ARITIMLA AKİFER TEMİZLEME TASARIMI ÜZERİNDEKİ ETKİLERİNİN İNCELENMESİ

Güngör Demirci, Gamze

Doktora, Çevre Mühendisliği Bölümü

Tez Yöneticisi: Doç. Dr. Ayşegül Aksoy

Mayıs 2009, 272 sayfa

Bu çalışmada, hidrolik iletkenlik (K), denge dağılım katsayısı (K_d) ve kütle transfer katsayısına (α) ait heterojenlik korelasyon boyutunun (λ) varyans ($\sigma^2_{\ln K}$) ile tanımlanmış farklı heterojenlik dereceleri ve farklı parametre dağılımları da göz önüne alınarak kütle transferi kısıtlı sorpsiyon şartları altında pompajı takip eden arıtımla akifer temizleme tasarımı ve maliyeti üzerindeki etkisi incelenmiştir. Ek olarak, temizleme başlamadan önce akiferde bulunan kirletici miktarı ve kirletici dağılımının etkisi de irdelenmiştir. Farklı K heterojenliği ve temizleme tasarımı şartlarının temizleme süresi üzerindeki etkisi, K 'nın λ anizotropisinin, K ve K_d , ve K_d ve α arasındaki korelasyonların ve iki-siteli denge/kinetik sorpsiyon modelinde dengenin sorpsiyon sitelerinin oranının (f) temizleme tasarımı ve maliyeti üzerindeki tesiri de incelenen diğer konulardır. Bu amaçlara ulaşmak için, bir yeraltı suyu akımı ve kirletici taşınımı simülasyonu modeli ile genetik algoritma (GA) kütüphanesinin birleştirilmesinden oluşan simülasyon-optimizasyon yaklaşımı kullanılmıştır. Elde edilen sonuçlar sadece başlangıçtaki kirletici

miktarının değil $\lambda_{\ln K}$ ile tanımlanan yüksek ve düşük K bölgelerinin yer ve boyutları ile geometrik ortalama ve $\sigma^2_{\ln K}$ ile belirlenen K büyüklüklerinin de temizleme tasarımı, maliyeti ve süresi üzerinde etkili olduğunu göstermiştir. Ayrıca, K açısından heterojen akiferlerde, çok sayıda ve düşük pompaj miktarı ile çalışan kuyudan oluşan tasarımların, yüksek pompaj miktarı ile çalışan tek bir kuyudan oluşan tasarımlara göre temizleme süresinin tahmini açısından daha sağlam olduğu bulunmuştur. Homojen K_d varsayımının temizleme tasarımı ve maliyeti açısından ciddi hatalara yol açabileceği ve bu hatanın büyüklüğünün K ve K_d 'nin mekansal dağılımı ile $\lambda_{\ln K_d}$, $\sigma^2_{\ln K_d}$ ve $\sigma^2_{\ln K}$ 'ya göre değişebileceği gösterilmiştir. α heterojenliğinin etkisinin K, K_d and α 'nın mekansal dağılımı, $\lambda_{\ln \alpha}$ ve $\sigma^2_{\ln \alpha}$ 'ya göre önemli veya önemsiz olabileceği sonucuna varılmıştır. Düşen f değeri ile tanımlanan kinetik olarak sorplanmış kirletici miktarının artmasının daha pahalı temizleme tasarımlarına yol açtığı gösterilmiştir.

Anahtar Kelimeler: Yeraltı Suyu, Pompajı Takip Eden Arıtımla Akifer Temizleme, Heterojenlik, Korelasyon Boyutu, Simülasyon-optimizasyon

To my beloved husband, Gökhan

ACKNOWLEDGEMENTS

I would like to thank Assoc. Prof. Dr. Ayşegül Aksoy, my supervisor, for her guidance, recommendations and support throughout this research. I would like to acknowledge my committee members, Prof. Dr. Kahraman Ünlü, Assoc. Prof. Dr. Ertan Durmuşoğlu, Dr. Emre Alp and Dr. Elçin Kentel for their time and valuable suggestions.

The financial support of this research was provided by State Planning Agency (Grant No: BAP-08-11-DPT2002K120510-DK17). A part of computational resources of this research was provided by The Scientific and Technological Research Council of Turkey (TÜBİTAK) through TR-Grid e-Infrastructure Project in which Middle East Technical University is a hosting institution. I thank people working in this project, especially to Feyza Eryol, for providing me the technical assistance about using the system. I extend my thanks to Hakan Moral for his technical help, guidance and patience during configuration of the computer systems used in this research.

I am thankful to colleagues from Department of Environmental Engineering of METU for sharing the difficulties of this long journey with me. I am also grateful to all friends who were always there for supporting me.

I spent one year in an extraordinary place, Massachusetts Institute of Technology. It was an incredible experience which have changed and broadened my viewpoint to life and science. I would like to thank everybody who made this visit possible. I would like to thank TÜBİTAK and State Planning Agency for providing me financial support by means of International Research Fellowship. I would like to

extend my gratitude to Assoc. Prof. Dr. Charles F. Harvey who was my supervisor during this visit and to Denis R. LeBlanc from United States Geological Survey for their continuous support and encouragement throughout my research there. Their good nature, willingness to advance my knowledge and their bright ideas always amazed me and made my visit more productive and fun. I feel a deep appreciation for the friends who made this visit so unforgettable: Selis Önel for being there every time I need her; Hanan Karam, Leila Farhadi, Mack Durham, Moji Bateni, Ashfaque Khandaker, Lavanya Sharan, Oyebanke Oyeyinka from MIT for their sincere and loyal friendship; people of Cambridge Musiki Cemiyeti, especially Feridun Özgören and Güliz Pamukoğlu, for sharing the songs with me; Meltem Arıkan for her sisterly interest.

I am grateful to my parents and sister for their endless support and encouragement at every step of my life. I am also thankful to my parents-in-law, sister-in-law and brother-in-law for their support and well-wishes.

Last, but certainly not the least, I would like to thank my beloved husband, my teammate, my endless supporter, Gökhan. His love, sense of humor, understanding, encouragement, help, patience and confidence made my life and this long and stressful period easier and bearable. Knowing his presence and love in my life always helps me to overcome difficulties on my way.

TABLE OF CONTENTS

ABSTRACT	iv
ÖZ	vi
DEDICATION	viii
ACKNOWLEDGEMENTS	ix
TABLE OF CONTENTS	xi
LIST OF TABLES	xiv
LIST OF FIGURES.....	xvi
LIST OF ABBREVIATIONS	xxiv
CHAPTERS	
1. INTRODUCTION.....	1
2. THEORETICAL BACKGROUND	6
2.1. Pump and Treat Remediation.....	6
2.2. Sorption Process in the Subsurface: Equilibrium vs. Nonequilibrium Sorption and Related Parameters.....	9
2.3. Geostatistical Characterization of Random Fields: Mean, Variance and Correlation Scale	15
2.4. Geostatistical Characteristics of Physically and Chemically Heterogeneous Aquifers	20
2.5. Correlation between Physical and Chemical Aquifer Properties	24
2.6. Impact of K Heterogeneity on Contaminant Transport and the Performance of Pump and Treat Remediation.....	27
2.7. Impact of K_d Heterogeneity on Contaminant Transport and the Performance of Pump and Treat Remediation.....	33

2.8.	Impact of Rate-limited Mass Transfer and the Heterogeneity in Mass Transfer Rate Coefficient on Contaminant Transport and the Performance of Pump and Treat Remediation.....	37
2.9.	Genetic Algorithms and Their Use in Pump and Treat Remediation Problems	43
3.	METHODOLOGY	48
3.1.	Generation of Heterogeneous Fields	48
3.1.1.	K-fields.....	50
3.1.2.	Anisotropic K-fields.....	59
3.1.3.	K_d -fields	60
3.1.4.	Correlated K_d -fields.....	61
3.1.5.	α -fields	64
3.1.6.	Correlated α -fields	64
3.2.	Groundwater flow and contaminant transport simulation model.....	67
3.3.	Problem Description.....	69
3.4.	Optimization Model	75
3.4.1.	The Optimal Design Model.....	77
3.4.2.	The Time-to-Compliance Model.....	88
3.5.	Summary of the Main Titles Studied in This Work.....	91
3.5.1.	Effect of Correlation Scale of K.....	91
3.5.2.	Effect of Correlation Scale Anisotropy of K.....	92
3.5.3.	Effect of Heterogeneity in K_d	92
3.5.4.	Effect of Correlation between K and K_d	93
3.5.5.	Effect of Heterogeneity in α	93
3.5.6.	Effect of Correlation between α and K_d	93
3.5.7.	Effect of f value.....	94
4.	RESULTS AND DISCUSSION	95
4.1.	Results of the Sensitivity Analysis for the Determination of Crossover and Coding Method	95
4.1.1.	The Optimal Design Model.....	96

4.1.2.	The Time-to-Compliance Model.....	104
4.2.	PCE Plume Simulations on Heterogeneous K-fields	108
4.3.	Effect of Correlation Scale of K.....	126
4.3.1.	Results of the Optimal Design Model	127
4.3.1.1.	Results of the Original Plume Case.....	127
4.3.1.2.	Results of the Average Plume Case	137
4.3.2.	Results of the Time-to-Compliance Model.....	150
4.3.2.1.	Results of the Original Plume Case.....	151
4.3.2.2.	Results of the Average Plume Case	158
4.4.	Effect of Correlation Scale Anisotropy	165
4.5.	Effect of Correlation Scale and Heterogeneity of K_d	168
4.5.1.	Uncorrelated K_d and K	168
4.5.2.	Correlated K_d and K	192
4.6.	Effect of Correlation Scale and Heterogeneity of α	205
4.6.1.	Uncorrelated α and K_d	205
4.6.2.	Correlated α and K_d	214
4.7.	Effect of f	219
5.	CONCLUSIONS	227
5.1.	Conclusions	227
5.2.	Recommendations for the Future Work	231
	REFERENCES.....	233
	APPENDICES	
A.	HETEROGENEOUS FIELD REPRESENTATIONS	252
B.	COVARIANCE FUNCTION COMPARISONS	262
	CURRICULUM VITAE	269

LIST OF TABLES

Table 2.1 Examples of real life P&T projects along with the aboveground treatment technology and the types of contaminants treated	8
Table 2.2. Summary of the values of α reported in literature	14
Table 2.3. Summary of the values of f reported in literature	16
Table 2.4. Summary of the field scale studies investigating spatial variability of K in terms of mean of $\ln K$, $\sigma^2_{\ln K}$ and $\lambda_{\ln K}$	21
Table 3.1. Summary of the statistical properties of the heterogeneous K -fields (The unit of K is m/s).....	52
Table 3.2. Summary of the statistical properties of the anisotropic heterogeneous K -fields (The unit of K is m/s).....	60
Table 3.3. Summary of the statistical properties of the heterogeneous K_d -fields (The unit of K_d is cm^3/g)	61
Table 3.4. Summary of the statistical properties of the negatively and positively correlated heterogeneous K_d -fields (The unit of K_d is cm^3/g).....	63
Table 3.5. Summary of the statistical properties of the heterogeneous α -fields (The unit of α is d^{-1}).....	65
Table 3.6. Summary of the statistical properties of the correlated heterogeneous α -fields (The unit of α is d^{-1})	66
Table 3.7. Aquifer physical properties	70
Table 3.8. Granulated activated carbon cost and design parameters	80
Table 3.9. Binary coding and Gray code representations of the integers 0 to15 (Wilf, 1989).....	85
Table 4.1. Results of the sensitivity analysis for the optimal design model (Cro = Crossover type; Prob = Crossover probability; Cod = Coding Type; TP =	

Two-point; Uni = Uniform; Bin = Binary; Gr = Gray; R = Replicate number; Best = Best solution among replicates)	98
Table 4.2. Average E_{rel} (%) within 5 replicate runs for different K-field cases for the optimal design model	102
Table 4.3. Results of the sensitivity analysis for the time-to-compliance model.	105
Table 4.4. Summary of the statistical properties of the modified heterogeneous K_d - fields of the constant total mass approach (The unit of K_d is cm^3/g)	171
Table 4.5. Percent remediation cost increase with respect to the cost on homogeneous K_d -field for the constant total mass and the constant K_{dg} approaches	190

LIST OF FIGURES

Figure 2.1. Schematic representation of a conventional P&T remediation system. Treated water is (a) injected back to the aquifer via an injection well, (b) discharged into a receiving water body (adapted from Simon et al. (2002)) ...	7
Figure 2.2. Histograms of (a) K, and (b) ln K for one of the heterogeneous fields used in this study	18
Figure 2.3. The negative exponential covariance function from Equation 2.8 (adapted from Gelhar (1993))	19
Figure 2.4. Flow diagram showing the steps of GAs	45
Figure 3.1. Comparison of the theoretical covariance function with the covariance function of the K-fields generated in this study for realization A (a) $\lambda_{\ln K, x} = 15$ m, (b) $\lambda_{\ln K, y} = 15$ m, (c) $\lambda_{\ln K, x} = 22.5$ m, (d) $\lambda_{\ln K, y} = 22.5$ m, (e) $\lambda_{\ln K, x} = 30$ m, (f) $\lambda_{\ln K, y} = 30$ m.....	53
Figure 3.2. Comparison of the theoretical covariance function with the covariance function of the K-fields generated in this study for realization B (a) $\lambda_{\ln K, x} = 15$ m, (b) $\lambda_{\ln K, y} = 15$ m, (c) $\lambda_{\ln K, x} = 22.5$ m, (d) $\lambda_{\ln K, y} = 22.5$ m, (e) $\lambda_{\ln K, x} = 30$ m, (f) $\lambda_{\ln K, y} = 30$ m.....	54
Figure 3.3. Comparison of the theoretical covariance function with the covariance function of the K-fields generated in this study for realization C (a) $\lambda_{\ln K, x} = 15$ m, (b) $\lambda_{\ln K, y} = 15$ m, (c) $\lambda_{\ln K, x} = 22.5$ m, (d) $\lambda_{\ln K, y} = 22.5$ m, (e) $\lambda_{\ln K, x} = 30$ m, (f) $\lambda_{\ln K, y} = 30$ m.....	55
Figure 3.4. Distribution of K values for field K21A	56
Figure 3.5. Distribution of K values for field K11A	57
Figure 3.6. Distribution of K values for field K11B	57
Figure 3.7. Distribution of K values for field K11C	58
Figure 3.8. Distribution of K values for field K12C	58

Figure 3.9. Distribution of K values for field K13C	59
Figure 3.10. The average plume used in the optimization model runs (Triangular area shows the contamination source, circles depict the potential well locations and the numbers for the optimization runs)	71
Figure 3.11. PCE plumes for the heterogeneous fields K11A, K11B, K11C, K12A, K12B, K12C, K13A, K13B and K13C	72
Figure 3.12. PCE plumes for the heterogeneous fields K21A, K21B, K21C, K22A, K22B, K22C, K23A, K23B and K23C	73
Figure 3.13. PCE plumes for the heterogeneous fields K31A, K31B, K31C, K32A, K32B, K32C, K33A, K33B and K33C	74
Figure 3.14. Schematic diagram of the simulation-optimization approach (adapted from Ko et al., 2005)	76
Figure 3.15. Representation of a GA string	82
Figure 3.16. Demonstration of the method for the generation of Gray code	84
Figure 3.17. Schematic representation of (a) two-point crossover (b) uniform crossover.....	87
Figure 3.18. Well locations for 1-well (gray shaded circle) and 7-well (gray and white shaded circles) policies used for the time-to-compliance model along with the average plume	89
Figure 4.1. F (the ratio of the best value obtained within replicates to the global optimum) values for different K-field cases for the optimal design model .	100
Figure 4.2. The average, minimum and maximum P&T remediation costs based on five replicate simulations for different K-field cases for the optimal design model.....	101
Figure 4.3. Average CPU times on Intel Xeon 5110 processors having 1.6 Ghz frequency and the generation numbers realized to reach the solutions (including all runs for all K-fields) for the optimal design model	103
Figure 4.4. Variation of the optimal remediation time within three replicates for different K-field cases for the time-to-compliance model	106

Figure 4.5. Average CPU times on Intel Xeon 5110 processors having 1.6 Ghz frequency and the generation numbers realized to reach the solutions (including all runs for all K-fields) for the time-to-compliance model.....	106
Figure 4.6. (a) PCE plume and (b) hydraulic head distributions for the homogenous K-field ($K = 4.5 \times 10^{-5}$ m/s).....	109
Figure 4.7. PCE plume and hydraulic head distributions for the heterogeneous fields K11A, K12A, K13A.....	110
Figure 4.8. PCE plume and hydraulic head distributions for the heterogeneous fields K11B, K12B, K13B	111
Figure 4.9. PCE plume and hydraulic head distributions for the heterogeneous fields K11C, K12C, K13C	112
Figure 4.10. PCE plume and hydraulic head distributions for the heterogeneous fields K21A, K22A, K23A.....	113
Figure 4.11. PCE plume and hydraulic head distributions for the heterogeneous fields K21B, K22B, K23B	114
Figure 4.12. PCE plume and hydraulic head distributions for the heterogeneous fields K21C, K22C, K23C	115
Figure 4.13. PCE plume and hydraulic head distributions for the heterogeneous fields K31A, K32A, K33A.....	116
Figure 4.14. PCE plume and hydraulic head distributions for the heterogeneous fields K31B, K32B, K33B	117
Figure 4.15. PCE plume and hydraulic head distributions for the heterogeneous fields K31C, K32C, K33C	118
Figure 4.16. Change in initial mass of PCE with respect to $\lambda_{\ln K}$	122
Figure 4.17. Change in area of the PCE plume with respect to $\lambda_{\ln K}$	123
Figure 4.18. Change in K_g in the plume area with respect to $\lambda_{\ln K}$	125
Figure 4.19. Change in total remediation costs with respect to $\lambda_{\ln K}$ for original plume case	128
Figure 4.20. Change in capital costs with respect to $\lambda_{\ln K}$ for original plume case.....	131

Figure 4.21. Change in treatment costs with respect to $\lambda_{\ln K}$ for original plume case	132
Figure 4.22. Change in total mass of PCE removed from the aquifer with respect to $\lambda_{\ln K}$ for original plume case.....	133
Figure 4.23. Variation in the total remediation costs with respect to $\lambda_{\ln K}$ (error bars represent one standard deviation): original plume case	135
Figure 4.24. Variation in the area and the initial mass of initial plume with respect to $\lambda_{\ln K}$ (error bars represent one standard deviation): original plume case ..	136
Figure 4.25. Variation in the unit cost of PCE removal with respect to $\lambda_{\ln K}$ (error bars represent one standard deviation): original plume case.....	138
Figure 4.26. Selected wells for average plume case along with the CoM (red cross) and centerline (blue line) of the average plume	139
Figure 4.27. Initial plume location and K distributions for fields K23A and K33A for the average plume case	139
Figure 4.28. Change in total remediation costs with respect to $\lambda_{\ln K}$ for average plume case	141
Figure 4.29. Change in treatment costs with respect to $\lambda_{\ln K}$ for average plume case	143
Figure 4.30. Change in pumping costs with respect to $\lambda_{\ln K}$ for average plume case	144
Figure 4.31. Change in capital costs with respect to $\lambda_{\ln K}$ for average plume case.....	145
Figure 4.32. Change in total mass of PCE removed from the aquifer with respect to $\lambda_{\ln K}$ for average plume case.....	147
Figure 4.33. Variation in the total remediation costs with respect to $\lambda_{\ln K}$ (error bars represent one standard deviation): average plume case	148
Figure 4.34. Change in the length of remediation periods with respect to $\lambda_{\ln K}$ for 1-well-policy and for original plume.....	153
Figure 4.35. Change in the length of remediation periods with respect to $\lambda_{\ln K}$ for 7-well-policy and for original plume.....	154

Figure 4.36. Variation in the time-to-compliance with respect to $\lambda_{\ln K}$ (error bars represent one standard deviation): 1-well-policy and for original plume case	157
Figure 4.37. Variation in the time-to-compliance with respect to $\lambda_{\ln K}$ (error bars represent one standard deviation): 7-well-policy and for original plume case	157
Figure 4.38. Change in the length of remediation periods with respect to $\lambda_{\ln K}$ for 1-well-policy and for average plume	159
Figure 4.39. Change in the length of remediation periods with respect to $\lambda_{\ln K}$ for 7-well-policy and for average plume	160
Figure 4.40. Comparison of percent change between minimum and maximum time-to-compliance among all K-fields for the 1-well and 7-well policies with the original and average plumes as the initial conditions (The percentage value was calculated by the division of difference between two values to minimum value)	162
Figure 4.41. Variation in the time-to-compliance with respect to $\lambda_{\ln K}$ (error bars represent one standard deviation): 1-well-policy and for average plume case	164
Figure 4.42. Variation in the time-to-compliance with respect to $\lambda_{\ln K}$ (error bars represent one standard deviation): 7-well-policy and for average plume case	164
Figure 4.43. Comparison of total remediation cost for isotropic and anisotropic K-fields	167
Figure 4.44. Change in total remediation cost with respect to anisotropy ratio ($\lambda_{\ln K,x}/\lambda_{\ln K,y}$). $\lambda_{\ln K,y}$ kept constant as 15 m and $\lambda_{\ln K,x}$ increased from 15 m to 22.5 and 30 m	168
Figure 4.45. Change in the initial total mass of PCE with respect to $\lambda_{\ln K_d}$ for the constant K_d approach	173
Figure 4.46. Change in K_d in the plume area with respect to $\lambda_{\ln K_d}$ for the constant K_d approach	174

Figure 4.47. Change in the remediation costs with respect to $\sigma^2_{\ln K}$ for K_d realizations a, b and c, K realizations A and B and $\lambda_{\ln K_d}$ of 15 m for the constant Kd_g approach.....	177
Figure 4.48. Change in the remediation costs with respect to $\sigma^2_{\ln K}$ for K_d realizations a, b and c, K realizations A and B and $\lambda_{\ln K_d}$ of 30 m for the constant Kd_g approach.....	178
Figure 4.49. Distribution of (a) K_d values on field Kd32a and (b) K values on field K33A along with the average plume.....	181
Figure 4.50. Distribution of (a) K_d values on field Kd32b, and (b) K values on field K33A along with the average plume.....	182
Figure 4.51. Distribution of (a) K_d values on field Kd32c and (b) K values on field K33A along with the average plume.....	183
Figure 4.52. Change in average, minimum and maximum remediation cost with respect to $\lambda_{\ln K_d}$ for K_d -fields of the constant Kd_g approach for different K cases (Error bars represent one standard deviation).....	185
Figure 4.53. Change in remediation cost with respect to $\sigma^2_{\ln K}$ for K_d realization a, K realization A and $\lambda_{\ln K_d}$ of 15 and 30 m for the constant Kd_g and the constant total mass approach.....	189
Figure 4.54. Change in the initial mass of PCE with respect to $\sigma^2_{\ln K}$ (bottom axis) and $\sigma^2_{\ln K_d}$ (top axis) for positively and negatively correlated K_d -fields.....	193
Figure 4.55. Change in remediation cost for correlated K_d -fields with respect to $\sigma^2_{\ln K}$ (bottom axis) and $\sigma^2_{\ln K_d}$ (top axis) for K realizations A, B and C and $\lambda_{\ln K} = \lambda_{\ln K_d}$ of 15 and 30 m.....	195
Figure 4.56. K distribution of field (a) K33C and (b) K31B along with the average plume.....	198
Figure 4.57. K distribution of field (a) K33B and (b) K31C along with the average plume.....	200
Figure 4.58. Change in average, minimum and maximum remediation cost with respect to $\lambda_{\ln K_d}$ for negatively and positively correlated K_d -fields (Error bars represent one standard deviation).....	203

Figure 4.59. Change in remediation cost with respect to $\sigma^2_{\ln K}$ for α realizations i, ii and iii, K realization A and $\lambda_{\ln \alpha}$ of 15 and 30 m	207
Figure 4.60. Change in remediation cost with respect to $\sigma^2_{\ln K_d}$ for K_d realization a, K-field 13A, $\lambda_{\ln \alpha}$ of 30 m	208
Figure 4.61. Change in average, minimum and maximum remediation cost with respect to $\lambda_{\ln \alpha}$ for uncorrelated α -fields and different K and K_d cases (Error bars represent one standard deviation)	212
Figure 4.62. Change in remediation cost with respect to $\sigma^2_{\ln K}$ and $\sigma^2_{\ln \alpha}$ for K_d -fields which are negatively correlated with K realizations A, B and C, $\lambda_{\ln \alpha}$ of 15 and 30 m	216
Figure 4.63. Change in remediation cost with respect to $\sigma^2_{\ln K}$ and $\sigma^2_{\ln \alpha}$ for K_d -fields which are positively correlated with K realizations A, B and C, $\lambda_{\ln \alpha}$ of 15 and 30 m	217
Figure 4.64. Change in average, minimum and maximum remediation cost with respect to $\lambda_{\ln \alpha}$ for correlated α -fields (Error bars represent one standard deviation)	220
Figure 4.65. Schematic representation of the final mass distribution resulting from the use of different f values	221
Figure 4.66. Comparison of total remediation costs for the original plume case when f = 0.25, 0.50 and 0.75	224
Figure 4.67. Comparison of total remediation costs for the average plume case when f = 0.25, 0.50 and 0.75	225
Figure A.1. Heterogeneous K-fields for realization A	252
Figure A.2. Heterogeneous K-fields for realization B	253
Figure A.3. Heterogeneous K-fields for realization C	254
Figure A.4. Anisotropic K-fields	255
Figure A.5. Heterogeneous K_d -fields for realization a	256
Figure A.6. Heterogeneous K_d -fields for realization b	257
Figure A.7. Heterogeneous K_d -fields for realization c	258
Figure A.8. Heterogeneous α -fields for realization i	259

Figure A.9. Heterogeneous α -fields for realization ii	260
Figure A.10. Heterogeneous α -fields for realization iii	261
Figure B.1. Comparison of the theoretical covariance function with the covariance function of the anisotropic K-fields generated in this study for realization B (a) $\lambda_{\ln K, x} = 22.5$ m, (b) $\lambda_{\ln K, y} = 15$ m, (c) $\lambda_{\ln K, x} = 30$ m, (d) $\lambda_{\ln K, y} = 15$ m	262
Figure B.2. Comparison of the theoretical covariance function with the covariance function of the K_d -fields generated in this study for realization a. (a) $\lambda_{\ln K_d, x} =$ 15 m, (b) $\lambda_{\ln K_d, y} = 15$ m, (c) $\lambda_{\ln K_d, x} = 30$ m, (d) $\lambda_{\ln K_d, y} = 30$ m	263
Figure B.3. Comparison of the theoretical covariance function with the covariance function of the K_d -fields generated in this study for realization b. (a) $\lambda_{\ln K_d, x} =$ 15 m, (b) $\lambda_{\ln K_d, y} = 15$ m, (c) $\lambda_{\ln K_d, x} = 30$ m, (d) $\lambda_{\ln K_d, y} = 30$ m	264
Figure B.4. Comparison of the theoretical covariance function with the covariance function of the K_d -fields generated in this study for realization c. (a) $\lambda_{\ln K_d, x} =$ 15 m, (b) $\lambda_{\ln K_d, y} = 15$ m, (c) $\lambda_{\ln K_d, x} = 30$ m, (d) $\lambda_{\ln K_d, y} = 30$ m	265
Figure B.5. Comparison of the theoretical covariance function with the covariance function of the α -fields generated in this study for realization i. (a) $\lambda_{\ln \alpha, x} = 15$ m, (b) $\lambda_{\ln \alpha, y} = 15$ m, (c) $\lambda_{\ln \alpha, x} = 30$ m, (d) $\lambda_{\ln \alpha, y} = 30$ m	266
Figure B.6. Comparison of the theoretical covariance function with the covariance function of the α -fields generated in this study for realization ii. (a) $\lambda_{\ln \alpha, x} = 15$ m, (b) $\lambda_{\ln \alpha, y} = 15$ m, (c) $\lambda_{\ln \alpha, x} = 30$ m, (d) $\lambda_{\ln \alpha, y} = 30$ m	267
Figure B.7. Comparison of the theoretical covariance function with the covariance function of the α -fields generated in this study for realization iii. (a) $\lambda_{\ln \alpha, x} =$ 15 m, (b) $\lambda_{\ln \alpha, y} = 15$ m, (c) $\lambda_{\ln \alpha, x} = 30$ m, (d) $\lambda_{\ln \alpha, y} = 30$ m	268

LIST OF ABBREVIATIONS

CoM	:	Center of mass
CPU	:	Central processing unit
CV	:	Coefficient of variation
f	:	Fraction of equilibrium sorption sites
GA	:	Genetic algorithm
GAC	:	Granular activated carbon
K	:	Hydraulic conductivity
K _d	:	Equilibrium distribution coefficient
K _g	:	Geometric mean of K-field
Kd _g	:	Geometric mean of K _d -field
NPL	:	National Priorities List
P&T	:	Pump-and-treat
PCE	:	Tetrachloroethene
α	:	Mass transfer rate
α_g	:	Geometric mean of α -field
λ	:	Correlation scale
σ	:	Standard deviation
σ^2	:	Variance

CHAPTER 1

INTRODUCTION

Of all the water available on the Earth, only 2.5% is fresh water. Groundwater constitutes 30.1% of the freshwater reserves. Considering that 68.7% of the freshwater is enclosed in the ice caps and glaciers, 0.3% is in the rivers, lakes and swamps as surface water and 0.9% is in other forms (Schneider, 1996), most of the freshwater which our lives depend on is below our feet under the ground. Although not all groundwater is available for our use, it is an important, reliable and good quality source of fresh water. Groundwater had been seen as a secondary source of water supply for human use after surface water for a long time. However, this picture is rapidly changing as groundwater is now preferred over surface water in many parts of the world as the major source for all types of water use, i.e. domestic, agricultural and industrial. This is mainly because surface water resources are diminishing as a result of climate change and their capture and storage is not always feasible (Villholth and Giordano, 2007). Surface waters are also faced with extensive pollution problems which limit their use. As in the other parts of the world, groundwater is an important source to supply demand in Turkey as well. In the year of 2001, 57.5% of all water distributed by water distribution networks in 3092 municipalities was obtained from wells and springs (TSI, 2009).

Although groundwater seems to be more protected against pollution problems compared to surface water, human activities threaten the water quality of groundwater in many parts of the world. Extensive use of fertilizers and other chemicals in agriculture, land disposal of untreated domestic and industrial

wastewaters, illegal hazardous liquid and solid waste dumps, leakages from the chemical storage tanks and pipelines of industrial facilities, leakages from landfills are only the few reasons of groundwater pollution. Because of all these polluting activities and insufficient measures, many pollutants, such as heavy metals, organic compounds and pesticides find their way to groundwater. As of September 2008, there are a total of 1258 contaminated sites in the United States in the National Priorities List (NPL). With the addition of 64 proposed sites, this total number may reach to 1322 (USEPA, 2009a). On the other hand, according to the assessment published in August 2007 by the European Environment Agency, the number of contaminated sites in Europe, including Turkey, is estimated as approximately 250,000. If the current trend continues, it is expected that the number of sites that requires remediation will increase by 50% by 2025 (EEA, 2009). In Turkey, unfortunately, there is no complete inventory of contaminated sites but the number is believed to be in the range of 1000-1500, of which 5-10% is predicted as the sites needing remediation (NATO/CCMS-Turkey, 2006).

Once being contaminated, it is not easy to restore the aquifers. Remediation of the contaminated aquifers is not only a hard but also an expensive and a lengthy task. There are various techniques currently available for this purpose. P&T remediation which consists of extraction of contaminated groundwater by pumping and then applying treatment is one of these techniques. In spite of all questions about its effectiveness which has been raised for decades (Mackay and Cherry, 1989; Travis and Doty, 1990; Bartow and Davenport, 1995; Mackay, 1998), it is still a widely preferred and used method all around the world. For example in the U.S., for the time period between 1982 to 2005, P&T remediation has been preferred, either alone or in combination with other remediation technologies, at 68% of NPL sites on which groundwater remediation has been implemented or planned (USEPA, 2007). There are also many examples of P&T remediation applications in Europe (ENVISAN, 2009). The main power of this technique lies behind being the method applicable for the plumes spread over a large area and providing both

hydraulic containment and cleanup of the plume at the same time (Hoffman, 1993; Marquis and Dineen, 1994). It is well known that P&T remediation systems are faced with some problems which are also the sources of the ongoing questions. The main problem is being unable to reach the cleanup goals at the end of very long operation which costs hundreds or even millions of dollars. This has become a motivation for a wealth of studies analyzing the reasons of this problem in the literature for ages. The study of Mackay and Cherry (1989) is a good example that reviews the reasons for not meeting the goals in the remediation of organic contaminants.

The problems associated with P&T may be as a result of some simplifying assumptions used in the design, such as homogeneous physical and chemical aquifer properties and equilibrium sorption of contaminant. Heterogeneity in physical and chemical aquifer properties is one of the basic reasons that impact the success of P&T remediation systems. In addition to heterogeneity, mass transfer limitations resulting from the nonequilibrium sorption of contaminants lead to great difficulties in P&T operations. In the field conditions, P&T operation starts with a relatively large drop in the contaminant concentration. After this early stage, the decline in the concentration gradually slows down resulting in a commonly observed phenomenon called “tailing”. Both heterogeneity and rate limited mass transfer are the reasons of tailing. These two factors also generate “rebound” effect, fairly rapid increase in the concentration after the shut down of the pumping operation (Eastern Research Group, Inc., 1996). As tailing behavior is observed, it may take several years or even decades to reach the remediation goals. The worse may be the exceedance of this goal due to rebound after the completion of the operation. Therefore, consideration of the aquifer heterogeneities and rate-limited mass transfer is crucial for the efficient remediation design and more accurate cost and operation time predictions. Furthermore, correlation between the physical and chemical aquifer properties is another factor which is worth to consider during the design of P&T remediation systems since it is well known that

the correlation between the physical and chemical parameters strongly affects the transport of contaminants (Garabedian, 1987; Bosma et al., 1993; Rabideau and Miller, 1994).

Finding the most efficient remediation design having the maximum performance with a minimum cost may be a tedious job with trial and error. Optimization tools help to make this job easier. In combination with numerical simulation models, optimization techniques have been used for optimal remediation system designs for decades not only for research (e.g. Gorelick et al., 1984; McKinney and Lin, 1996; Yan and Minsker, 2006) but also for real life applications (e.g. optimization case studies at Federal Remediation Technologies Roundtable member sites (FRTR, 2009)).

Considering how expensive and lengthy the P&T remediation of contaminated aquifers is, even a small percent improvement in the performance can make a significant difference in the total cost and prediction of the length of remediation period. On the other hand, without defining how different factors affect the P&T remediation design and cost, it is not possible to get any improvement. The motivation of this study lies behind the idea that the scale of physical and chemical heterogeneity may be an important factor affecting P&T design and cost. Specifically the objective of this study is to evaluate the influence of correlation scale of hydraulic conductivity (K), the equilibrium distribution coefficient (K_d) and mass transfer rate (α) on the P&T remediation design and cost under different degrees of heterogeneity using simulation-optimization approach. The study also aims to investigate the effect of contaminant mass present in the heterogeneous aquifer on the P&T design and cost. In addition, the change in the length of remediation period under different heterogeneity and design conditions is addressed in order to find a more robust design approach for physically heterogeneous aquifers. Hypothesizing that the correlation between K and K_d and K_d and α might have significant influence on the P&T performance, the study also

focuses to define this influence under different heterogeneity conditions. Furthermore, the effect of correlation scale anisotropy of K and the fraction of equilibrium/nonequilibrium sorption sites on the P&T design and cost is purposed to be revealed.

This dissertation is composed of six chapters. Chapter 1, the current chapter, makes a general introduction with the subject by specifically emphasizing the motivations and the objective of the study. Chapter 2 provides brief theoretical information about the key concepts as well as extensive reviews of the literature about different aspects of the study. Chapter 3 gives the description of the methodological tools along with the definition of the problem and the main titles studied. Chapter 4 presents all results obtained and discussions of these results. Chapter 5 covers the conclusions drawn out of the results of this work and the recommendations for future work.

CHAPTER 2

THEORETICAL BACKGROUND

2.1. Pump and Treat Remediation

P&T has been the most widely used technology for the remediation of contaminated groundwater for decades. A conventional P&T remediation system consists of extraction of contaminated groundwater and treatment of it above ground. Pumping wells are placed at selected locations into the aquifer to be treated and contaminated groundwater is pumped to the surface for subsequent treatment. For the aboveground treatment of the contaminants, various treatment technologies are used including biological (e.g. activated sludge systems, rotating biological contactors, etc.) and physical/chemical (e.g. air stripping, granular activated carbon (GAC), ion exchange, chemical oxidation, etc.) ones. The treated water may then be either discharged to a receiving water body nearby or injected back into the aquifer (Eastern Research Group, Inc., 1996). Figure 2.1 is the schematic representation of a conventional P&T remediation system.

P&T remediation is applied to the sites contaminated with variety of contaminants such as chlorinated VOCs (e.g. trichloroethene (TCE), tetrachloroethene (PCE), dichloroethene (DCE), etc.), nonchlorinated VOCs (e.g. benzene, toluene, xylene, etc.) and metals. Table 2.1 gives some examples of real life P&T projects along with the treatment technology used aboveground and the types of contaminants treated. More examples can be found on the Annual Status Report Remediation Database of U.S. Environmental Protection Agency (EPA) (USEPA, 2009b).

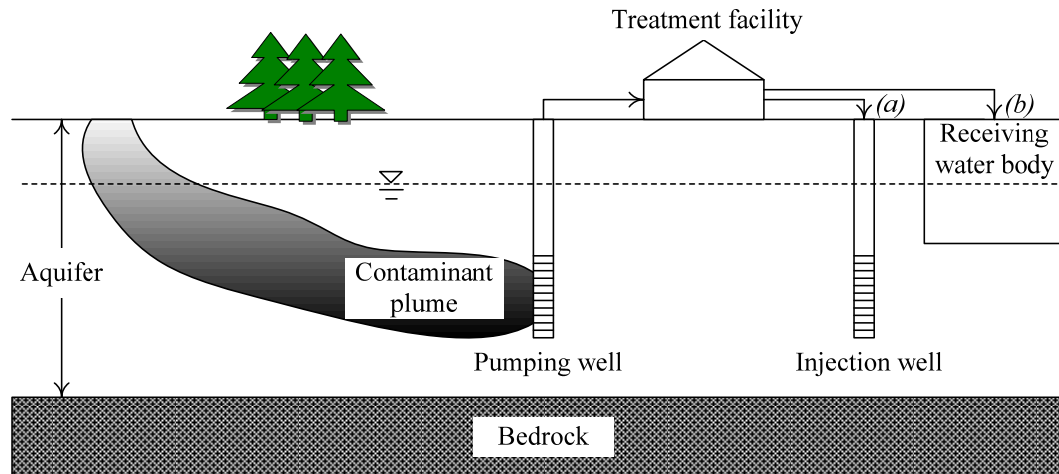


Figure 2.1. Schematic representation of a conventional P&T remediation system. Treated water is (a) injected back to the aquifer via an injection well, (b) discharged into a receiving water body (adapted from Simon et al. (2002))

Other than being a contaminated groundwater cleanup method, P&T is also a useful method for hydraulic containment of the contaminant plumes by controlling their movements and preventing the expansion of the contaminated zone. Hence, for large contaminant plumes, P&T is superior to the other alternative remediation techniques (Hoffman, 1993; Marquis and Dineen, 1994). Between 1982 and 2005, P&T remediation has been preferred, either alone (45%) or in combination with other remediation technologies (23%), at 68% of NPL sites on which groundwater remediation has been implemented or is planned. When the P&T projects on NPL sites are investigated, it is seen that 72% of them are still operational while only 10% has already been completed or shut down. It is interesting that only 38% of this 10% had met the remediation goals while remaining 62% were shut down because of various reasons such as technical/operational problems or replacement with other remediation technologies (USEPA, 2007).

Table 2.1 Examples of real life P&T projects along with the aboveground treatment technology and the types of contaminants treated

Site, Location	Treatment Technology	Contaminant treated	Reference
Engelhard Corporation Facility, MA	Metal removal, air stripping, filtration, GAC adsorption	1,2-DCE; 1,1-DCE; 1,1,-DCA; 1,1,1-TCA; TCE; PCE	USEPA, 2005(a)
The Eaton Corporation Facility, NE	Air stripping	TCE	USEPA, 2005(b)
Chemko Technical Services, Inc. Facility, FL	Air stripping	PCE; TCE; 1,2-DCE	USEPA, 2005(c)
The Otis Air National Guard Base/Camp Edwards, MA	GAC adsorption	PCE; TCE; benzene; EDB	AFCEE, 2007
Twin Cities Army Ammunition Plant, MN	Air stripping	1,2-DCE; 1,1,1-TCA; TCE; PCE	USEPA, 2001
Former Firestone Facility, CA	GAC adsorption and air stripping	1,1-DCE; TCE; PCE; 1,1-DCA; benzene; toluene; xylene	USEPA, 2001
U.S. Department of Energy, Savannah River, SC	Air stripping	TCE; PCE; 1,1,1-TCA	USEPA, 2001
Old Mill, OH	GAC adsorption and air stripping	TCE; PCE; 1,2-DCE; ethylbenzene	USEPA, 2001
Mystery Bridge at Highway 20, WY	Air stripping	1,2-DCE; TCE; PCE; 1,1,1-TCA; 1,1-DCE	USEPA, 2001
LaSalle Electrical, IL	GAC adsorption and air stripping	PCBs; TCE; 1,2-DCE; 1,1,1-TCA; VC; 1,1-DCA; PCE	USEPA, 2001

1,1,-DCA = 1,1-dichloroethene; 1,2-DCA = 1,2-dichloroethane; 1,1-DCE = 1,1-Dichloroethene; 1,2-DCE = 1,2-dichloroethene; 1,1,1-TCA = 1,1,1-trichloroethane; VC = vinyl chloride; EDB = Ethylene dibromide, MTBE = Methyl tertiary-butyl ether; PCBs = Polychlorinated biphenyls

The major concerns in using P&T remediation technology are the long cleanup times to reach the water quality goals and high cost of operation in addition to the high capital cost. An analysis of 32 P&T sites revealed that the capital cost per site ranged from \$290,000 to \$19,000,000 with an average of \$4,900,000, while operating cost per year ranged from \$110,000 to \$4,600,000 with an average of \$770,000 (USEPA, 2001). On the other hand, Mackay (1998) stated that 1 to 10 years of time range was generally expected for the completion of remediation by P&T but the anticipations were barely satisfied. The prolonged cleanup times and the high cost mostly depend on the aquifer complexity in terms of spatially variable physical and chemical properties, rate-limited mass transfer due to chemical and/or physical nonequilibrium, the size of the aquifer, the contaminant properties, the magnitude of the contaminated groundwater plume, including the plume area, depth and the concentrations of contaminants within the plume, performance goals and discharge limits, and the adequacy of the system design (Mackay and Cherry, 1989; Berglund, 1995; Berglund and Cvetkovic, 1995; Berglund, 1997; USEPA, 1999; Zhang and Brusseau, 1999; Marquis and Dineen, 1994).

2.2. Sorption Process in the Subsurface: Equilibrium vs. Nonequilibrium Sorption and Related Parameters

Sorption is one of the key processes affecting the fate and transport of contaminants and should be included in the simulation models. The typical approach used in most groundwater flow and contaminant transport models is the linear equilibrium sorption which assumes instantaneous sorption and a linear reversible relationship for the transfer of the solute between aqueous and sorbed phases such that

$$S = K_d C \quad (2.1)$$

where S = the total mass of solute sorbed per unit mass of soil [M/M]; K_d = the equilibrium distribution coefficient; and C = the aqueous phase concentration of solute [M/L³].

Equilibrium sorption assumption is valid when the sorption process is fast enough relative to the other processes affecting the solute concentration, such as advection and hydrodynamic dispersion. Equilibrium between the aqueous and sorbed phases can be established only for such a case. Under the natural groundwater flow conditions in the subsurface, equilibrium sorption assumption can be valid. However, detailed laboratory and field observations have shown that equilibrium sorption assumption fails in many cases such as in flow conditions under induced gradients with increased velocities (Ptacek and Gillham, 1992; Pickens et al., 1981; Brusseau and Rao, 1989a; Brusseau et al., 1991a; Valocchi 1985). In induced flow conditions, as in P&T remediation, nonequilibrium sorption has a special importance affecting the remediation performance (Brusseau, 1992a). Aksoy and Culver (2000) showed that neglecting nonequilibrium sorption in P&T remediation design resulted in underestimated time, cost and pumped water volume predictions for remediation.

Processes responsible for nonequilibrium sorption can have either physical or chemical base. Physical nonequilibrium is the result of presence of mobile and immobile regions in the flow domain and the diffusive solute transfer between them (Nkedi-Kizza et al., 1984). The process has been described by the two-region model developed by Coats and Smith (1964) and van Genuchten and Wierenga (1976). Although it is more properly classified as a hydrodynamic feature of the flow domain, physical nonequilibrium is usually discussed as a sorption nonequilibrium mechanism (Brusseau and Rao, 1989b). On the other hand, chemically based nonequilibrium sorption is described by two-site model developed by Selim et al. (1976) and Cameron and Klute (1977). Because the two-site model is used in this study in order to represent the mass transfer limited

sorption, two-region model is not mentioned here in detail. However, it is worth to point out that the two-site model is mathematically equivalent to the two-region model which assumes contaminant exchange between mobile and immobile water zones (Nkedi-Kizza et al., 1984).

The two-site model hypothesizes that sorption sites in soils can be divided into two fractions. Sorption is at instantaneous equilibrium for one fraction (Type 1) and rate-limited or kinetic for the other (Type 2) (van Genuchten and Wagenet, 1989; Nkedi-Kizza et al., 1984; Brusseau and Rao, 1989a). The sorption at equilibrium sites (S_1) is described by linear equilibrium sorption equation (Equation 2.1) such that

$$\frac{\partial S_1}{\partial t} = fK_d \frac{\partial C}{\partial t} \quad (2.2)$$

where f = the fraction of equilibrium sorption sites (Type 1) [-].

On the other hand, the sorption on the nonequilibrium sites (S_2) is given by the following reversible first order kinetic equation.

$$\frac{\partial S_2}{\partial t} = \alpha[(1-f)K_d C - S_2] \quad (2.3)$$

where α = first order mass transfer rate coefficient [$1/T$].

Considering that the summation of S_1 and S_2 gives the total sorption, the governing transport equations for two-site model are

$$\left[1 + \frac{f\rho_b K_d}{n}\right] \frac{\partial C}{\partial t} + \frac{\rho_b}{n} \frac{\partial S_2}{\partial t} = D \frac{\partial^2 C}{\partial x^2} - v \frac{\partial C}{\partial x} \quad (2.4)$$

where D = hydrodynamic dispersion coefficient [L^2/T]; n = effective porosity [-]; t = time [T]; v = linear average velocity [L/T]; and ρ_b = dry bulk density of porous media [M/L^3].

Equation 2.3 can be used for both rate-limited surface reactions and diffusion limited access to sorption sites, called intrasorbent diffusion. The rate-limited reaction is assumed to occur between the sorbate and specific sites on the surface of sorbent particles for the first case. The rate limitation is due to the diffusion of the sorbate into or out of the sorbent matrix for the second case. Intrasorbent diffusion is thought to be the cause of the nonequilibrium sorption of nonionic, low-polarity, hydrophobic organic compounds, such as PCE, by the sorbent organic matter (Brusseau and Rao, 1989a, b; Brusseau et al., 1991a).

The three important parameters included in the two-site model are K_d , α and f . Assuming K_d and α as homogenous or completely neglecting α by equilibrium sorption assumption may oversimplify the remediation design and result in improper remediation systems. Although, to author's knowledge, it has not been mentioned in any studies in literature, f value may also have a considerable impact on the design, cost and time estimates.

K_d is the expression describing the partitioning of a solute between water and soil. It depends on both soil and contaminant properties and it is obtained by the multiplication of soil organic carbon/water partition coefficient (K_{oc}) of the contaminant and fraction of organic carbon (f_{oc}) of the soil. For a single contaminant which has a certain K_{oc} value at certain temperature, different K_d values can be observed depending on the organic carbon content of the soil. Therefore, K_d is usually regarded as the chemical property of the aquifer and can show spatial variation at the field in relation to the organic carbon content of the soil.

One of the two kinetics-associated parameters of two-site model is α . It represents the rate of the sorption/desorption on the rate-limited sorption sites. Its value shows variation depending on various factors, such as the properties of the contaminant and soil, scale of the experiment (i.e. lab or field), time scale of the experiment, pore water velocity used in the experiment, etc. (Ptacek and Gillham, 1992; Maraqa, 2001; Brusseau et al., 1991a; Brusseau and Rao, 1989b; Zimmerman, 1998). The accurate determination of α is one of the limitations which has been experienced in nonequilibrium sorption studies. The most commonly used method for this purpose is to perform laboratory column experiments. Then, the least square regression analysis is conducted usually using a computer program to fit the breakthrough curve data and to predict α . The major difficulty associated with this method is that application of the coefficients determined from the laboratory studies to the field situations may introduce error. This is due to the higher flow rates used in column experiments compared to the actual field situation and presence of other nonideal factors in the field such as aquifer heterogeneity (Zimmerman, 1998, Brusseau et al., 1991a; Pang and Close, 1999). Therefore, α determined at the field scale is generally much lower than the counterpart determined in the laboratory (Maraqa, 2001; Brusseau et al., 1991a). In addition, α for long term contaminated soils can be much lower than α measured in the laboratory using very recently contaminated soils. Many studies in literature showed that the rate of desorption decreases with increasing time of exposure (Koller et al., 1996; Culver et al., 1997; Pignatello and Xing, 1996; Connaughton et al., 1993; Deitsch and Smith, 1995). The summary of α values reported in literature for different types of contaminants and soils are given in Table 2.2. The great variation of the values in Table 2.2 is the result of these mentioned factors.

The other kinetics-associated parameter of the two-site model is f . It represents the fraction of sorbent for which sorption is instantaneous. With this description, it is a soil related parameter such that for the same type of contaminant, different f values

Table 2.2. Summary of the values of α reported in literature

Contaminant	Type of experiment	Type of soil material	α (d ⁻¹)	Reference
TCE	Batch	Soil with f_{oc} = 1.04%	0.0018	Sahoo, 1997
TCE	Batch Column	Long term contaminated soil with f_{oc} = 1.04	0.0018 – 0.0058 0.0041 – 0.0076	Culver et al., 1997
TCE PCE Xylene Naphthalene	Column	2 sandy aquifer materials with f_{oc} = 0.007 and 0.025%	2.88 1.68 1.44 1.92	Brusseau et al., 1991a
PCE p-xylene Naphthalene 1,4-DCB	Column	3 aquifer materials with f_{oc} = 0.1, 0.02 and 0.03%	4.32 – 338.4 9.12 – 400.8 6.24 – 158.4 19.2 – 518.4	Brusseau, 1992b
TCE PCE	Column	Soil with f_{oc} = 0.47	460.8 280.8	Piatt, 1997
Naphthalene Phenanthrene Pyrene	Batch	Sediment with f_{oc} = 0.019%	3.36 – 1.37 0.89 – 2.26 0.72 – 1.61	Piatt et al., 1996
TCE PCE Benzene	Gas purge Column	4 soils with f_{oc} = 0.007 and 0.025% Soil with f_{oc} = 0.39% Soil with f_{oc} = 18% Soil with f_{oc} = 0.39%	41.75 – 410.4 172.8 31.68 564	Brusseau et al., 1990
Naphthalene	Column	Sand f_{oc} = 0.66% Sand f_{oc} = 0.036%	0.132 11.8	Liu et al., 1991
BROM CTET PCE DCB HCA	Column	Borden sand with f_{oc} = 0.02%	4.1 – 133.9 3.7 – 37.8 1.5 – 69.1 1.8 – 52.3 1.5 – 40.7	Ptacek and Gillham, 1992

1,4-DCB = 1,4-dichlorobenzene, BROM = bromoform, CTET = carbon tetrachloride, HCA = hexachloroethane.

have been reported for different types of soils (Zimmerman, 1998; Brusseau, 1992b). On the other hand, Brusseau et al. (1991a, b) shows a relation between f and K_{ow} , octanol-water partition coefficient, which is a contaminant property. According to this relation, f increases with increasing $\log K_{ow}$. In addition, for the same type soil, different f values were reported for different contaminants (Zimmerman, 1998; Brusseau, 1992b). This shows that values of f vary depending on the type of soil and the contaminant (Brusseau, 1992c). The value of f for different contaminants and different types of aquifer materials has been reported in a number of studies. A compilation of these studies is given in Table 2.3.

2.3. Geostatistical Characterization of Random Fields: Mean, Variance and Correlation Scale

Natural environment is continuous and spatially variable with great complexity. Geostatistics has arisen with the need of estimation of the parameters which vary in space and description of this spatial distribution since it is impossible to measure these parameters at every single point of the system of interest. For a subsurface flow system, examples of spatially variable parameters include K and f_{oc} of the soil. Geostatistics helps to predict these parameters in the large scale with the use of limited number of local measurements. The aim of geostatistical analysis is to define the spatial correlation structure of measured data, to construct a model that describes the observed data, and predict the values in the areas where data are not available or measured (Webster and Oliver, 2007).

Geostatistical analysis is applied to quantify the degree of heterogeneity of an aquifer in terms of statistical parameters such as mean, variance and the correlation scale. For a set of observations which is normally distributed, the mean is the central value (Kitanidis, 1997) and computed as

Table 2.3. Summary of the values of f reported in literature

Contaminant	Type of experiment	Type of soil material	F	Reference
Naphthalene	Column	Sand with $f_{oc} = 0.05\%$ and 2 soils with $f_{oc} = 0.3$ and 1%	0.02 – 0.70	Zimmerman, 1998
Benzene			0.10 – 0.85	
Toluene			0.55 – 0.83	
Xylene			0.52 – 0.85	
TCE	Column	2 sandy aquifer materials with $f_{oc} = 0.007$ and 0.025%	0.42	Brusseau et al., 1991a
PCE			0.49	
Xylene			0.46	
Naphthalene			0.60	
Benzene	Column	Sandy soil with $f_{oc} = 0.39\%$	0.38	Brusseau et al., 1991b
Naphthalene			0.46	
Anthracene			0.51	
PCE	Column	3 aquifer materials with $f_{oc} = 0.1, 0.02$ and 0.03%	0.28 – 0.48	Brusseau, 1992b
p-xylene			0.52 – 0.76	
Naphthalene			0 – 0.70	
1,4-DCB			0.36 – 0.74	
TCE	Batch	Soil with $f_{oc} = 1.04\%$	0.06	Sahoo, 1997
Naphthalene	Batch	Sediment with $f_{oc} = 0.019\%$	0.20 – 0.31	Piatt et al., 1996
Phenanthrene			0.31 – 0.34	
Pyrene			0.24 – 0.27	
Naphthalene	Column	Sand $f_{oc} = 0.66\%$	0.62	Liu et al., 1991
		Sand $f_{oc} = 0.036\%$	0.49	
BROM	Column	Borden sand with $f_{oc} = 0.02\%$	0.31 – 0.62	Ptacek and Gillham, 1992
CTET			0.19 – 0.47	
PCE			0.31 – 0.61	
DCB			0.33 – 0.46	
HCA			0.44 – 0.62	

$$\bar{X} = \frac{1}{N} \sum_{i=1}^N X_i \quad (2.5)$$

where X_i = measured value; \bar{X} = arithmetic mean; and N = number of observations.

When deviations from the normality occur, the measured values may be transformed to a new scale on which their distribution is closer to normal. Logarithmic transformation, in which the distribution of the logarithm or natural logarithm of the data X is normal, is one of them. Log-normal distribution is generally used to characterize the subsurface parameters. For example, K is one of the parameters shown to be log-normally distributed in nature. An example distribution of K values ranging from 9.4×10^{-6} to 1.8×10^{-4} m/s is shown as a histogram in Figure 2.2a. The K histogram belongs to one of the K -fields used in this study as will be discussed in the next chapter. As seen in Figure 2.2a, the distribution is not symmetric and it is obvious that K is not normally distributed. On the other hand, the histogram of $\ln K$ is presented in Figure 2.2b. It is almost symmetric and taking the natural logarithm of K has normalized the data quite effectively. In the light of this information, then, the geometric mean of the same set of observations is expressed by the following formula (Webster and Oliver, 2007):

$$\ln \bar{G} = \frac{1}{N} \sum_{i=1}^N \ln X_i \quad (2.6)$$

where \bar{G} = geometric mean.

The variance is the term used to describe the spread of observations (Gelhar, 1993; Webster and Oliver, 2007). Its square root is the standard deviation. The variance is computed as

$$\sigma^2 = \frac{1}{N-1} \sum_{i=1}^N (X_i - \bar{X})^2 \quad (2.7)$$

where σ^2 = variance; and σ = standard deviation.

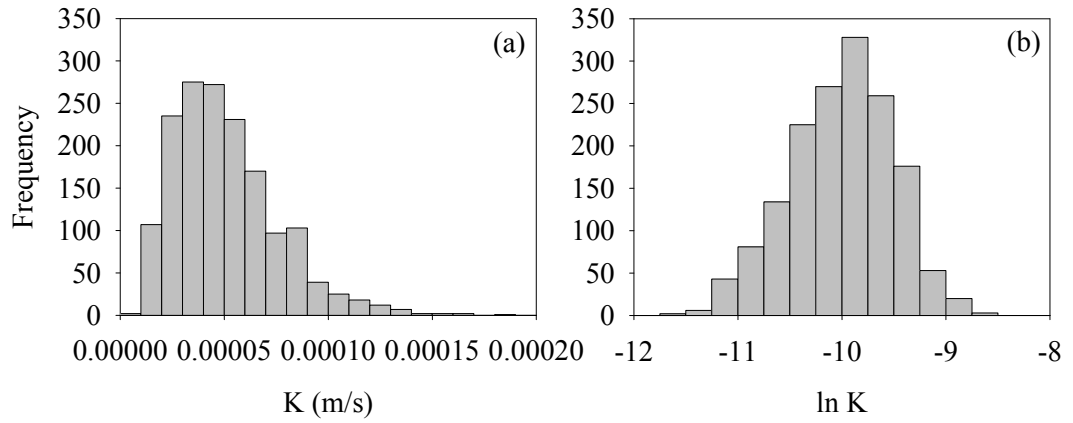


Figure 2.2. Histograms of (a) K, and (b) ln K for one of the heterogeneous fields used in this study

The mean and σ^2 are the terms used to describe the normal distribution of measurements independent of their location. In order to describe the variation of measurements in space or the relation among them based on their location, the concept of covariance is used. A measure of linear relationship between two measurements is shown by the covariance function. Physically, the covariance function is the indicator of the degree of correlation between the measurements at adjacent points in space. Since the subsurface is continuous, a high correlation is expected for points which are close to each other, while this correlation decreases as the separation between the points increases (Gelhar, 1993). In literature, the negative exponential covariance function is generally assumed to characterize the spatial continuity of aquifer properties (Eggleston et al., 1996; Eggleston, 1997; Woodbury and Sudicky, 1991; Pfleiderer and Moltyaner, 1993; Byers and Stephens, 1983; Rehfeldt et al., 1992; Sudicky, 1986; Hess et al., 1992; Bjerg et al., 1992). The negative exponential covariance function ($R(h)$) is represented by the following equation and graphically shown in Figure 2.3 (Gelhar, 1993).

$$R(h) = \sigma^2 e^{(-h/\lambda)} \quad (2.8)$$

where h = separation (lag) distance; and λ = correlation scale (λ_x , λ_y , λ_z are correlation scales in principal directions).

The separation at which the correlation decreases from σ^2 to (σ^2/e) is λ (Figure 2.3). It is, physically, the scale at which two measurements of the variable become practically uncorrelated (Kitanidis, 1997). In other words it is the limit of spatial dependence and starting from that distance, measurements become spatially independent (Webster and Oliver, 2007). Aquifer properties are said to be statistically isotropic if the λ s are the same in different directions and statistically anisotropic if directional λ s are different.

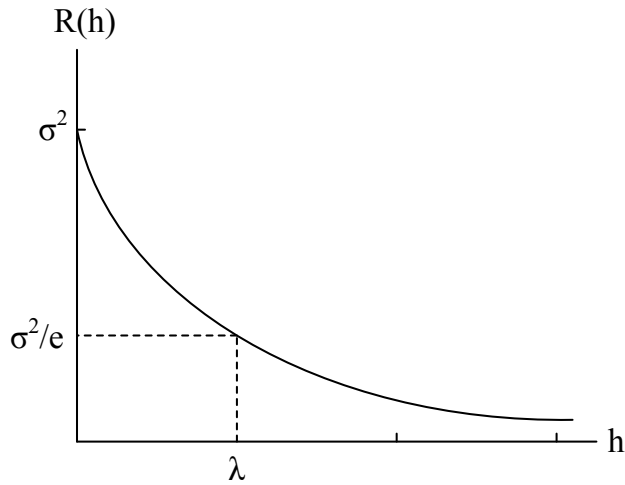


Figure 2.3. The negative exponential covariance function from Equation 2.8 (adapted from Gelhar (1993))

2.4. Geostatistical Characteristics of Physically and Chemically Heterogeneous Aquifers

Spatial variations in aquifer physical and chemical properties, has known to have strong influences on groundwater flow and transport since movement and dispersion of the solutes are controlled by the heterogeneity of these properties (Zinn and Harvey, 2003; Dynamac Corporation, 1998; Cvetkovic and Shapiro, 1990; Hu et al., 2004; Mishra et al., 1999; Mishra and Gutjahr, 1999). Therefore, information about subsurface variations of aquifer properties is critical for a successful prediction of contaminant transport. In addition, remediation method selection and implementation for contaminated aquifers require knowledge of spatial heterogeneity of aquifer properties affecting groundwater flow and contaminant transport.

The spatial variability of K has been investigated at the field scale in a number of studies in literature. A short summary composed of several different field sites from different parts of the world is given in Table 2.4. K statistics from other field sites are summarized by Gelhar (1993). In Table 2.4, the range of $\sigma^2_{\ln K}$ is 0.14 to 12.25 showing that the degree of variation in K can be expressed by several orders of magnitude in the field. In the study of Welhan and Reed (1997), K range spans even six orders of magnitude. On the other hand, $\lambda_{\ln K}$ ranges from 1 m to 55 m in Table 2.4. All these studies have shown that, in reality, aquifers can be highly heterogeneous in K which is one of the critical parameters for the flow of groundwater and the transport of contaminants. Some of these studies also have shown that aquifers can either be statistically isotropic or anisotropic in nature. For example, Sudicky (1986), Hess et al. (1992), Thompson (1990) and Byers and Stephens (1983) reported the Borden, Cape Cod, Lawrence Livermore National Lab (LLNL) and Sevilleta Wildlife Refuge aquifers, respectively, as isotropic. On the other hand, Snake River Plain (Welhan and Reed, 1997), Borden (Woodbury

Table 2.4. Summary of the field scale studies investigating spatial variability of K in terms of mean of $\ln K$, $\sigma^2_{\ln K}$ and $\lambda_{\ln K}$

Site	Mean of $\ln K$	$\sigma^2_{\ln K}$	$\lambda_{\ln K}$ (m)	Unit of K	Reference
Borden, Ontario, Canada	-4.94	0.38	2.8	cm/s	Sudicky, 1986
Borden, Ontario, Canada	-4.68	0.356	5.14, 8.33	cm/s	Woodbury and Sudicky, 1991
Borden, Ontario, Canada	-4.96	0.585	4.8	cm/s	Turcke and Kueper, 1996
Twin Lake, Ontario, Canada	-3.86	0.23	1.5	cm/s	Indelman et al., 1999
Cape Cod, Flowmeter	-2.21	0.24	3.5, 8	cm/s	Hess et al., 1992
MA, USA Permeameter	-3.35	0.14	2.9, 4.2	cm/s	
Cape Cod, MA, USA	-2.18	0.28	8.08	cm/s	Eggleson et al., 1996
Cape Cod, MA, USA	-2.57	0.061	1.0	cm/s	Foster-Reid, 1994
Columbus AFB, MS, USA	-5.23	4.5	12.8	cm/s	Rehfeldt et al., 1992
Columbus AFB, MS, USA	-8.02	0.893	-	m/s	MacIntyre et al., 1998
Columbus AFB, MS, USA	-	4.5, 2.8	12, 5.3	cm/s	Boggs and Rehfeldt, 1990; Boggs et al., 1990
Columbus AFB, MS, USA	-5.4	4.4	12.5	cm/s	Eggleson, 1997
LLNL site, CA, USA	0.20	3.24	55	m/d	Tompson, 1990
Snake River Plain, ID, USA	4.1	12.25	-	m/d	Welhan and Reed, 1997
Sevilleta Wildlife Refuge, NM, USA	-4.275	0.534	1.5	cm/s	Byers and Stephens, 1983
Vejen aquifer, Denmark	-7.59	0.37	1, 2.5	m/s	Bjerg et al., 1992
Horkheimer Insel, Germany	-7.33	2.34	-	m/s	Ptak and Teutsch, 1994; Zlotnik et al., 2001
Krauthausen, Germany	-6.65	1.3	6.66	m/s	Vereecken et al., 2000

and Sudicky, 1991) and Schoolcraft (Biteman, 2002) aquifers were found to be anisotropic with the λ_x/λ_y ratios of 4, 1.6, and 2.6, respectively. For an aquifer in Schoolcraft, Hyndman et al. (2000) reported λ_x/λ_y ratio of 3.5. In majority of the field scale studies, K has been found to be log-normally distributed (Byers and Stephens, 1983; MacIntyre et al., 1998; Rehfeldt et al., 1992; Sudicky, 1986; Turcke and Kueper, 1996; Hess et al., 1992; Bjerg et al., 1992; Tompson, 1990) although there are a few exceptions (Eggleston et al., 1996; Woodbury and Sudicky, 1991; Pfleiderer and Moltyaner, 1993; Robin et al., 1991). Indeed, K following a log-normal distribution is a common assumption in stochastic groundwater analysis (Tompson, 1993; Destouni and Cvetkovic, 1991; Brusseau and Srivastava, 1997; Bosma et al., 1993; Rabideau and Miller, 1994; Abulaban and Nieber, 2000). In addition, the most frequently used covariance function to determine λ is the negative exponential covariance function (Eggleston et al., 1996; Eggleston, 1997; Woodbury and Sudicky, 1991; Pfleiderer and Moltyaner, 1993; Byers and Stephens, 1983; Rehfeldt et al., 1992; Sudicky, 1986; Hess et al., 1992; Bjerg et al., 1992).

Besides physical heterogeneity, heterogeneity of the chemical properties of soil has also a major impact on the transport of reactive solutes. The number of field scale studies about the determination of chemical heterogeneity in terms of K_d is very limited (Robin et al., 1991; Allen-King et al., 1998; Mackay et al., 1986; MacIntyre et al., 1991, 1998; Foster-Reid, 1994). Robin et al. (1991) measured K_d for strontium at Borden aquifer and found the contrast between the highest and the lowest K_d as almost sevenfold and the mean and $\sigma^2_{\ln K_d}$ as 2.25 and 0.072 (as mL/g), respectively. $\lambda_{\ln K_d}$ was estimated to be 0.3-2 m. At the same site, Mackay et al. (1986) measured the K_d of PCE ranging over an order of magnitude. Allen-King et al. (1998) found the mean of $\ln K_d$ and $\sigma^2_{\ln K_d}$ for PCE as -0.54 and 0.39 (as mL/g) for a single core taken from the Borden aquifer. Eight years later, Allen-King et al. (2006) analyzed 11 cores from the Borden aquifer and found the mean of $\ln K_d$ and $\sigma^2_{\ln K_d}$ for PCE as -1.05 and 0.37 (as mL/g). Zhao et al. (2005)

measured K_d values for PCE in 216 different samples taken from a contaminated aquifer near Schoolcraft, MI. They found the horizontal and vertical $\lambda_{\log K_d}$ as 18.9 m and 2.5 m, respectively. Hoffman (1995) analyzed 132 K_d data for PCE from LLNL site and found the average K_d value as 0.44 mL/g with σ of 0.62. Another study conducted at the Columbus Air Force Base aquifer by MacIntyre et al. (1991) revealed an order of magnitude variation in K_d of naphthalene. Seven years later, at the same site, MacIntyre et al. (1998) found that the mean of $\ln K_d$ and $\sigma^2_{\ln K_d}$ of naphthalene were -1.618 and 0.466 (as L/kg), respectively. Foster-Reid (1994) determined the mean of $\ln K_d$ (as l/mg) of benzene, TCB (trichlorobenzene) and PentCB (pentachlorobenzene) by analyzing 73 soil samples taken from the Handy Cranberry Bog on Cape Cod, MA as -4.205, -1.003 and 0.849, respectively. $\sigma^2_{\ln K_d}$ of benzene, TCB and PentCB was found as 0.1386 while $\lambda_{\ln K_d}$ was 1 m. Among this small number of studies, Robin et al. (1991) and Allen-King et al. (1998, 2006) observed that K_d showed neither normal nor log-normal distributions at Borden site. On the other hand, MacIntyre et al. (1998), Hoffman (1995), Foster-Reid (1994) and Painter et al. (2001) have found log-normally distributed K_d at Columbus Air Force Base, LLNL, Cape Cod and Yucca Mountain site, respectively. Zhao et al. (2005) also used log-normal distribution to describe the K_d distribution at Schoolcraft site. Although it is not possible to make a general log-normal distribution assumption based on field scale studies, similar to K , K_d is almost always assumed to be log-normally distributed in modeling studies (Bosma et al., 1993; Tompson, 1993; Cvetkovic et al., 1998; Rabideau and Miller, 1994).

Another parameter to represent the chemical heterogeneity is α . Unfortunately, there is no field scale study giving the spatial correlation structure of α in the literature. However, it is clear that α is a spatially distributed parameter since the properties controlling the rate of mass transfer include the types of minerals and their spatial distribution, the types and amounts of natural organic matter, the volume, size and geometry of macropores, mesopores, and micropores within

grains and aggregates; the geometry, chemistry and mineralogy of coatings on the surfaces (Hollenbeck et al., 1999; Li and Brusseau, 2000).

2.5. Correlation between Physical and Chemical Aquifer Properties

In addition to the spatial variability of parameters such as K , K_d and α , the correlation between any two of these parameters might affect the transport of a solute in the subsurface. For example, the numerical simulation studies have shown that not only the individual variability of K and K_d , but also the correlation between these two key parameters is an important factor for the transport of a solute (Garabedian, 1987; Burr et al., 1994; Bellin and Rinaldo, 1995; Bosma et al., 1993; Rabideau and Miller, 1994). In several field scale studies, negative correlation between K and K_d was found (Robin et al., 1991; Thompson, 1993; Hess et al., 1993; Foster-Reid, 1994; Barber et al., 1992) and this was attributed to the presumption of greater sorption by smaller particles. On the other hand, some researchers found positive correlation between K and K_d (MacIntyre et al., 1998; Allen-King et al., 1998, 2006; Hess et al., 2002). This was thought to be the result of the high organic carbon content of coarse sediments (Ball and Roberts, 1991) or remained unexplained (MacIntyre et al., 1998). There are also field scale studies reporting K and K_d as uncorrelated with each other (Zhao et al., 2005). In other words, there is no consensus about the type of correlation between K and K_d . Therefore, different correlation types have been assumed in many numerical simulation studies (Thompson, 1993; Bosma et al., 1993; Burr et al., 1994; Thompson et al., 1998; Brusseau and Srivastava, 1999; Cvetkovic et al., 1998).

Tompson (1993) reported negative correlation between K and K_d of PCE based on the preliminary field observations conducted on mixed sands, silts and clays in the alluvial materials of the eastern Livermore Valley of California by Bishop et al. (1990). In the study of Thompson (1993), the equation relating K and K_d has been given as follows.

$$\ln K_d = 1.02 - 0.32 \ln K \quad (2.9)$$

Similarly, in a field study at Cape Cod, MA, Foster-Reid (1994) has shown that there is a significant negative correlation between K and K_d with a slope of -0.341 for benzene, TCB and PentCB. Hess et al. (1993) have found negative correlation between K and K_d of lead as well as K_d of zinc. Robin et al. (1991) have observed negative correlation between K and K_d of strontium.

In contrast to studies reported negative correlation, Allen-King et al. (1998) observed positive correlation between K and K_d of PCE on the aquifer materials taken from Borden aquifer and has expressed the relation with the following equation.

$$\ln K_d = 2.14 + 0.53 \ln K \quad (2.10)$$

MacIntyre et al. (1998) have found positive correlation between K and K_d of naphthalene at Columbus Air Force Base site. In a reactive tracer test conducted at Cape Cod, MA, Hess et al. (2002) have observed a positive correlation between K and K_d for nickel.

In addition to correlation between K and K_d , the type and the degree of correlation between α and K_d has been investigated in several different studies using different types of contaminants and soils. Brusseau and Rao (1989b) compiled data on the nonequilibrium sorption of hydrophobic and nonhydrophobic organic chemicals, separately, from the literature. An inverse log-log linear relationship between K_d (mL/g) and α (h^{-1}) has been found for both types of chemicals. The equation relating $\log \alpha$ and $\log K_d$ for hydrophobic organic chemicals was

$$\log \alpha = 0.301 - 0.668 \log K_d \quad (2.11)$$

Brusseau et al. (1991a) investigated the transport of 12 organic chemicals, including PCE, with three aquifer materials having low organic carbon content ($f_{oc} = 0.007, 0.015$ and 0.025%) by column experiments. According to their findings, there was a log-log linear inverse relationship between α (h^{-1}) and K_d (mL/g) such that

$$\log \alpha = -1.676 - 0.7 \log K_d \quad (2.12)$$

Brusseau and Reid (1991) made column experiments using five different low organic carbon aquifer materials ($f_{oc} < 0.05\%$) and four different organic chemicals, including PCE. They have found the inverse relationship between α (h^{-1}) and K_d (mL/g). When least-squares regression analysis was applied to the data reported in this study, the following equation has been found.

$$\log \alpha = 0.473 - 0.504 \log K_d \quad (2.13)$$

Brusseau and Rao (1991) conducted column experiments with 26 different organic chemicals, including PCE, and a sandy aquifer material with a moderately low organic carbon content ($f_{oc} = 0.13\%$). The equation reported for the group of chemicals, in which PCE was present, was

$$\log \alpha = 0.56 - 0.47 \log K_d \quad (2.14)$$

$\log \alpha - \log K_d$ relationship reported by Brusseau et al. (1991b) for a series of chlorinated benzenes and a sandy soil with 0.39% organic carbon content was

$$\log \alpha = 0.75 - 0.63 \log K_d \quad (2.15)$$

This inverse log-log linear relationship has also been found in some other studies (Brusseau, 1992b; Nkedi-Kizza et al., 1989; Piatt, 1997; Brusseau et al., 1990; Hu

et al., 1995a) and has successfully been used to predict the α values using the K_d values (Brusseau, 1992c; Brusseau et al., 1989).

It is believed that some type of diffusion limited mechanism (i.e. diffusional rate-limited transfer of the sorbate mass from the exterior surface of the organic matter into the interior matrix) is responsible for the nonequilibrium sorption of organic solutes. An increase in diffusional constraint is expected with the increasing molecular size of the sorbate. The inverse relationship between α and K_d was suggested to be the result of this diffusive mass transfer where former represents the degree of diffusional constraint and the latter is related with the molecular size of the sorbate (i.e. K_d increases in relation with the increase in K_{oc} when molecular size of the sorbate increases (Piwoni and Keeley, 1990)) (Brusseau and Rao, 1989a, b; Brusseau et al., 1991a, b).

2.6. Impact of K Heterogeneity on Contaminant Transport and the Performance of Pump and Treat Remediation

Impact of physical heterogeneity on contaminant transport and groundwater remediation has been an interest of researchers for a long time. In this section of the study, a review of these studies is presented by giving an emphasis on K heterogeneities. The study of Dekker and Abriola (2000) is an example showing the effect of physical aquifer heterogeneity on contaminant transport. They considered the influence of permeability heterogeneity on the migration and entrapment of the dense nonaqueous phase liquids (DNAPLs) by employing model simulations on multiple realizations of permeability fields having different $\sigma_{\ln K}^2$ and $\lambda_{\ln K}$. Higher $\sigma_{\ln K}^2$ resulted in an obvious increase in lateral spreading of PCE with higher saturation regions at the interfaces between high and low permeability regions and a decrease in penetration depth of spill. Higher $\sigma_{\ln K}^2$ also caused an increased variability among the model outputs. Penetration depth of the spill increased but the spread of the spill decreased with increasing vertical $\lambda_{\ln K}$,

especially for more heterogeneous formation. On the other hand, spreading and the penetration depth of the spill were relatively insensitive to the horizontal $\lambda_{\ln K}$ examined in the study. This was attributed to the small spill release area relative to the horizontal $\lambda_{\ln K}$.

Effect of physical heterogeneity on the different aspects of P&T remediation, such as design, costs and cleanup time has been studied by several researchers. Some of these researchers employed pumping only for hydraulic containment while some others considered P&T systems to clean up the contaminated aquifer. Zheng and Wang (1999) integrated heterogeneous transmissivity (T) into the P&T remediation design through Monte Carlo analysis in a simulation-optimization study. The aim of the remediation system design was to hydraulically contain the contaminant plume. Therefore, system constraints did not include any term related to contaminant concentration. The results showed that both the total remediation costs and the uncertainty in it (i.e. ratio of standard deviation over mean of remediation cost) increased with the uncertainty in the K-field. Morgan et al. (1993) aimed to minimize the total pumping rate in order to provide hydraulic containment of a contaminant plume. Results showed that as the fields became more heterogeneous, the total pumping rate increased for the same degree of solution reliability. Similar to Morgan et al. (1993), Ricciardi et al. (2007) minimized the cost of P&T remediation in order to assure hydraulic plume containment by optimizing the pumping rate. Their results were in agreement with the results of Morgan et al. (1993) such that pumping rates were higher when $\sigma^2_{\ln K}$ was greater. They also found that the cost of the optimal solution decreased with the decreasing $\sigma^2_{\ln K}$. Bayer et al. (2004) aimed to find the efficiency of a P&T remediation system under different heterogeneity conditions. Efficiency was determined in terms of the minimum pumping rate of a single well at a fixed location which supplied hydraulic containment of a contaminant plume. As a result, they did not consider the amount of removed contaminant. The different heterogeneity characteristics were defined with different $\sigma^2_{\ln T}$ and $\lambda_{\ln T}$. Results

showed that increasing $\sigma_{\ln T}^2$ and $\lambda_{\ln T}$ led to a considerable rise of the mean pumping rate. On the other hand, the increase in $\sigma_{\ln T}^2$ and $\lambda_{\ln T}$ also resulted in a variation in the pumping rate σ^2 (i.e. σ^2 of pumping rate among 500 $\ln T$ realizations). The magnitude of this rise was higher for the higher values of $\sigma_{\ln T}^2$ and $\lambda_{\ln T}$. The assessment in the study of Bayer et al. (2004) did not focus on the extent of mass removal. The authors noted that the efficiency of the remediation system in terms of mass removal would probably be different than the efficiency in terms of the minimum pumping rate.

McKinney and Lin (1996) used simulation-optimization approach in order to investigate the effect of K heterogeneity on the cost of P&T remediation system. They considered the reduction of the contaminant concentration to a certain level at the observation points. The results indicated that heterogeneity of K did not have a significant impact on the remediation system cost and the number of wells for the problem studied. However, it did affect the remediation system design such that well locations and pumping rates were different for homogeneous and two different heterogeneous cases. Huang and Mayer (1997) applied simulation-optimization approach to search for the optimal pumping rates and the well locations for a P&T system on both homogenous and heterogeneous aquifers. The remediation goal was to reduce the aqueous phase contaminant concentration to a certain level at monitoring points within a certain remediation period. They found that the optimal locations of the wells were different for homogenous and heterogeneous aquifers. In a heterogeneous aquifer, optimal wells were located in high permeability zones, which reduced the total remediation cost because of the decrease in pumping cost. They also found that the heterogeneous aquifer condition required an additional pumping well as well as the higher remediation cost compared to the homogenous conditions. Aksoy and Culver (2004) examined the impact of K heterogeneity on optimal P&T remediation design and cost and demonstrated that the remediation cost generally increased as the K heterogeneity increased. They also added that the variability in the remediation costs increased

with increasing K heterogeneity. The number of pumping wells and the pumping rates changed when the degree of heterogeneity changed as well. Chan Hilton and Culver (2005) conducted a simulation-optimization study on a hypothetical heterogeneous aquifer having a single heterogeneous K-field with two different σ^2 in K. For this single K-field case, they found that more pumping wells were required and higher volume of water was pumped out resulting in higher remediation cost for the more heterogeneous K-field. Pinder et al. (2004) applied simulation-optimization approach to find the optimum pumping schedules on homogeneous and heterogeneous aquifers in K. They found that heterogeneous aquifer required more pumping than the homogeneous one. When they applied the pumping schedule obtained using the homogeneity assumption to different heterogeneous fields, they found that the remediation goal was exceeded at 80% of the heterogeneous fields. Then they created another heterogeneous field by averaging all of the heterogeneous fields tested. Then, they found the optimal pumping policy for this field and applied it to individual heterogeneous fields. In this case, the remediation goal was exceeded at 64% of the fields.

Russell and Rabideau (2000) applied decision analysis in order to investigate the effect of K heterogeneity on the failure probability of different P&T remediation system designs which were developed based on the assumption of homogeneity. In the study two failure definitions were used: failure in the hydraulic containment of the contaminant plume and failure in compliance monitoring. $\sigma^2_{\ln K}$ was the only parameter defining K heterogeneity. Results showed that inclusion of K heterogeneity caused high failure probabilities especially for the more heterogeneous aquifer. For heterogeneous aquifers, the escape of contaminant via preferential flow paths and local drawdown failure was noted. It was also noted that for a less heterogeneous aquifer, the probability of failure in compliance monitoring was higher than the probability of failure in the hydraulic containment. On the other hand, for more heterogeneous aquifer, the probability of failure in the hydraulic containment was higher. In the same study, the effect of heterogeneity

on cleanup times was also investigated. For most of the P&T designs, the cleanup time required for the more heterogeneous aquifer was higher but the opposite was also observed. Therefore, the impact was not consistent among all designs. Lee et al. (2000) applied modeling approach to compare a design of a P&T remediation system on a homogenous and two different heterogeneous aquifers in terms of time required for contaminant cleanup. One of the heterogeneous aquifers contained an embedded clay lens within the unconsolidated sand. The second one was a stratified system consisting of two layers of unconsolidated sand and silt. A single well located near the center of the plume was used to cleanup the aquifer. The results showed that cleanup of the aquifer containing a small clay lens was longer than the homogenous aquifer while the most adverse impact of heterogeneity on remediation time was observed on the two-layer system. Rabideau and Miller (1994) modeled P&T remediation in a vertically heterogeneous aquifer. They found that cleanup times were highly sensitive to the degree of K heterogeneity and observed to increase as the degree of heterogeneity increased. Berglund and Cvetkovic (1995) assessed the effect of K heterogeneity on cleanup times under rate-limited mass transfer conditions. Although their results showed a general trend of increasing cleanup times with increasing σ^2 in K, the magnitude of this effect was found to be small under the conditions assumed in the study. Cleanup time converged to a limit value as the pumping rate increased. This limit value was determined by the rate-limited mass transfer. This indicated that for low pumping rates, K heterogeneity was the controlling factor on the remediation process while for large pumping rates mass transfer process took the control.

James and Gorelick (1994) made an analysis in order to find the number of sampling wells to minimize the P&T remediation cost (including both remediation and sampling cost) of contaminated aquifer where the plume location and extent were uncertain due to the unknown source location, source loading time and aquifer heterogeneity. The optimum number of sampling wells increased with the

increase of $\sigma_{\log K}^2$. Because the travel range of plume and its extent increased with the increase of $\sigma_{\log K}^2$, the optimum total cost increased. However, this increase was mainly due to the increase in the number of sampling wells and remediation cost remained relatively constant in the $\sigma_{\log K}^2$ range of 0.1 to 3. They added that the change in the cost was due to uncertainty in the plume location. Similar to $\sigma_{\log K}^2$, the number of sampling wells increased with the increase in λ of the spatially distributed K in the range of Δx to $3\Delta x$. The cost of the remediation also rose with the rise of λ in the same range because of the higher cost of sampling. For λ range of $3\Delta x$ to $9\Delta x$, the optimum sampling and remediation design was relatively insensitive.

Maxwell et al. (2008) performed a risk assessment study in order to investigate the effect of application of a P&T remediation system on the exposure of the individuals to PCE on a heterogeneous aquifer that is used as a municipal water source. They used seven different realizations of K in order to represent the heterogeneous nature of the aquifer. The average concentration obtained in the municipal wells with the application of P&T system changed from realization to realization. For some realizations, using P&T decreased the concentration in the municipal wells while it increased the concentration for some others. This was because of the presence of hydraulic channels connecting the contaminant source with the wells at different locations for different realizations. This study emphasized the importance of the role of uncertainty in aquifer heterogeneity on groundwater flow and transport as well as the remediation of contaminated aquifers. Mylopoulos et al. (1999) performed a simulation-optimization study for a P&T remediation system on a real aquifer which was heterogeneous in terms of K. Because of the high degree of hydrogeologic uncertainty, they applied stochastic simulation through Monte Carlo technique (200 realizations). System constraints did not include any term related to the contaminant concentration. The results showed the spatial distribution of K-field, in other words the relative locations of

high and low K regions, had a significant impact on the pumping rates and operating cost of cleanup wells.

Although there are studies investigating the effect of K heterogeneity on the optimal P&T remediation design and costs in literature, none of the studies mentioned above focused on the systematic analysis of the impact of λ of K . This study did not only focus on the effect of λ of K on the P&T remediation design and cost but also on the impact of λ of K on the remediation time. For time-to-compliance analysis, the effect of number of wells used for the remediation was investigated in addition to the effect of λ . A comparison of two different P&T remediation designs was made in order to find a more robust design approach when heterogeneity was present. For both remediation designs and associated cost and time analyses, importance of spatial distribution of K was explored by working on three different realizations of K . This study also considered the influence of different initial plume masses and configurations on the remediation design and cost. Therefore, validity of the results for different initial plume conditions was evaluated. Furthermore, the effect of anisotropy in λ of K on the P&T remediation design and cost was analyzed.

2.7. Impact of K_d Heterogeneity on Contaminant Transport and the Performance of Pump and Treat Remediation

Heterogeneity in K_d and its correlation with other aquifer properties, such as K , is another important issue in the contaminant transport and groundwater remediation studies. Hu et al. (2004) investigated the effect of heterogeneity of K and K_d on solute transport process. They found that under natural flow conditions, solute dispersion increased with the increase in σ^2 in both K and K_d and the effect of σ^2 in K_d was more obvious than that in K . They also studied the influence of λ of K and K_d . Their results showed that solute dispersion decreased with the decrease in λ of both K and K_d . Bosma et al. (1993) conducted numerical Monte Carlo simulations

to investigate transport of adsorbing solute in a porous media which was heterogeneous in terms of K and K_d . They studied the effect of $\sigma^2_{\ln K}$, $\sigma^2_{\ln K_d}$ and $\lambda_{\ln K_d}$ on solute spreading. They found that decrease in $\lambda_{\ln K_d}$, while keeping $\lambda_{\ln K}$ constant, diminished the plume spreading in the longitudinal direction. Accordingly, an increase in $\lambda_{\ln K_d}$ enhanced the longitudinal spreading. They explained this situation with the larger distance between low and high K_d regions with increasing $\lambda_{\ln K_d}$. Transverse spreading was not affected by the change in $\lambda_{\ln K_d}$. They observed significant enlargement of the plume in the longitudinal direction with a relatively mild increase in $\sigma^2_{\ln K_d}$. On the other hand, transverse spreading was, once again, found to be independent from the chemical heterogeneity. They also observed enhanced longitudinal spreading with larger $\sigma^2_{\ln K}$. Unlike K_d case, increase in $\sigma^2_{\ln K}$ increased the transverse spreading. Bosma et al. (1993) also assessed the effect of correlation between K and K_d assuming both negative and positive correlations in addition to the uncorrelated case. They found that plume spreading in the longitudinal direction was enhanced in the case of negative correlation compared to the uncorrelated case as can be expected from the theory. Because the high K s combined with low sorption and low K s combined with high sorption resulted in large solute spreading. On the other hand, longitudinal plume spreading was smaller for the positively correlated case compared to the uncorrelated case. They also revealed that the magnitude of the effect of correlation between K and K_d on longitudinal spreading was different for different geometric means of K_d . Their results on plume spreading in the transverse direction showed that correlation between K and K_d did not have an effect on it. Findings of Hu et al. (1995b) was similar to that of Bosma et al. (1993) when the effect of correlation between K and K_d on longitudinal plume spreading was considered. However for transverse spreading, unlike Bosma et al. (1993), Hu et al. (1995b) found that positive correlation decreased the spreading while negative correlation enhanced it. Cvetkovic and Shapiro (1990) performed a stochastic solute arrival time analysis on a sorptive solute on heterogeneous porous media. For the equilibrium sorption assumption, they assumed constant K_d as well as

heterogeneous K_d which was uncorrelated and negatively correlated with K . The results showed that heterogeneity in K_d caused notably longer mass arrival time and this effect was greater when K and K_d were negatively correlated compared to the case where K and K_d were uncorrelated. They also pointed out that the effect of K_d heterogeneity was less pronounced for smaller σ^2 s.

Above studies focused on the impact of K and K_d heterogeneity on plume migration under natural flow conditions. Aksoy and Culver (2004) investigated the effect of K_d heterogeneity, in combination with K heterogeneity, on optimal P&T remediation design and costs. They found that lower K_d heterogeneity ($\sigma^2_{\ln K_d} = 0.007$) resulted in similar remediation costs with the homogenous K_d assumption but higher K_d heterogeneity ($\sigma^2_{\ln K_d} = 0.177$) caused significant increase in the remediation cost up to 50%. They also added that increasing K heterogeneity may have decreased the impact of K_d heterogeneity. Rabideau and Miller (1994) made simulations for fields having heterogeneous characteristics in both K and K_d in the vertical direction. First, $\sigma^2_{\ln K_d}$ was the same with $\sigma^2_{\ln K}$ and there was no correlation between K and K_d . For this case, they found no significant difference in P&T performance in terms of cleanup time. The simulations performed with correlated $\ln K$ and $\ln K_d$ fields showed that a perfect positive correlation between $\ln K_d$ and $\ln K$ resulted in considerably shorter cleanup times while a perfect negative correlation significantly increased it. This was because the negative correlation resulted in the presence of a higher fraction of sorbed contaminant mass in the low conductivity regions where the groundwater flow was slow. They also stated that since the type of correlation had a significant impact on P&T remediation performance, serious consideration of spatial structure of sorption capacity was necessary for the sites where P&T remediation was planned to be implemented.

Schäfer and Kinzelbach (1992) investigated the effect of heterogeneity in K and K_d on the performance of in-situ bioremediation, which was composed of one injection and one pumping well, by Monte Carlo analysis. The performance of the

remediation was measured by the time to achieve 90% pollutant removal (RMT_{90}) and compared with the homogeneous case. Four different heterogeneity conditions were tested. The first one was the heterogeneity in both K and K_d with a high σ and long λ . In the second condition, both K and K_d were heterogeneous with low σ in order to test the effect of σ in these parameters. For the third condition, K_d was assumed as homogenous while K was heterogeneous with high σ . The fourth, and the last, condition was to show the sensitivity of the results to λ such that λ of both K and K_d was decreased by half while σ remained as high. They measured the relative dominance of the pollutant removal by biodegradation and extraction and found 80% removal by biodegradation and 20% removal by extraction. Aquifer heterogeneity in all of the four cases decreased the microbial activity and resulted in prolonged RMT_{90} compared to the homogeneous case. An increase in $\sigma_{\ln K}$ and $\sigma_{\ln K_d}$ (comparison of first and the second condition) had a significant effect on RMT_{90} as remediation with very long durations became more probable. RMT_{90} increased with $\sigma_{\ln K}$ and $\sigma_{\ln K_d}$ exponentially. Assuming K_d heterogeneity instead of homogeneity (comparison of the first and the third condition) had also a clear unfavorable effect on RMT_{90} . When K and K_d were assumed to be negatively correlated, further deterioration of the remediation performance was observed by a considerable increase in RMT_{90} compared to the uncorrelated case. Shorter λ led to a shorter RMT_{90} but the effect was not as noticeable as the effects of σ and the presence of K_d heterogeneity. This result was attributed to the increased probability of channeling with large K which connected the injection and pumping wells when λ was longer. When there was such a short-circuiting, DO distribution in the aquifer was not favorable for an efficient remediation and most of the injected DO was extracted without reaching to some polluted regions of the aquifer.

Up to now, there is a single study in literature (Aksoy and Culver, 2004) investigating the effect of K_d heterogeneity on P&T remediation design and associated costs. However, they did not consider the impact of λ of K_d . In addition,

they studied on just a single K realization as a background K heterogeneity condition. However, changing K distribution, when K_d is heterogeneous, might be important for the understanding of the relative importance of K and K_d heterogeneities and may have significant impact on the remediation design and cost. This study also considered the effect of correlation between K and K_d on the remediation. Rabideau and Miller (1994) made a similar study but considering only the vertical heterogeneity and its impact on cleanup time. Schäfer and Kinzelbach (1992) studied the effect of $\lambda_{\ln K}$ and $\lambda_{\ln K_d}$ together on the cleanup time of an in-situ bioremediation system. Their analysis was basically about the performance of in-situ bioremediation system based on the remediation time. They only considered negative correlation but not positive correlation between K and K_d . Moreover, they applied Monte Carlo analysis and did not investigate the impact of realizations itself on the results. Therefore, this study is the first one investigating the impact of λ of K_d for different degrees of heterogeneity conditions together with different K realizations on optimal P&T remediation design and cost. In addition, the study is novel in terms of studying the effect of both positive and negative correlation between K and K_d in horizontal scale on optimal P&T remediation design and cost.

2.8. Impact of Rate-limited Mass Transfer and the Heterogeneity in Mass Transfer Rate Coefficient on Contaminant Transport and the Performance of Pump and Treat Remediation

The effect of rate-limited mass transfer or nonequilibrium sorption and the heterogeneity in mass transfer rate coefficient on contaminant transport and groundwater remediation is the last issue reviewed. Studies in the literature have shown that neglecting rate-limited mass transfer or nonequilibrium sorption may cause erroneous results in both solute transport and remediation design. For example, Zhang and Brusseau (1999) simulated the TCE plume behavior subjected to P&T remediation in Tucson, AZ. When equilibrium sorption was assumed, it

was seen that the simulation results did not match the observed data. When nonequilibrium sorption defined by the two-site model was taken into account, a slightly improved match was obtained, at least for a certain part of the remediation period. Therefore, nonequilibrium sorption affected the TCE transport. Andersson and Destouni (2001) conducted a risk-cost analysis in groundwater transport and found that ambiguous risk and cost estimates may have been obtained if kinetic sorption (described by the first-order nonequilibrium sorption desorption process) was disregarded and only equilibrium sorption was assumed. Their results also showed that estimation errors in risk and cost may have even been higher when sorption was completely ignored. Aksoy and Culver (2000) investigated the effect of sorption assumptions on P&T remediation design and cost. They showed that the optimal design found with the use of equilibrium sorption assumption may not satisfy the remediation goals in a mass transfer limited aquifers in the same remediation period. On the other hand, in literature, there are also examples which shows that inclusion of nonequilibrium sorption do not provide improvement in the prediction of solute behavior. Brusseau and Srivastava (1997) studied the impact of rate-limited sorption on PCE plume displacement in Borden aquifer under natural flow conditions. When homogeneous K was assumed, rate-limited sorption and local scale heterogeneity/mass transfer had a minimal impact on plume displacement. Both equilibrium and rate-limited sorption simulations did not match the observed data. When K and K_d heterogeneities were taken into account, for both equilibrium and rate-limited sorption cases, it was seen that heterogeneity in K and K_d , which were negatively correlated, did not improve the match between the simulated and the observed data for the center of plume mass displacement, either.

In addition to consideration of rate-limited mass transfer, the value of mass transfer coefficient may be important in terms of both solute transport and remediation design and has been studied by some researchers. For example, Berglund (1997) investigated the effect of rate-limited mass transfer (described by

a linear expression) from the DNAPL phase to the aqueous phase within an analytical framework on DNAPL transport in heterogeneous aquifers. The breakthrough curves obtained with different mass transfer rate coefficients showed that lower mass transfer rate coefficients resulted in enhanced tailing. Breakthrough curve changed its character from simulating the equilibrium conditions to rate-limited mass transfer conditions over a relatively small interval of mass transfer rate coefficient. This showed that concentration change over time was highly sensitive to this parameter. When the same analysis was performed on an aquifer with higher degree of K heterogeneity, it was seen that an increase in $\sigma^2_{\ln K}$ led to enhanced tailing for all mass transfer rate coefficients. The effect of $\sigma^2_{\ln K}$ on the later stages of breakthrough became more pronounced with the increasing mass transfer rate coefficient. Therefore, increase in the degree of K heterogeneity and advection related tailing decreased the sensitivity of DNAPL transport to mass transfer rate coefficient at the later stages of breakthrough.

Berglund and Cvetkovic (1995) studied the effect of rate-limited mass transfer (described by a first-order linear expression) on P&T remediation time. They stated that cleanup times were significantly longer for mass transfer rate-limited case compared to the nonreactive case. When the mass transfer was taken into account, only a small decrease in cleanup times with increasing pumping rate was observed. Unlikely, for the nonreactive case the cleanup times gradually declined with the increasing pumping rate. For the mass transfer limited case, the cleanup time increased as the rate coefficient decreased such that for very small rate coefficients the cleanup time was significantly long. In addition, as the mass transfer became slower, the sensitivity of the cleanup time to the pumping rate became less. In another study presented by Brogan and Gailey (1995) very similar findings with the study of Berglund and Cvetkovic (1995) were obtained. Brogan and Gailey (1995) found that there was a significant influence of the nonequilibrium solute transport (described by reversible first-order expression) on the cleanup time and cleanup time increased with the decreasing mass transfer rate

coefficient. They also showed less sensitive cleanup time to pumping rate for slow mass transfer conditions. In their study, Aksoy and Culver (2000) showed that P&T remediation time exponentially increased while mass transfer rate decreased and the heterogeneity in K resulted in a reduction in the magnitude of the effect of mass transfer. Rabideau and Miller (1994) modeled P&T remediation in a vertically heterogeneous aquifer assuming nonequilibrium sorption conditions. They found that slow mass transfer rates dramatically increased the projected cleanup time and the cleanup time got longer as the rate of mass transfer got slower. The relative significance of the mass transfer rate effect was slightly decreased as the degree of heterogeneity in K increased. On the other hand, the relative significance of sorption nonequilibrium and K heterogeneity depended on the values of the parameters defining these processes. Either of them may dominate over the other depending on the values of these parameters in elongating the cleanup times. Harvey et al. (1994) compared slow and rapid mass transfer (described by a first-order model) for the performance evaluation of P&T remediation with pulsed pumping. They found that rapid mass transfer rates resulted in much shorter remediation time whereas for slow mass transfer rates remediation time was very long. In addition, they pointed out that for rapid mass transfer, equilibrium was reached just at the beginning of the resting periods while for slow mass transfer, concentration came to only 18% of equilibrium during the resting periods. Pumping more water did not result in shorter cleanup period by the same ratio since rate-limited mass transfer put a lower limit on the length of the cleanup period. Haggerty and Gorelick (1994) found that total pumping rate increased with the decreasing mobile-immobile phase mass transfer rate. For a 3-year cleanup, the effect of mass transfer could be seen more obviously compared to a 15-year cleanup. Thus they stated that long term remediation schemes were less affected by the mass transfer limitations.

The effect of heterogeneity in mass transfer rate coefficient and its correlation with other aquifer parameters, such as K , may be as critical as the value of it for

transport and remediation studies. Mishra et al. (1999) investigated the solute transport in the case of spatially variable sorption and desorption rates used in the linear kinetic model. They found that spatially variable rates resulted in lower peak concentrations, shifted peak positions and longer tails in the breakthrough curve showing that understanding of the heterogeneity in the sorption and desorption rates is important in predicting the transport behaviors of the solutes. In another study, Mishra and Gutjahr (1999) examined the effect of spatially varying sorption and desorption rates on the spreading of the linearly sorbing solute plume in transverse direction. They stated that when σ^2 of the sorption rates was small, the variability in groundwater velocity, or in other words variability in K , had more pronounced effect on the transverse dispersion than the sorption rate variability. Li and Brusseau (2000) studied the effect of heterogeneous rate-limited mass transfer described by the two-region model on solute transport. Their results showed that when the mean rate coefficient was too small or large, the effect of heterogeneity in rate-limited mass transfer was minimal. However, for intermediate rate coefficients, the effect was observable with greater tailing for heterogeneous case. This implied that assuming the rate coefficient as homogenous may result in overestimated mass removal and underestimated cleanup times. Cvetkovic and Shapiro (1990) performed a stochastic solute arrival time analysis to a sorptive solute on heterogeneous porous media by considering both equilibrium and nonequilibrium sorption governed by the first-order linear kinetics. The results of the equilibrium sorption case were given above. For the nonequilibrium sorption case, they assumed variability in forward and reverse rate coefficients and in K with depth. They also assumed that forward and reverse rate coefficients were negatively correlated with K . They found that the cumulative mass arrival time with variable forward and reverse rate coefficients was generally larger than the cumulative mass arrival time with constant sorption parameters. The effect of sorption coefficient variability was greater for larger $\sigma^2_{\ln K}$. Destouni and Cvetkovic (1991) assumed negative, positive and no correlation between K and sorption and desorption rate coefficients of the kinetic sorption model in order to investigate the

effect of spatially variable sorption parameters on the field scale mass arrival of a sorbing solute. For the negative correlation case, when the rate coefficients were spatially variable, an increased and early peak in the breakthrough curve was observed compared to the case with constant rate coefficient. In addition, for large rate coefficients, double-peak behavior was noticed. For the positive correlation case, an increased and narrowed peak was observed in the breakthrough curve. In the case of no correlation, the effect was similar to the negative correlation case in which double-peak behavior was detected.

Aksoy and Culver (2004) considered the spatial variability in the mass transfer rate coefficient of the two-site nonequilibrium sorption model for the optimum design and cost of P&T remediation. They took both K and K_d as spatially variable. When the mass transfer coefficient heterogeneity was taken into account, it was seen that nonequilibrium sorption heterogeneity affected the remediation design and cost for low K heterogeneity but this effect was negligible for high K heterogeneity. Berglund (1997) evaluated the effect of rate-limited mass transfer from DNAPL phase to aqueous phase on the P&T remediation time and found that sensitivity of cleanup times to K heterogeneity decreased with decreasing mass transfer rate coefficient. Berglund (1997) also assumed rate coefficient as spatially variable and positively correlated with mean groundwater velocity (i.e. K) and found that spatial variability in the rate coefficient resulted in enhanced tailing and prolonged cleanup times.

Among the above studies, only the study of Aksoy and Culver (2004) investigated the effect of α heterogeneity on the P&T remediation design and associated costs. They considered a single $\sigma^2_{\ln\alpha}$ but this study considered two different $\sigma^2_{\ln\alpha}$ in order to see the effect of changing $\sigma^2_{\ln\alpha}$ on the P&T remediation design and cost. They also did not explore the impact of λ . Berglund (1997) evaluated the effect of spatially variable rate-limited mass transfer coefficient on the P&T remediation time, but the mass transfer model used in Berglund's (1997) study described the

mass transfer from DNAPL phase to aqueous phase, not the transfer due to nonequilibrium sorption and it only considered the P&T remediation time as the comparison indicator. In addition to the effect of $\sigma_{\ln\alpha}^2$ and λ , this study also aims to explore the effect of correlation between α and K_d . This analysis was also extended to the effect of correlation between α and K by the use of the positive and negative correlation between K and K_d . Different from Berglund's (1997) study, this study considered the effect of correlation of α with both K and K_d under nonequilibrium sorption conditions on the P&T remediation design and cost.

Furthermore, the effect of f value on the P&T remediation design and cost was investigated. In literature, there are studies comparing equilibrium and rate-limited mass transfer in terms of both transport and remediation of contaminants but there is no single study, to author's knowledge, investigating the effect of f value which specifies the fraction of equilibrium sorption sites in two-site nonequilibrium sorption model on the P&T remediation design and cost. This study is unique because of these mentioned features. Therefore, this study aims to fill the gaps in the mentioned subjects above in the literature.

2.9. Genetic Algorithms and Their Use in Pump and Treat Remediation Problems

Genetic algorithms (GAs) are probabilistic search algorithms which were first introduced in the 1960's by John Holland. However, the first important theoretical analysis presented by Holland was in 1975 (Holland, 1975). GAs are based on the mechanics of natural selection and natural genetics. The inspiration of them comes from the modification of successive generations to reach an optimum form and the survival of the fittest (Hopgood, 2001).

GAs differ from the traditional optimization methods in some particular ways. They use probabilistic rules rather than the deterministic rule as in the case of

traditional optimization methods. They do not require the objective function to have certain characteristics such as differentiability or convexity since they use directly the objective function information. They search from a population of policies instead of a single policy as in the traditional methods. Besides these favorable characteristics which have made GAs a common method for the optimization of large-scale, complex problems, they also have some weak points in their application. The real performance of a particular algorithm can be problem specific. Some experimentation with the GA parameters, such as population size, crossover and mutation probability, may be necessary to reach the optimum form of the algorithm. A globally optimum solution is not guaranteed with GA but they generate near-optimal solutions robustly (Weck et al., 1999). Their operation may be computationally intensive but this problem can be surpassed with the implementation on parallel computers.

The first step of a basic GA is the random creation of an initial population of strings which represents the set of decision variables or a set of possible solutions. Strings are composed of bits. Binary encoding which represents the decision variables as 1s and 0s is the most often used type of encoding. The initial population of strings is then evaluated according to the objective function and the constraints to determine how well each string fits the objectives of the problem. A temporary mating pool is formed based on the fitness values of the strings. The strings with higher fitness values have higher probability of being in the mating pool. Following selection, crossover operator works on randomly selected pairs of strings, called as the parent strings, with a certain probability. Information is exchanged between two strings by crossover operation to generate two new strings for the next generation. The purpose of the crossover is to combine the useful segments of the parents on new individuals (Goldberg, 1989). The simplest crossover type is one-point crossover. During one-point crossover a single location is randomly chosen on the selected strings and bits beyond this point are swapped between the parent strings. In two-point crossover, two locations on the selected

strings are determined randomly and the bits between these crossover sites are exchanged. In uniform crossover each bit position of the two parents are considered for swapping. A detailed description of uniform and two-point crossover operators can be found in Section 3.4.1. The last operator is the mutation in which the value of a randomly selected bit on a randomly selected string is altered with a small probability. The aim of mutation is to put diversity into the population and to prevent the probable loss of some useful genetic material (Goldberg, 1989). After the mutation a new generation of strings is created. This cycle of selection, crossover and mutation continues until the stopping criterion is met. Figure 2.4 shows the flow diagram showing all steps of GAs.

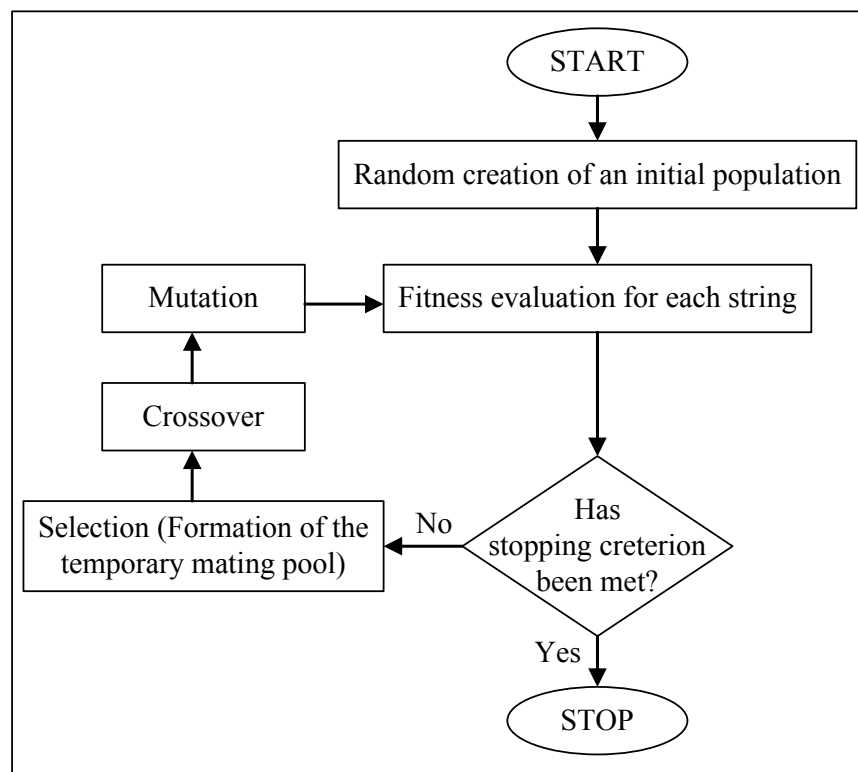


Figure 2.4. Flow diagram showing the steps of GAs

GAs have been in use for more than a decade for the solution of P&T remediation problems which might have discontinuous, nonlinear and nonconvex cost functions (McKinney and Lin, 1994; Liu et al., 2000; Zheng and Wang, 2002; Aksoy and Culver, 2004; Ayvaz and Karahan, 2008). The complexity of a P&T remediation system optimization problem depends on several factors including the choice for objective function, associated constraints, the number and the type of decision variables. The objective function can take a form of minimization of the P&T system cost (i.e. pumping, well construction, water treatment costs or various combinations of these), minimization of the cleanup time, minimization of the sum of pumping rates or pumping volumes assuming linear relationship between these two and the cost of remediation or maximization of contaminant removal. The remediation system may aim to contain the contaminant plume hydraulically or prevent the increase in the downgradient contaminant concentration or any point in the aquifer above a certain limit. The goal of the remediation system is generally integrated with constraints functions of the optimization model (Rogers and Dowla, 1994). Therefore, constraints can be related with the groundwater quality (e.g. maximum contaminant concentration at monitoring points or any point in the aquifer, maximum contaminant mass remained in the aquifer), pumping rates (e.g. maximum pumping rate in a well, maximum total pumping rate in all extraction wells) or hydraulic head (e.g. maximum drawdown observed in the pumping wells) (Cunha, 2002; Mayer et al., 2002). The decision variables generally include pumping rate, number of wells and their locations or time of the cleanup.

In this study, two different optimization models are used. The aim of the first one is to minimize the total cost of remediation including both installation and operating costs of pumping wells and aboveground treatment unit. The second model aims to minimize the cleanup time. For both problems, the objective function includes nonlinear and discontinuous cost terms as will be given in Sections 3.4.1 and 3.4.2. Inclusion of the nonlinear and discontinuous terms complicates the optimization problem but the power of GA lies behind the success

of solving these kinds of problems. Inclusion of nonlinear pumping cost term is especially important for heterogeneous aquifers since optimal pumping rates and well locations may easily be affected from the drawdown which may greatly change by the local K (Huang and Mayer, 1997). Constraints are the other factors determining the complexity of the optimization problem. In this study, both concentration and hydraulic constraints are considered. As Mayer et al. (2002) stated, the introduction of contaminant constraints increases the complexity of the problem considerably. Unlike many other studies (Espinoza et al., 2005; Sinha and Minsker, 2007; McKinney and Lin, 1994; Wang and Zheng, 1997; Chang and Hsiao, 2002; Aral and Guan, 1996; Zheng and Wang, 2002; Ko et al., 2005), in this study the dissolved contaminant concentration constraint is applied to all points in the aquifer, not to a few monitoring points. In addition, a total concentration constraint is used in order to prevent the concentration rebound which is considered as one of the drawbacks of P&T remediation systems since it is not considered in the designs. This approach was used in only a few studies in literature (Aksoy, 2000; Aksoy and Culver, 2000; Aksoy and Culver, 2004). In summary, the objective function and the constraints of this study were selected to obtain more realistic optimum solutions in comparison to other P&T optimization studies in literature.

CHAPTER 3

METHODOLOGY

3.1. Generation of Heterogeneous Fields

Random field generation is a commonly used technique to create fields describing continuous (or discrete) distribution of aquifer parameters. In this study, the turning bands method was used in order to generate the heterogeneous fields. The turning bands method was first developed by Matheron (1973). The method involves the generation of two- or higher-dimensional random fields by generating a sequence of one-dimensional line processes (Fenton, 1990; Harter, 1994). The details of the method can be found elsewhere (e.g. Mantoglou and Wilson, 1982; Tompson et al., 1989).

In order to generate the random fields, a two dimensional turning bands code, Turn2D.F, written in Fortran and developed by Tompson et al. (1989) was used. This code generates the line processes using the standard spectral integration method. It can simulate both isotropic and anisotropic fields. For this reason, it is deemed to be sufficient for the generation of various fields of heterogeneity characteristics for this study.

The random fields that were used in this study represent a two dimensional aquifer of 300 m \times 300 m. The fields consist of 1600 square elements with 1681 grid points. The grid spacing between the grid points is 7.5 m in both x and y directions. In the study, three different realizations were generated for each

heterogeneous field. The seed used for the generation of a specific random field is referred to as a realization. Fields generated using the same seed have the similar parameter distribution pattern in terms of respective locations of high and low values throughout the field.

In order to label the heterogeneous fields, a naming convention was used. This convention can be described as follows:

- 1) The first component is 1-2 characters which defines the type of the heterogeneous field; K, K_d and r for K, K_d and α -fields, respectively.
- 2) The second component is a number indicating σ^2 , in other words, the degree of heterogeneity. As the number increases, σ^2 , the distance between the minimum and the maximum values of the specific aquifer parameter increases.
- 3) The third component is a number representing λ . Similar to the convention used for σ^2 , as the number increases, the magnitude of λ increases.
- 4) The fourth and the last component is the realization indicator given by a letter. This indicator defines the seed used in the generation of heterogeneous fields. The low and high values are spatially distributed similarly (in respective locations) in the fields having the same realization indicator. Upper case letters (A, B, C), lower case letters (a, b, c) and roman numerals (i, ii, iii) are used to define the different realizations of K, K_d and α -fields, respectively. For the correlated fields the realization indicator of the field with which they are correlated is used.
- 5) For the combination of different heterogeneity cases, individual labels representing each heterogeneous field and a sign defining the relation (i.e. correlation) between these heterogeneous fields are used together. The signs -, + and / were used for negatively correlated, positively correlated and uncorrelated cases, respectively.

Given the above labeling convention, K11A stands for the heterogeneous K-field having the lowest σ^2 and the smallest λ for the first realization (realization A) while K33A represents the field having the highest σ^2 and the largest λ . For the combination of K-field of the medium σ^2 and the medium λ in realization A with K_d-field of the highest σ^2 and the highest λ in realization b, the label used is K22A/Kd32b. For the representation of the use of the K-field having the lowest σ^2 and the smallest λ and the K_d-field which is positively correlated with the K-field, K11A+Kd11A is used as the label.

3.1.1. K-fields

Isotropic, log-normally distributed K-fields were generated with the geometric mean (K_g) of 4.5×10^{-5} m/s (mean of $\ln K = -10$) based on the values given for fields in the literature (Table 2.4). This value is typical for a sandy aquifer (Domenico and Schwartz, 1990; Freeze and Cherry, 1979). K_g in the range of 5.6×10^{-6} – 1.2×10^{-3} m/s have been used in the example groundwater management problems in literature (e.g. McKinney and Lin, 1996; Lee et al., 2000; Aksoy and Culver, 2004; Chan Hilton and Culver, 2005; Elder et al., 2002). In order to get different degrees of heterogeneity in terms of $\sigma^2_{\ln K}$ and $\lambda_{\ln K}$, three different $\sigma^2_{\ln K}$ (0.2500, 0.7225 and 1.3225) and three different $\lambda_{\ln K}$ values (15, 22.5 and 30 m) were used. The $\sigma^2_{\ln K}$ values represent approximately 50%, 100% and 150% coefficient of variation (CV), respectively. K values range over approximately 1.5 orders of magnitude for $\sigma^2_{\ln K}$ of 0.2500 while they spanned nearly 2.5 and 3.5 orders of magnitude for $\sigma^2_{\ln K}$ of 0.7225 and $\sigma^2_{\ln K}$ of 1.3225, respectively. $\lambda_{\ln K}$ values were selected based on two criteria given by Tompson et al. (1989). The first is related with the size of the domain such that the size of the domain in any direction should necessarily be much larger than the λ in the same direction, nominally by a factor of 10 or more, to estimate the spatial statistics. In this study, since the domain size is 300 m in both x and y directions the largest $\lambda_{\ln K}$ was chosen as 30 m. The second criterion is related with the grid size such that the grid

spacing in any direction should be less than λ in the same direction, preferably by a factor of 0.5 or less. In this study, since the grid spacing is 7.5 m in both x and y directions the smallest $\lambda_{\ln K}$ was chosen as 15 m. Table 3.1 shows the summary of the properties of these heterogeneous K-fields, as $\lambda_{\ln K}$, the range of the K, the arithmetic mean, σ_K , K_g and $\sigma_{\ln K}^2$. In literature, heterogeneity has generally been reported as the $\sigma_{\ln K}^2$ but some researchers also report it in terms of σ_K . Similarly, although the mean value of K in the field is commonly given with K_g value, there are some studies reported arithmetic mean values. Therefore, all these values are presented in Table 3.1.

After generating the heterogeneous K-fields, the covariance function obtained from the random field generator for each field was compared with the theoretical negative exponential covariance function given in Equation 2.8. Figures 3.1 to 3.3 show this comparison for each realization. According to the Equation 2.8, λ is equal to the lag distance where the covariance function reaches the value of (σ^2/e) (Figure 2.3). In these figures, it was observed that the covariance functions obtained from the random field generator almost perfectly fitted the theoretical ones.

The K-fields, obtained using the random field generator, were visualized using MATLAB® and presented in Figures A.1 - A.3 in Appendix A. Examples of these fields are shown in Figures 3.4 to 3.9. In the figures, the green color represents the K values around 4.5×10^{-5} m/s, which is K_g , while blue and red colors show low and high ends of the K range, respectively. When Figures 3.4 and 3.5 are compared, the impact of the degree of heterogeneity in K values throughout the aquifer can be seen. In these figures, the respective locations of the higher and lower Ks are similar because of the use of the same seed for the random field generation. However, the magnitude difference between the low and high K values is greater for the more heterogeneous case (K21A) than the less heterogeneous one

Table 3.1. Summary of the statistical properties of the heterogeneous K-fields (The unit of K is m/s)

Field	$\lambda_{\ln K}$ (m)	Range of K	Ar. Mean	σ_K	K_g	$\sigma_{\ln K}^2$
K11A	15	$7.5 \times 10^{-6} - 2.5 \times 10^{-4}$	5.1×10^{-5}	2.6×10^{-5}	4.5×10^{-5}	0.2500
K11B	15	$9.0 \times 10^{-6} - 2.9 \times 10^{-4}$	5.1×10^{-5}	2.9×10^{-5}	4.5×10^{-5}	0.2500
K11C	15	$6.9 \times 10^{-6} - 2.3 \times 10^{-4}$	5.1×10^{-5}	2.7×10^{-5}	4.5×10^{-5}	0.2500
K12A	22.5	$7.7 \times 10^{-6} - 1.8 \times 10^{-4}$	5.1×10^{-5}	2.5×10^{-5}	4.5×10^{-5}	0.2500
K12B	22.5	$5.5 \times 10^{-6} - 1.9 \times 10^{-4}$	5.1×10^{-5}	2.6×10^{-5}	4.5×10^{-5}	0.2500
K12C	22.5	$1.1 \times 10^{-5} - 3.7 \times 10^{-4}$	5.1×10^{-5}	2.8×10^{-5}	4.5×10^{-5}	0.2500
K13A	30	$9.4 \times 10^{-6} - 1.8 \times 10^{-4}$	5.1×10^{-5}	2.5×10^{-5}	4.5×10^{-5}	0.2500
K13B	30	$7.5 \times 10^{-6} - 2.1 \times 10^{-4}$	5.1×10^{-5}	2.7×10^{-5}	4.5×10^{-5}	0.2500
K13C	30	$9.6 \times 10^{-6} - 2.7 \times 10^{-4}$	5.1×10^{-5}	2.7×10^{-5}	4.5×10^{-5}	0.2500
K21A	15	$2.1 \times 10^{-6} - 8.1 \times 10^{-4}$	6.4×10^{-5}	6.0×10^{-5}	4.5×10^{-5}	0.7225
K21B	15	$2.9 \times 10^{-6} - 1.1 \times 10^{-3}$	6.5×10^{-5}	7.5×10^{-5}	4.5×10^{-5}	0.7225
K21C	15	$1.8 \times 10^{-6} - 7.0 \times 10^{-4}$	6.4×10^{-5}	6.6×10^{-5}	4.5×10^{-5}	0.7225
K22A	22.5	$2.3 \times 10^{-6} - 4.5 \times 10^{-4}$	6.3×10^{-5}	5.6×10^{-5}	4.5×10^{-5}	0.7225
K22B	22.5	$1.2 \times 10^{-6} - 5.1 \times 10^{-4}$	6.4×10^{-5}	6.0×10^{-5}	4.5×10^{-5}	0.7225
K22C	22.5	$3.9 \times 10^{-6} - 1.6 \times 10^{-3}$	6.5×10^{-5}	7.6×10^{-5}	4.5×10^{-5}	0.7225
K23A	30	$3.1 \times 10^{-6} - 5.0 \times 10^{-4}$	6.3×10^{-5}	5.4×10^{-5}	4.5×10^{-5}	0.7225
K23B	30	$2.1 \times 10^{-6} - 6.2 \times 10^{-4}$	6.5×10^{-5}	6.4×10^{-5}	4.5×10^{-5}	0.7225
K23C	30	$3.3 \times 10^{-6} - 9.5 \times 10^{-4}$	6.4×10^{-5}	6.8×10^{-5}	4.5×10^{-5}	0.7225
K31A	15	$7.3 \times 10^{-7} - 2.3 \times 10^{-3}$	8.4×10^{-5}	1.2×10^{-4}	4.5×10^{-5}	1.3225
K31B	15	$1.1 \times 10^{-6} - 3.3 \times 10^{-3}$	9.1×10^{-5}	1.8×10^{-4}	4.5×10^{-5}	1.3225
K31C	15	$6.0 \times 10^{-7} - 1.8 \times 10^{-3}$	8.6×10^{-5}	1.4×10^{-4}	4.5×10^{-5}	1.3225
K32A	22.5	$7.8 \times 10^{-7} - 1.0 \times 10^{-3}$	8.3×10^{-5}	1.1×10^{-4}	4.5×10^{-5}	1.3225
K32B	22.5	$3.5 \times 10^{-7} - 1.2 \times 10^{-3}$	8.5×10^{-5}	1.2×10^{-4}	4.5×10^{-5}	1.3225
K32C	22.5	$1.6 \times 10^{-6} - 5.7 \times 10^{-3}$	9.0×10^{-5}	2.0×10^{-4}	4.5×10^{-5}	1.3225
K33A	30	$1.2 \times 10^{-6} - 1.2 \times 10^{-3}$	8.1×10^{-5}	1.0×10^{-4}	4.5×10^{-5}	1.3225
K33B	30	$7.3 \times 10^{-7} - 1.6 \times 10^{-3}$	8.7×10^{-5}	1.3×10^{-4}	4.5×10^{-5}	1.3225
K33C	30	$1.3 \times 10^{-6} - 2.8 \times 10^{-3}$	8.7×10^{-5}	1.5×10^{-4}	4.5×10^{-5}	1.3225

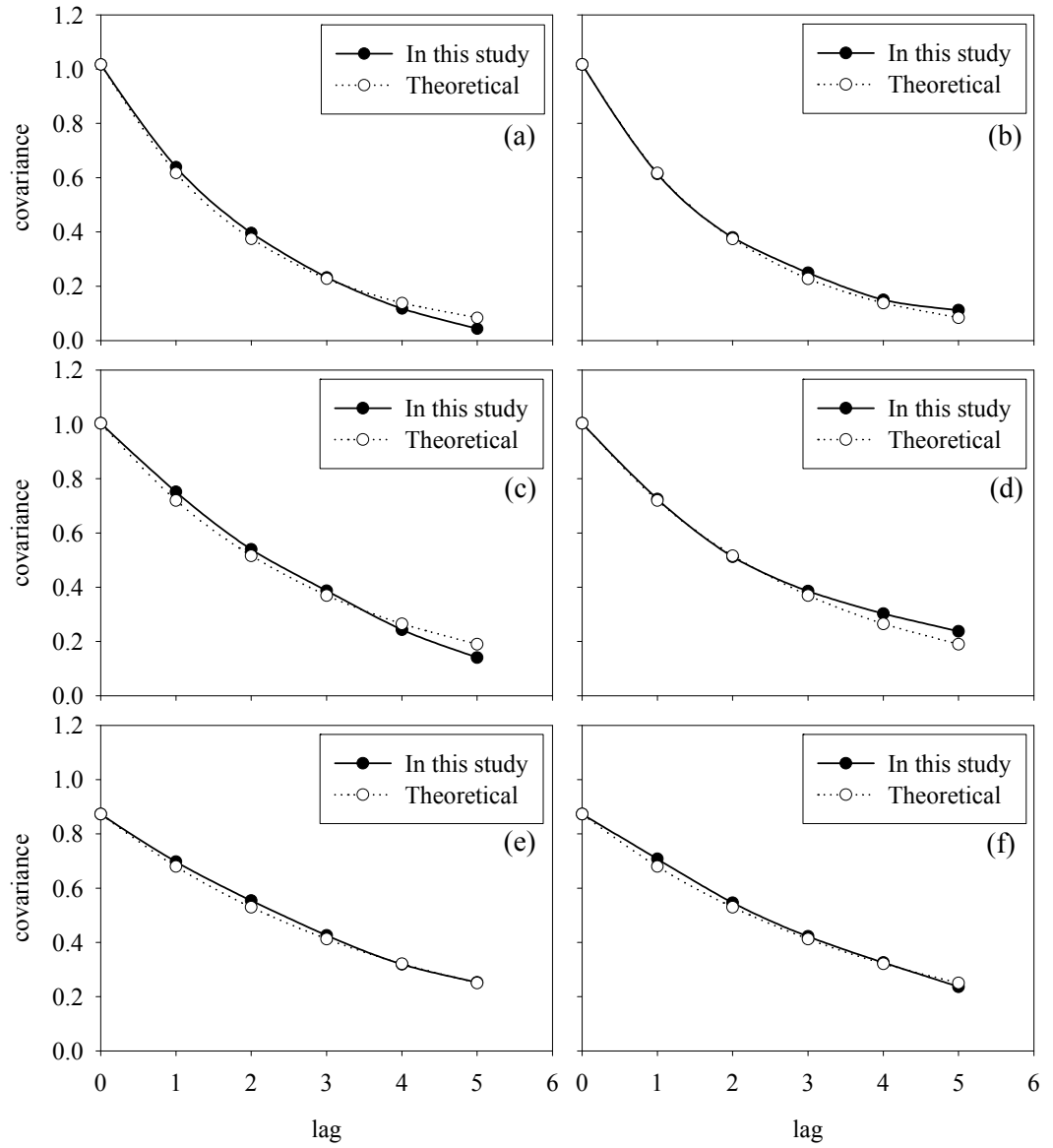


Figure 3.1. Comparison of the theoretical covariance function with the covariance function of the K-fields generated in this study for realization A (a) $\lambda_{\ln K, x} = 15$ m, (b) $\lambda_{\ln K, y} = 15$ m, (c) $\lambda_{\ln K, x} = 22.5$ m, (d) $\lambda_{\ln K, y} = 22.5$ m, (e) $\lambda_{\ln K, x} = 30$ m, (f) $\lambda_{\ln K, y} = 30$ m

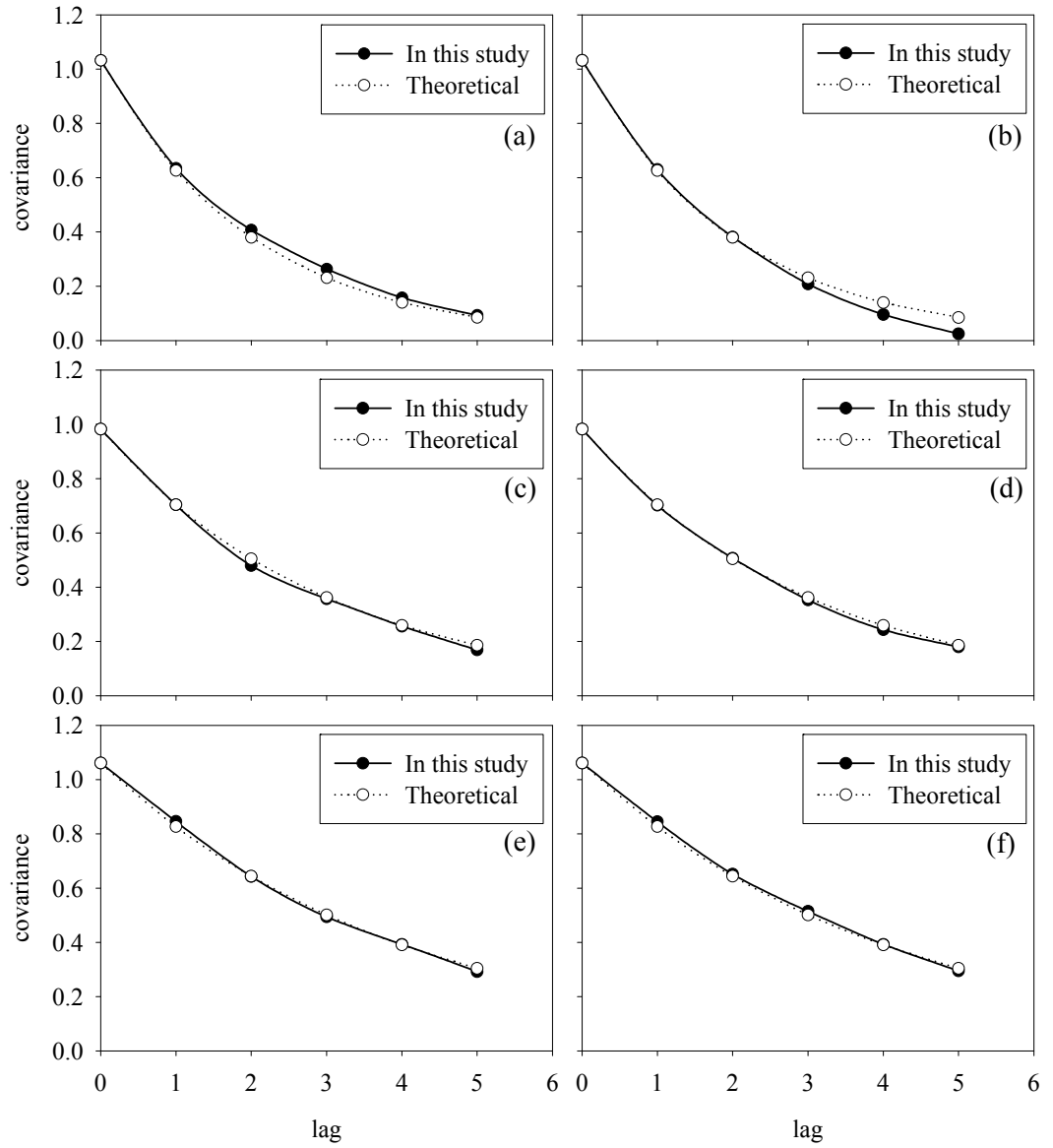


Figure 3.2. Comparison of the theoretical covariance function with the covariance function of the K-fields generated in this study for realization B (a) $\lambda_{\ln K, x} = 15$ m, (b) $\lambda_{\ln K, y} = 15$ m, (c) $\lambda_{\ln K, x} = 22.5$ m, (d) $\lambda_{\ln K, y} = 22.5$ m, (e) $\lambda_{\ln K, x} = 30$ m, (f) $\lambda_{\ln K, y} = 30$ m

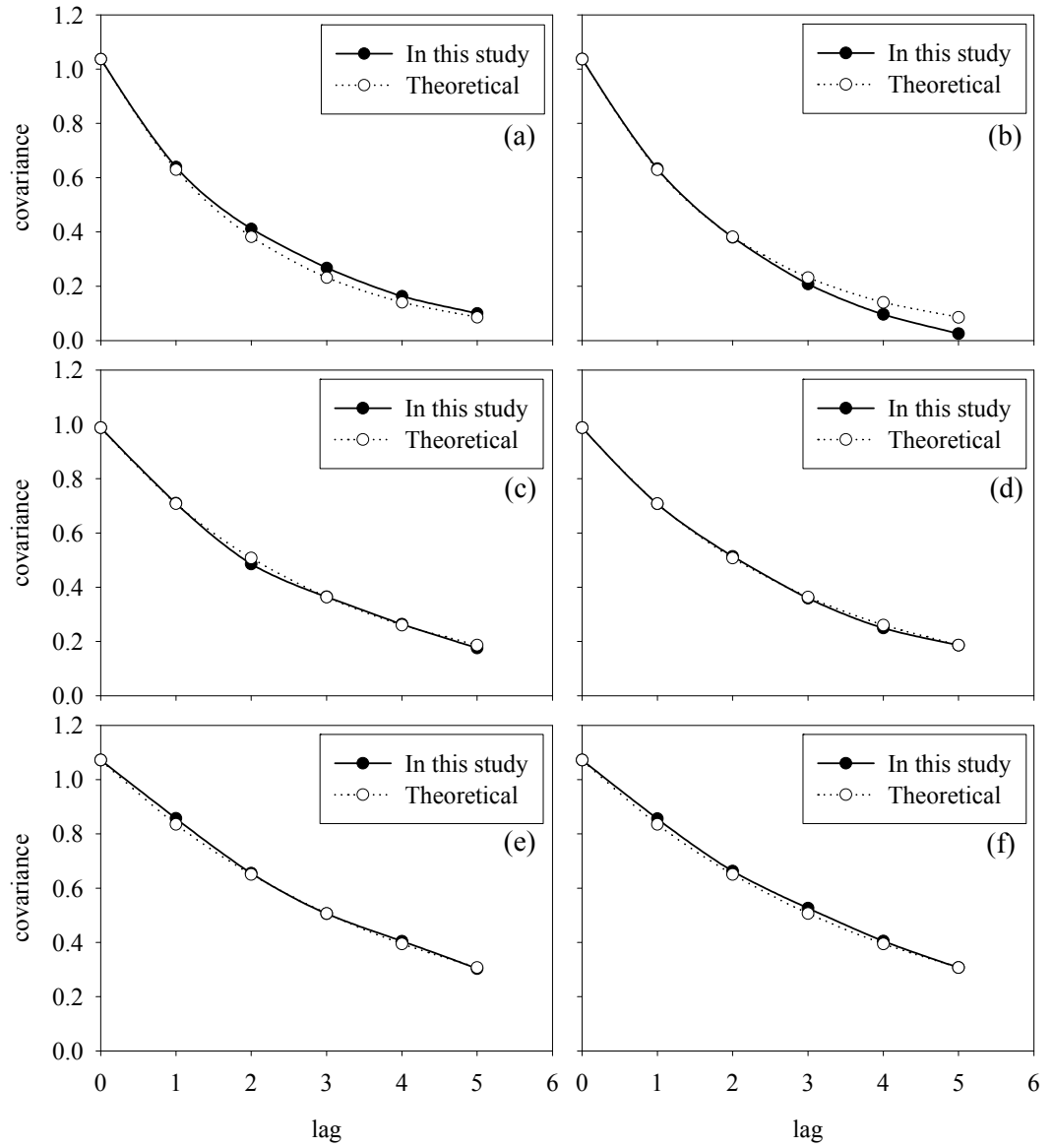


Figure 3.3. Comparison of the theoretical covariance function with the covariance function of the K-fields generated in this study for realization C (a) $\lambda_{\ln K, x} = 15$ m, (b) $\lambda_{\ln K, y} = 15$ m, (c) $\lambda_{\ln K, x} = 22.5$ m, (d) $\lambda_{\ln K, y} = 22.5$ m, (e) $\lambda_{\ln K, x} = 30$ m, (f) $\lambda_{\ln K, y} = 30$ m

(K11A). This is represented by the contrast between the blue and red colors. Figures 3.5 to 3.7 show the K distribution for three different realizations of the

field K11. Although these fields have the same K_g , $\sigma^2_{\ln K}$ and $\lambda_{\ln K}$ the locations of low and high K values are different for different realizations. Figures 3.7 to 3.9 show the effect of changing $\lambda_{\ln K}$ s on the K-field distribution (K11C, K12C and K13C). As $\lambda_{\ln K}$ increases, the distance between the areas of high and low K zones increases. At the same time, the areas of such zones grow as well.

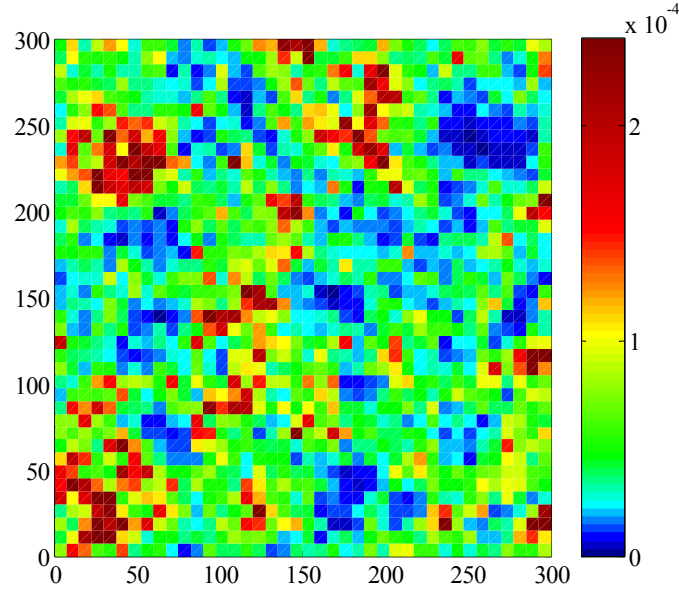


Figure 3.4. Distribution of K values for field K21A

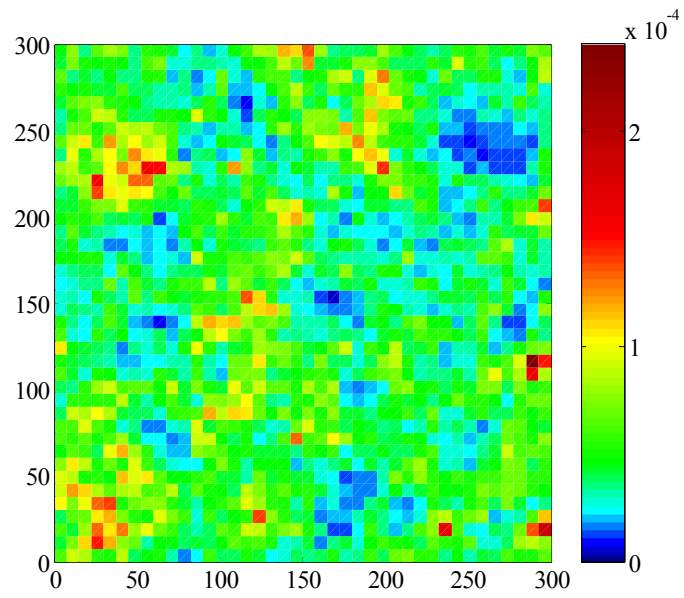


Figure 3.5. Distribution of K values for field K11A

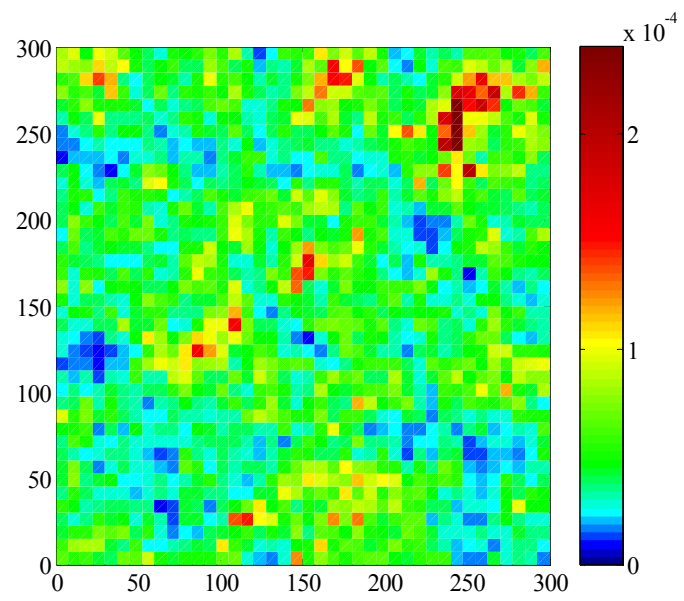


Figure 3.6. Distribution of K values for field K11B

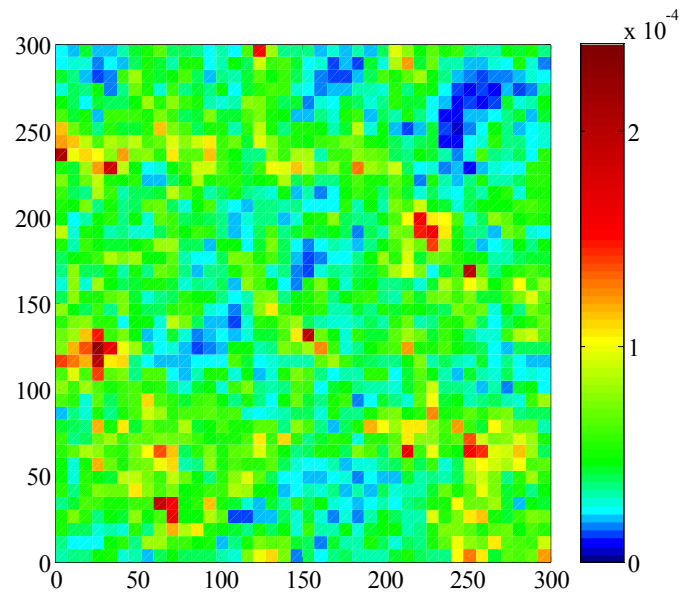


Figure 3.7. Distribution of K values for field K11C

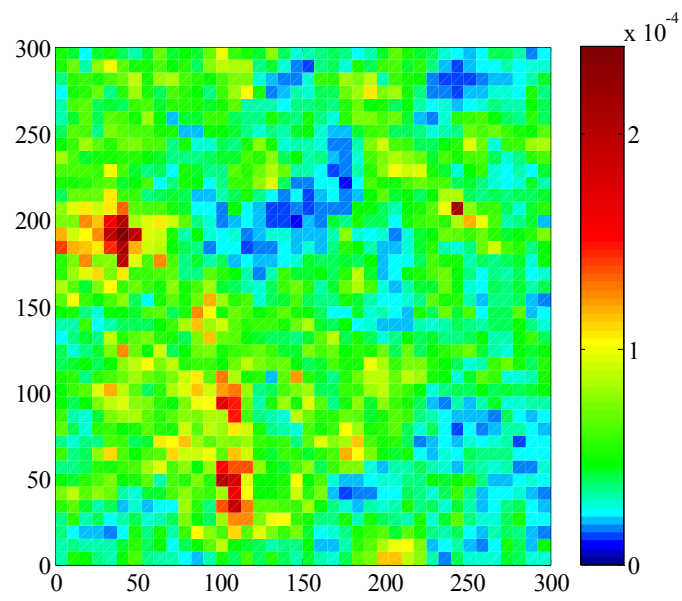


Figure 3.8. Distribution of K values for field K12C

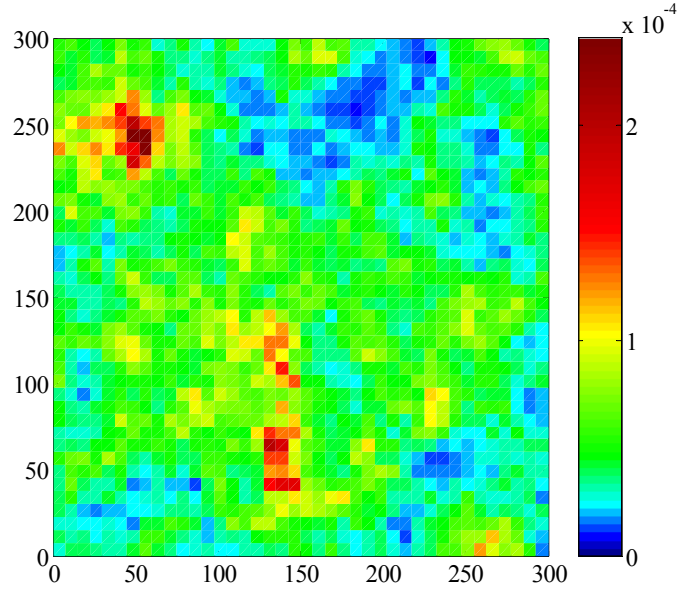


Figure 3.9. Distribution of K values for field K13C

3.1.2. Anisotropic K-fields

In order to investigate the effect of λ anisotropy on P&T remediation system design and cost, K-fields with anisotropy ratio of 1.5:1 ($\lambda_{\ln K, x} = 22.5\text{m}$: $\lambda_{\ln K, y} = 15\text{m}$) and 2:1 ($\lambda_{\ln K, x} = 30\text{m}$: $\lambda_{\ln K, y} = 15\text{m}$) were generated for realization B. The covariance functions of anisotropic fields of realization B provided better fits with the theoretical covariance functions compared to realizations A and C. These covariance functions are presented in Figure B.1 in Appendix B. These anisotropic fields were generated for two different $\sigma^2_{\ln K}$, 0.2500 and 1.3225. Colored representations of anisotropic fields are given in Figure A.4 in Appendix A. Table 3.2 shows the statistical summary of anisotropic K-fields.

Table 3.2. Summary of the statistical properties of the anisotropic heterogeneous K-fields (The unit of K is m/s)

Field	$\lambda_{\ln K, x}$ (m)	$\lambda_{\ln K, y}$ (m)	Range of K	Ar. Mean	σ_K	K_g	$\sigma_{\ln K}^2$
K10B_AN1	22.5	15	$1.0 \times 10^{-5} - 2.3 \times 10^{-4}$	5.1×10^{-5}	2.6×10^{-5}	4.5×10^{-5}	0.2500
K10B_AN2	30	15	$1.0 \times 10^{-5} - 2.0 \times 10^{-4}$	5.1×10^{-5}	2.6×10^{-5}	4.5×10^{-5}	0.2500
K30B_AN1	22.5	15	$1.6 \times 10^{-6} - 1.9 \times 10^{-3}$	8.5×10^{-5}	1.2×10^{-4}	4.5×10^{-5}	1.3225
K30B_AN2	30	15	$1.5 \times 10^{-6} - 1.4 \times 10^{-3}$	8.5×10^{-5}	1.2×10^{-4}	4.5×10^{-5}	1.3225

3.1.3. K_d -fields

For the K_d -fields, the geometric mean (K_{dg}) value was selected as $0.36 \text{ cm}^3/\text{g}$ based on the study of Aksoy (2000). On the other hand, based on laboratory measurements, Allen-King et al. (2006) reported K_{dg} for PCE as 0.35 mL/g for Borden aquifer. This shows that the selected K_d value is compatible with the field scale studies in literature as well. Similar to K-fields, a log-normal distribution was assumed for K_d -fields based on the findings of the field scale studies (e.g. Hoffman, 1995; Painter et al., 2001) and the assumptions used in modeling studies (e.g. Bosma et al., 1993; Tompson, 1993). Fields having three different $\sigma_{\ln K_d}^2$ values (0.0256, 0.0740 and 0.1354) and two different $\lambda_{\ln K_d}$ (15 and 30 m) for each $\sigma_{\ln K_d}^2$ values were generated by the random field generator. At these $\sigma_{\ln K_d}^2$ values, CV was 16%, 28% and 38%, respectively. For each K_d -field, three different realizations were considered. Table 3.3 shows the statistical summary of the heterogeneous K_d -fields. The covariance function obtained from the random field generator for each K_d -field was compared with the theoretical negative exponential covariance function given in Equation 2.8 and almost a perfect fit was observed for these two. This comparison is given in Figures B.2 - B.4 in Appendix B. The colored representations of the K_d -fields are given in Figures A.5 to A.7 in Appendix A. These heterogeneous K_d -fields were used in combination with the

selected heterogeneous K-fields to investigate the effect of $\lambda_{\ln K_d}$ on P&T remediation design and cost.

Table 3.3. Summary of the statistical properties of the heterogeneous K_d -fields
(The unit of K_d is cm^3/g)

Field	$\lambda_{\ln K_d}$ (m)	Range of K_d	Ar. Mean	σ_{K_d}	K_{d_g}	$\sigma^2_{\ln K_d}$
Kd11a	15	0.21 – 0.60	0.36	0.0588	0.36	0.0256
Kd11b	15	0.21 – 0.59	0.36	0.0589	0.36	0.0256
Kd11c	15	0.21 – 0.61	0.36	0.0586	0.36	0.0256
Kd12a	30	0.20 – 0.64	0.36	0.0587	0.36	0.0256
Kd12b	30	0.23 – 0.62	0.36	0.0591	0.36	0.0256
Kd12c	30	0.23 – 0.62	0.36	0.0590	0.36	0.0256
Kd21a	15	0.15 – 0.85	0.37	0.1036	0.36	0.0740
Kd21b	15	0.14 – 0.84	0.37	0.1039	0.36	0.0740
Kd21c	15	0.14 – 0.88	0.37	0.1031	0.36	0.0740
Kd22a	30	0.13 – 0.95	0.37	0.1037	0.36	0.0740
Kd22b	30	0.16 – 0.90	0.37	0.1046	0.36	0.0740
Kd22c	30	0.16 – 0.91	0.37	0.1042	0.36	0.0740
Kd31a	15	0.11 – 1.15	0.38	0.1466	0.36	0.1354
Kd31b	15	0.10 – 1.13	0.38	0.1471	0.36	0.1354
Kd31c	15	0.10 – 1.21	0.38	0.1456	0.36	0.1354
Kd32a	30	0.09 – 1.34	0.38	0.1474	0.36	0.1354
Kd32b	30	0.12 – 1.24	0.38	0.1486	0.36	0.1354
Kd32c	30	0.13 – 1.26	0.38	0.1477	0.36	0.1354

3.1.4. Correlated K_d -fields

Since both positive and negative correlation between K and K_d were observed in the literature (see Section 2.5), both types of correlation were considered in this study. In order to construct K_d -fields which are correlated with K-fields either positively or negatively, the following model of correlation was used.

$$\ln K_d = a \pm b \ln K \quad (3.1)$$

Here, K_d is log-normally distributed and varies with the “b” power of K . In this equation, “a” and “b” define the mean of $\ln K_d$ and $\sigma^2_{\ln K_d}$, respectively. This type of model has been applied to the field measurements conducted at Borden site in order to define the correlation between K and K_d s of strontium (Robin et al., 1991) and PCE (Allen-King et al., 1998; Thompson, 1993). Thompson (1993) has reported the value of “b” in Equation 3.1 as -0.32 based on the K and K_d measurements associated with PCE sorption at LLNL site (see Section 2.5). This value is also used in the study of Thompson et al. (1998). Motivated by these early studies, -0.32 and +0.32 were used as the “b” term of Equation 3.1 in order to represent the negative and positive correlation between K and K_d in this study. The “a” values were selected as -4.225 for negative and 2.181 for positive correlation cases in order to make K_{d_g} as $0.36 \text{ cm}^3/\text{g}$. In the light of this information, the following equations were used for the generation of negatively and positively correlated K_d -fields.

$$\ln K_d = -4.225 - 0.32 \ln K \quad (3.2)$$

$$\ln K_d = 2.181 + 0.32 \ln K \quad (3.3)$$

Correlated K_d -fields were constructed in correlation with the K -fields of all three $\sigma^2_{\ln K}$ (0.2500, 0.7225 and 1.3225) and three realizations but for two $\lambda_{\ln K}$ s (15 and 30 m) (Section 3.1.1) as only these two $\lambda_{\ln K_d}$ s were used to generate the uncorrelated K_d -fields in Section 3.1.3. Since the correlated K_d -fields constructed at this step have the same spatial structure with the K -fields with which these fields are correlated, their covariance functions are the same with that of K -fields (Figures 3.1 to 3.3). Table 3.4 shows the statistical summary of correlated K_d -fields. It is worth to note that the realization indicators of K -fields were used to label the correlated K_d -fields. Because the distribution of the low and high K_d

Table 3.4. Summary of the statistical properties of the negatively and positively correlated heterogeneous K_d -fields (The unit of K_d is cm^3/g)

Field	$\lambda_{\ln K_d}$ (m)	Range of K_d	Ar. Mean	σ_{K_d}	K_{d_g}	$\sigma^2_{\ln K_d}$
K11A-Kd11A	15	0.21 – 0.64	0.36	0.0593	0.36	0.0256
K11B-Kd11B	15	0.20 – 0.60	0.36	0.0583	0.36	0.0256
K11C-Kd11C	15	0.21 – 0.66	0.36	0.0593	0.36	0.0256
K13A-Kd12A	30	0.23 – 0.59	0.36	0.0597	0.36	0.0256
K13B-Kd12B	30	0.22 – 0.64	0.36	0.0585	0.36	0.0256
K13C-Kd12C	30	0.20 – 0.59	0.36	0.0589	0.36	0.0256
K21A-Kd21A	15	0.14 – 0.95	0.37	0.1054	0.36	0.0740
K21B-Kd21B	15	0.13 – 0.86	0.37	0.1026	0.36	0.0740
K21C-Kd21C	15	0.15 – 1.00	0.37	0.1057	0.36	0.0740
K23A-Kd22A	30	0.17 – 0.84	0.37	0.1061	0.36	0.0740
K23B-Kd22B	30	0.16 – 0.95	0.37	0.1028	0.36	0.0740
K23C-Kd22C	30	0.14 – 0.83	0.37	0.1040	0.36	0.0740
K31A-Kd31A	15	0.10 – 1.35	0.39	0.1505	0.36	0.1354
K31B-Kd31B	15	0.09 – 1.17	0.38	0.1451	0.36	0.1354
K31C-Kd31C	15	0.11 – 1.44	0.39	0.1518	0.36	0.1354
K33A-Kd32A	30	0.13 – 1.14	0.39	0.1513	0.36	0.1354
K33B-Kd32B	30	0.12 – 1.35	0.38	0.1457	0.36	0.1354
K33C-Kd32C	30	0.10 – 1.12	0.39	0.1472	0.36	0.1354
K11A+Kd11A	15	0.20 – 0.62	0.36	0.0580	0.36	0.0256
K11B+Kd11B	15	0.22 – 0.65	0.36	0.0593	0.36	0.0256
K11C+Kd11C	15	0.20 – 0.60	0.36	0.0583	0.36	0.0256
K13A+Kd12A	30	0.22 – 0.57	0.36	0.0575	0.36	0.0256
K13B+Kd12B	30	0.20 – 0.59	0.36	0.0589	0.36	0.0256
K13C+Kd12C	30	0.22 – 0.64	0.36	0.0585	0.36	0.0256
K21A+Kd21A	15	0.14 – 0.91	0.37	0.1014	0.36	0.0740
K21B+Kd21B	15	0.15 – 0.99	0.37	0.1055	0.36	0.0740
K21C+Kd21C	15	0.13 – 0.87	0.37	0.1026	0.36	0.0740
K23A+Kd22A	30	0.15 – 0.78	0.37	0.0995	0.36	0.0740
K23B+Kd22B	30	0.14 – 0.83	0.37	0.1040	0.36	0.0740
K23C+Kd22C	30	0.16 – 0.96	0.37	0.1028	0.36	0.0740
K31A+Kd31A	15	0.09 – 1.26	0.38	0.1425	0.36	0.1354
K31B+Kd31B	15	0.11 – 1.43	0.39	0.1512	0.36	0.1354
K31C+Kd31C	15	0.09 – 1.18	0.38	0.1451	0.36	0.1354
K33A+Kd32A	30	0.11 – 1.02	0.38	0.1383	0.36	0.1354
K33B+Kd32B	30	0.10 – 1.12	0.39	0.1472	0.36	0.1354
K33C+Kd32C	30	0.12 – 1.35	0.38	0.1458	0.36	0.1354

values over the field is exactly the same with that of K-field with which it is correlated.

3.1.5. α -fields

Heterogeneous α -fields were generated with the geometric mean (α_g) value of 0.0025 d^{-1} based on the study of Aksoy (2000). Two different $\sigma_{\ln\alpha}^2$ (0.0057 and 0.0299) and two different $\lambda_{\ln\alpha}$ (15 and 30 m) for each $\sigma_{\ln\alpha}^2$ value were used for the generation of the fields. CV was 7.5% and 17.5% with these $\sigma_{\ln\alpha}^2$ s. Similar to K and K_d -fields, for each α -field, three different realizations were considered. Table 3.5 shows the statistical summary of the α -fields and colored visualizations of them are given in Figures A.8 to A.10 in Appendix A. As in the case of K and K_d -field generation, the covariance function obtained from the random field generator for each α -field was compared with the theoretical one and graphs of this comparison are shown in Figures B.5 to B.7 in Appendix B.

3.1.6. Correlated α -fields

Since only negative correlation between α and K_d were reported in the literature, (see Section 2.5), only negative correlation was considered in this study. Review of literature about the correlation between α and K_d has shown that there is an inverse log-log linear relationship between these two parameters (for details of the literature review, see Section 2.5). However, in order to be compatible with the model of correlation given for the K and K_d (Equation 3.1) ln-ln linear relationship was preferred over log-log linear relationship. Shifting from log-log relationship to ln-ln relationship does not change the “b” value which defines $\sigma_{\ln\alpha}^2$. Since “a” value of this relationship will already have to be different from the value given in literature in order for the adjustment of α_g value to 0.0025 d^{-1} , this shift does not affect anything in terms of the compatibility with the literature value. The f_{oc} of the

Table 3.5. Summary of the statistical properties of the heterogeneous α -fields (The unit of α is d⁻¹)

Field	$\lambda_{\ln\alpha}$ (m)	Range of α	Ar. Mean	σ_{α}	α_g	$\sigma^2_{\ln\alpha}$
r11i	15	0.0020 – 0.0033	0.0025	0.0002	0.0025	0.0057
r11ii	15	0.0020 – 0.0032	0.0025	0.0002	0.0025	0.0057
r11iii	15	0.0019 – 0.0033	0.0025	0.0002	0.0025	0.0057
r12i	30	0.0015 – 0.0047	0.0025	0.0004	0.0025	0.0299
r12ii	30	0.0015 – 0.0042	0.0025	0.0004	0.0025	0.0299
r12iii	30	0.0014 – 0.0047	0.0025	0.0004	0.0025	0.0299
r21i	15	0.0020 – 0.0032	0.0025	0.0002	0.0025	0.0057
r21ii	15	0.0019 – 0.0033	0.0025	0.0002	0.0025	0.0057
r21iii	15	0.0020 – 0.0032	0.0025	0.0002	0.0025	0.0057
r22i	30	0.0015 – 0.0043	0.0025	0.0004	0.0025	0.0299
r22ii	30	0.0014 – 0.0046	0.0025	0.0004	0.0025	0.0299
r22iii	30	0.0015 – 0.0045	0.0025	0.0004	0.0025	0.0299

aquifer material of this study was calculated as 0.14% when K_{oc} of PCE was taken as 251 mL/g which was the representative K_{oc} value for a range of 44 to 525 mL/g (European Commission, 2005). Based on the correlation equation reported for a sandy aquifer material with $f_{oc} = 0.13\%$ by Brusseau and Rao (1991) (Equation 2.14), the following equation which relates α to K_d has been used for the generation of the negatively correlated α -fields.

$$\ln \alpha = -6.47 - 0.47 \ln K_d \quad (3.4)$$

The “a” value was selected as -6.47 in order to make α_g as 0.0025 d⁻¹. Correlated α -fields were constructed in correlation with the correlated K_d -fields with K (Section 3.1.4) of two $\sigma^2_{\ln K_d}$ (0.0256 and 0.1354), two $\lambda_{\ln K_d}$ (15 and 30 m) and three realizations. Since the correlated α -fields constructed at this step have the same spatial structure with the correlated K_d -fields with K with which these fields

are correlated, their covariance functions are the same with that of correlated K_d -fields with K . Table 3.6 shows the statistical summary of correlated α -fields.

Table 3.6. Summary of the statistical properties of the correlated heterogeneous α -fields (The unit of α is d^{-1})

Field	$\lambda_{\ln\alpha}$ (m)	Range of α	Ar. Mean	σ_α	α_g	$\sigma_{\ln\alpha}^2$
K11A-Kd11A-r11A	15	0.0019 – 0.0032	0.0025	0.0002	0.0025	0.0057
K11B-Kd11B-r11B	15	0.0020 – 0.0033	0.0025	0.0002	0.0025	0.0057
K11C-Kd11C-r11C	15	0.0019 – 0.0032	0.0025	0.0002	0.0025	0.0057
K13A-Kd12A-r12A	30	0.0020 – 0.0031	0.0025	0.0002	0.0025	0.0057
K13B-Kd12B-r12B	30	0.0019 – 0.0032	0.0025	0.0002	0.0025	0.0057
K13C-Kd12C-r12C	30	0.0020 – 0.0033	0.0025	0.0002	0.0025	0.0057
K31A-Kd31A-r21A	15	0.0013 – 0.0045	0.0025	0.0004	0.0025	0.0299
K31B-Kd31B-r21B	15	0.0014 – 0.0048	0.0025	0.0004	0.0025	0.0299
K31C-Kd31C-r21C	15	0.0013 – 0.0044	0.0025	0.0004	0.0025	0.0299
K33A-Kd32A-r22A	30	0.0015 – 0.0041	0.0025	0.0004	0.0025	0.0299
K33B-Kd32B-r22B	30	0.0013 – 0.0043	0.0025	0.0004	0.0025	0.0299
K33C-Kd32C-r22C	30	0.0015 – 0.0047	0.0025	0.0004	0.0025	0.0299
K11A+Kd11A-r11A	15	0.0019 – 0.0033	0.0025	0.0002	0.0025	0.0057
K11B+Kd11B-r11B	15	0.0019 – 0.0032	0.0025	0.0002	0.0025	0.0057
K11C+Kd11C-r11C	15	0.0020 – 0.0033	0.0025	0.0002	0.0025	0.0057
K13A+Kd12A-r12A	30	0.0020 – 0.0032	0.0025	0.0002	0.0025	0.0057
K13B+Kd12B-r12B	30	0.0020 – 0.0033	0.0025	0.0002	0.0025	0.0057
K13C+Kd12C-r12C	30	0.0019 – 0.0032	0.0025	0.0002	0.0025	0.0057
K31A+Kd31A-r21A	15	0.0014 – 0.0047	0.0025	0.0004	0.0025	0.0299
K31B+Kd31B-r21B	15	0.0013 – 0.0044	0.0025	0.0004	0.0025	0.0299
K31C+Kd31C-r21C	15	0.0014 – 0.0048	0.0025	0.0004	0.0025	0.0299
K33A+Kd32A-r22A	30	0.0015 – 0.0043	0.0025	0.0004	0.0025	0.0299
K33B+Kd32B-r22B	30	0.0015 – 0.0047	0.0025	0.0004	0.0025	0.0299
K33C+Kd32C-r22C	30	0.0013 – 0.0043	0.0025	0.0004	0.0025	0.0299

3.2. Groundwater flow and contaminant transport simulation model

In this study, BIO2D-KE (Culver et al., 1996; Earles, 1996), a two-dimensional, depth averaged, finite element groundwater flow and contaminant transport model was used as the simulation model. It can simulate the advective and dispersive transport of contaminants that may undergo abiotic and/or biotic degradation and equilibrium and/or kinetic sorption. In this study biodegradation was assumed to be negligible with respect to advection, dispersion, and sorption for the fate and removal of the contaminant. This provided a more conservative approach since biodegradation helps P&T remediation by decreasing the amount of contaminant mass present in the aquifer. The outputs from the model are the hydraulic heads and contaminant concentrations. It was assumed that the hydrological system responds quickly and reaches a steady state within a pumping period. Therefore, within a pumping period, the steady state, saturated flow is described by the following equation:

$$\frac{\partial}{\partial x} \left(T \frac{\partial H}{\partial x} \right) + Q_w = 0 \quad (3.5)$$

where T = transmissivity [L^2/T]; H = hydraulic head [L]; and Q_w = well flow rate [L^3/T].

In addition to groundwater flow, BIO2D-KE can also simulate the contaminant transport by assuming that the transport of contaminant is governed by advection, dispersion and sorption. In order to describe the mass transfer limited sorption process, the two-site model is used. The details about the two-site sorption concept are given in Section 2.2. As a result, the governing equation for solute transport undergoing rate-limited sorption is expressed with the following equation which is equal to the combination of Equations 2.3 and 2.4.

$$b_s(n + \rho_b f K_d) \frac{\partial C}{\partial t} = b_s D n \frac{\partial^2 C}{\partial x^2} - b_s v n \frac{\partial C}{\partial x} - b_s \alpha \rho_b [(1-f) K_d C - S_k] \quad (3.6)$$

where b_s = saturated aquifer depth [L]; and S_k = mass of contaminant sorbed kinetically per unit mass of soil [M/M].

Before starting the model runs, the simulation model was checked for numerical accuracy according to two criteria (dimensionless numbers) and some model parameters were selected based on them. The first criterion is the “Peclet Number”, which determines the dominance of advective and dispersive fluxes. A grid Peclet number for the two coordinate directions are (Kinzelbach, 1986)

$$Pe_x = (v_x \Delta x) / D_{xx} = (v_x \Delta x) / v_x \alpha_L = \Delta x / \alpha_L \quad (3.7)$$

$$Pe_y = (v_y \Delta y) / D_{yy} = (v_y \Delta y) / v_y \alpha_T = \Delta y / \alpha_T \quad (3.8)$$

where $Pe_{x,y}$ = the grid Peclet number in x and y directions, respectively [-]; $v_{x,y}$ = velocity of groundwater in x and y directions [L/T]; $\Delta x, \Delta y$ = size of the element in x and y direction [L]; $D_{xx,yy}$ = dispersion coefficient [L^2/T]; and $\alpha_{L,T}$ = longitudinal and transverse dispersivities [L].

To avoid numerical problems Pe should be kept smaller than 2 everywhere in the simulation domain (Huyakorn and Pinder, 1983; Kinzelbach, 1986), although some references say that Pe smaller than 4 is also acceptable (Campbell et al., 1981; Anderson and Woessner, 1992). In this study, the size of the elements, Δx and Δy , are selected as 7.5 m. In order to keep Pe smaller than 2 in y-direction, α_T was taken as 4 m. Since α_L can be 5-20 times bigger than α_T (Freeze and Cherry, 1979) α_L was taken as 20 m. According to Kinzelbach (1986), to control numerical dispersion, the size of elements should not exceed α_L . By taking α_L as 20 m, this condition was also satisfied.

The “Courant Number” which should be satisfied in the selection of the time step, Δt , is the second criterion. The Courant number for the two coordinate directions is (Kinzelbach, 1986)

$$Co_x = | \Delta t v_x / \Delta x | \quad (3.9)$$

$$Co_y = | \Delta t v_y / \Delta y | \quad (3.10)$$

where $Co_{x,y}$ = Courant numbers in x and y directions, respectively [-]; and Δt = time step [T].

In physical terms, the criterion says that “not more pollutant mass can leave the cell via convection (advection) during the time interval $[t, t+\Delta t]$ than is inside it at the beginning of the time interval” (Kinzelbach, 1986). This means that Co should be smaller than 1 (Huyakorn and Pinder, 1983; Kinzelbach, 1986; Anderson and Woessner, 1992). In order to satisfy this criterion, several model simulations were performed under the pumping conditions expected to occur during simulation optimization model runs with changing time steps. According to the results of these simulations, Δt was selected as 1 day.

3.3. Problem Description

The aquifer for which the simulation-optimization model was applied is a confined aquifer with the dimensions of 300 m \times 300 m. 1600 uniform square elements with 1681 grid points were used to discretize it. Constant head boundaries of 35.0 and 33.0 m on the west and east sides of the aquifer, respectively, form a steady flow in the east direction. No-flow conditions existed on the north and south boundaries. This aquifer configuration is commonly used in groundwater remediation research (Huang and Mayer, 1997; Hsiao and Chang, 2002; Aksoy and Culver, 2004; McKinney and Lin, 1996; Morgan et al., 1993; Ricciardi et al., 2007; Chan Hilton and Culver, 2005; Guan and Aral, 1999; Uçankuş and Ünlü,

2008). The bottom of the aquifer had a 1% slope from west (d = 61m) to east (d = 64m). Constant concentration (0 mg/L) boundaries were used on the east and west sides of the aquifer. The physical properties of the aquifer are given in Table 3.7.

Table 3.7. Aquifer physical properties

Parameter	Value
K_g (m/s)	4.5×10^{-5}
Longitudinal dispersivity, α_L (m)	20
Transverse dispersivity, α_T (m)	4
Saturated thickness, b_s (m)	30.5
Effective porosity, n	0.2
Soil bulk density, ρ_b (g/cm ³)	1.81

PCE, a chlorinated organic compound, was selected as the contaminant to be used in this study. PCE is the second most frequently treated contaminant by P&T remediation at Superfund sites in the United States after TCE (USEPA, 2007). Several long-term transport and sorption field studies, such as at the Borden site, have shown that PCE can be fairly conservative at the field scale (Roberts et al., 1986; Harmon and Roberts, 1994; Cushey and Rubin, 1997; Brusseau and Srivastava, 1997).

Initial PCE plumes were generated by BIO2D-KE simulating a continuous area source over a period of 7 years with a peak concentration of 30 mg/L. Contamination source is assumed to be removed before remediation period starts. Equilibrium sorption with a K_d value of 0.36 cm³/g was assumed during the plume generation simulations. Assuming that site characterization has been completed and that a contaminant transport simulation model has been calibrated to the initial conditions of the plume, PCE plume was generated for each heterogeneous K-field

(Section 3.1.1) separately, resulting in 27 different PCE plumes. Then, a single PCE plume was created by taking the average of these 27 plumes. This averaging approach was used in previous studies in literature (Aksoy and Culver, 2004; Chan Hilton and Culver, 2005). Both the plumes which have been originally generated for each heterogeneous K-field and the single plume which is the average of all 27 different plumes were used as the initial concentration conditions for the optimization model runs. The former is called as the “original plume” while the latter is named as the “average plume”. The average plume used in the model runs is presented in Figure 3.10 while the plumes for 27 different heterogeneous fields are shown in Figures 3.11 to 3.13. Non-equilibrium sorption was assumed during the simulation-optimization model runs.

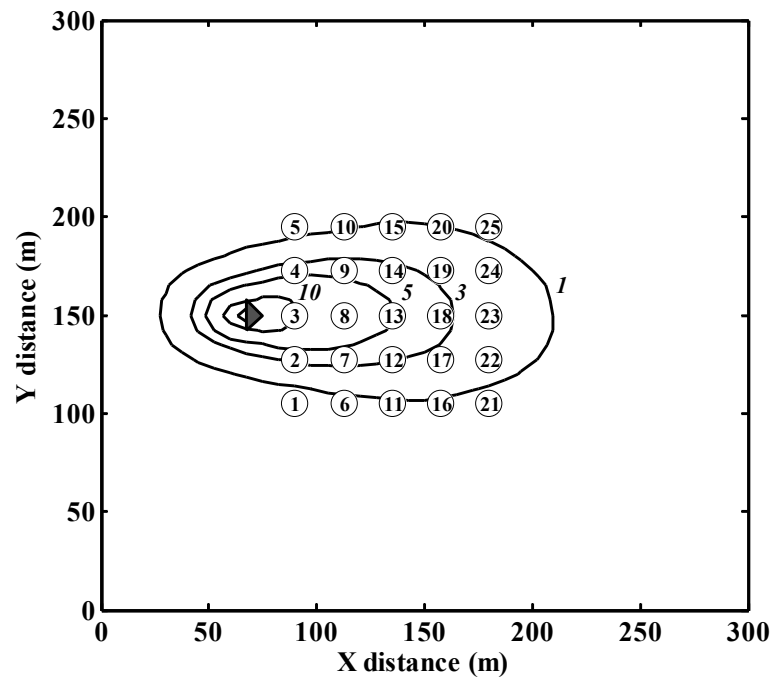


Figure 3.10. The average plume used in the optimization model runs (Triangular area shows the contamination source, circles depict the potential well locations and the numbers for the optimization runs)

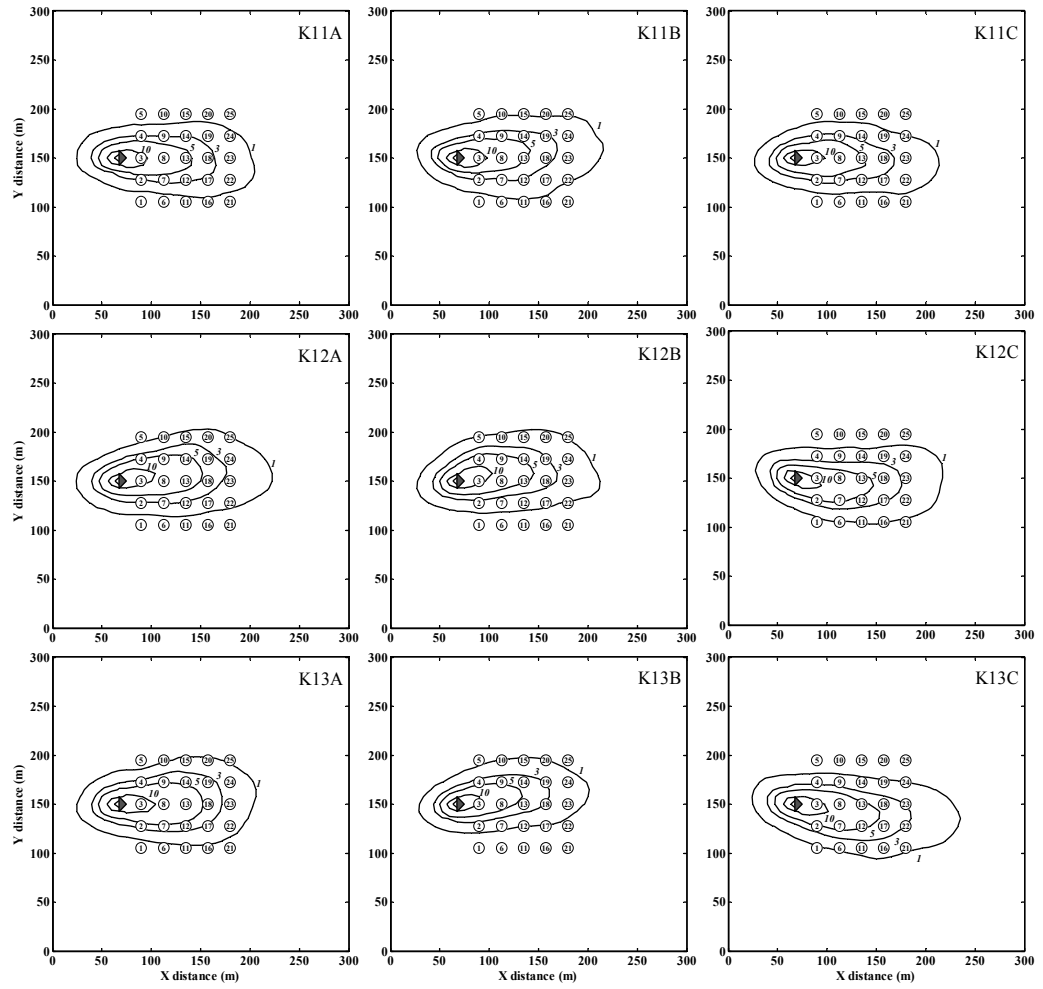


Figure 3.11. PCE plumes for the heterogeneous fields K11A, K11B, K11C, K12A, K12B, K12C, K13A, K13B and K13C

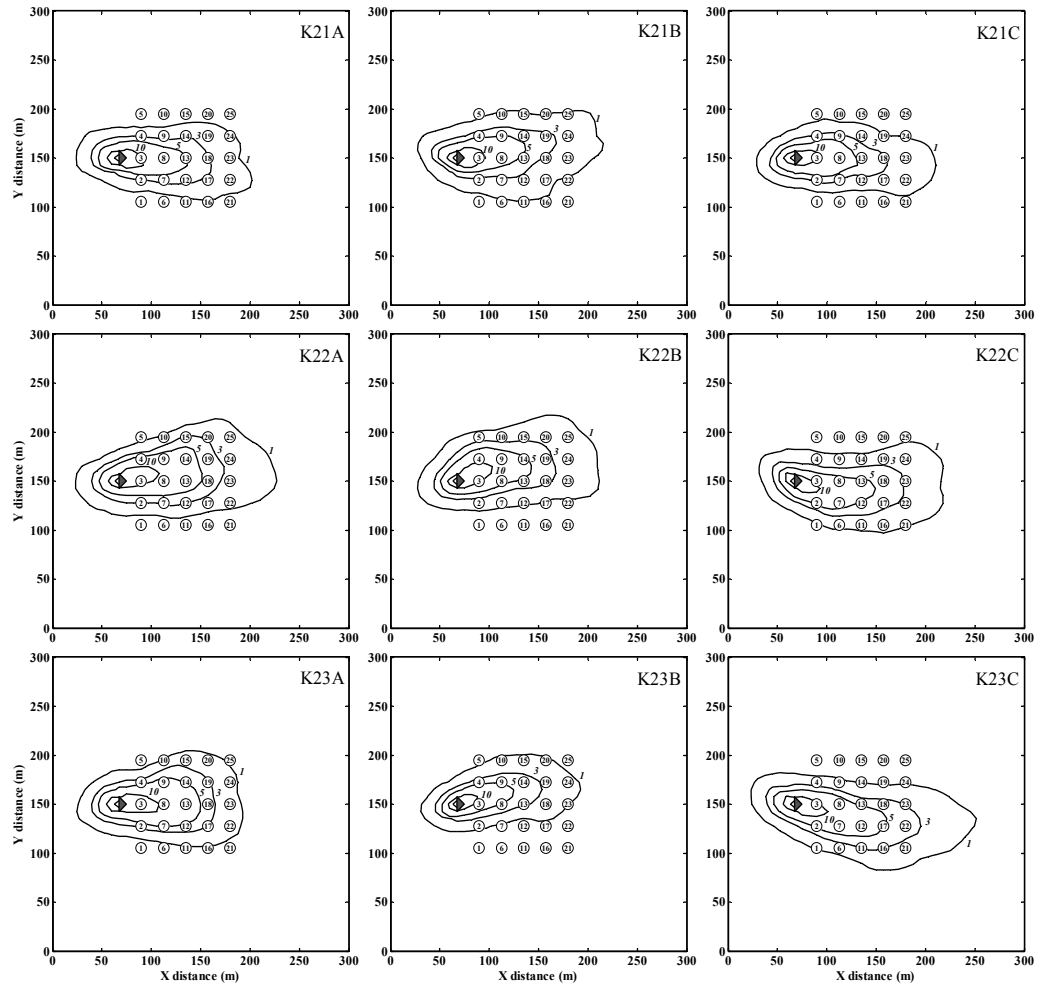


Figure 3.12. PCE plumes for the heterogeneous fields K21A, K21B, K21C, K22A, K22B, K22C, K23A, K23B and K23C

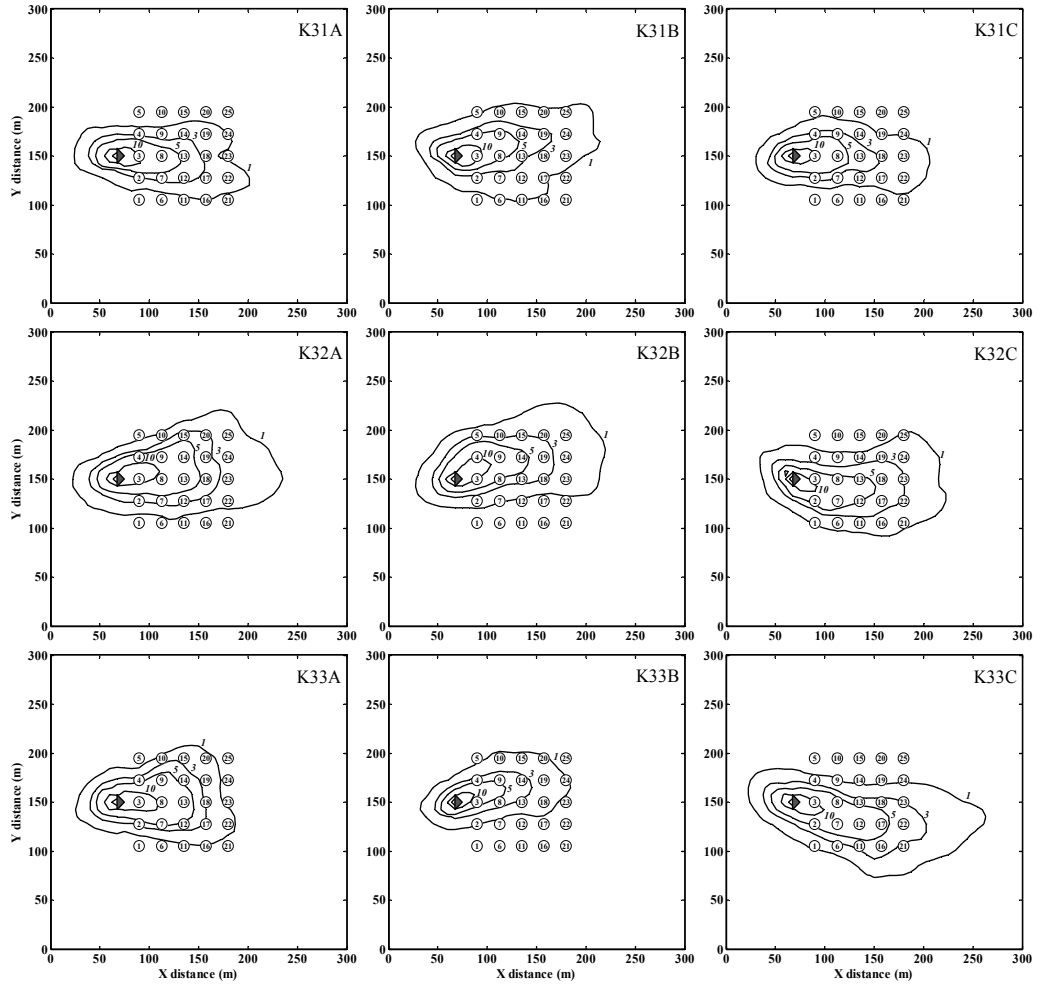


Figure 3.13. PCE plumes for the heterogeneous fields K31A, K31B, K31C, K32A, K32B, K32C, K33A, K33B and K33C

After creating the PCE plumes, the representative center point of the PCE plume mass, called as the center of mass (CoM), for both original plumes and average plume was calculated. CoM can be described as the first moment of inertia of the mass at each sampling location within the plume about specified x and y axes (Hyman and Dupont, 2001). Here, in this study, every single grid point on the aquifer area was taken as a sampling point for the calculation of CoM. The CoM

of the plumes was calculated using the Equations (3.11) and (3.12) (Hyman and Dupont, 2001). Then, a line was drawn between the source and the CoM in order to find the centerline of the plume.

$$X = \frac{\sum_{i=1}^{GP} x_i \times \text{mass}_i}{\sum_{i=1}^{GP} \text{mass}_i} \quad (3.11)$$

$$Y = \frac{\sum_{i=1}^{GP} y_i \times \text{mass}_i}{\sum_{i=1}^{GP} \text{mass}_i} \quad (3.12)$$

where X = x coordinate of the CoM; Y = y coordinate of the CoM; x_i = x coordinate of the grid point i ; y_i = y coordinate of the grid point i ; and mass_i = amount of contaminant mass at grid point i .

The total amount of mass over the aquifer area was calculated as follows:

$$\sum_{i=1}^{GP} \text{mass}_i = \sum_{i=1}^{GP} A_i \times b_s \times ((C_i \times n) + (C_i \times K_d \times \rho_b)) \div 1000 \quad (3.13)$$

where A_i = Surface area associated with each grid point ($3.75 \times 3.75 \text{ m}^2$ for corner grid points, $7.5 \times 3.75 \text{ m}^2$ for side grid points and $7.5 \times 7.5 \text{ m}^2$ for inside grid points).

3.4. Optimization Model

In this study, the simulation-optimization approach is used. GA were selected as the optimization method while PGAPack (Levine, 1996), a GA library, was used as an optimization model. In general, there are two sets of variables in a P&T remediation system: decision variables and state variables. Decision variables,

which can be specified and controlled by the system engineer, include well locations, number of the wells, pumping rates, length of the remediation period and the treatment technology capacity. The state variables are the hydraulic head and the solute concentration where the former is a dependent variable in the groundwater flow equation, and the latter is a dependent variable in the transport equation (Wang and Zheng, 1997; Aksoy and Culver, 2004). In the simulation-optimization approach, decision variables which are assigned by the optimization model are used as inputs into the simulation model in order to update the state variables. In this study, PGAPack, the GA library, selects the candidate values for the decision variables and sends them to BIO2D-KE. BIO2D-KE evaluates the response of the aquifer to the specified decision variables and reflects in the values of the state variables. Then, the fitness of the policy under consideration is evaluated through an objective function which is dependent on both the decision variables and the state variables returned by the simulation model. Figure 3.14 represents simulation-optimization approach schematically using one of the optimization models of this study as an example.

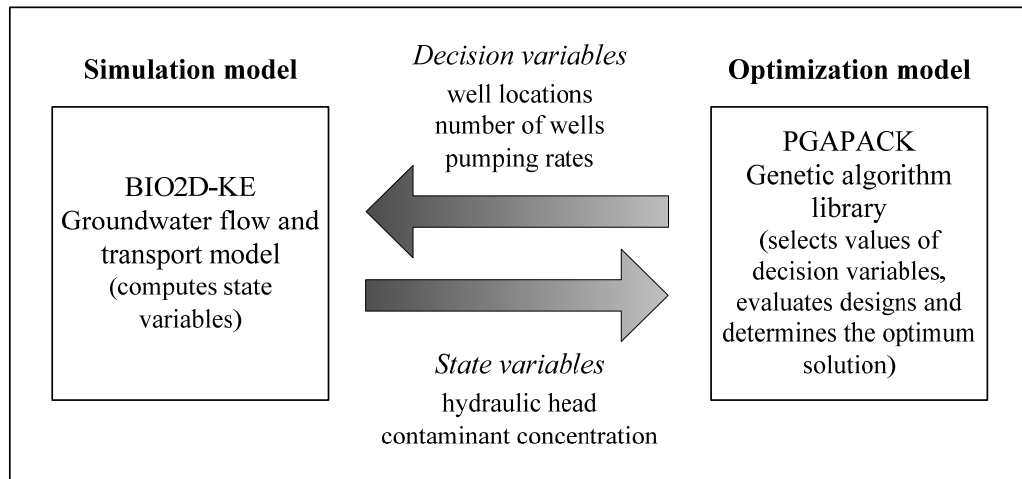


Figure 3.14. Schematic diagram of the simulation-optimization approach (adapted from Ko et al., 2005)

In this study, two different optimization models were used: the optimal design model and the time-to-compliance model. The optimal design model was used in every step of this study with all kinds of heterogeneous fields while time-to-compliance model was just used for the optimization model runs conducted for cases of K heterogeneity only.

3.4.1. The Optimal Design Model

The aim of the optimal design model is to find the best P&T remediation policy with the minimum cost, including the operating and the capital costs, within a fixed management time while satisfying the specified constraints. The decision variables are the well locations, the number of the wells and the pumping rates. In order to cleanup the contaminated aquifer, 25 candidate pumping wells were placed arbitrarily to cover the plume area of relatively higher contaminant concentrations (Figures 3.10 to 3.13). The distance between the wells is 22.5 m in both x and y direction. GA determines the active pumping well(s) by the help of a pointer which is 1 if a well is active and 0 if it is inactive. In order to reduce the computational demand, it was assumed that active pumping wells operate at the same pumping rate. The details of this GA procedure will be given later in this section. Remediation (management) time was selected as 1260 days (Aksoy and Culver, 2004). GAC, the second most common P&T aboveground treatment technology after air stripping (USEPA, 2004), was used to treat the contaminated groundwater on the ground.

The constraints for the optimal design model are:

- upper bound on the maximum aqueous concentration in the aquifer at the end of the remediation time,
- upper bound on the maximum total concentration in the aquifer at the end of the remediation time,

- upper bound on the maximum allowable hydraulic head decline, and
- upper and lower bounds for pumping rates.

The optimization model adapted from Aksoy and Culver (2004) is mathematically expressed as

$$\text{Minimize}_{Q_z, I_z} \left[C_{\text{pump}} + \sum_{t=1}^{ST} C_{\text{carbon},t} + \sum_{e=1}^E C_{\text{capwell},e} + C_{\text{captreat}} \right] \times [1 + \text{Pen}] \quad (3.14)$$

where;

$$C_{\text{pump}} = \frac{0.002725 S_p t_m}{\varepsilon} \sum_{e=1}^E [Q_e (H_z - h_e + 0.7 \text{Pa})] \quad (3.15)$$

$$C_{\text{carbon},t} = \frac{S_c t_s}{d_c} \beta(C_t)^\eta Q_{\text{tot}} \quad (3.16)$$

$$C_{\text{capwell},e} = 5,543 I_z (d_z)^{0.299} \quad (3.17)$$

$$C_{\text{captreat}} = A n_{\text{ads}} \quad (3.18)$$

$$n_{\text{ads}} = \text{integer} \left[\left(\frac{t_a}{V_a} Q_{\text{tot}} \right) + 0.5 \right] \quad (3.19)$$

$$Q_{\text{tot}} = \sum_{e=1}^E Q_e \quad (3.20)$$

$$C_t = \frac{1}{Q_{\text{tot}}} \sum_{e=1}^E Q_e \left(\frac{C_{e,t0} - C_{e,t1}}{2} \right) \quad (3.21)$$

$$\text{Pen} = \frac{\text{Equation 3.25}}{\sum_{b=\text{Equation 3.23}} \omega_b v_b} \quad (3.22)$$

subject to;

$$C_{aq \max} \leq C_{aq}^* = 1 \text{ mg/L} \quad (3.23)$$

$$C_{tot \max} \leq C_{tot}^* = C_{aq}^* (K_d \rho_b + n) = 0.852 \text{ mg/ (L aquifer)} \quad (3.24)$$

$$\text{Max } |h_{o, gp} - h_{f, gp}| \leq 15 \text{ m; } gp = 1, \dots, GP \quad (3.25)$$

$$0.0 \leq Q_z \leq 691.2 \text{ m}^3/\text{day}; z \in Z \quad (3.26)$$

where C_{pump} = pumping operational costs for management period [\$]; $C_{carbon,t}$ = operational cost of GAC treatment facility during simulation time step t [\$]; $C_{capwell,z}$ = capital and installation cost for well z [\$]; $C_{captreat}$ = capital cost of GAC adsorbers [\$]; Z = total number of potential pumping wells [-]; E = total number of active pumping wells [-]; ST = total number of simulation time steps [-]; t_m = length of management period m [T]; Q_e = volumetric pumping rate at active well e [L^3/T]; Q_z = volumetric pumping rate at potential well z [L^3/T]; h_e = hydraulic head relative to well depth at end of management period m at pumping well e [L]; t_s = length of simulation time step [T]; d_z = depth of well z [L]; C_t = weighted average influent concentration to adsorbers for simulation time step t [M/L^3]; Q_{tot} = total pumping rate during management period [L^3/T]; n_{ads} = number of adsorbers required for treatment system [-]; $C_{e,t0}$ = aqueous contaminant concentration at pumping well e at beginning of simulation time step t [M/L^3]; $C_{e,t1}$ = aqueous contaminant concentration at pumping well e at end of simulation time step t [M/L^3]; I_z = pointer [=1 if well is active, =0 if well is inactive]; GP = number of grid points [-]; $h_{o, gp}$ = initial head at grid point gp [L]; $h_{f, gp}$ = final head at grid point gp [L]; C_{aq}^* = aqueous concentration goal [M/L^3]; C_{tot}^* = total concentration goal [M/L^3 aquifer]; $C_{aq \max}$ = maximum aqueous concentration in aquifer at end of remediation period [M/L^3]; $C_{tot \max}$ = maximum total concentration in aquifer at end of remediation period [M/L^3 aquifer]; Pen = total penalty due to constraint violations; ω_b = constraint weight on b^{th} constraint; and v_b = constraint violation on b^{th} constraint.

The descriptions of other parameters associated with the GAC cost and design are given in Table 3.8. The cost and design parameters in Table 3.8 are based on

Culver and Shenk (1998) while Freundlich isotherm parameters for PCE are from the study of Faust and Aly (1987). Equation 3.26 is not included in the penalty function as its violation is impossible since the pumping rate is one of the decision variables of the model and the range of values the pumping rate can get is defined by the user. The total concentration constraint (Equation 3.24) equalizes the maximum total concentration to the total concentration in the aquifer when the system is in equilibrium with the maximum allowable aqueous concentration. This approach helps the selection of a remediation policy which prevents concentration rebound after remediation ceases (Aksoy and Culver, 2000).

Table 3.8. Granulated activated carbon cost and design parameters

Coefficient	Value
Energy cost, S_p (\$/kWh)	0.07
Wire to pump efficiency, ϵ	0.5
Depth to datum, H_z (m)	61
Pressure required for adsorber, Pa (psi)	15
Fraction of carbon used at time of removal, d_c	0.9
Carbon cost coefficient, S_c (\$/kg)	2.2
Cost per adsorber unit, A (\$/unit)	100,000
Freundlich isotherm coefficient for PCE-carbon, β	0.017
Freundlich isotherm exponent for PCE-carbon, η	0.52
Required contact time, t_a (min)	15
Pore volume of adsorber, V_a (m ³)	20

For the handling of constraint violations, the multiplicative penalty method was used (Chan Hilton and Culver, 2000). This approach was shown to be a robust method for constraint enforcement in GA applications for groundwater remediation problems. In this method, a penalty factor was calculated in proportion to the magnitude of the violations of each constraint. Actual cost was then multiplied by this factor given below

$$\text{Pen} = \sum_{b=1}^B \omega_b v_b \quad (3.27)$$

$$v_b = \max[0, g_b(x) - B_b] \quad (3.28)$$

where B = total number of constraints; B_b = constant constraint bound for constraint b ; and $g_b(x)$ = value corresponding to the violation in b^{th} constraint.

If there is no constraint violation, then the total cost of the potential policy would be equal to the true value of the evaluation cost function. Otherwise, the cost will be increased by a factor of $(1+\text{Pen})$ as shown in Equation 3.14. In this study, the constraint weights for each constraint, ω_b , were selected as 50 based on the study of Aksoy (2000).

The GA steps followed by optimization model PGAPack are as follows:

- First, a set of decision variables represented by an initial population of strings is created randomly. The population size was selected as 120 as a result of a sensitivity analysis. Binary representation in which the bits of strings are shown as 1s and 0s was used for the representation of the decision variables. The length of an individual string is determined according to the number of decision variables as well as discretization of these variables. In the optimal design model, it is assumed that there are 25 candidate wells to remediate the contaminated aquifer and active wells pump at the same rate. Thus, a single decision variable, represented by the first 6 bits in a GA string, was used for the pumping rate. The next 25 bits were the pointers that specify whether a candidate well is active or not. The pointer value “1” represents an active well pumping with the rate determined by the first 6 bits of GA string. On the other hand, the pointer value “0” shows that the candidate well is not active. Therefore, each individual GA string has 31 bits (Figure 3.15).

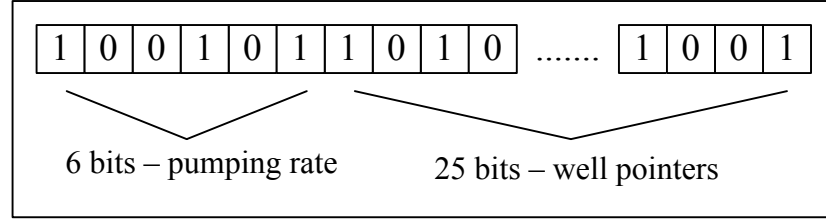


Figure 3.15. Representation of a GA string

The translation of a string value to the actual value of the decision variable (in this case, pumping rate) is performed as follows. First, the number of possible pumping rates for the decision variable is calculated by

$$N_y = 2^{k_y} \quad (3.29)$$

where N_y = number of possible values; and k_y = length of the string for decision variable y .

For this study, $2^6 = 64$ different pumping rates could be considered. Then the translation could be performed according to the following formula

$$x_y = x_y^{\min} + j \frac{(x_y^{\max} - x_y^{\min})}{N_y - 1} \quad j = 0, \dots, N_y - 1 \quad (3.30)$$

where x_y = value of the decision variable y ; x_y^{\max} = maximum value of the decision variable y ; x_y^{\min} = minimum value of the decision variable y ; and j = integer indicating the j^{th} possible value for the decision variable y .

In this study, coding of the bits in a binary string to an integer value, in other words calculation of the value of j , is done in two different ways. The first method is the “binary coding” in which a binary string is decoded into an integer $m \in [0, N_y - 1]$ according to

$$m = \sum_{i=1}^{k_y} b_i 2^{i-1} \quad (3.31)$$

where b_i = the value of the i^{th} bit.

In this method, binary representations of two numbers may be far from each other although they are contiguous in their decimal representations. For example, 7 and 8 are two consecutive integers but their four-bit binary representations, 0111 and 1000 respectively, differ in the maximum number of bit positions (the far left of the string). This may decrease the probability of convergence to the most optimal solution and affect the performance of GA. In order to overcome this problem another method of coding, called as the “Gray code” or sometimes as the “reflected binary code”, was used. Gray code uses different, and may be a preferable (Reeves and Rowe, 2003), mapping of binary strings to an integer value than given by Equation 3.31 such that only one bit changes between subsequent numbers. The code is called as reflected since it can be generated by reflecting the bits. Reflection is done by listing the original bits in reverse order and coupling the reversed bits to the original ones. Then a binary 0 and binary 1 are added as a first bit to the original and reflected bits, respectively (Wilf, 1989). The schematic demonstration of this process is given in Figure 3.16. More details about Gray coding can be found in Wilf (1989).

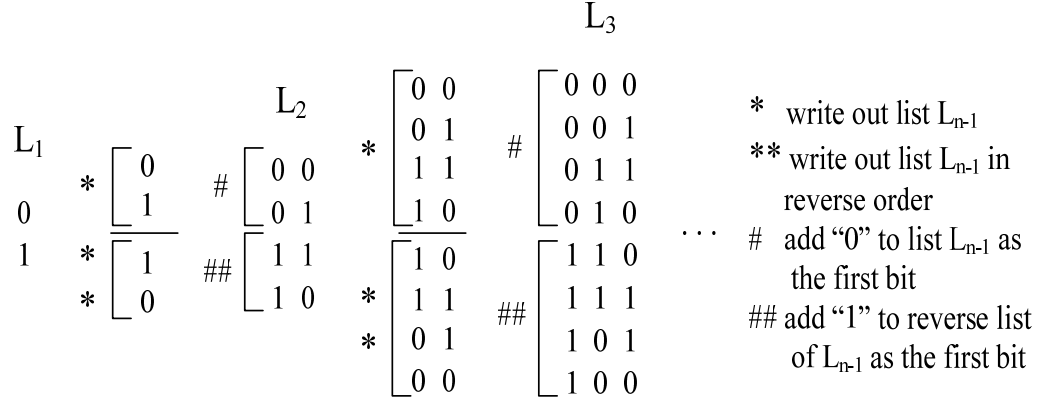


Figure 3.16. Demonstration of the method for the generation of Gray code

Table 3.9 shows the mapping of the integers 0 to 15 with both binary coding and Gray code representations. Gray coding is known to overcome the problem of “Hamming cliffs” which is observed in binary coding. The distance between two strings is measured by Hamming distance which can simply be defined as the number of bits that differ. The Hamming distance is always one in Gray coding. This means that if two adjacent integers are represented bitwise, there will be a single bit difference. However, for binary coding, there are Hamming cliffs where all bits change with a change of one unit in the integer value. In other words, in binary coding complementary bits can represent adjacent integers. For example, binary representations of 7 (0111) and 8 (1000) are complements of each other (Mathias and Whitley, 1994; Rowe et al, 2004; Chakraborty and Janikow, 2003).

- Next, the initial population of strings is evaluated via the objective function and the constraints in order to find the fitness of the policies represented by the strings. A ranking fitness value is given to each string based on its evaluation value. A specified number of strings with the best fitness values are always

Table 3.9. Binary coding and Gray code representations of the integers 0 to15
(Wilf, 1989)

m	Binary coding	Gray code	m	Binary coding	Gray code
0	0000	0000	8	1000	1100
1	0001	0001	9	1001	1101
2	0010	0011	10	1010	1111
3	0011	0010	11	1011	1110
4	0100	0110	12	1100	1010
5	0101	0111	13	1101	1011
6	0110	0101	14	1110	1001
7	0111	0100	15	1111	1000

copied to the new generation to preserve the good solutions in the population for longer than one generation. This approach used in this study is called an “elitist approach”. According to the results of a sensitivity analysis on convergence, this number was chosen as 10% of the initial population, which was 12. After the ranking process, the selection process begins. Tournament selection was chosen as the selection method. In this method, two strings are selected randomly and the one with the better ranking fitness value is copied into a temporary mating pool as a parent string in order to be used in the crossover operation (Dumitrescu et al., 2000). This procedure is repeated until the number of strings in the temporary mating pool reaches the desired number of replacement strings.

- The selection process is followed by crossover to exchange the bits between two strings. In this study, uniform crossover with 50% crossover probability was selected since it outperformed two-point crossover in the sensitivity analysis for convergence. The detailed results of the sensitivity analysis are given in Section 4.1. Two-point crossover is an enhancement over the one-point crossover in which a single bit position was considered for information swapping. Two-point crossover supplied enhanced diversity in the population.

Providing that a template identifying the similarities at certain bit positions among strings is referred to as the “schema” (Holland, 1975), one-point crossover may not combine all possible schemas in a search. Moreover, one-point crossover may destroy the schemas with long defining lengths (Mitchell, 1996). This situation was called as the “positional bias” by Eshelman et al. (1989). Two-point crossover, on the other hand, may have less probability of breaking the schemas with long defining lengths and higher probability of combining more schemas. However, it is not free of positional bias. Conversely, uniform crossover provides no positional bias. Yet, uniform crossover may be computationally intensive (Mitchell, 1996; Ashlock, 2000). In two-point crossover, two locations are determined on parent strings and the bits between these crossover sites are exchanged (Figure 3.17(a)). In uniform crossover, each bit position of the two parent strings are considered for information swapping based on a randomly generated crossover mask. If the mask value for the corresponding bit location in the string is 1, then the bits of the parents are not swapped. However, if it is 0, the bits at the corresponding locations are exchanged (Chipperfield, 1997). An example application is depicted in (Figure 3.17(b)). Strings that do not undergo crossover will also be the members of the next generation without any modification unless they are subject to mutation.

- After crossover, the mutation process is operated with a certain probability and some of the bits on the strings are altered. The aim of mutation is to maintain population diversity and minimize premature convergence to a local minimum. Mutation probability is generally applied with a low percentage, 1% to 4% (Wang and Zheng, 1997). In this study it was employed as 3% according to the sensitivity analysis on convergence. The mutation results in a new generation of strings with the same number of strings as the previous generation.

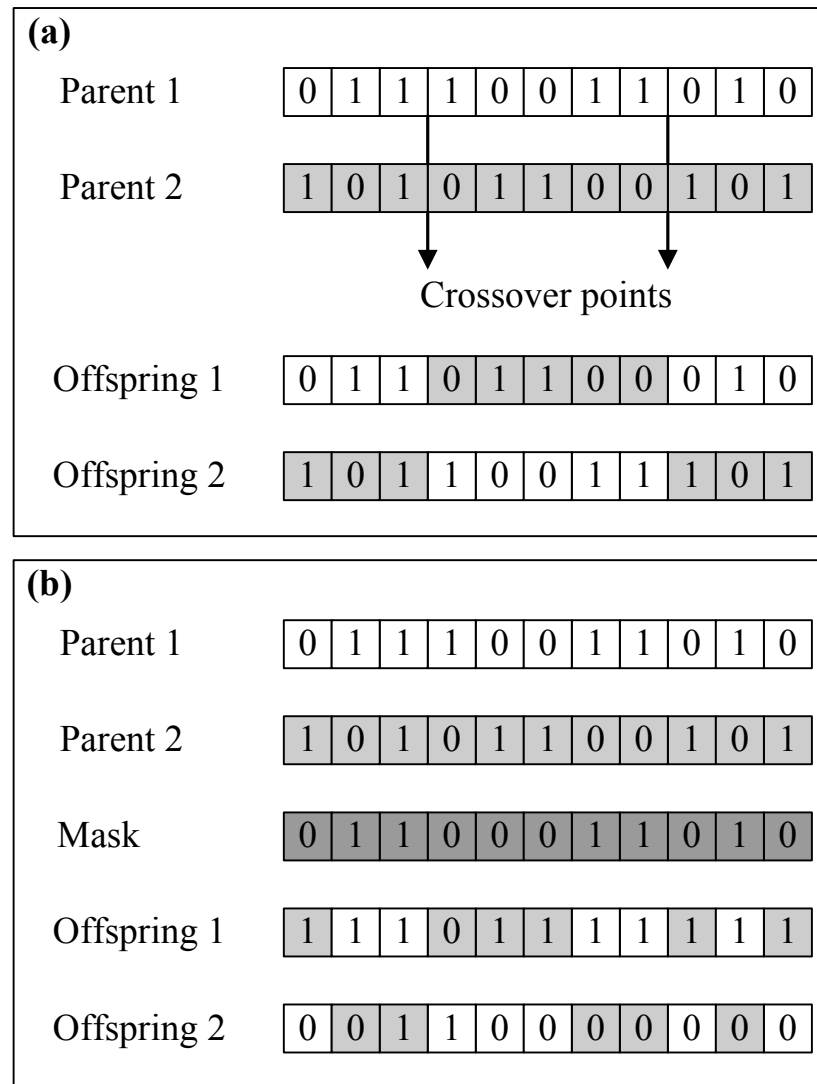


Figure 3.17. Schematic representation of (a) two-point crossover (b) uniform crossover

- All of the above steps, except the random generation of the initial population, are repeated until a stopping criterion is satisfied (Figure 2.4). For this study, it was set to no change after 30 consecutive generations. This means that the GA procedure is terminated if there is no change in the value of the best evaluation after 30 consecutive generations.

For the optimal design model, the best solution obtained among at least 5 replicates is regarded as the optimal policy for a given problem. This approach is used since the GA is a random search method and under the complexity of the optimization problem studied, the possibility of convergence to a local minimum exists.

3.4.2. The Time-to-Compliance Model

The second optimization model employed in this study is the time-to-compliance model which focuses on finding the shortest remediation time to reach the target water quality criteria with a fixed remediation scheme. In this model, the objective function aims to minimize the capital and operational costs of P&T remediation system with a single decision variable which is the length of the remediation period while satisfying the constraints on the aqueous and total PCE concentration and allowable hydraulic head decline in the aquifer. This optimization model was applied for the fields with K heterogeneity only.

In order to cleanup the aquifer contaminated with PCE, two different remediation schemes were considered in order to compare the effect of the selection of the well locations and pumping rates on the optimal cleanup time. First scheme, called as the “7-well-policy”, consists of seven different wells (wells 3, 7, 9, 13, 17, 19 and 23) spread over the contaminant plume. The wells pump at a flow rate of 25 m³/day each where the total pumping rate equals to 175 m³/day. The second scheme, called as the “1-well-policy”, includes a single well (well 13) pumping at a flow rate of 175 m³/day. Therefore, the total pumping rate for these two different remediation schemes considered for the time-to-compliance model are the same. The locations of the wells are shown in Figure 3.18 on the average plume as an example. For this model, the maximum candidate remediation period is 7156 days or approximately 20 years. Similar to the optimal design model, GAC was selected as the aboveground treatment method.

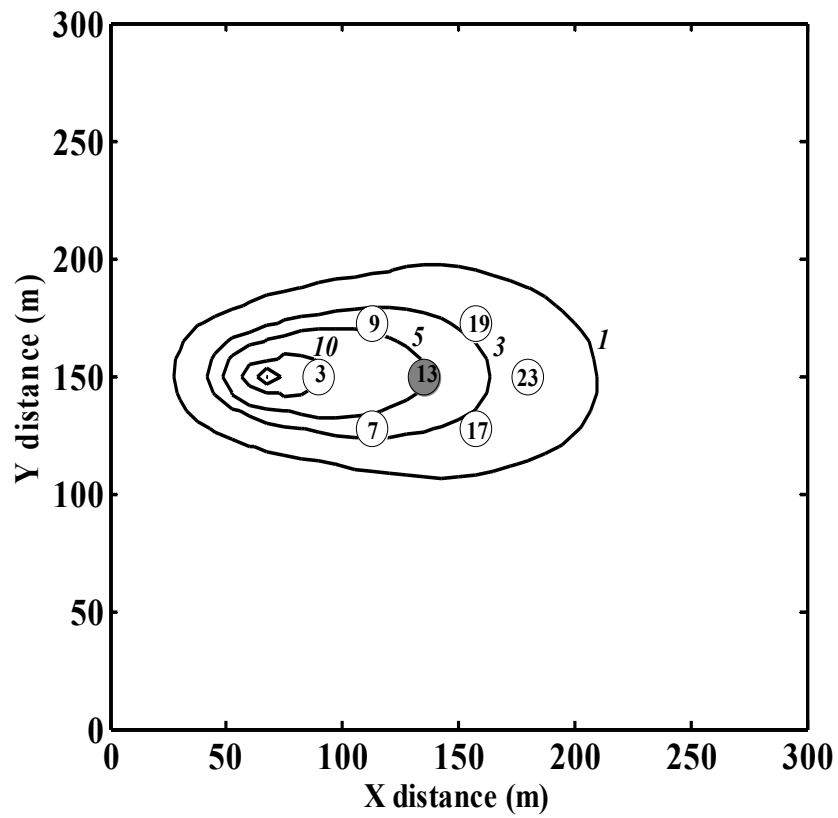


Figure 3.18. Well locations for 1-well (gray shaded circle) and 7-well (gray and white shaded circles) policies used for the time-to-compliance model along with the average plume

The constraints for the time-to-compliance model are:

- upper bound on the maximum aqueous concentration in the aquifer at the end of the remediation time,
- upper bound on the maximum total concentration in the aquifer at the end of the remediation time,
- upper bound on the maximum allowable hydraulic head decline,
- upper and lower bounds for remediation time.

The mathematical expression of the time-to-compliance optimization model is

$$\text{Minimize}_{t_m} \left[C_{\text{pump}} + \sum_{t=1}^{ST} C_{\text{carbon},t} + \sum_{e=1}^E C_{\text{capwell},e} + C_{\text{captreat}} \right] \times [1 + \text{Pen}] \quad (3.32)$$

where;

$$C_{\text{pump}} = \frac{0.002725 S_p t_m}{\varepsilon} \sum_{e=1}^E [Q_e (H_z - h_e + 0.7 \text{Pa})] \quad (3.33)$$

$$C_{\text{carbon},t} = \frac{S_c t_s}{d_c} \beta(C_t)^n Q_{\text{tot}} \quad (3.34)$$

$$C_{\text{capwell},e} = 5543 (d_e)^{0.299} \quad (3.35)$$

$$C_{\text{captreat}} = A n_{\text{ads}} \quad (3.36)$$

$$n_{\text{ads}} = \text{integer} \left[\left(\frac{t_a}{V_a} Q_{\text{tot}} \right) + 0.5 \right] \quad (3.37)$$

$$Q_{\text{tot}} = \sum_{e=1}^E Q_e \quad (3.38)$$

$$C_t = \frac{1}{Q_{\text{tot}}} \sum_{e=1}^E Q_e \left(\frac{C_{e,t0} - C_{e,t1}}{2} \right) \quad (3.39)$$

$$\text{Pen} = \frac{3.43}{\sum_{b=3.41} \omega_b v_b} \quad (3.40)$$

subject to;

$$C_{\text{aq max}} \leq C_{\text{aq}}^* = 1 \text{ mg/L} \quad (3.41)$$

$$C_{\text{tot max}} \leq C_{\text{tot}}^* = C_{\text{aq}}^* (K_d \rho_b + n) = 0.852 \text{ mg/ (L aquifer)} \quad (3.42)$$

$$\text{Max } |h_{0,\text{gp}} - h_{f,\text{gp}}| \leq 15 \text{ m; gp} = 1, \dots, \text{GP} \quad (3.43)$$

$$1 \leq t_m \leq 7156 \text{ days} \quad (3.44)$$

In time-to-compliance optimization model, since the well locations and pumping rates were selected beforehand, the only decision variable is the length of remediation period (management time) which is represented by a 10-bit string. The first 9 bit encodes the remediation time with a maximum value of 3578 days. The 1-bit code pointer was added as a 10th bit in order to multiply the remediation time with 1 or 2 to be able to get longer remediation periods when necessary. The GA steps followed in the optimal design model are also followed in time-to-compliance model. The GA parameters, such as population size, crossover probability, mutation probability and the methods used in the GA operations, such as tournament selection, uniform crossover, are all the same as for the optimal design model. The few differences in this model are that only Gray coding was used for coding of the binary strings to integer values and the best solution was obtained among the 3 replicates. The number of the replicates decreased because the problem in this model is simpler than the previous one so that GA generally reaches the same result almost in all replicates. Another reason was the computational time needed to reach the best result in time-to-compliance model. Since the remediation times in this model can be much longer than 1260 days, which is the remediation time of the optimal design model, the computational time of a single GA run with this model is longer than that of a single GA run compared to the optimal design model. The discussion about the computational times for both models will be given in Section 4.1.

3.5. Summary of the Main Titles Studied in This Work

3.5.1. Effect of Correlation Scale of K

Optimization runs were performed first assuming only K heterogeneity. Heterogeneous K-fields generated in Section 3.1.1 were used in order to investigate the effect of λ of K heterogeneity on P&T remediation design and cost, and P&T remediation time. For the first analysis, the optimal design model was

used while in the second analysis the time-to-compliance model was employed. Three different $\lambda_{\ln K}$ (15, 22.5 and 30 m) were used at this step. In order to see the effect of $\sigma^2_{\ln K}$ and the relative locations of high and low K zones, these GA runs were repeated for three different $\sigma^2_{\ln K}$ (0.2500, 0.7225 and 1.3225) and three different realizations of K-fields. K_g was kept constant among the heterogeneous K-fields. In addition, optimization runs were performed with both original and average plume in order for the investigation of the effect of initial plume distribution on the results.

3.5.2. Effect of Correlation Scale Anisotropy of K

In order to investigate the effect of λ anisotropy on P&T remediation system design and cost, two different anisotropy conditions were considered in this study. Two different $\sigma^2_{\ln K}$ (0.2500 and 1.3225) of a single realization were used. Only the average plume was used for this step of the study.

3.5.3. Effect of Heterogeneity in K_d

Optimization runs were performed for the heterogeneous K_d -fields generated in Section 3.1.3 in order to investigate the effect of λ of K_d on P&T remediation design and cost. For this purpose the optimal design model was used. Heterogeneous K-fields, selected based on the results of the optimization runs performed in Section 3.5.1, were used in combination with the heterogeneous K_d -fields. Two different $\lambda_{\ln K_d}$ (15 and 30 m) were used at this step. In order to see the effect of σ^2 and relative locations of high and low K_d zones, runs were repeated for three different $\sigma^2_{\ln K_d}$ (0.0256, 0.0740 and 0.1354) and three different realizations of heterogeneous K_d -fields. Two approaches were used. In one of them K_{d_g} was kept constant among the heterogeneous K_d -fields. In the other, K_{d_g} was varied. The detailed descriptions of these approaches will be provided in the relevant

section of Chapter 4. For both approaches, only the average initial plume was considered.

3.5.4. Effect of Correlation between K and K_d

Since both negative and positive correlations between K and K_d are reported in literature (see Section 2.5), the effects of both types of correlation on P&T remediation design and cost were investigated in this study. For this purpose, optimization runs were performed on correlated K_d -fields generated in Section 3.1.4. Two different $\lambda_{\ln K_d}$ (15 and 30 m), three different $\sigma^2_{\ln K_d}$ (0.0256, 0.0740 and 0.1354) and three different realizations were considered. At this step, optimization runs were performed only for the initial average plume.

3.5.5. Effect of Heterogeneity in α

Optimization runs were performed on heterogeneous α -fields generated in Section 3.1.5 in order to study the effect of λ of α on P&T remediation design and cost. For this purpose, the optimal design model was used. Heterogeneous K and K_d -fields, selected based on the results of the runs performed in Section 3.5.1 and 3.5.3, were used in combination with the heterogeneous α -fields. Two different $\lambda_{\ln \alpha}$ (15 and 30 m) were investigated at this step. The optimization runs were repeated for two different $\sigma^2_{\ln \alpha}$ (0.0057 and 0.0299) and three different realizations of α -fields considering only the initial average plume in order to see the effects of σ^2 and relative locations of high and low α zones on the remediation cost and design. α_g was kept constant among the heterogeneous α -fields.

3.5.6. Effect of Correlation between α and K_d

Since only a negative correlation between α and K_d is reported in literature (see Section 2.5), the optimization runs were performed on α -fields negatively

correlated with the heterogeneous correlated K_d -fields with K considering the initial average plume. Two $\sigma_{\ln\alpha}^2$ (0.0057 and 0.0299) and two $\lambda_{\ln\alpha}$ (15 and 30 m) with three realizations were studied.

3.5.7. Effect of f value

“ f ” value is one of the parameters of the two-site nonequilibrium sorption model. It is defined as the fraction of the equilibrium sorption sites. f value used in the all of the optimization runs in this study is 0.75 (see Section 3.3 for details). In order to see the effect of f value on P&T remediation design and cost, optimal design model runs for the heterogeneous K -fields (Section 3.1.1) were repeated with two other f values, 0.5 and 0.25. These values were selected based on the literature survey summarized in Table 2.3. Optimization runs at this step were performed for three $\lambda_{\ln K}$ (15, 22.5 and 30 m) and the lowest and the highest $\sigma_{\ln K}^2$ values (0.2500 and 1.3225) considering both the original and the average initial plumes.

CHAPTER 4

RESULTS AND DISCUSSION

4.1. Results of the Sensitivity Analysis for the Determination of Crossover and Coding Method

Before starting optimization runs, a sensitivity analysis was performed to choose the best method of crossover and coding, which are two critical parameters for the performance of GA. In addition, two different crossover probability values for each crossover operator were tested to find the optimum crossover probability. For this purpose, nine different heterogeneous K-fields (K11A, K12A, K13A, K21A, K22A, K23A, K31A, K32A and K33A) were used. The selection was made between two-point and uniform crossover as the crossover method and binary and Gray coding as the coding method. The detailed information about these methods was given in Section 3.4.1. In PGAPack, the default crossover probabilities employed were 0.85 and 0.5 for two-point and uniform crossover, respectively. The probability of two-point crossover was defined as the probability that a selected string will undergo crossover while for uniform crossover it was the probability of a bit being selected from the first parent string (Levine, 1996). In the sensitivity analysis, these default values were used. In addition, crossover probabilities were exchanged so that probability values of 0.85 and 0.5 were tested for uniform and two-point crossover, respectively, as well. The GA simulations were first performed for optimal design model and then for the time-to-compliance model. The results of the sensitivity analysis executed for both models are presented as separate sections below.

4.1.1. The Optimal Design Model

In complex engineering problems, the best solution obtained through optimization is generally regarded as the “optimum” solution. This is due to the fact that for such problems mostly conditional, discontinuous, non-linear and non-convex functions may be of concern and this may result in convergence to a local optima. However, since the aim of the sensitivity analysis was to investigate the performance of GA for different GA parameters, the global optimum solution for a specific case was critical for the evaluation of the goodness of the result. Therefore, the global optimum P&T policies were determined using the trial-and-error approach where the starting point for search was the optimal GA solutions to the corresponding cases. Results obtained by GA optimization for different GA parameters and initial populations of strings were compared against the global optimum values. For comparison, an F value was defined which indicated the ratio of the best solution obtained within replicates to the global optimum for a specific K-field case.

The efficacy of GA for different GA parameters was also evaluated by the repeatability of the outcome for a K-field case or checking the variation in solutions obtained from replicate GA runs. In these replicate runs for a specific K-field case, the only difference was the initial populations of strings. All other assumptions were the same. The variations within the replicate runs were additionally defined by the relative errors (Andre et al., 2001). For a specified K-field case, first, the relative error for each individual simulation was calculated. Then, the average of replicates was taken to find out the average relative error for each K-field case. The relative error was estimated as follows:

$$E_{rel} = \frac{S_{simulation} - S_{global}}{S_{global}} \quad (4.1)$$

where E_{rel} = relative error; $S_{simulation}$ = solution obtained through optimization, and S_{global} = global optimum solution.

The last criterion used to assess the efficiency of GA optimization for P&T remediation design was the convergence rate. This was defined both by the CPU time spent during the simulations and the number of generations needed to reach the solution. The simulations were performed on Intel Xeon 5110 processors having 1.6 Ghz frequency.

For optimal design model, initially, simulations were conducted for binary coding using different crossover probabilities and types. Then based on the results obtained for binary coding, GA runs were employed for Gray coding. All results are summarized in Table 4.1. For optimal design model, five replicate runs were conducted for each K-field case.

As seen in Table 4.1, regardless of the crossover probabilities tested in this study, uniform crossover with Gray coding outperformed the others. In fact 49% of the 45 total runs for all K-field cases ended up with the global optimum values for the crossover probability of 0.85. For 0.5 crossover probability, this quantity was 51%. It was possible to reach the global optimum solution within five replicates in all of the K-field cases using uniform crossover with Gray coding. This is also shown by F values in Figure 4.1. However, this was not the case for the other crossover and decision variable coding combinations. For example, two-point crossover with binary coding and 0.5 crossover probability was not sufficient to converge to the global optimum solution in any of the K-field cases (Figure 4.1). In 4 out of 9 K-fields cases it was possible to attain the global optimums for the crossover probability of 0.85. Therefore, for two-point crossover with binary coding, the crossover probability of 0.85 resulted in a better efficiency in terms of the number of runs reaching the global optimums compared to the crossover probability of 0.5.

Table 4.1. Results of the sensitivity analysis for the optimal design model (Cro = Crossover type; Prob = Crossover probability; Cod = Coding Type; TP = Two-point; Uni = Uniform; Bin = Binary; Gr = Gray; R = Replicate number; Best = Best solution among replicates)

K-field	Cro(Prob)/Cod	R1	R2	R3	R4	R5	Best
K11A	TP(0.85)/Bin	162,741	161,614	161,614	162,741	161,614	161,614
	TP(0.5)/Bin	189,505	166,290	190,638	189,574	189,709	166,290
	Uni(0.85)/Bin	189,358	161,614	189,382	176,339	175,494	161,614
	Uni(0.5)/Bin	188,925	161,614	161,614	176,349	162,741	161,614
	TP(0.85)/Gr	167,515	163,262	169,930	165,540	161,614	161,614
	Uni(0.85)/Gr	161,614	162,741	161,614	162,741	161,614	161,614
	Uni(0.5)/Gr	162,740	163,262	167,515	175,199	161,614	161,614
K12A	TP(0.85)/Bin	165,038	165,038	165,038	165,038	165,038	165,038
	TP(0.5)/Bin	165,052	193,044	172,600	193,044	193,226	165,052
	Uni(0.85)/Bin	165,038	193,558	163,761	192,071	165,038	163,761
	Uni(0.5)/Bin	165,052	165,052	165,038	165,052	165,038	165,038
	TP(0.85)/Gr	172,600	186,059	182,064	170,020	184,607	170,020
	Uni(0.85)/Gr	163,761	163,761	163,761	163,761	163,761	163,761
	Uni(0.5)/Gr	163,761	164,386	163,761	164,386	163,761	163,761
K13A	TP(0.85)/Bin	169,800	169,631	169,631	169,631	169,631	169,631
	TP(0.5)/Bin	193,330	195,573	184,751	194,011	194,846	184,751
	Uni(0.85)/Bin	180,210	193,985	169,631	193,448	194,105	169,631
	Uni(0.5)/Bin	169,631	169,631	169,631	169,800	170,646	169,631
	TP(0.85)/Gr	170,646	169,631	192,864	173,825	171,289	169,631
	Uni(0.85)/Gr	180,210	169,801	169,631	169,631	176,894	169,631
	Uni(0.5)/Gr	179,722	169,631	169,800	169,631	169,631	169,631
K21A	TP(0.85)/Bin	188,560	169,594	188,560	188,560	188,600	169,594
	TP(0.5)/Bin	180,685	188,848	188,560	189,348	178,659	178,659
	Uni(0.85)/Bin	165,299	187,614	189,049	188,560	189,161	165,299
	Uni(0.5)/Bin	180,938	165,299	168,338	180,283	188,858	165,299
	TP(0.85)/Gr	168,737	180,406	168,737	169,215	165,678	165,678
	Uni(0.85)/Gr	166,611	165,299	178,596	180,283	168,338	165,299
	Uni(0.5)/Gr	178,657	174,704	165,299	165,299	165,299	165,299
K22A	TP(0.85)/Bin	168,078	194,969	168,078	168,078	168,078	168,078
	TP(0.5)/Bin	191,853	195,245	195,735	195,816	169,814	169,814
	Uni(0.85)/Bin	194,969	168,078	168,078	168,078	194,969	168,078
	Uni(0.5)/Bin	194,970	196,500	168,078	194,970	186,025	168,078
	TP(0.85)/Gr	190,014	175,303	194,455	171,312	172,867	171,312
	Uni(0.85)/Gr	168,078	169,814	168,078	168,078	169,387	168,078
	Uni(0.5)/Gr	169,813	168,079	168,078	168,078	172,867	168,078
K23A	TP(0.85)/Bin	183,007	183,007	195,079	185,882	185,541	183,007
	TP(0.5)/Bin	198,982	194,649	210,168	205,188	195,790	194,649
	Uni(0.85)/Bin	185,541	197,405	195,079	195,079	185,541	185,541
	Uni(0.5)/Bin	194,648	185,541	195,126	186,229	197,405	185,541
	TP(0.85)/Gr	194,325	184,803	194,780	184,268	184,188	184,803
	Uni(0.85)/Gr	188,027	184,803	184,268	183,007	183,007	183,007
	Uni(0.5)/Gr	184,268	183,598	183,599	183,007	184,268	183,007

Table 4.1. Results of the sensitivity analysis for the optimal design model
(continued)

K-field	Cro(Prob)/Cod	R1	R2	R3	R4	R5	Best
K31A	TP(0.85)/Bin	187,621	175,459	188,106	175,459	175,459	175,459
	TP(0.5)/Bin	188,115	187,923	187,923	188,563	189,198	187,923
	Uni(0.85)/Bin	188,115	188,106	187,621	187,621	180,135	180,135
	Uni(0.5)/Bin	188,387	188,034	188,034	188,374	187,621	187,621
	TP(0.85)/Gr	168,161	189,138	186,352	180,955	184,188	168,161
	Uni(0.85)/Gr	167,070	175,459	167,070	172,343	183,833	167,070
	Uni(0.5)/Gr	167,070	181,587	167,070	178,512	175,458	167,070
K32A	TP(0.85)/Bin	195,878	195,878	195,878	195,878	195,878	195,878
	TP(0.5)/Bin	198,128	202,581	195,878	197,594	198,134	195,878
	Uni(0.85)/Bin	194,356	174,636	174,636	197,594	174,636	174,636
	Uni(0.5)/Bin	177,800	197,594	195,878	196,502	195,878	177,800
	TP(0.85)/Gr	177,801	179,203	177,093	195,665	177,232	177,094
	Uni(0.85)/Gr	174,636	174,636	174,636	175,317	187,467	174,636
	Uni(0.5)/Gr	175,289	174,636	174,636	174,636	174,636	174,636
K33A	TP(0.85)/Bin	184,664	185,894	184,664	185,894	184,664	184,664
	TP(0.5)/Bin	205,128	205,428	205,088	205,759	217,910	205,088
	Uni(0.85)/Bin	185,894	184,664	185,894	205,128	221,977	184,664
	Uni(0.5)/Bin	205,263	204,881	171,851	188,059	171,851	171,851
	TP(0.85)/Gr	185,894	204,677	195,794	203,593	202,143	185,894
	Uni(0.85)/Gr	201,478	171,851	197,554	201,541	193,052	171,851
	Uni(0.5)/Gr	171,851	201,592	198,459	171,851	171,851	171,851

This indicated that the crossover probability of 0.5 was not sufficient to explore the search space and the algorithm was not able to move away from the local optimum points when two-point crossover and binary coding were used given the other GA parameter values used in the study. When all K-fields were considered, 29% of the total 45 runs ended up at the global optimum for the crossover probability of 0.85. This value was 0% for the crossover probability of 0.5. When two-point crossover with the crossover probability of 0.85 was tested for Gray coding, in only 2 of the 9 K-field cases the global optimums were obtained within replicates. In overall runs for all fields, just 4% of 45 runs had the global optimum. Therefore, in this context, Gray coding deteriorated the performance of GA for two-point crossover. Uniform crossover with binary coding had

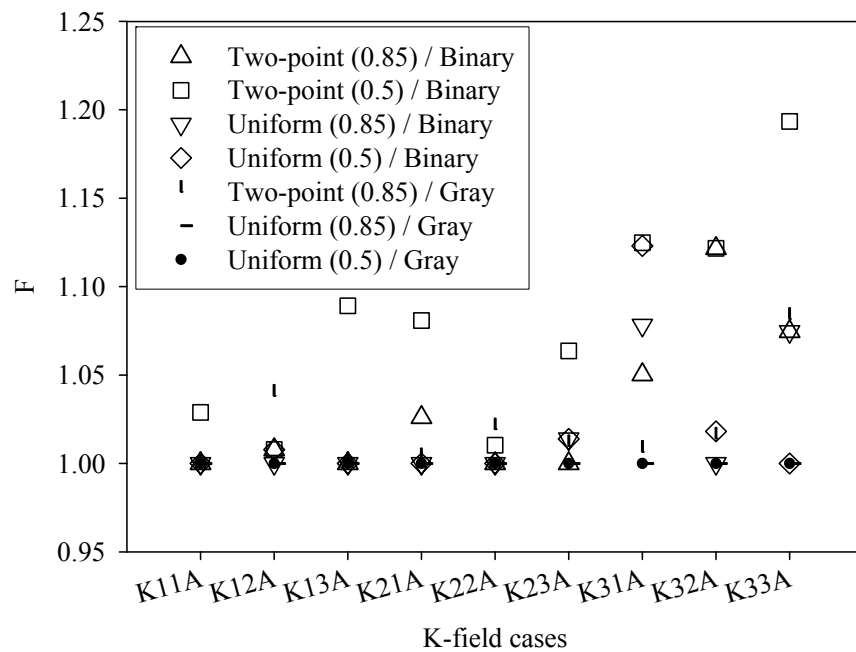


Figure 4.1. F (the ratio of the best value obtained within replicates to the global optimum) values for different K-field cases for the optimal design model

intermediate performance compared to two-point crossover with binary coding and uniform crossover with Gray coding. For the crossover probabilities of 0.85 and 0.5, 6 and 5 K-field cases, respectively, resulted in the global optimum values. In overall, in 22% and 20% of the total 45 runs for all K-fields, it was possible to get the global optimum for the crossover probabilities of 0.85 and 0.5, respectively.

Figure 4.2 shows the average, minimum and maximum of five replicate simulations conducted for 9 different K-field cases for different decision variable coding alternatives, crossover methods and crossover probability values. In this figure, the difference between the minimum and the maximum remediation costs shows the extent of the variations in the optimal results when different initial

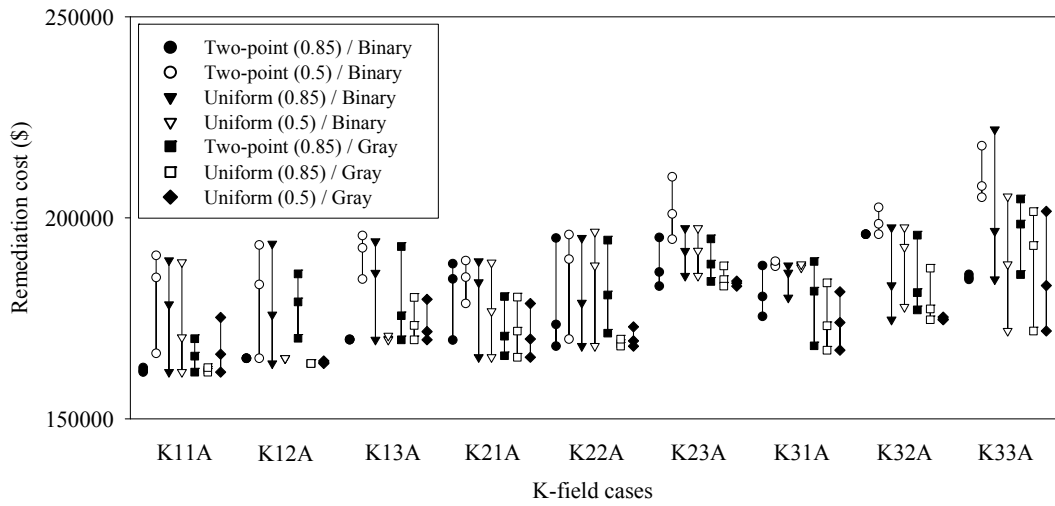


Figure 4.2. The average, minimum and maximum P&T remediation costs based on five replicate simulations for different K-field cases for the optimal design model

population of strings is considered. Table 4.2 summarizes the relative error in each run with respect to the global optimum. In Figure 4.2, when all K-fields were considered, the average variation in remediation costs achieved within five replicates (i.e. difference between the maximum and minimum solutions within 5 replicates) was \$8,123 for the combination of binary coding and two-point crossover with a crossover probability of 0.85. The second and third rankings for the smallest variations in solutions within replicates were for the crossover probabilities of 0.5 and 0.85, respectively, for uniform crossover with Gray coding. The respective values were \$9,847 and \$10,303. The worst difference was \$23,656 for binary coding and uniform crossover with the crossover probability of 0.85. Yet, these values alone are not conclusive in terms of the efficacy of a certain GA parameters combination. For example, replicates for a certain combination of GA parameters may end up in the same local optimum which would results in a variation of \$0. In fact, when Table 4.2 is examined, it is noticed that the minimum

Table 4.2. Average E_{rel} (%) within 5 replicate runs for different K-field cases for the optimal design model

K-fields	TP(0.85) /Bin	TP(0.5) /Bin	Uni(0.85) /Bin	Uni(0.5) /Bin	TP(0.85) /Gr	Uni(0.85) /Gr	Uni(0.5) /Gr
K11A	0.3	14.6	10.4	5.3	2.5	0.3	2.8
K12A	0.8	12.0	7.4	0.8	9.4	0.0	0.2
K13A	0.0	13.5	9.8	0.2	3.6	2.1	1.2
K21A	11.8	12.1	11.3	6.9	3.2	4.0	2.8
K22A	3.2	12.9	6.4	11.9	7.6	0.4	0.8
K23A	1.9	9.8	4.8	4.8	3.0	0.9	0.4
K31A	8.0	12.7	11.5	12.6	8.8	3.6	4.1
K32A	12.2	13.6	4.9	10.4	3.9	1.6	0.1
K33A	7.7	21.0	14.5	9.6	15.5	12.4	6.6
AVG	5.1	13.6	9.0	6.9	6.4	2.8	2.1

average E_{rel} values (2.1% and 2.8%) are for uniform crossover with Gray coding. For two-point crossover with the crossover probability of 0.85, Gray coding increased the average E_{rel} to 6.4%. The highest average E_{rel} (13.6%) was for the combination of two-point crossover, binary coding, and crossover probability of 0.5. The next highest average E_{rel} quantities (9.0% and 6.9%) were for the combinations constituting of uniform crossover and binary coding with different crossover probabilities.

Figure 4.3 depicts the average CPU time and the average number of GA generations required to reach the solution in all runs conducted for a specific combination of GA parameters. In general, the uniform crossover consumed more CPU time compared to two-point crossover regardless of the coding and crossover probability. This observation is in line with Ashlock's (2000). However, in return of higher CPU time for simulations, a higher percentage of the total runs with a specific combination of GA parameters ended up in the global optimum solution. For example, only an average of 23.7 hours of CPU was spent for runs with two-point crossover, crossover probability of 0.5, and binary coding. Yet, all of the

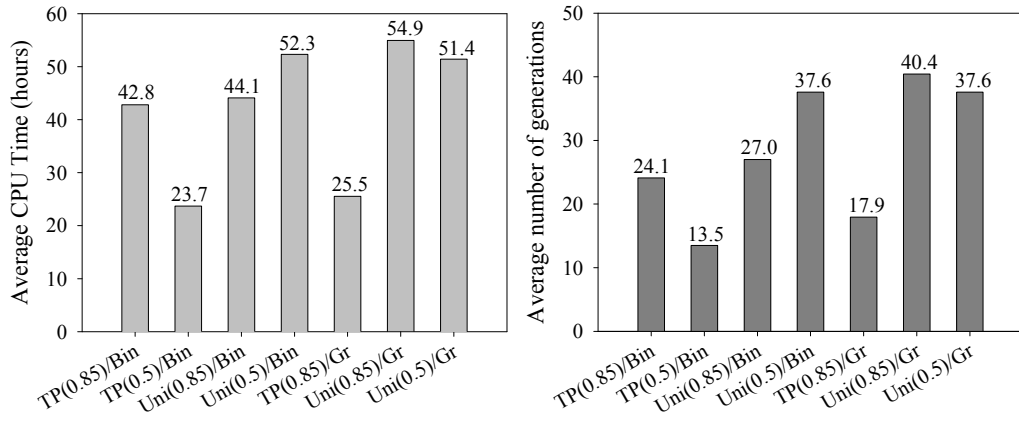


Figure 4.3. Average CPU times on Intel Xeon 5110 processors having 1.6 Ghz frequency and the generation numbers realized to reach the solutions (including all runs for all K-fields) for the optimal design model

runs finalized at local optimum points. With the crossover probability of 0.5, it was not possible for the GA algorithm to jump into another search region for the mutation rate and stopping criteria applied. The highest CPU hours were for the uniform crossover with Gray coding. On the average, 54.9 and 51.4 hours were required for the crossover probabilities of 0.85 and 0.5, respectively. For these cases, 22 and 23 of the runs (out of 45), respectively, resulted in the global optimum value. The number of generations required to reach the solutions were in agreement with the CPU times. In general, compared to two-point crossover, uniform crossover required higher number of GA generations to reach the solutions. Two-point crossover, binary coding and crossover probability of 0.5 converged in an average of 13.5 generations for all K-field cases. Yet, none of the final solutions were the global optimums. For uniform crossover, Andre et al. (2001) and Sharma and Irwin (2003) reported that the use of Gray coding increased the convergence rate of GA in terms of less number of evaluations required for the optimal solution. On the other hand, Haupt and Haupt (1998) stated that Gray code slowed down the GA optimization. Results obtained from

this sensitivity analysis showed that Gray coding and uniform crossover demanded higher CPU time but in return, it was possible to obtain the global optimum with higher possibility. According to the results of this sensitivity analysis, it was decided to use the uniform crossover with 0.5 probability and Gray coding for the rest of the study because of its distinct outperformance compared to other alternatives.

4.1.2. The Time-to-Compliance Model

Since the time-to-compliance model was simpler in terms of the number of the decision variables and the string length used for coding of the decision variables, 3 replicate runs were conducted for each GA parameter set and the K-field case. For the time-to-compliance model, comparison was made between coding and crossover types. However, only a single crossover probability value was chosen for each crossover type. This value was 0.85 and 0.5 for two-point and uniform crossovers, respectively, based on the results of the optimal design model.

In general, for this simpler optimization problem relative to the optimal design model, both crossover types performed equally well with either binary or Gray coding as summarized in Table 4.3. It was possible to reach the global optimum values for all K-field cases except K11A. However, for K11A the difference between the best solution and the global optimum was only one day which is negligible compared to the total remediation time of 3459 days for the optimal solution (Table 4.3). Figure 4.4 shows the variation of solutions for each K-field case within the three replicates. Except for uniform crossover for K23A, the variation among the solutions was either negligibly small or did not exist. This indicated that both coding and crossover types were successful in finding the global optimum solution within three replicates. Figure 4.5 depicts the efficiency of algorithms in terms of both the CPU time spent during the simulations and the number of generations needed to reach the solution. For all four different

Table 4.3. Results of the sensitivity analysis for the time-to-compliance model

K-field	Cro(Prob)/Cod	R1	R2	R3	Best
K11A	TP(0.85)/Bin	3459	3474	3473	3459
	TP(0.85)/Gr	3460	3459	3459	3459
	Uni(0.5)/Bin	3473	3460	3460	3460
	Uni(0.5)/Gr	3459	3459	3460	3459
K12A	TP(0.85)/Bin	3642	3628	3628	3628
	TP(0.85)/Gr	3628	3628	3628	3628
	Uni(0.5)/Bin	3642	3628	3628	3628
	Uni(0.5)/Gr	3628	3628	3628	3628
K13A	TP(0.85)/Bin	4048	4048	4048	4048
	TP(0.85)/Gr	4048	4048	4048	4048
	Uni(0.5)/Bin	4048	4048	4048	4048
	Uni(0.5)/Gr	4048	4048	4048	4048
K21A	TP(0.85)/Bin	3684	3698	3698	3684
	TP(0.85)/Gr	3684	3684	3684	3684
	Uni(0.5)/Bin	3684	3684	3684	3684
	Uni(0.5)/Gr	3684	3684	3684	3684
K22A	TP(0.85)/Bin	3922	3922	3922	3922
	TP(0.85)/Gr	3922	3922	3922	3922
	Uni(0.5)/Bin	3922	3922	3922	3922
	Uni(0.5)/Gr	3922	3922	3922	3922
K23A	TP(0.85)/Bin	4384	4482	4384	4384
	TP(0.85)/Gr	4384	4384	4482	4384
	Uni(0.5)/Bin	4384	4482	4384	4384
	Uni(0.5)/Gr	4384	4384	4482	4384
K31A	TP(0.85)/Bin	3936	3936	3936	3936
	TP(0.85)/Gr	3936	3936	3936	3936
	Uni(0.5)/Bin	3936	3936	3936	3936
	Uni(0.5)/Gr	3936	3936	3936	3936
K32A	TP(0.85)/Bin	4258	4258	4258	4258
	TP(0.85)/Gr	4258	4258	4258	4258
	Uni(0.5)/Bin	4258	4258	4258	4258
	Uni(0.5)/Gr	4258	4258	4258	4258
K33A	TP(0.85)/Bin	4146	4146	4146	4146
	TP(0.85)/Gr	4146	4146	4146	4146
	Uni(0.5)/Bin	4146	4146	4146	4146
	Uni(0.5)/Gr	4146	4146	4146	4146

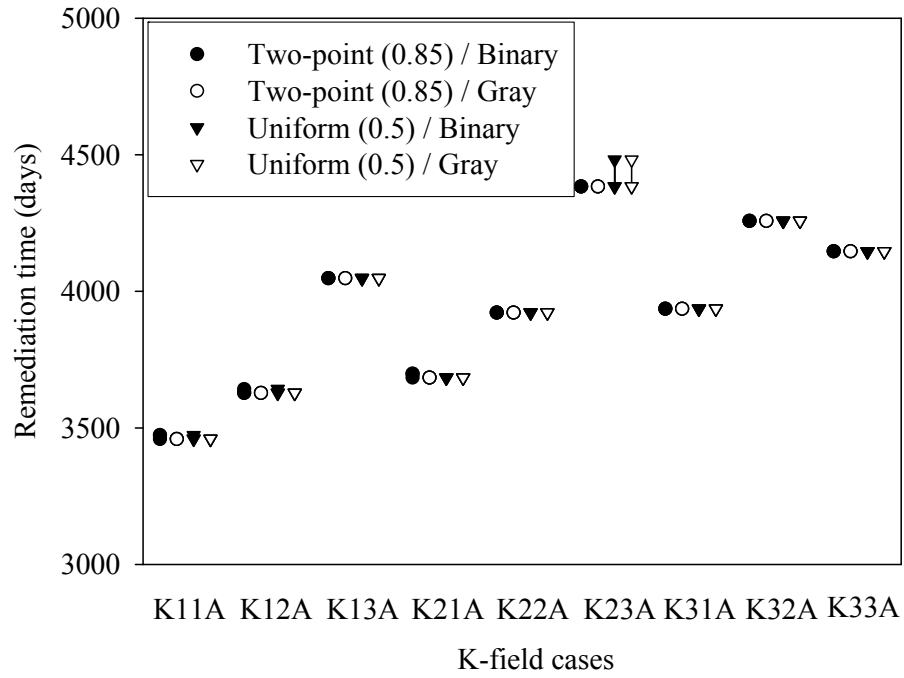


Figure 4.4. Variation of the optimal remediation time within three replicates for different K-field cases for the time-to-compliance model

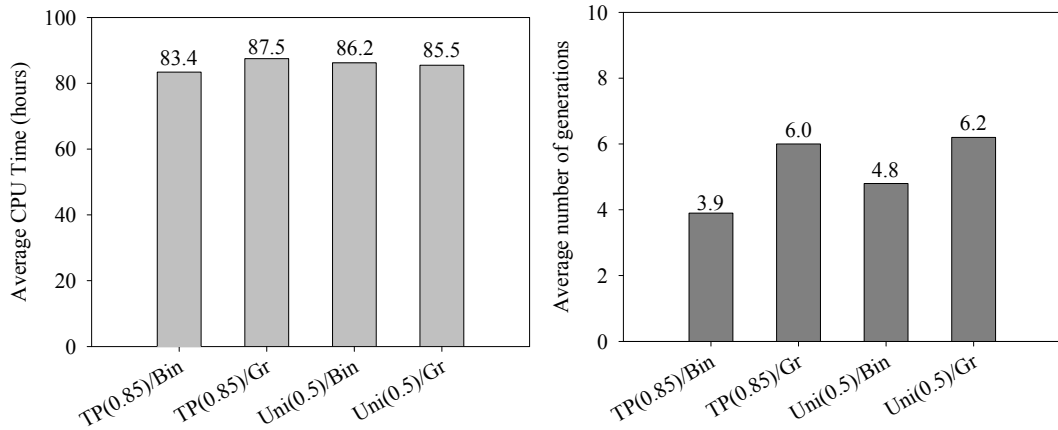


Figure 4.5. Average CPU times on Intel Xeon 5110 processors having 1.6 Ghz frequency and the generation numbers realized to reach the solutions (including all runs for all K-fields) for the time-to-compliance model

combinations of crossover and coding types, the average simulation time was almost the same showing that none of the crossover and coding types provided an advantage over the other in terms of convergence rate. All of these results showed that for this simpler problem, any of the four options can be used and optimization result will be insensitive to the GA parameters tested in this sensitivity analysis. Therefore, it was decided to use the uniform crossover with 0.5 of probability and Gray coding for the rest of the study.

The rationale behind the better performance of uniform crossover over the two-point crossover, for relatively complex P&T optimization problem (optimal design model), may be due to the fact that uniform crossover can put the features together without considering their relative locations on the string. This ability, in turn, can offset the disruptive behavior of uniform crossover on the good features of the population (Dumitrescu et al., 2000; Mitchell, 1996). De Jong and Spears (1992) compared two-point and uniform crossover in terms of “crossover productivity”. They defined productivity as the ability of a crossover operator to destroy the homogeneity of the population. They found that uniform crossover was more productive than two-point crossover for the uniform crossover probability of 0.5. De Jong and Spears (1992) also mentioned about the superiority of uniform crossover over n-point crossover operators in terms of the exploratory power. They stated that an offspring can be created with uniform crossover anywhere in the space but two-point crossover is restricted to smaller subsets. In this study, this exploratory power of uniform crossover may also be the reason of the better performance over two-point crossover. As De Jong and Spears (1992) stated, there should be a balance between exploration and exploitation for an efficient algorithm and this balance point may change depending on the complexity of the problem, the population size, selection pressure and mutation rate. On the other hand, Gray coding eliminates the Hamming cliffs problem and significantly alters the number of local optima (Mathias and Whitley, 1994). Elimination of Hamming cliffs, in

other words the process followed in the representation of adjacent numbers by the Gray code, may improve the GA performance.

Since the best GA operator parameters to reach the optimal solution were selected through the sensitivity analysis, from herein the best solution found thorough GA optimization will be referred to as the optimum solution.

4.2. PCE Plume Simulations on Heterogeneous K-fields

Before analyzing the results of the optimization runs, the steady-state distributions of PCE and hydraulic head under different heterogeneity conditions were investigated. First, the distributions of PCE plume and head under the homogeneous aquifer condition with the K value of 4.5×10^{-5} m/s were found in order to compare them with the ones obtained for the heterogeneous field conditions. Distributions for the homogeneous case are shown in Figure 4.6. In a steady-state homogeneous aquifer, hydraulic head changed only along the x direction for the conditions assumed in this study (i.e. constant head boundaries on the west and east sides and no-flow conditions on the north and south boundaries) and this created one-dimensional, uniform groundwater flow. Under such conditions the head distribution was independent of K. Head contours were placed equally throughout the aquifer and parallel to each other. Under uniform flow conditions, the shape of the plume was regular and elliptic.

The steady-state PCE plume and head distributions simulated on the heterogeneous K-fields are shown in Figure 4.7 to 4.15 with the heterogeneous K distributions at the background. These plumes were called as the “original plume” and used in the optimization runs as the initial condition of the PCE plume (see Section 3.3). One of the determinants of the shape and the extent of the plume is the head distribution in the aquifer. On the other hand, distribution of hydraulic

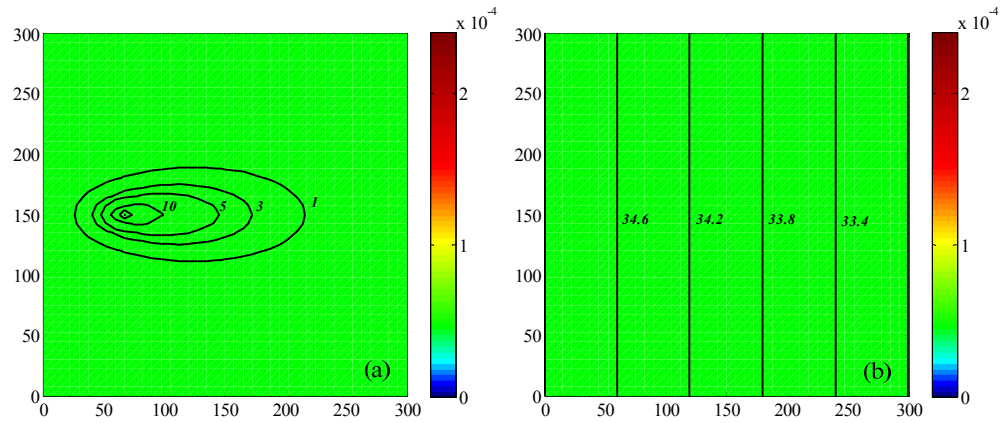


Figure 4.6. (a) PCE plume and (b) hydraulic head distributions for the homogenous K-field ($K = 4.5 \times 10^{-5}$ m/s)

head depends on the existing K distribution in the aquifer. Spatially variable K creates non-uniform flow fields in heterogeneous aquifers. Unlike homogenous K-field, the flow field is two-dimensional for the heterogeneous K-fields. In Figure 4.7 to 4.15, it was observed that the spacing between equally labeled head contours was large in high K zones whereas it was small for low K. The reason of this situation lies behind the Darcy's Law. Groundwater flows from the regions having higher hydraulic head to the regions having lower hydraulic head. Therefore, hydraulic head changes along a groundwater flow path. This head change per unit distance is called "hydraulic gradient" (Barackman and Brusseau, 2004). Darcy's Law states that groundwater flux is proportional to the hydraulic gradient (represented with " $\partial H / \partial x$ " in Equation 3.5) and K. For a constant groundwater flux, when ∂H is constant, K and ∂x becomes directly proportional and ∂x increases when K increases.

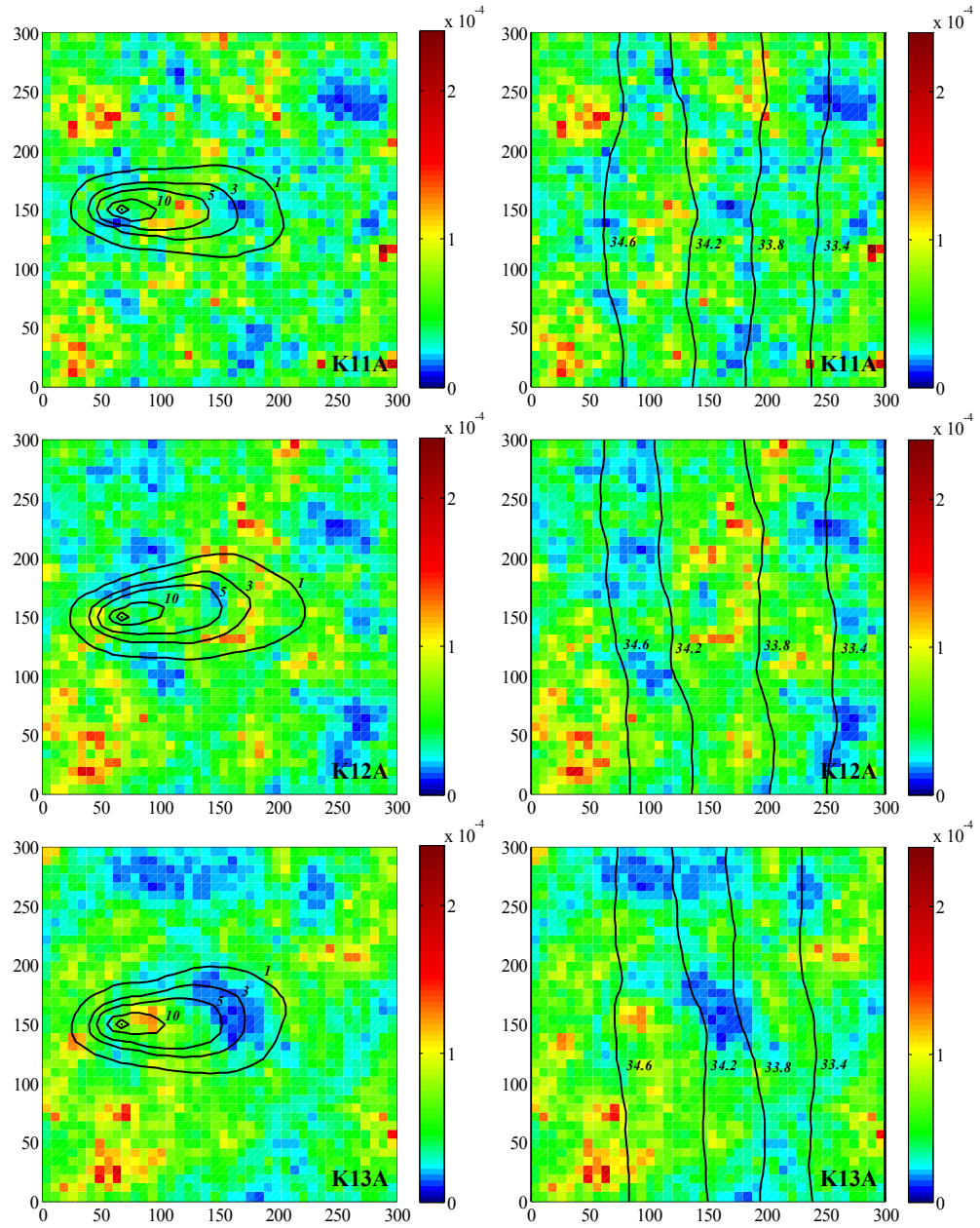


Figure 4.7. PCE plume and hydraulic head distributions for the heterogeneous fields K11A, K12A, K13A

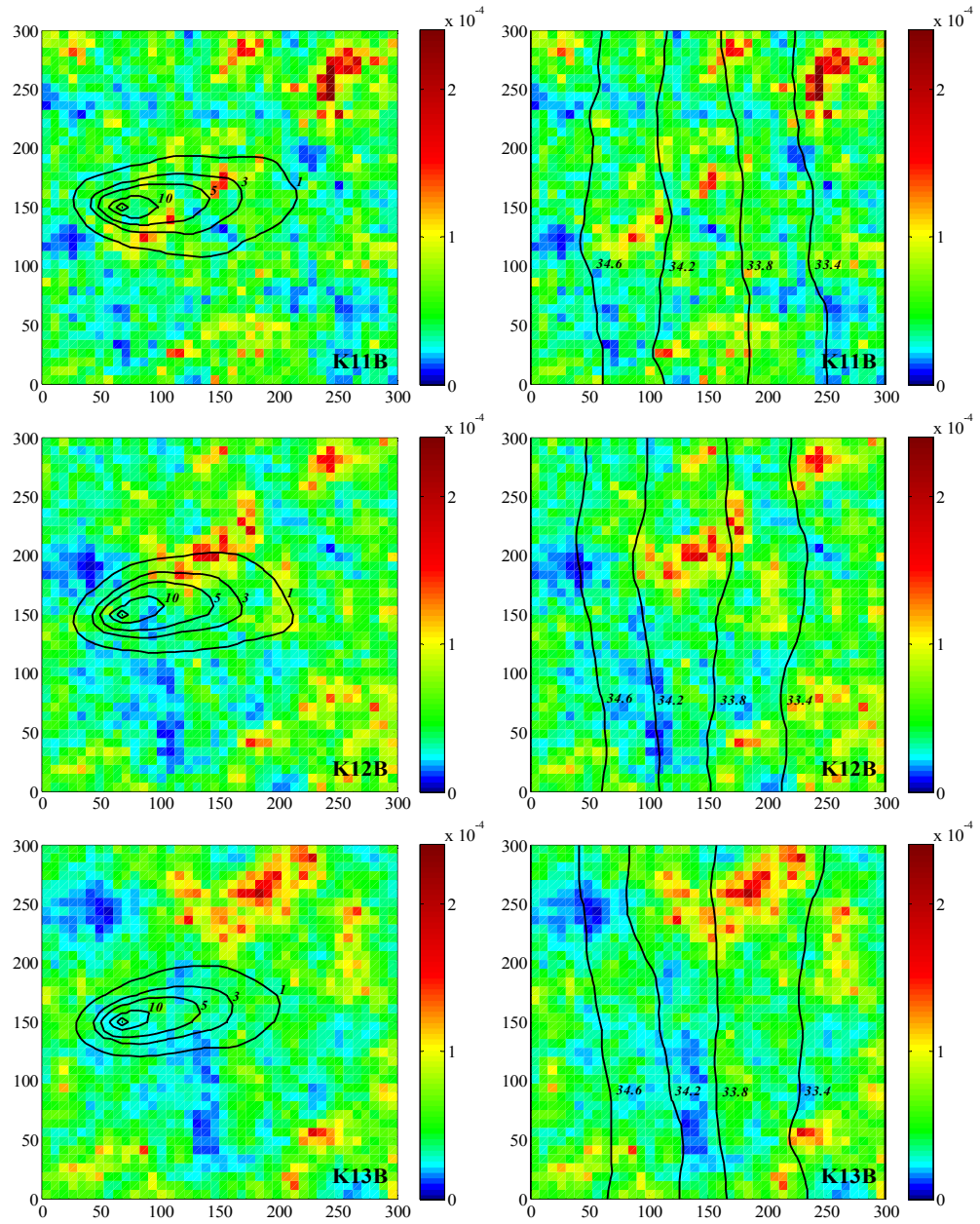


Figure 4.8. PCE plume and hydraulic head distributions for the heterogeneous fields K11B, K12B, K13B

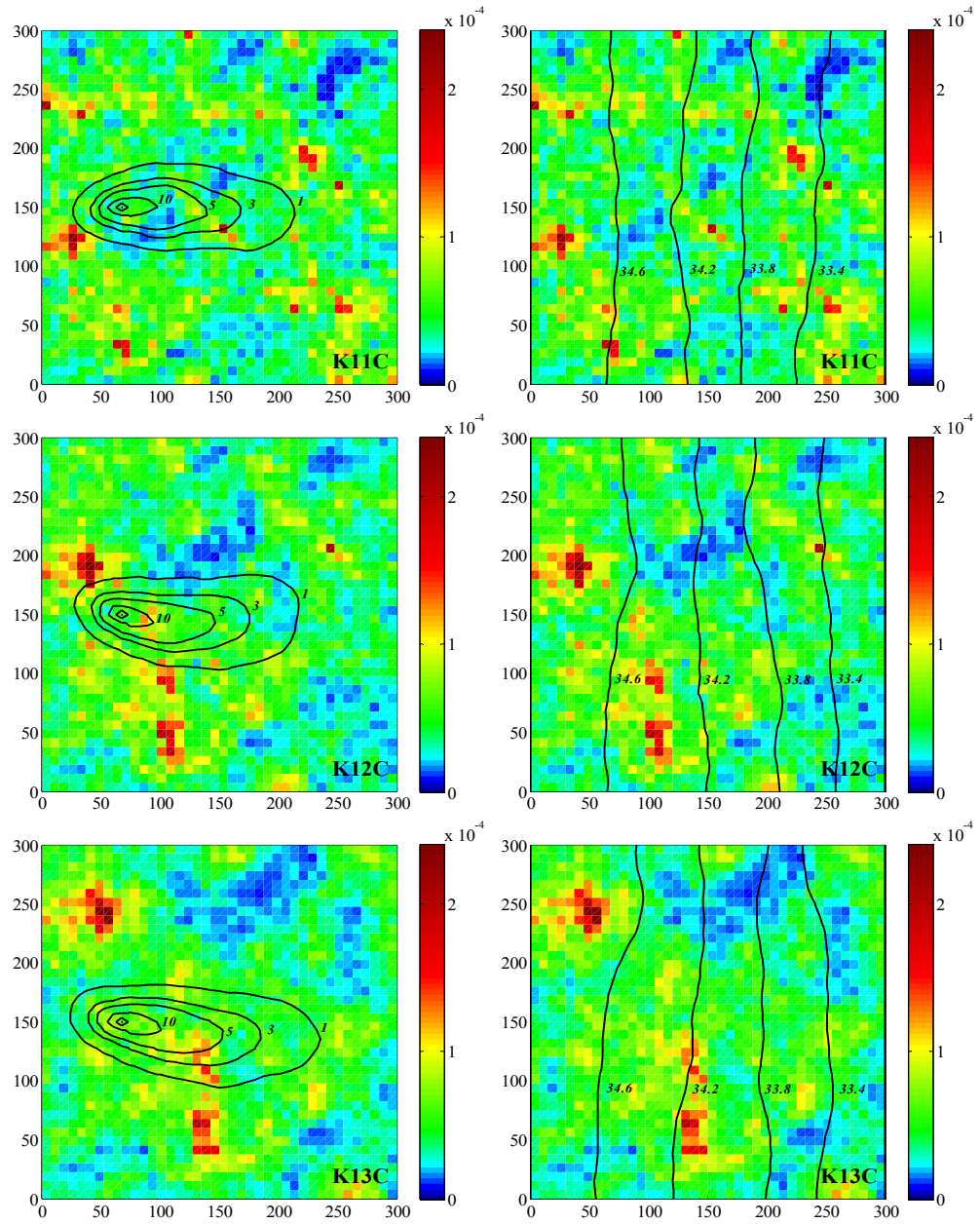


Figure 4.9. PCE plume and hydraulic head distributions for the heterogeneous fields K11C, K12C, K13C

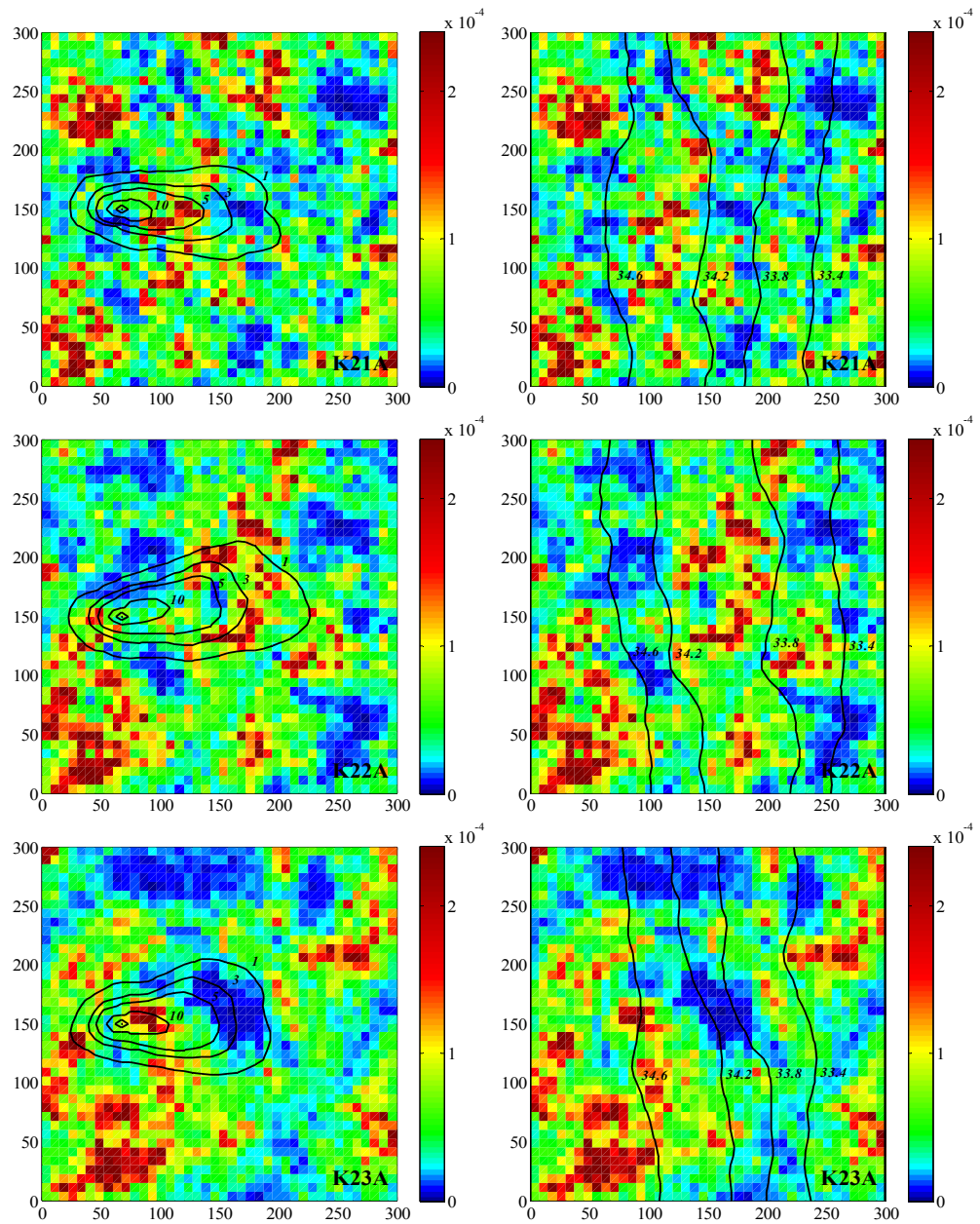


Figure 4.10. PCE plume and hydraulic head distributions for the heterogeneous fields K21A, K22A, K23A

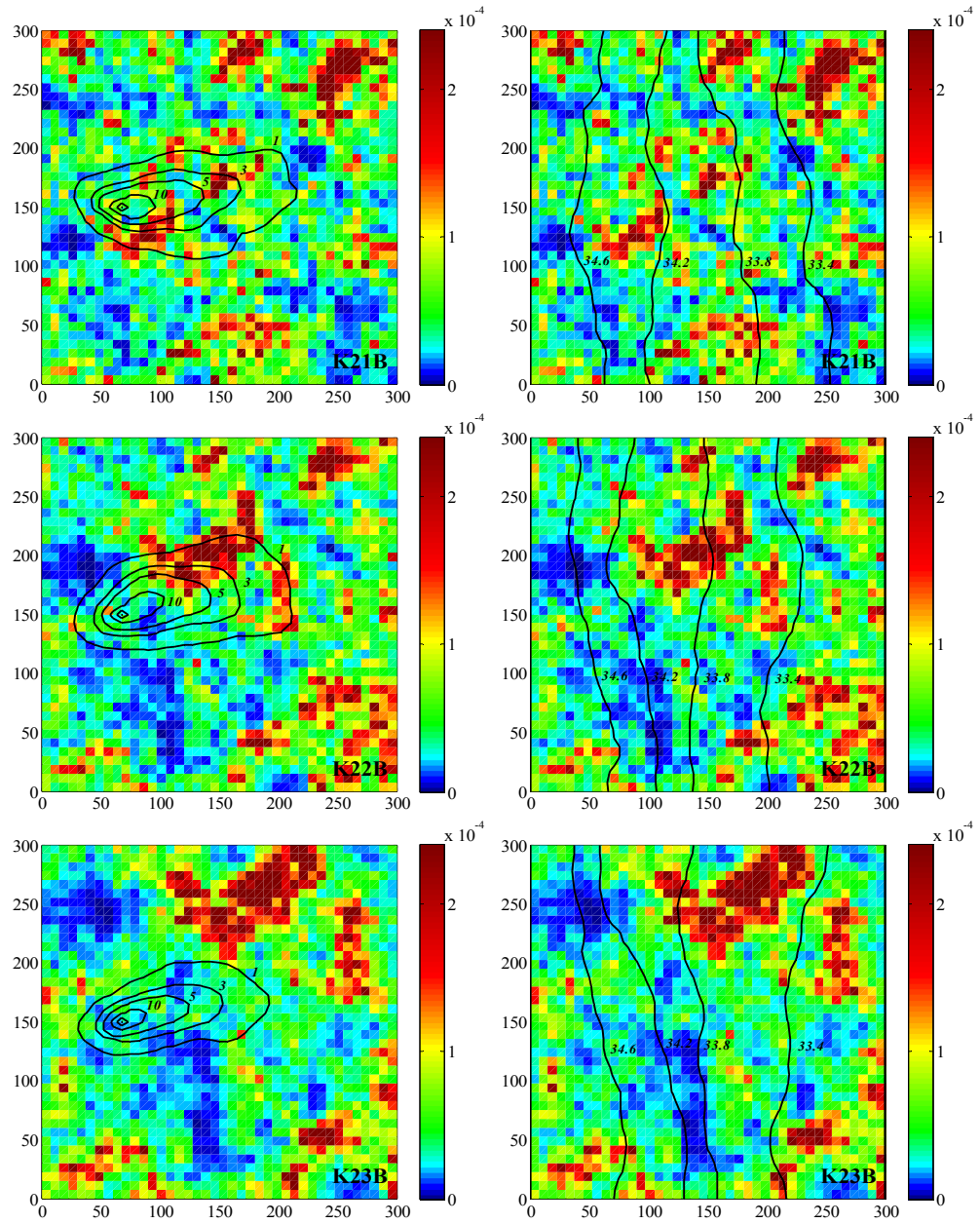


Figure 4.11. PCE plume and hydraulic head distributions for the heterogeneous fields K21B, K22B, K23B

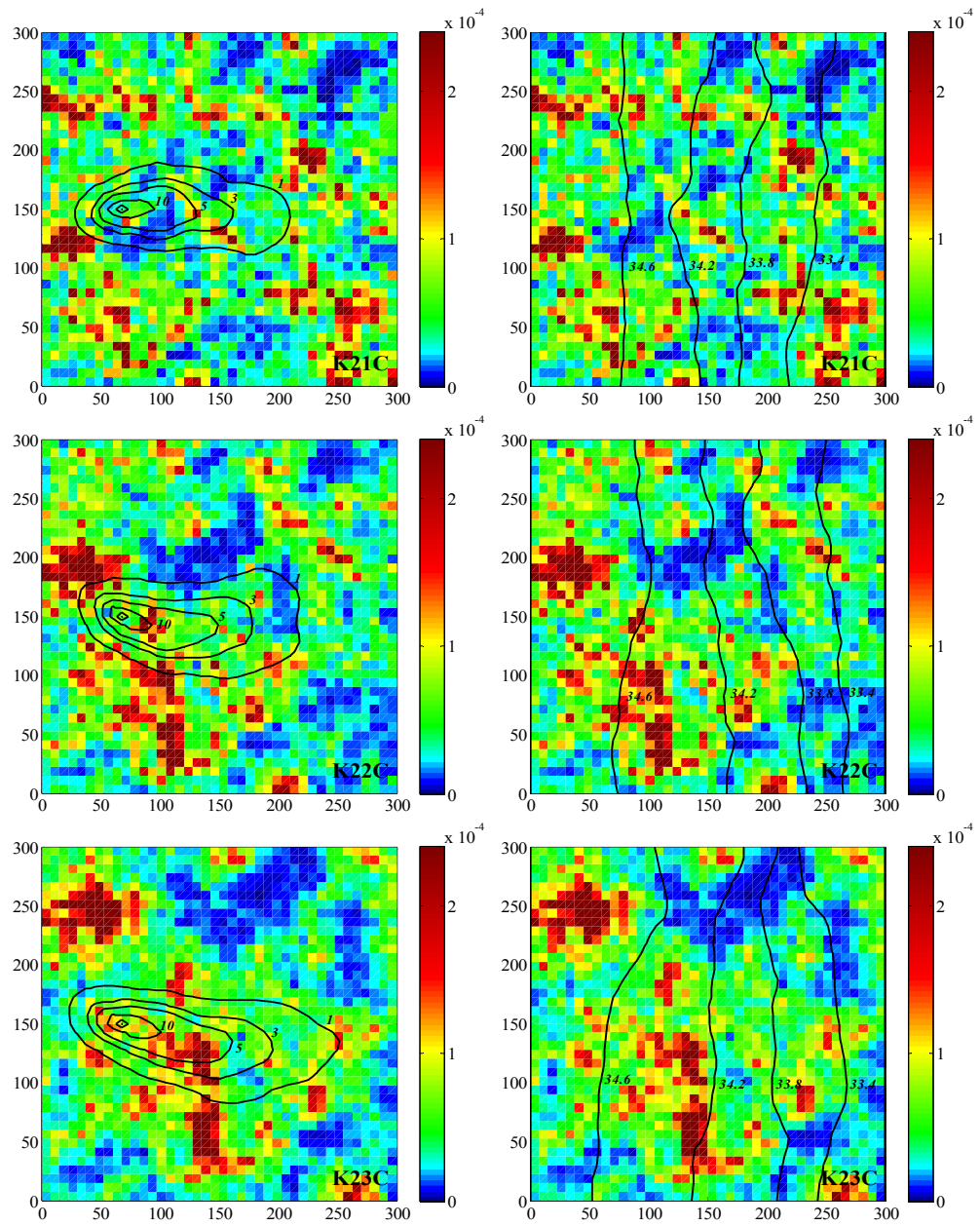


Figure 4.12. PCE plume and hydraulic head distributions for the heterogeneous fields K21C, K22C, K23C

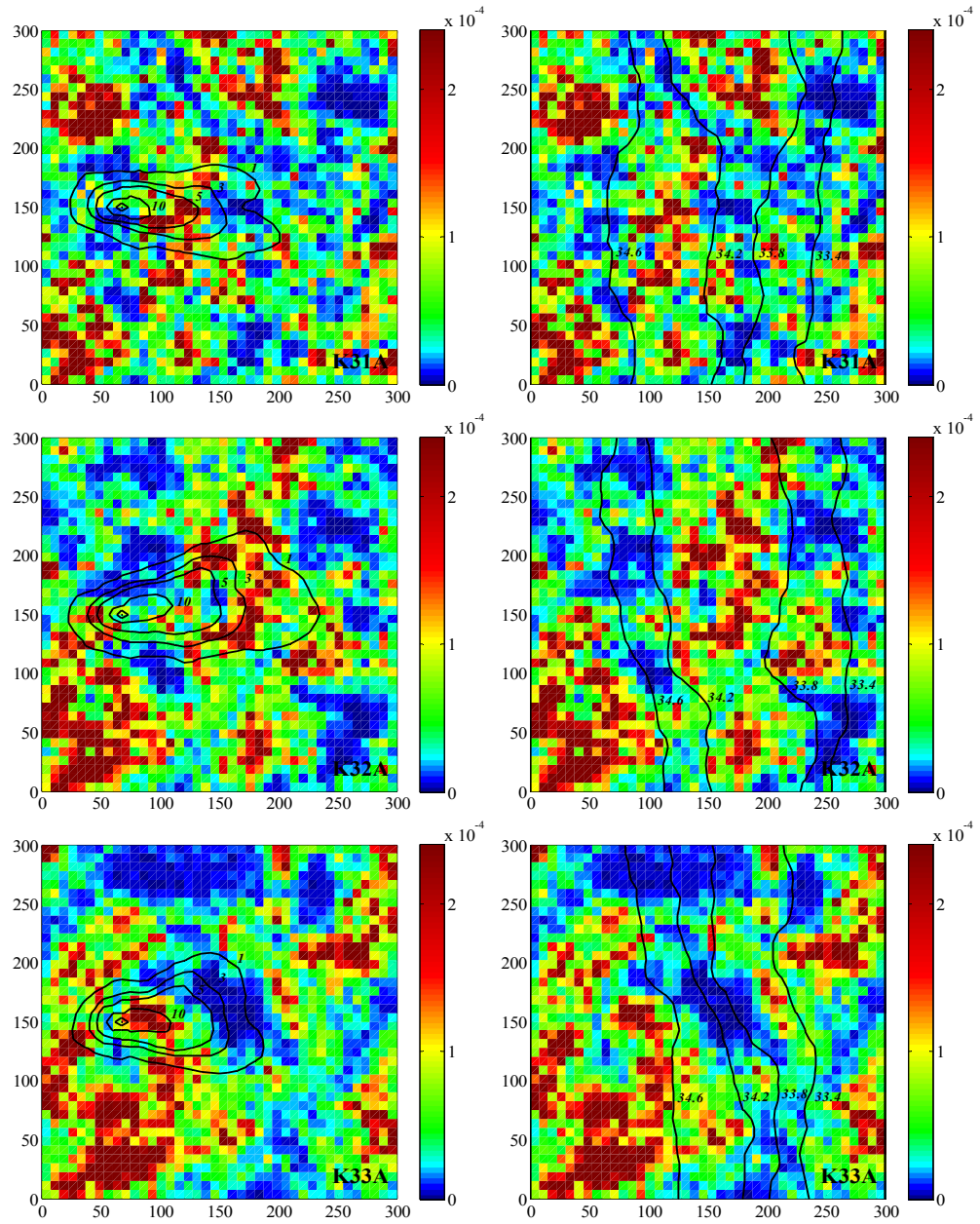


Figure 4.13. PCE plume and hydraulic head distributions for the heterogeneous fields K31A, K32A, K33A

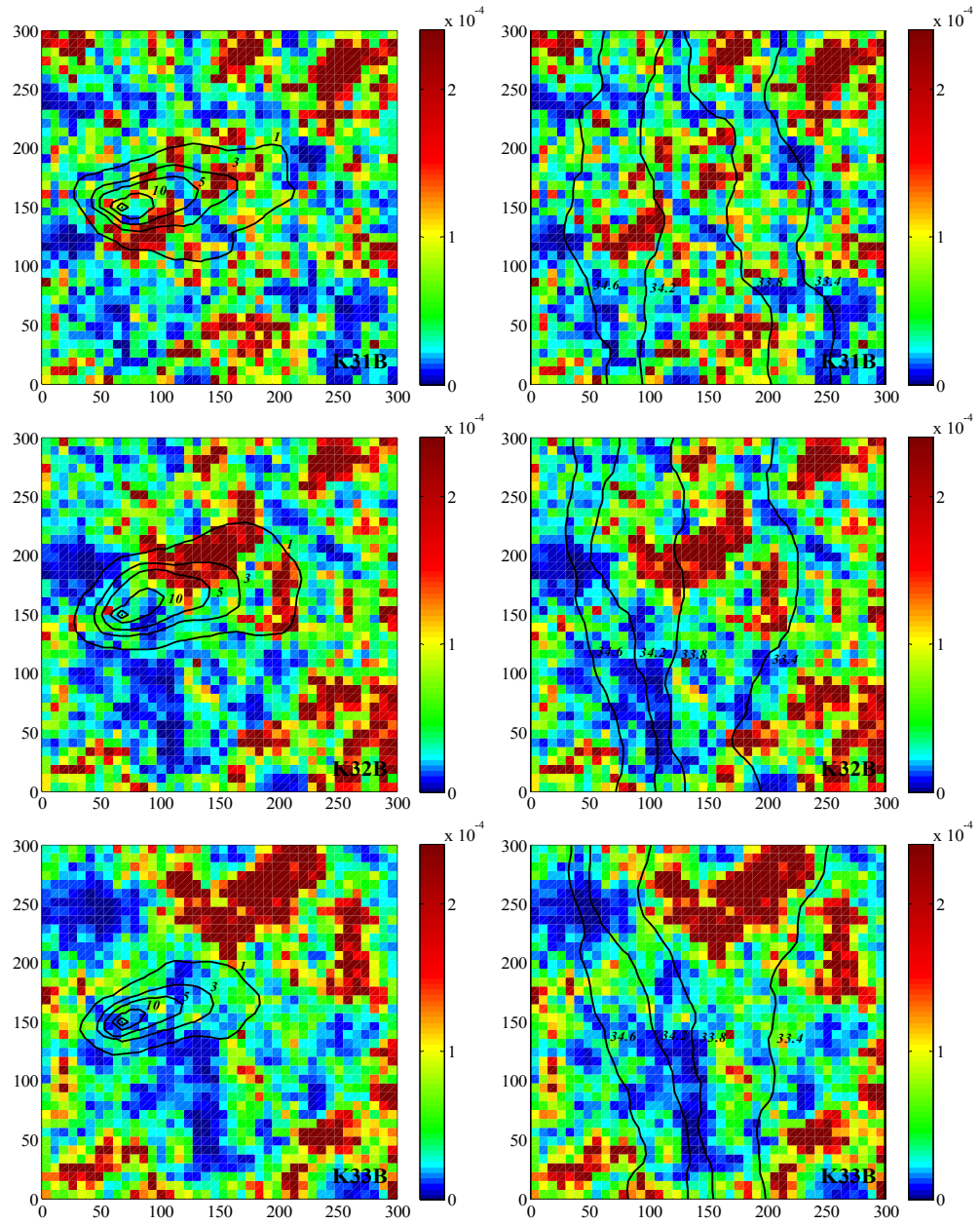


Figure 4.14. PCE plume and hydraulic head distributions for the heterogeneous fields K31B, K32B, K33B

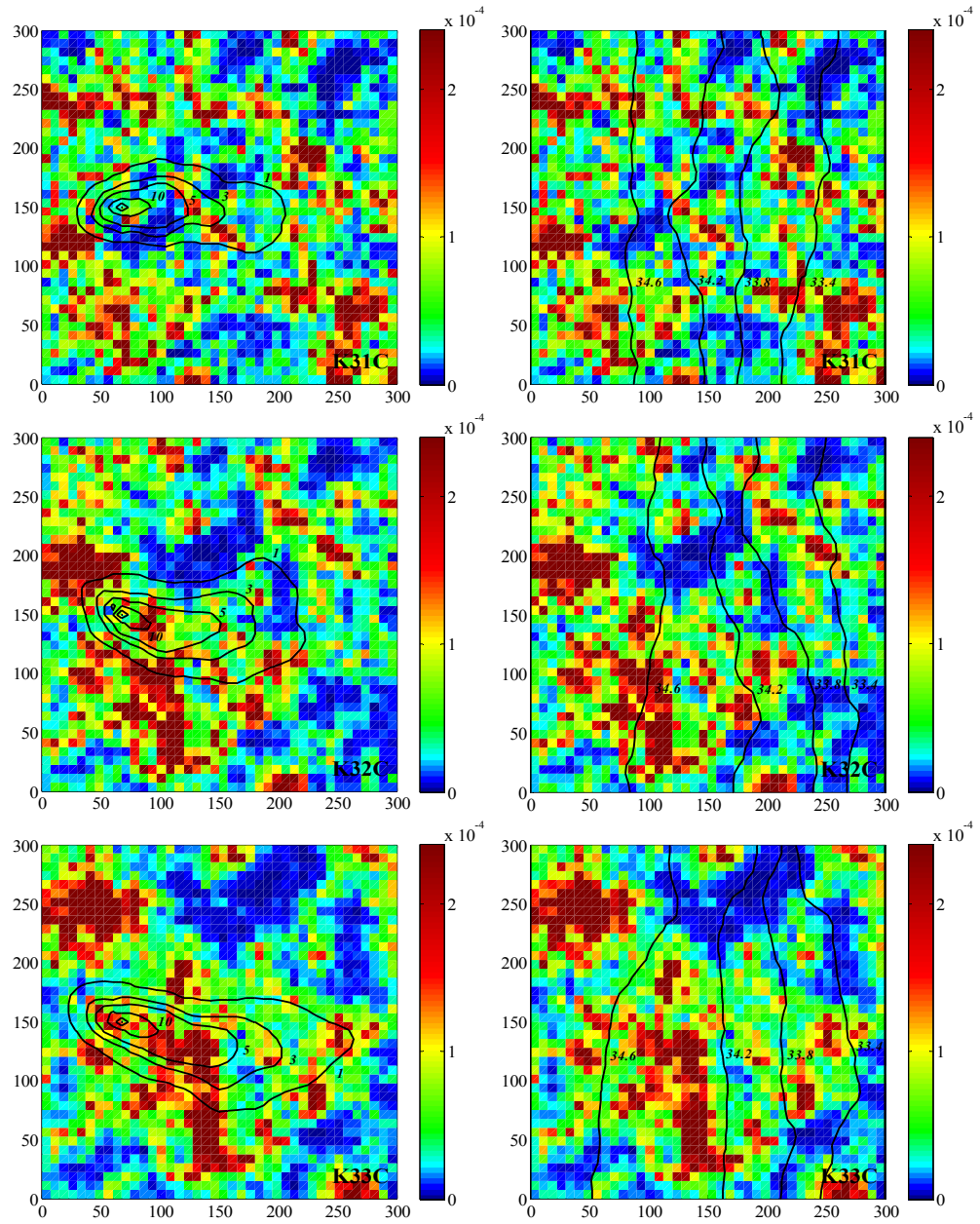


Figure 4.15. PCE plume and hydraulic head distributions for the heterogeneous fields K31C, K32C, K33C

For the heterogeneous K-fields, the shape of head contours became more irregular with increasing $\sigma_{\ln K}^2$ such that the spacing between them changed more and the number of the bends increased. The shape of the head contours were affected by the change in $\lambda_{\ln K}$ since change in $\lambda_{\ln K}$ caused the change in locations of high and low K zones. However there was no noticeable trend as in the case of $\sigma_{\ln K}^2$. These findings are in line with the findings of Uçankuş and Ünlü (2008).

Non-uniform flow conditions observed in heterogeneous aquifers resulted in irregular shape and distribution of contaminant plumes. As the heterogeneity condition changed, the plume shape and distribution changed, too. When $\sigma_{\ln K}^2$, in other words difference between high and low K values, increased, distortion in the plume shape increased and the plume distribution was affected from this change more remarkably. For the K-fields having the lowest $\sigma_{\ln K}^2$, the plume was more or less elliptic while it became more irregular depending on the distribution of low and high K zones as $\sigma_{\ln K}^2$ increased. These findings are in line with the literature. Storck et al. (1997) stated that in aquifers with large $\sigma_{\ln K}^2$, contaminant plumes had more irregular shapes and the travel direction of the plume became more uncertain. On the other hand, in a more homogeneous aquifer, the contaminant plumes had more uniform shapes and followed more predictable pathways. Hemsı and Shackelford (2006) evaluated the effect of K heterogeneity on the plume patterns for four different levels of heterogeneity. For higher $\sigma_{\ln K}$, distinct contrasts between plume shapes emerged either as strongly divergent or strongly convergent plumes but for lower $\sigma_{\ln K}$, the contrast diminished and plumes diverged or converged in a narrower range. Uçankuş and Ünlü (2008) studied the effect of K heterogeneity in terms of CV on the behavior of a BTEX plume which was subjected to biodegradation. They obtained more irregular and distorted plume shapes with increasing CV.

As $\lambda_{\ln K}$ increases, the distance between the areas of high and low K zones increased. At the same time, the areas of such zones grown. Therefore, distribution

and the location of low and high K zones were different for different $\lambda_{\ln K}$ even the same seed was used to generate them. The plume distribution was inevitably affected by these differences but it was not possible to see a general trend for the distribution of contaminant plume with changing $\lambda_{\ln K}$ as this was the case for head contours. The general behavior of the plume was consistent with the head distribution. Plume elongated through the high K regions while low K regions on the way of the plume prevented it from spreading. The plumes of fields K32A and K33A (Figure 4.13) can be taken as the examples to explain this phenomenon. In field K32A, where $\lambda_{\ln K}$ was 22.5 m, there was a wide high K region along the flow path of the plume. The presence of this high K zone caused the plume to gain length along x direction. On the other hand, in field K33A, which had $\lambda_{\ln K}$ of 30 m, there was a large low K region almost at the same place with the high K region of K32A. The existence of low K region suppressed the expansion of the plume, made it shorter in width compared to K32A. The effect of the location and the shape of the high and low K regions on plume shape was significant. For example in fields K12C (Figure 4.9), K22C (Figure 4.12) and K32C (Figure 4.15), the presence of low K region just north of the PCE plume made the upper edge of the plume to bend inside. This effect became more significant with increasing $\sigma^2_{\ln K}$. In literature, Uçankuş and Ünlü (2008) studied the effect of $\lambda_{\ln K}$ on the behavior of a BTEX plume which was subjected to biodegradation for a single K realization. They detected smaller plumes for higher CV and $\lambda_{\ln K}$. Although the present study did not consider biodegradation, it showed that this may or may not be the case depending on the K realization. Because, the change in location of high and low K regions with changing realization and $\lambda_{\ln K}$ may significantly affect the shape of the plume. For example, for realization B, plume shrunk with increasing $\lambda_{\ln K}$ for $\sigma^2_{\ln K}$ of 0.2500 (i.e. fields K11B, K12B and K13B in Figure 4.8) but for realization C, it expanded with increasing $\lambda_{\ln K}$ for the same $\sigma^2_{\ln K}$ (i.e. fields K11C, K12C and K13C in Figure 4.9). On the other hand, the plume shrunk with increasing $\sigma^2_{\ln K}$ for realization B and $\lambda_{\ln K}$ of 30 m (K13B, K23B and K33B in Figures 4.8, 4.11 and

4.14) whereas it expanded with increasing $\sigma^2_{\ln K}$ for realization C and $\lambda_{\ln K}$ of 30 m (i.e. fields K13C, K23C and K33C in Figures 4.9, 4.12 and 4.15).

Since plumes were generated assuming the contaminant source as the constant concentration boundary condition, which is a common practice in groundwater and contaminant transport modeling (Bakr et al., 2003), the amount of mass emanated from the source during the 7 years of simulation time was different for each heterogeneous K-field. Even for the K-fields where the amount of contaminant mass was similar, the distribution of this mass over the aquifer area was different because of the different heterogeneity conditions. Presence of different amounts of mass and different distributions of the plume also influenced the area of the PCE plume. The amount of mass emanated from the source and present in the each heterogeneous aquifer at the beginning of the GA simulations was calculated and its change with respect to $\lambda_{\ln K}$ was shown in Figure 4.16. The area delineated by 1 mg/L contour line of plume was also found and its change with respect to $\lambda_{\ln K}$ was shown in Figure 4.17.

Comparison of Figures 4.16 and 4.17 shows that the areal extents of the PCE plumes were directly correlated with the total (sorbed + aqueous) PCE mass and exhibited similar trends with respect to $\lambda_{\ln K}$. When different realizations were considered, there was no common trend between the initial total PCE mass (and also the area covered by the plume) and $\lambda_{\ln K}$. For instance, for realization B, the initial total PCE mass increased for $\lambda_{\ln K}$ of 22.5 m compared to 15 m. Then, among the three $\lambda_{\ln K}$ considered, the minimum initial plume mass was achieved for $\lambda_{\ln K}$ of 30 m. However, this trend was not unique and dependent on the heterogeneity condition. For realization C, for example, the initial contaminant mass increased for greater $\lambda_{\ln K}$ values. Since the locations and the size of the high and low K regions change with changing $\lambda_{\ln K}$, this situation might be expected. On the other hand, as shown in Figures 4.16 and 4.17, $\sigma^2_{\ln K}$ resulted in variation in the

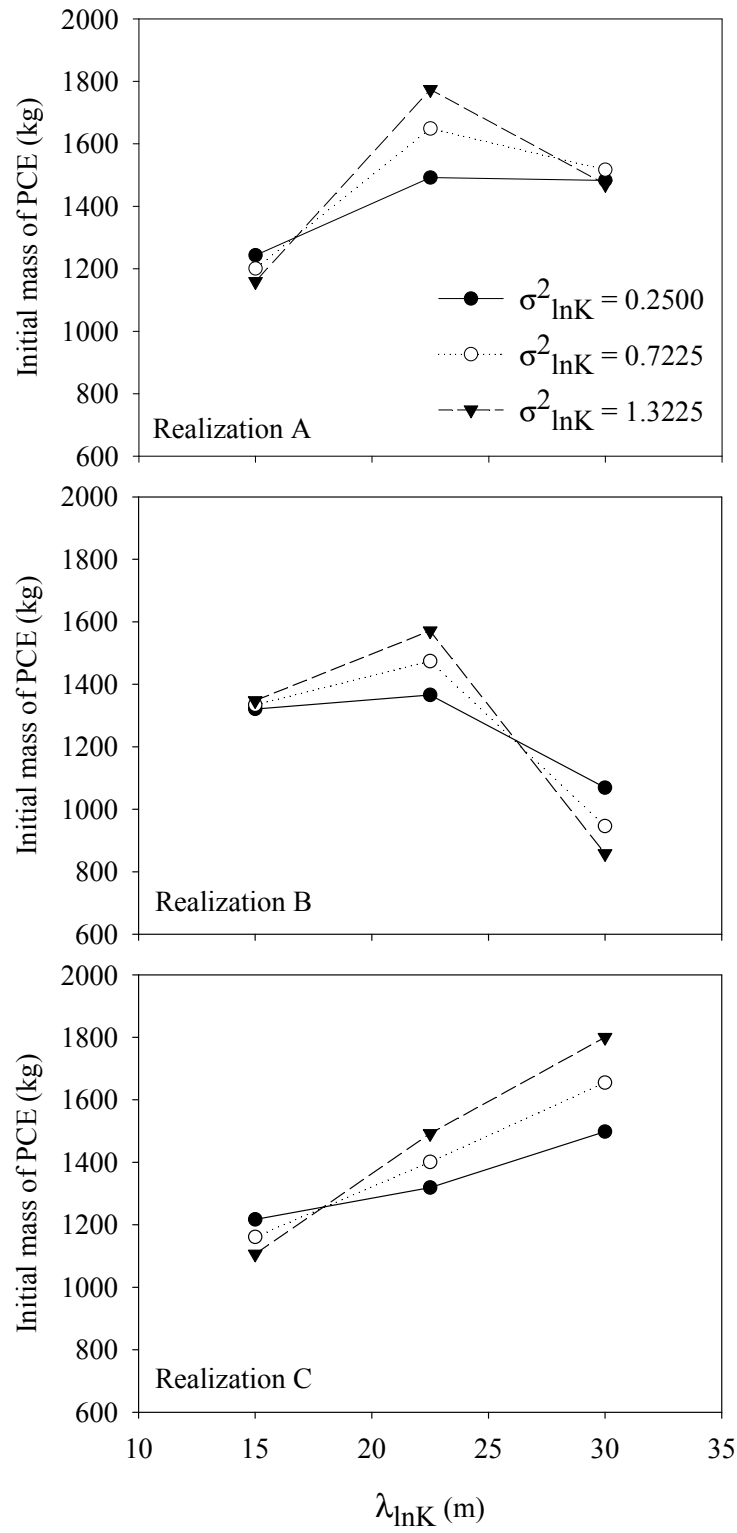


Figure 4.16. Change in initial mass of PCE with respect to $\lambda_{\ln K}$

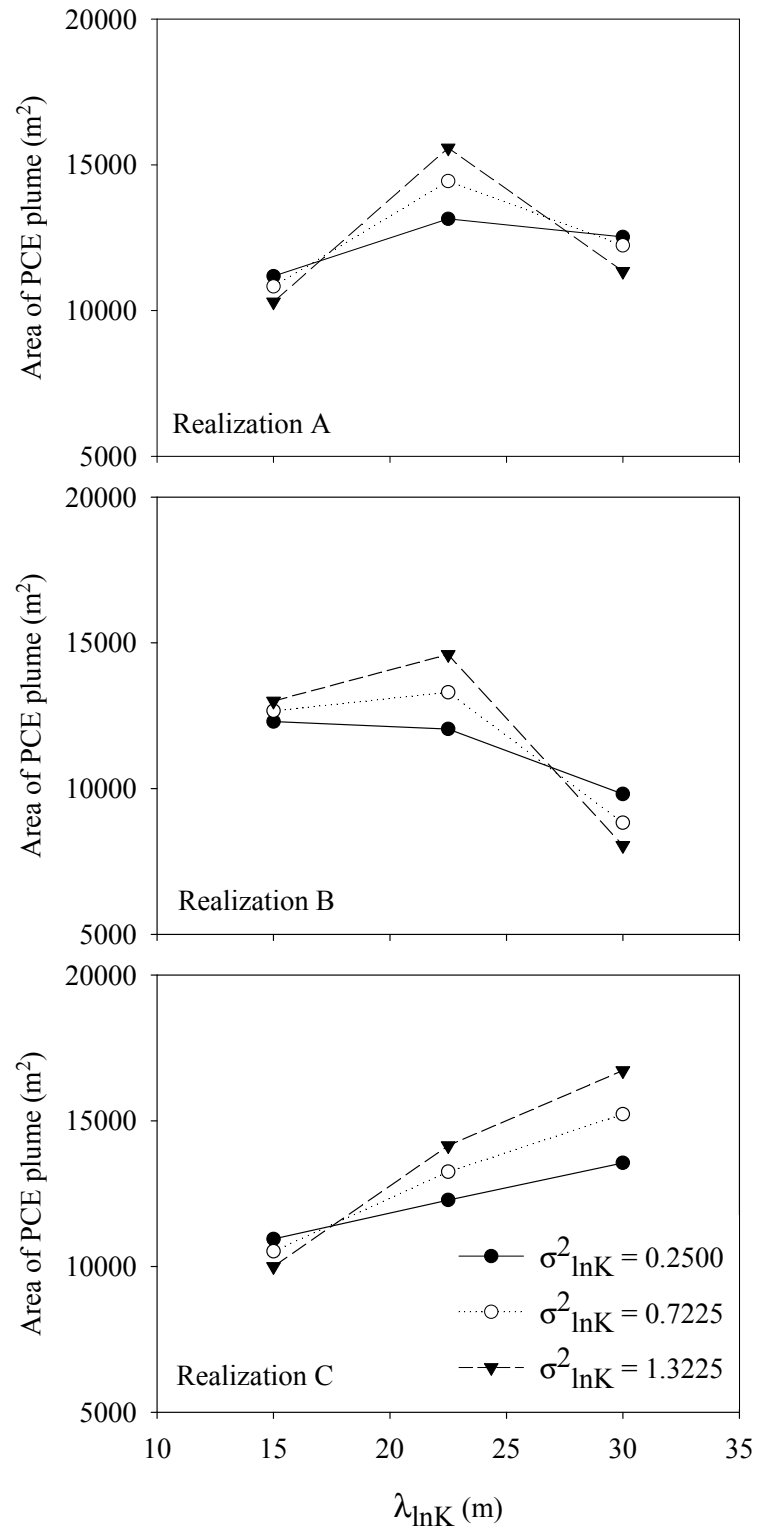


Figure 4.17. Change in area of the PCE plume with respect to $\lambda_{\ln K}$

initial plume mass and area as well. When $\lambda_{\ln K}$ was 22.5 m the mass and the area of the plume increased with increasing $\sigma_{\ln K}^2$ for all three realizations but this regular trend could not be observed for $\lambda_{\ln K}$ of 15 and 30 m for all realizations. This might also be the result of different K distributions in different realizations. The variation in PCE mass and plume area with respect to $\sigma_{\ln K}^2$ was expected since higher $\sigma_{\ln K}^2$ meant higher contrast between the low and high K values in the field which led to enhanced preferential pathways for the contaminant transport. For the same K_g , as $\sigma_{\ln K}^2$ increased, K values in the high conductivity zones became even higher. On the other hand, the resistance of the low K zones to the groundwater flow increased. Therefore, the distribution of high and low K zones in terms of respective locations (represented by realization) had a major impact on movement of the contaminant plume as well as $\sigma_{\ln K}^2$ and $\lambda_{\ln K}$.

A statistical analysis was conducted for the K values of the area where PCE plumes sit on in order to see if there was any relation between the extent of the plume and the statistical properties of K in the corresponding area. Figure 4.18 shows the change in K_g in the plume area with respect to $\lambda_{\ln K}$. The change in K_g in the plume area and the area of the PCE plume (Figure 4.17) with respect to $\lambda_{\ln K}$ were in close agreement. K_g of the plume area of field K33C was the highest among 27 heterogeneous fields with 7.6×10^{-5} m/s. This field also had the largest plume area and the highest amount of initial mass. When the colored representation of this field was investigated (Figure 4.15), it was seen that there was hardly any low K region in the plume area. On the contrary, there was a wide high K zone on the flow path of the plume. The high K resulted in an increase in the groundwater velocity and plume spreading. The field which had the lowest K_g of plume area was K33B. The area of the plume of this field was the smallest with the lowest amount of contaminant mass. The colored representation of this field (Figure 4.14) revealed that there was no high K region in the plume area. This slowed down the movement of the plume and prevented it from spreading. As a

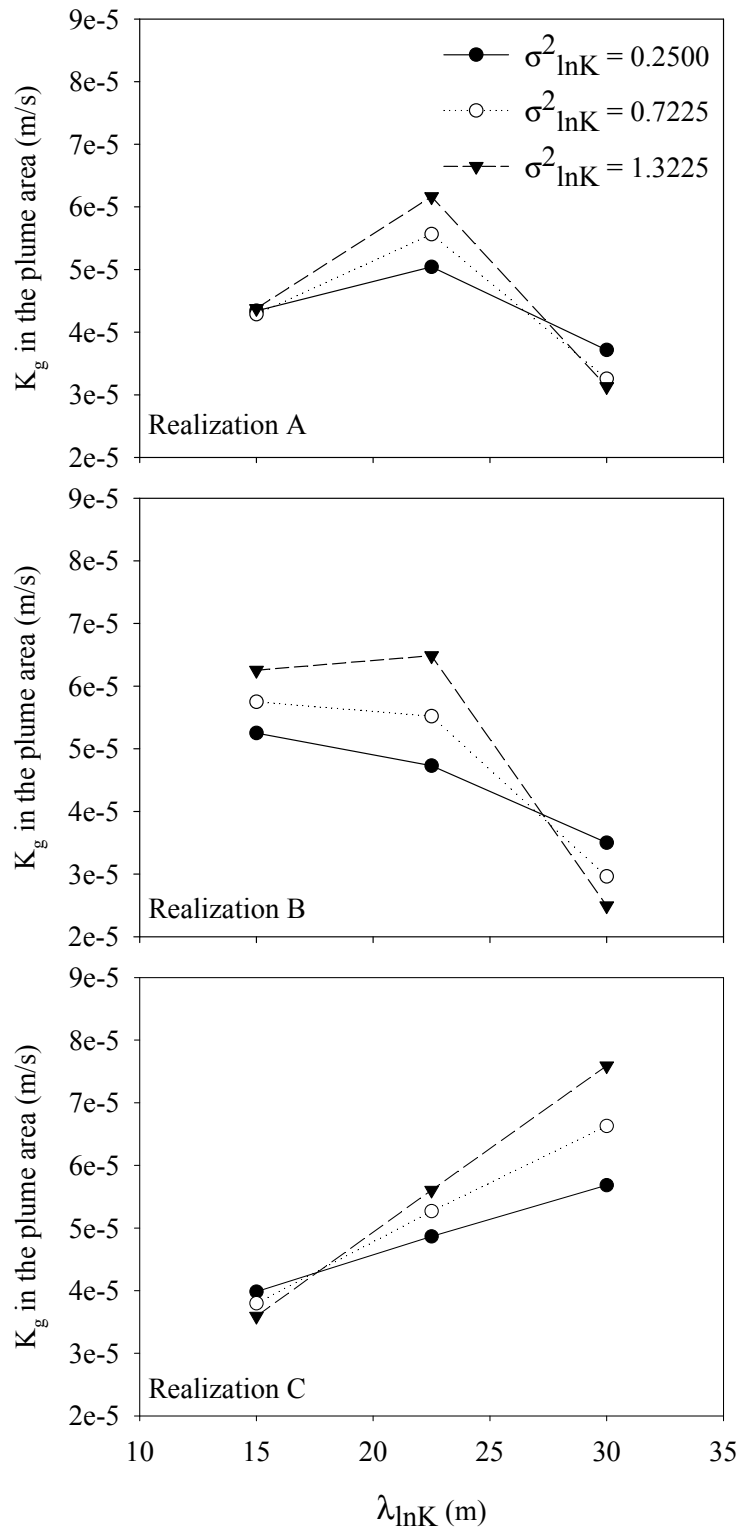


Figure 4.18. Change in K_g in the plume area with respect to $\lambda_{\ln K}$

support to this discussion, the number of elements with small K values in the plume areas were counted. Results showed that 81% of the total number of elements had a K value smaller than the overall K_g value (i.e. 4.5×10^{-5} m/s) on field K33B. 81% was the highest percentage among 27 heterogeneous fields. On the other hand, for K33C, this value was 26% which was the smallest percentage value among 27 fields. These results showed that the total mass and the area of the contaminant plume were in correlation with the K_g of the plume area, not the K_g of the whole aquifer. Therefore, although all heterogeneous $300\text{m} \times 300\text{m}$ fields had the same K_g , plume formations were diverse and local K values had a significant impact on plume distribution.

4.3. Effect of Correlation Scale of K

In the following sections, the effect of $\lambda_{\ln K}$ on P&T remediation design and cost and time-to-compliance were investigated. The optimization runs of this step were conducted both with original plume, the plume of the corresponding field, and average plume, the average of 27 different original plumes (see Section 3.3 for the details).

In the original plume case, both the mass and the area of the contaminant plume over the aquifer changed depending on the heterogeneity condition (i.e. $\sigma_{\ln K}^2$ and $\lambda_{\ln K}$) and the distribution of K for the same continuous contaminant source and contamination period as discussed in Section 4.2. It was assumed that characteristics of the site and plume configurations were fully known and the calibration of the model was made accordingly. The impact of heterogeneity both on contamination and remediation was taken into consideration at the same time. Hence, the original plume case represented the conditions where we were fully aware of the heterogeneity conditions and therefore the plume conditions (i.e. migration).

The average plume case, on the other hand, examined the impact of heterogeneity and $\lambda_{\ln K}$ for the same initial mass. As declared in Section 3.3, the initial plume for the average plume case was generated by averaging the initial plumes of the 27 plumes of the original plume case. Therefore, it may be possible that the average plume disregarded the local deviations in K for the initial plume formation. However, such a bias can be expected in real life remediation designs as well, due to improper sampling and field characterization.

4.3.1. Results of the Optimal Design Model

4.3.1.1. Results of the Original Plume Case

The results of the optimization runs conducted with original plumes showed that the single-well designs predominated on the 27 different heterogeneous fields. The only design which consisted of 2 wells was the one for K23A. Among 26 different single well designs, well 13 (Figure 3.11 to 3.13) was the most selected active well in 10 different cases. When the locations of the selected wells were analyzed, it was seen that for most of the K -fields, the active pumping wells were the wells either on the centerline of the plumes or the wells adjacent to the wells on the centerline. In addition, selected wells were also very close or at down gradient of the CoM for all K -fields. These findings were similar to Chan Hilton and Culver's (2005) and Huang and Mayer's (1997).

When the total remediation costs of the optimal designs were analyzed (Figure 4.19), it was observed that the relationships between costs and $\lambda_{\ln K}$ did not follow a regular trend for different realizations of the heterogeneous fields. However, trends in initial mass of PCE with respect to $\lambda_{\ln K}$ were in close agreement with the trends in total cost of remediation with respect to $\lambda_{\ln K}$ except for field K23A. Since the remediation goal for all fields was the same, higher contaminant mass was

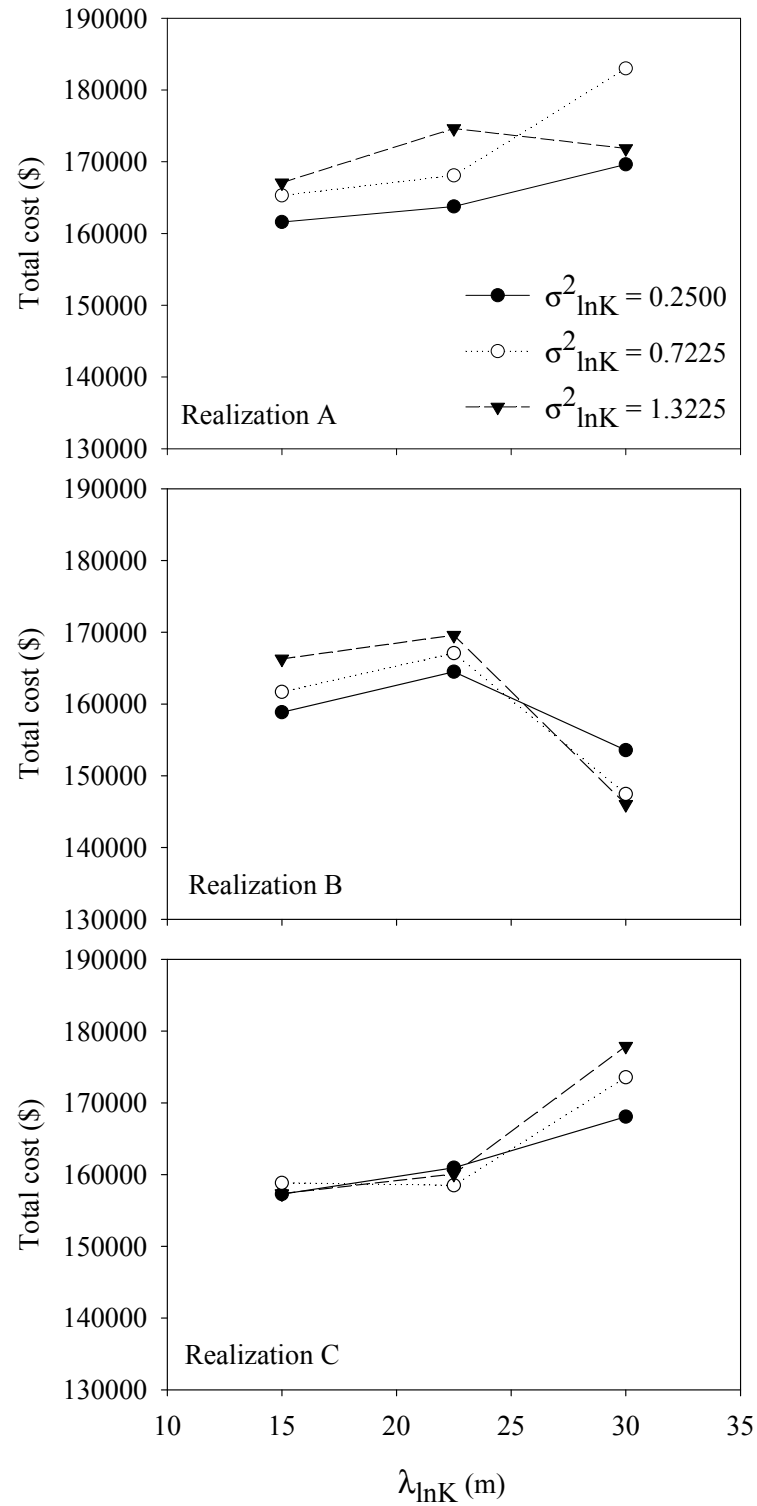


Figure 4.19. Change in total remediation costs with respect to $\lambda_{\ln K}$ for original plume case

removed in fields that had higher initial contaminant mass. As a result, the remediation cost increased accordingly. The deviation in the similar trend in total cost with the initial mass of PCE versus $\lambda_{\ln K}$ was due to field K23A. For field K23A, 2-well design was used unlike all other 26 fields for which single-well designs were chosen. Although $\sigma^2_{\ln K}$ of field K33A was higher than field K23A and the initial PCE mass was almost the same for both fields, the single-well design was used for field K33A whereas 2-well design was chosen for field K23A. This may be due to the fact that the area of the initial plume for K33A was 93% of that for K23A (Figure 4.17). This slight difference may result in the selection of two wells for field K23A. In addition, from the figures of initial plumes (Figures 4.10 and 4.13) it can be understood that there was less PCE mass in the low K region, located in the center of the aquifer area, in field K33A when compared to field K23A. This may be another reason why 2 wells were chosen for field K23A but not for field K33A.

The minimum and the maximum total remediation costs for all 27 designs were \$146,000 (for field K33B) and \$183,000 (for field K23A), respectively. Therefore, the total cost changed up to 25% with respect to the minimum cost, depending on the heterogeneity condition, the respective locations of high and low K zones and the contaminant mass initially present in the aquifer. When the variation in remediation costs for different heterogeneity conditions were examined within a specific realization, the percent change in remediation costs for different heterogeneous K-fields are 13% for realization A, 16% for realization B and 13% for realization C.

The effect of heterogeneity condition on P&T remediation system cost could be understood more clearly if the elements of the total cost (i.e. pumping cost, operational cost of GAC treatment facility which is referred to as “treatment cost” from now on, capital and installation costs for wells and capital cost of GAC treatment facility) were investigated individually. This approach was necessary

since all optimal designs included a single GAC adsorber and the capital cost of GAC unit (\$100,000) constituted a great percentage, 55-68%, of the total cost. When the capital cost of GAC unit was excluded from the total cost and a similar analysis was performed, it was seen that the cost could change up to 80% among all realizations depending on the heterogeneity condition, the respective locations of high and low K zones and the contaminant mass initially present in the aquifer. The percent change among different heterogeneous cases was 35% for realization A, 51% for realization B and 36% for realization C. On the other hand, the capital and installation cost of a well depended only on the number of the wells and the well depth. The change in depth of active wells for different K-fields was not very significant because of the 1% slope of the aquifer bottom. As an example, the well installation cost changed only by \$20 between two adjacent wells (i.e. distance between these wells was 22.5 m). When the locations of active wells for different K-fields were considered (wells 8, 9, 13, 14, 17, 18, 19, and 23 in Figures 3.10 to 3.13), the maximum downstream distance between these wells was 67.5 m. Therefore, the capital costs, including the installation costs of GAC treatment facility and the pumping wells, were almost the same as long as the numbers of active wells were the same (Figure 4.20). However, as for field K23A, increased number of active wells resulted in a significant increase in the overall remediation cost as depicted in Figure 4.19 for realization A.

Under these conditions, it was not surprising that treatment and pumping cost determined the general trend of total remediation cost with respect to λ_{lnK} for the single well designs. Figure 4.21 shows the change in treatment costs with respect to λ_{lnK} . The trends were similar with the trend in total cost except for K23A. It was also noticeable that the trends in the treatment cost were the same with the trends in the amount of PCE mass removed from the aquifer except for the field K23A (Figure 4.22). The reason of the difference in the treatment cost for field K23A was the use of two wells. Treatment cost was a function of both PCE concentration

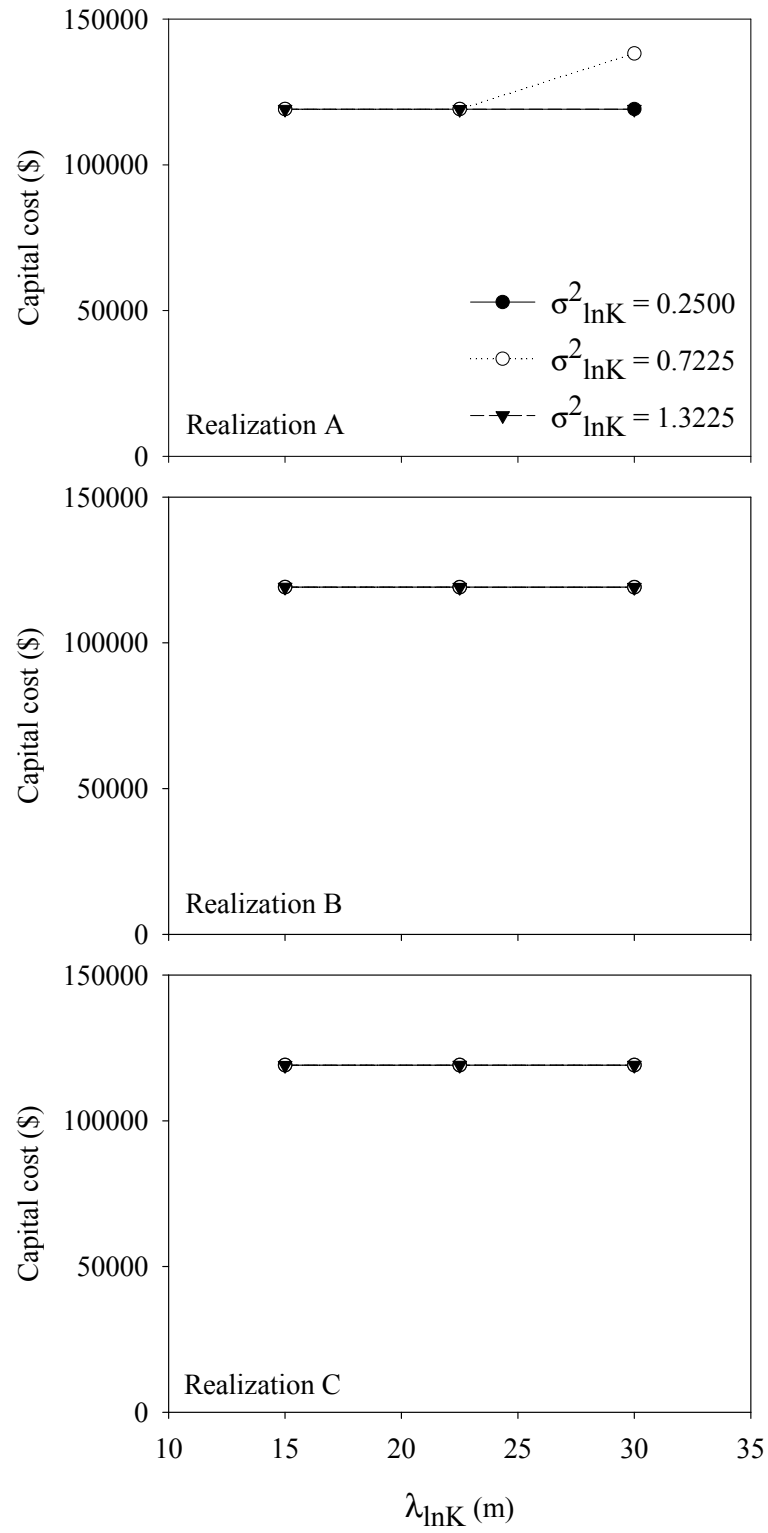


Figure 4.20. Change in capital costs with respect to $\lambda_{\ln K}$ for original plume case

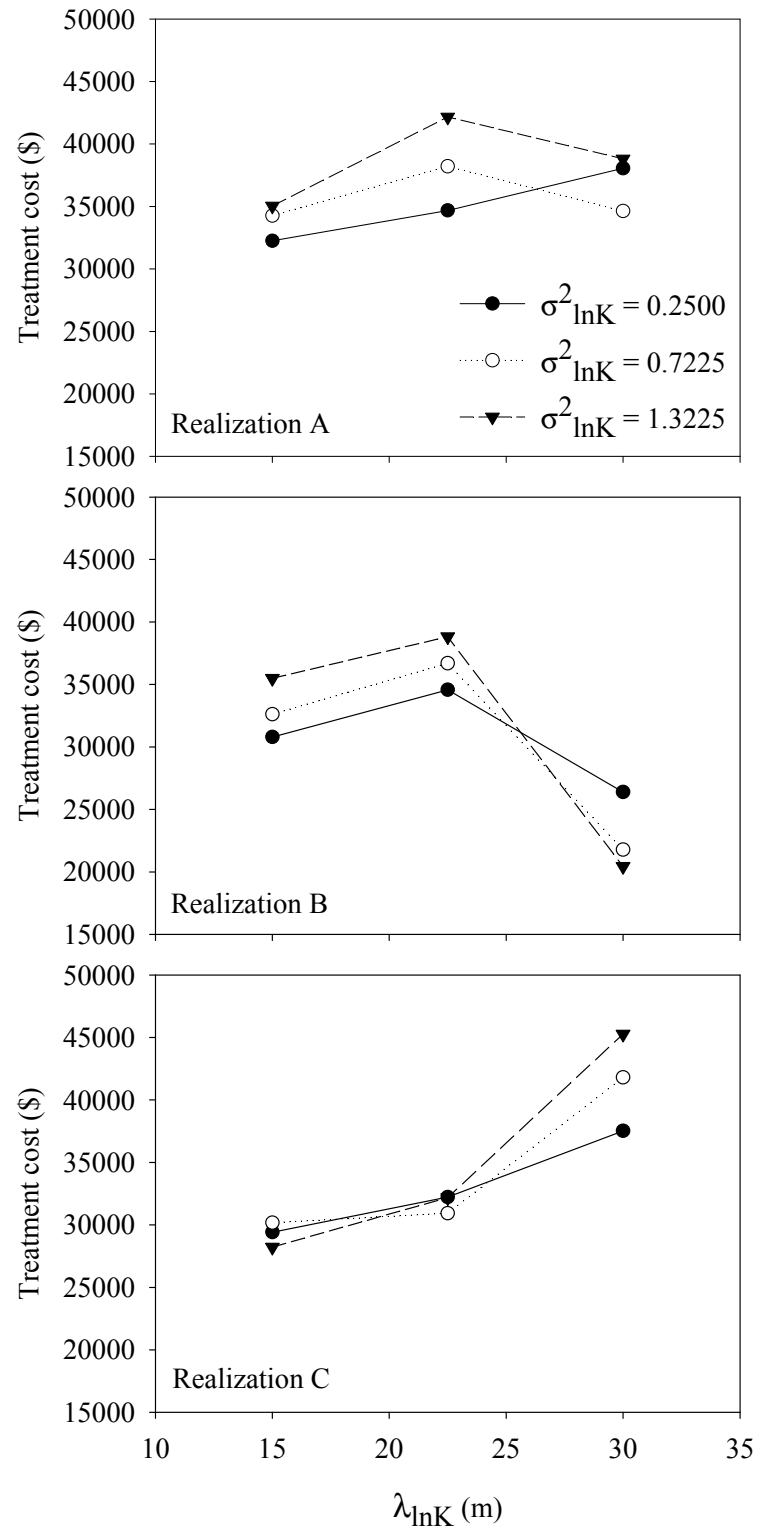


Figure 4.21. Change in treatment costs with respect to $\lambda_{\ln K}$ for original plume case

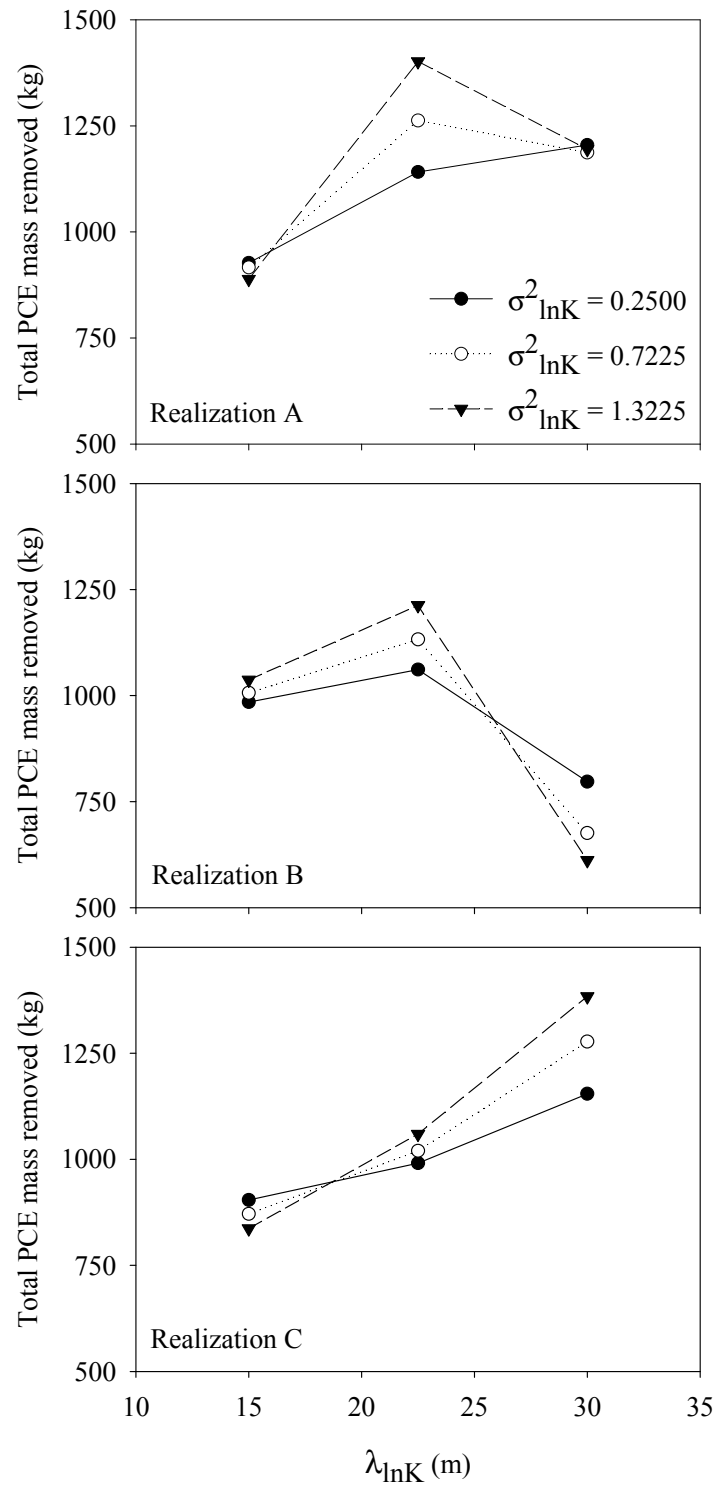


Figure 4.22. Change in total mass of PCE removed from the aquifer with respect to $\lambda_{\ln K}$ for original plume case

coming to the GAC unit and the total pumping rate. For field K23A, the total pumping rate was significantly lower compared to other $\sigma_{\ln K}^2$ cases for realization A and $\lambda_{\ln K}$ of 30 m because of the use of two wells. Total pumping rate was 615.6 and 680.4 m³/day for K13A and K33A, respectively while it was 475.2 m³/day for K23A. It seems that pumping from two different locations of the aquifer with a smaller pumping rate was enough to satisfy the remediation goal despite higher total cost. As a result, the incoming water to the GAC column was more concentrated for K23A. In fact, when all heterogeneous K-fields were considered, K23A exhibited the highest level of mass of PCE removed per each unit of water withdrawn from the aquifer. The range of PCE mass removed per volume of water withdrawn for different fields was 1.1 gr/m³ to 2.0 gr/m³. The maximum rate of removal for single well designs was 1.9 gr/m³.

There was also a direct correlation between PCE mass initially present in the aquifer and the total PCE mass removed during remediation. The trends with respect to $\lambda_{\ln K}$ and $\sigma_{\ln K}^2$ were the same for initial PCE mass (Figure 4.16) and PCE mass removed from the aquifer (Figure 4.22). Since the remediation goal for all fields was the same, higher contaminant mass was removed in fields that had higher initial contaminant mass.

Figure 4.23 summarizes the variation in the total remediation costs for 27 different fields having different heterogeneity conditions. For each $\lambda_{\ln K}$, the average, standard deviation, minimum and maximum values obtained for fields of different $\sigma_{\ln K}^2$ and realizations were considered. In Figure 4.23 there was a slight increase in the average value when $\lambda_{\ln K}$ increased from 15 m to 22.5 m. The average cost value remained constant between $\lambda_{\ln K}$ of 22.5 m and 30 m. The noticeable trend in Figure 4.23 was that when $\lambda_{\ln K}$ increased, the variation of cost values around the average also increased. This might be understood better if the variation of initial mass and plume area with respect to $\lambda_{\ln K}$ was investigated in the same way. Figure

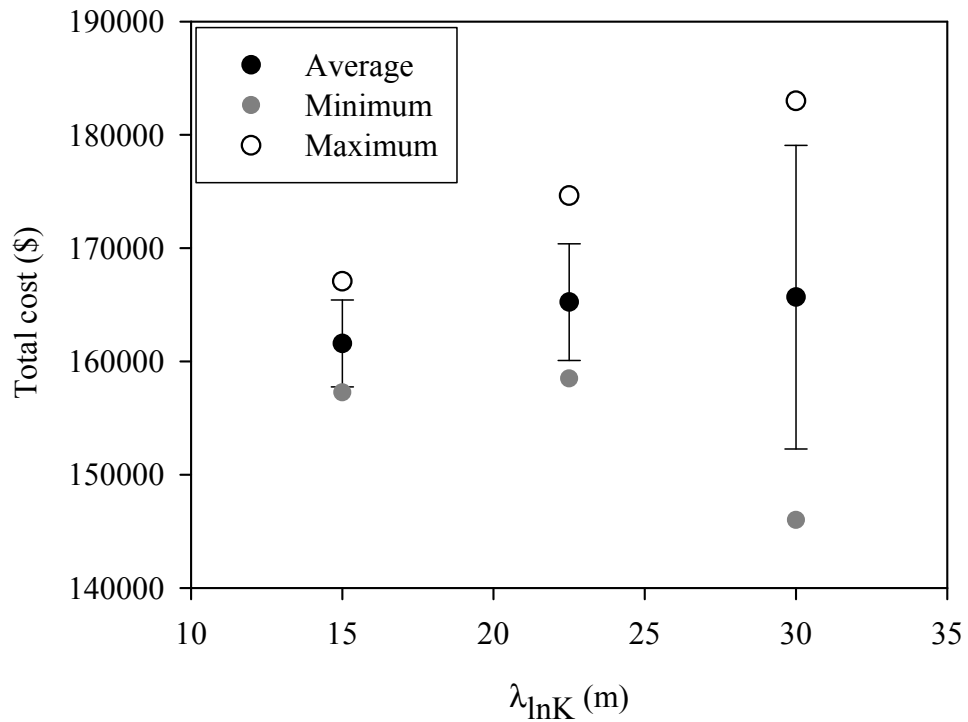


Figure 4.23. Variation in the total remediation costs with respect to $\lambda_{\ln K}$ (error bars represent one standard deviation): original plume case

4.24 shows these analyses. The trend was a little different than the trend of total cost such that average mass and area decreased when $\lambda_{\ln K}$ increased from 22.5 to 30 m. This was because the high cost of field K23A made the average of total cost for $\lambda_{\ln K}$ of 30 m higher. Similar to total cost, variation around the average of initial PCE mass and plume area increased with increasing $\lambda_{\ln K}$. Therefore, although the impact of a realization of a heterogeneous K-field on the results was shown, in overall, high $\lambda_{\ln K}$ promoted more variation in the costs. For larger $\lambda_{\ln K}$, the distance between the high and low K zones and the areas associated with these zones were larger. Therefore, together with the relative locations of high and low K zones, $\lambda_{\ln K}$

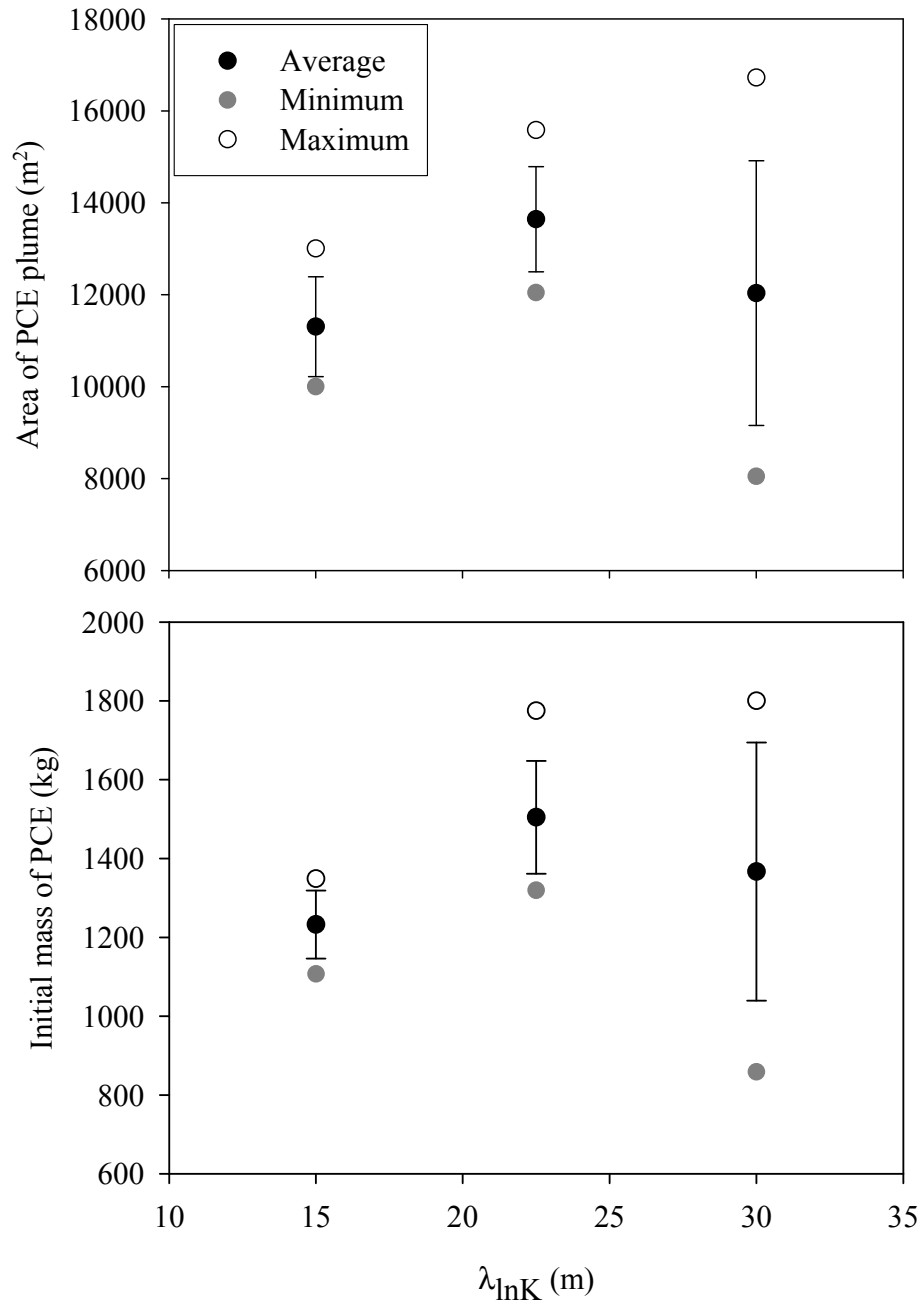


Figure 4.24. Variation in the area and the initial mass of initial plume with respect to $\lambda_{\ln K}$ (error bars represent one standard deviation): original plume case

of the field impacted the spreading and then the remediation of contamination. This in turn, resulted in either higher or lower remediation costs.

When the variation in the unit cost of PCE removal was analyzed with respect to λ_{lnK} (Figure 4.25), it was noted that the observed trend was negatively correlated with the relationships between the area of PCE plume and λ_{lnK} and the PCE mass and λ_{lnK} as given in Figure 4.24. Yet, the maximum variation was still observed for the highest λ_{lnK} . For fields having λ_{lnK} of 15 m, the lowest and highest remediation cost per mass of PCE removal were \$160/kg PCE and \$188/kg PCE, respectively. These values were \$125/kg PCE and \$162/kg PCE for λ_{lnK} of 22.5 m, and \$129/kg PCE and \$239/kg PCE for λ_{lnK} of 30 m, respectively. 91% variation (with respect to minimum) in the unit cost of PCE mass removal was observed for different heterogeneity conditions. Therefore, λ_{lnK} impacted the migration and mass of the contamination and, therefore, the unit cost of remediation.

4.3.1.2. Results of the Average Plume Case

For the average plume case, the optimal remediation designs for 25 of the 27 heterogeneous fields resulted in the selection of a single active well. For fields K23A and K33A, 2 wells were required for the cleanup. Among 25 different single well designs, well 13 was the most frequently selected active well for 13 K-fields. In 10 of the 27 fields (37%), the locations of the active wells for the average plume case were the same as for the original plume case. Nevertheless, for majority of these fields (8 out of 10), the pumping rates were different compared to the original plume case. In 17 of the fields, different locations were selected for active wells compared to the original plume case. Therefore, the change in the configuration of the initial plume and heterogeneity governed the optimum remediation design and costs. Realization B exhibited the highest resemblance between the optimal remediation designs for original and average plume cases

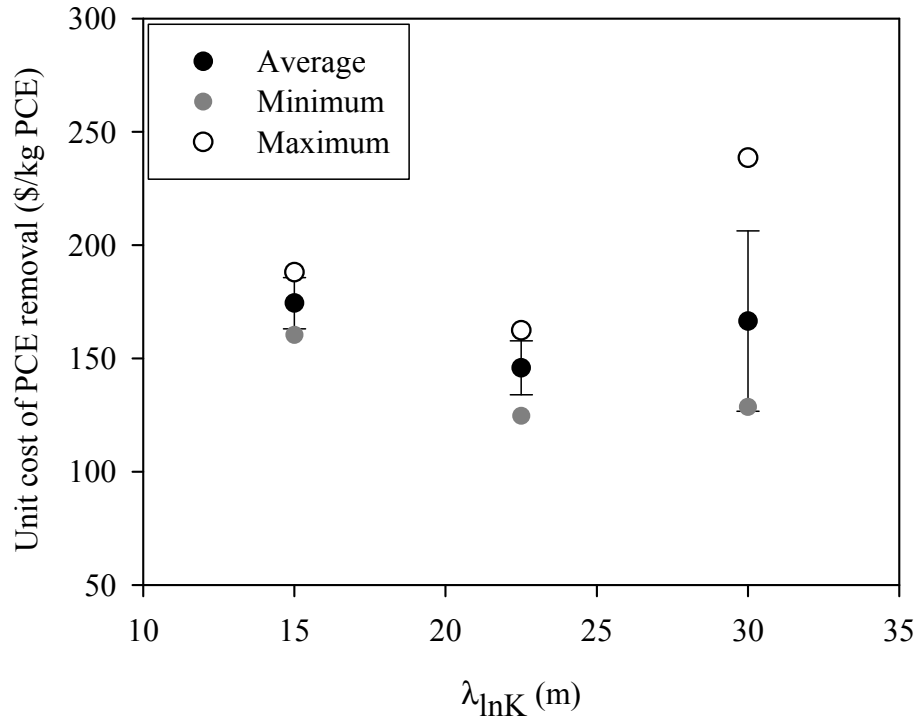


Figure 4.25. Variation in the unit cost of PCE removal with respect to $\lambda_{\ln K}$ (error bars represent one standard deviation): original plume case

compared to other realizations. Similar to the original plume case, active pumping wells in all designs (wells 7, 8, 13, 14, 17, 18) were the wells either on the centerline of the plumes or the wells adjacent to the wells on the centerline (Figure 4.26).

The only fields for which two wells were required for the cleanup were K23A and K33A. For K23A two wells were chosen for both original and average plume case but the well locations were different (wells 14 and 18 for original plume case but wells 13 and 18 for average plume case). In Figure 4.27, it was seen that average plume covered the low K region at the center of the aquifer as it was in the original

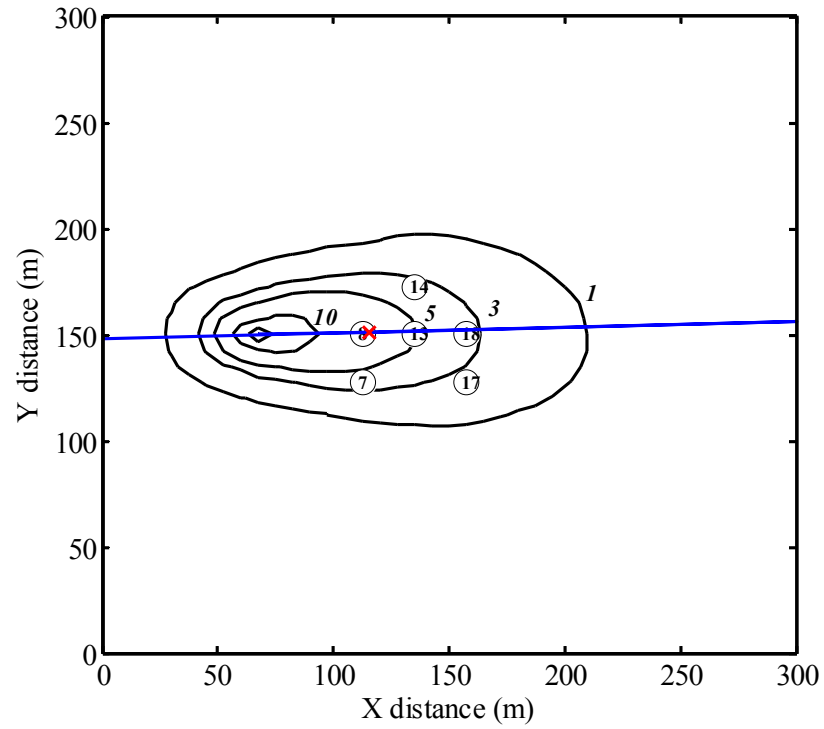


Figure 4.26. Selected wells for average plume case along with the CoM (red cross) and centerline (blue line) of the average plume

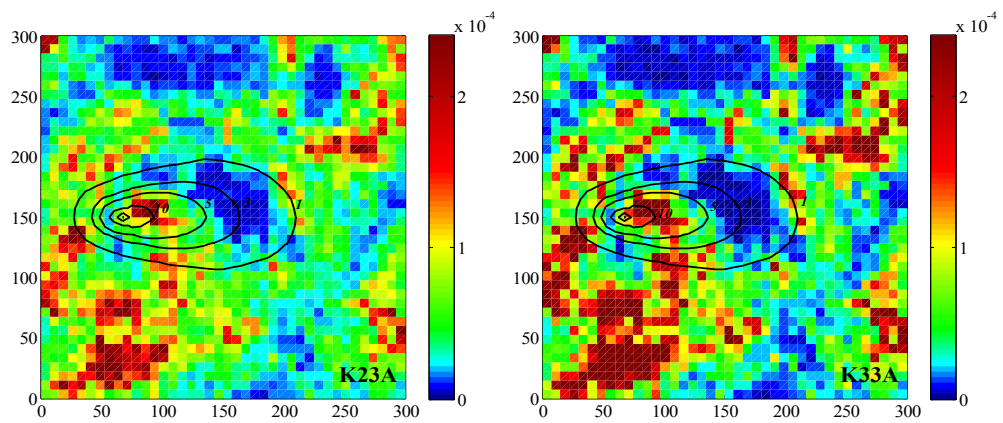


Figure 4.27. Initial plume location and K distributions for fields K23A and K33A for the average plume case

plume case. This might be the reason of the selection of the same number of wells for the average plume case but different plume shapes and masses might cause selection of different well locations. The other difference between average and original plume case for the remediation system design for K23A was the pumping rate of the wells. For average plume case pumps operated at a lower rate (216 m³/day) compared to the original plume case (237.6 m³/day) at active wells. This was because the total mass initially present in the aquifer was less for average plume case (Figure 4.27) compared to the original plume case (Figure 4.10). For K33A single well (well 13) was selected in the original plume case but two wells (wells 14 and 18) were selected for the average plume case. Although initial mass was higher for K33A in original plume case, more costly 2-well design was chosen in the average plume case. This might be due to the slightly larger plume area and potentially unrealistic accumulation of contaminants (especially the sorbed phase) in the low K zones (Figures 4.13 and 4.27). Therefore, as stated before, it may be possible that the average initial plume disregarded the local deviations in K for initial plume formation. This showed that although the amount of PCE mass initially present in the aquifer was very important in terms of P&T design and cost, the location and size of the high and low K regions as well as the magnitude of K was also important.

The minimum and maximum total remediation cost for all 27 designs were \$156,100 (for field K22C) and \$177,100 (for field K23A), respectively, when the initial plume was the same for all heterogeneous fields (Figure 4.28). Therefore, the total cost changed by up to 13% with respect to the minimum cost depending on the heterogeneity condition and the respective locations of high and low K zones. This percent variation was the half of the percent variation observed for the original plume case and showed the decrease in variation in the cost when average plume was used in the simulations. The levels of percent change in the remediation costs for different heterogeneity conditions were 11% for realization A, 4% for

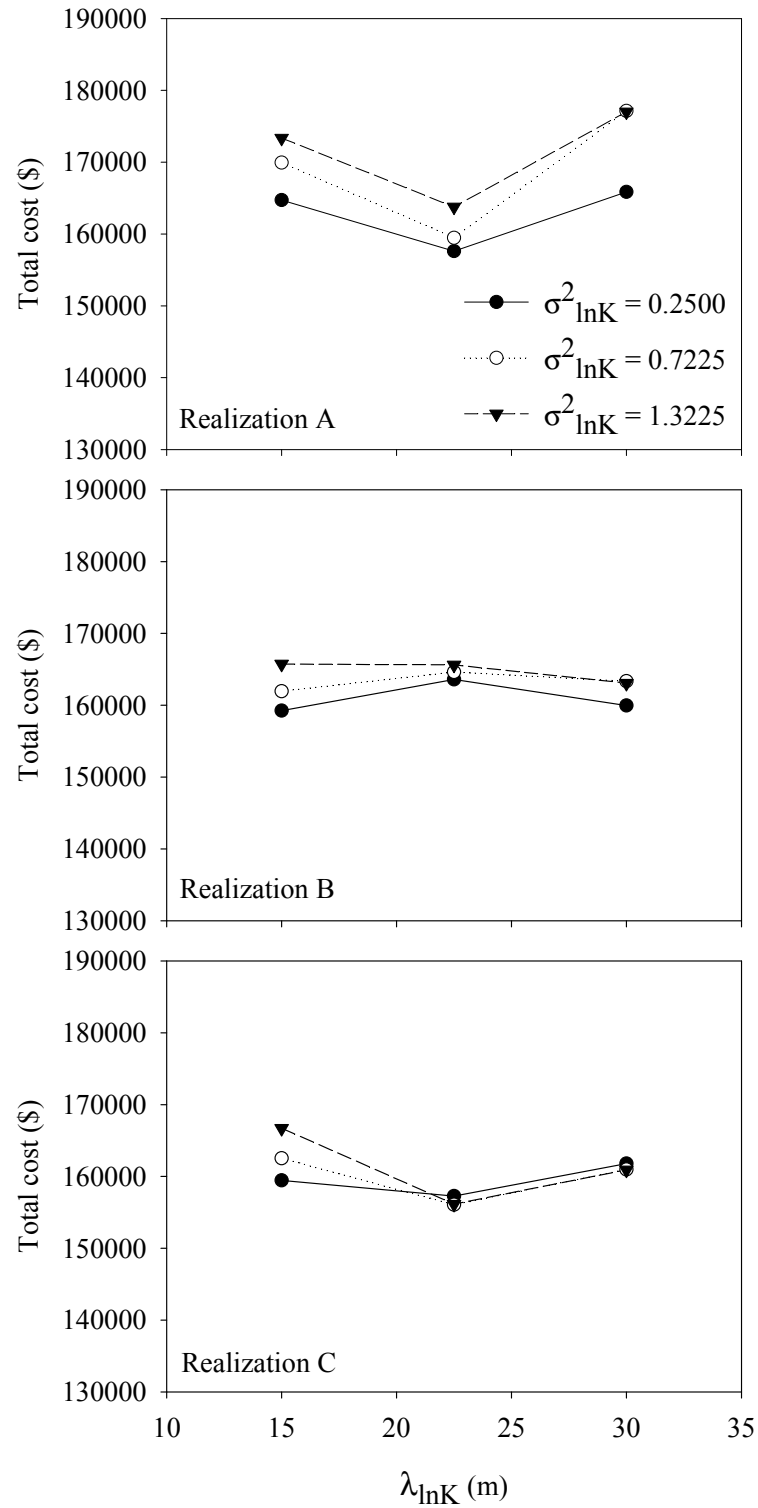


Figure 4.28. Change in total remediation costs with respect to $\lambda_{\ln K}$ for average plume case

realization B and 7% for realization C. When the capital cost of GAC unit was excluded, the remaining costs changed by up to 38% among all realizations depending on the heterogeneity condition and the respective locations of high and low K zones. This value was 30% for realization A, 11% for realization B and 19% for realization C, individually.

When the total remediation costs presented in Figure 4.28 was investigated, it was observed that the relationships between costs and $\lambda_{\ln K}$ were divergent for different realizations of the heterogeneous fields, as also observed for the original plume case. However, since the initial contaminant mass was similar, the extent of variation for different $\lambda_{\ln K}$ values was less significant compared to the original plume case.

Total cost got higher with increasing $\sigma^2_{\ln K}$ for some fields but there were also fields for which total cost was the same for different $\sigma^2_{\ln K}$. Aksoy and Culver (2004) found the optimum well locations and the pumping rates in order to minimize the cost of remediation of a single contaminant plume on heterogeneous aquifers with different $\sigma^2_{\ln K}$ values and different K distributions (i.e. realizations). Their results showed that for one of the realizations cost increased with increasing $\sigma^2_{\ln K}$ but for the other two realizations a slight decrease was observed at low $\sigma^2_{\ln K}$ values. The findings of this study were in line with that of Aksoy and Culver (2004) such that a slight decrease may be observed with increasing $\sigma^2_{\ln K}$ as it was for realization C with $\lambda_{\ln K}$ of 22.5 and 30 m.

Similar to the original plume case, treatment and pumping costs determined the general trend of total remediation costs with respect to $\lambda_{\ln K}$ for the single well designs (Figures 4.29 and 4.30). All optimal designs employed only one GAC adsorber. Figure 4.31 shows the change in capital costs (i.e. sum of capital cost of well(s) and GAC unit) with respect to $\lambda_{\ln K}$. Except fields K23A and K33A, which

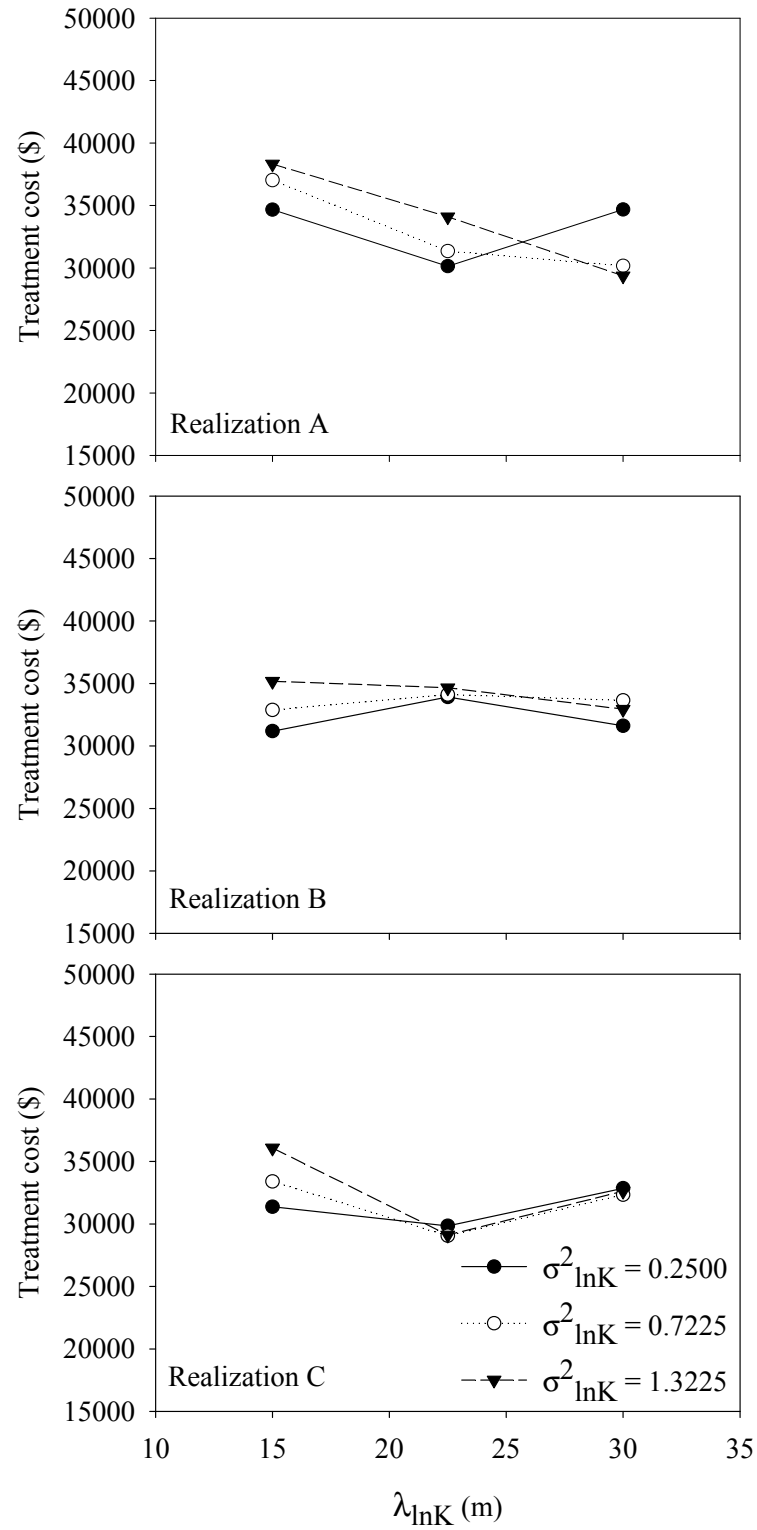


Figure 4.29. Change in treatment costs with respect to $\lambda_{\ln K}$ for average plume case

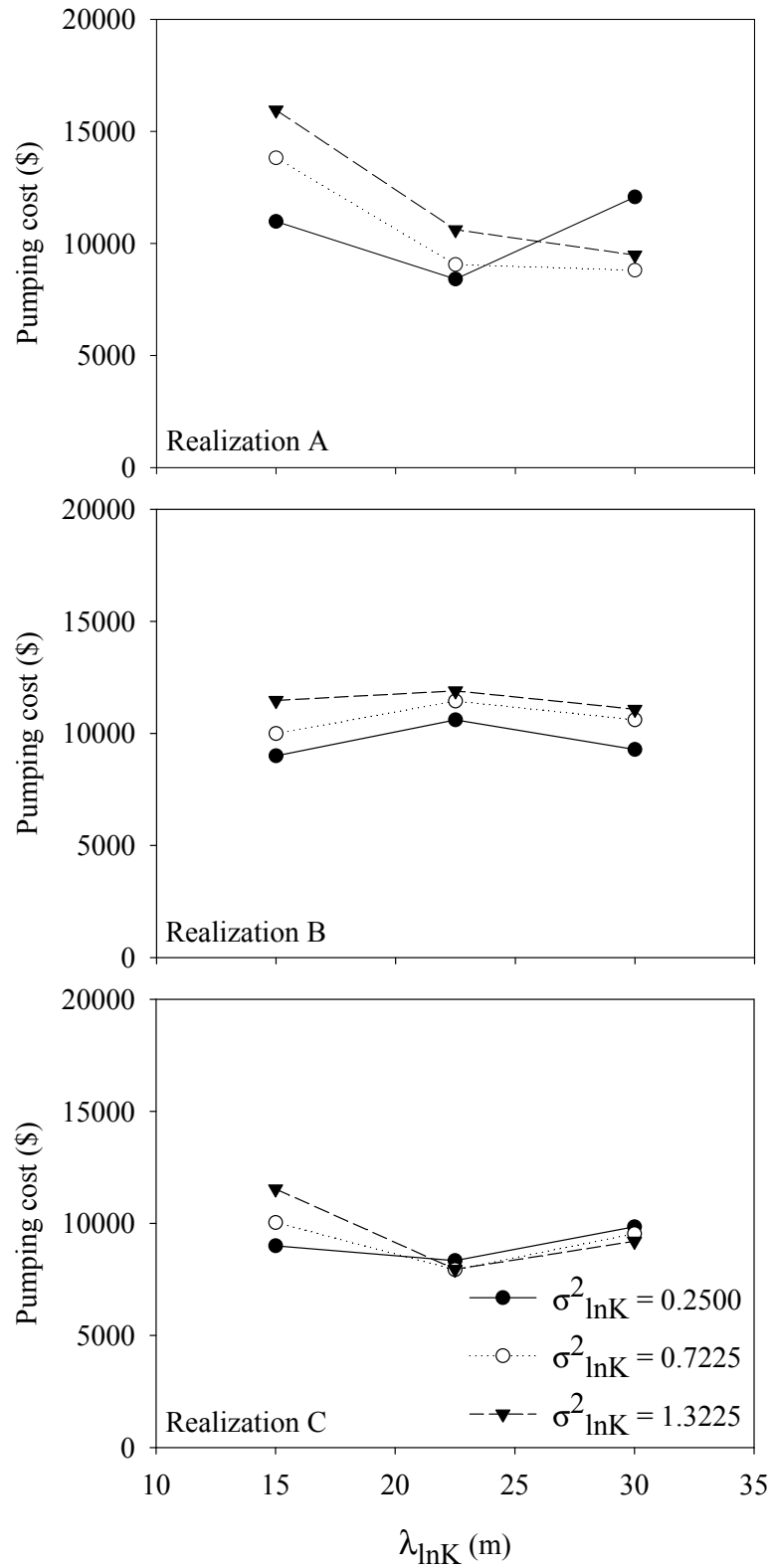


Figure 4.30. Change in pumping costs with respect to $\lambda_{\ln K}$ for average plume case

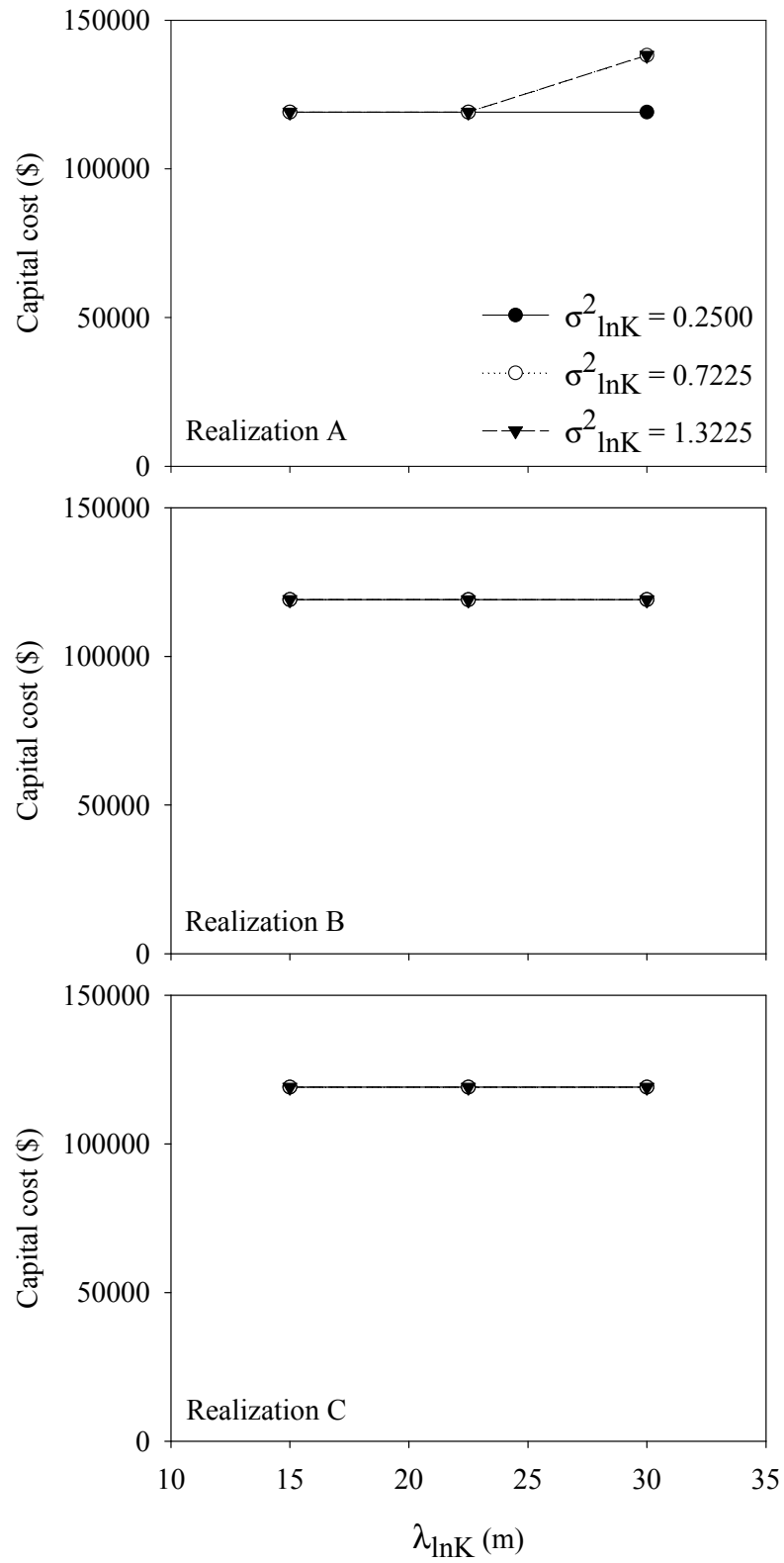


Figure 4.31. Change in capital costs with respect to $\lambda_{\ln K}$ for average plume case

used two active wells, capital costs were similar. When the locations of active wells for different K-fields were considered (wells 7, 8, 13, 14, 17, 18 in Figure 3.10), the maximum downstream distance between these wells was 45 m. Therefore, the capital costs, including the installation costs of GAC treatment facility and the pumping wells, were almost the same as long as the numbers of active wells were the same. Figures 4.29 and 4.30 show the change in treatment and pumping costs with respect to λ_{lnK} . The trends were similar with the total cost for both pumping and treatment costs except K23A and K33A. Treatment cost was a function of both PCE concentration coming to the GAC unit and the total pumping rate while pumping cost depended on pumping rate and the hydraulic head relative to well depth at end of management period. For fields K23A and K33A, the pumping rate was lower than field K13A because of the use of two wells and this made these costs lower. Total pumping rate was 540 m³/day for K13A but it was 432 and 410.4 m³/day for K23A and K33A, respectively.

The amount of PCE removed from the aquifer was fairly constant among different heterogeneity conditions since mass of PCE initially present in the aquifer was constant for the average plume case (Figure 4.32). The quantity of PCE removed from the aquifer to reach the remediation goals for the original plume case had the range of 610 to 1400 kg. This range was 970 to 1070 kg for the average plume case. The minimum unit remediation costs to reach the water quality standards were \$125/kg PCE and \$156/kg PCE for the original and average plume cases, respectively. The respective values for the maximum unit remediation costs were \$239/kg and \$183/kg. Therefore, when all heterogeneity conditions were considered for the average plume case, the variation (with respect to minimum) in the unit cost of PCE mass removal was 17% which was significantly low compared to the 91% variation observed for the original plume case. The range of PCE mass removed per volume of water withdrawn for different fields was 1.3

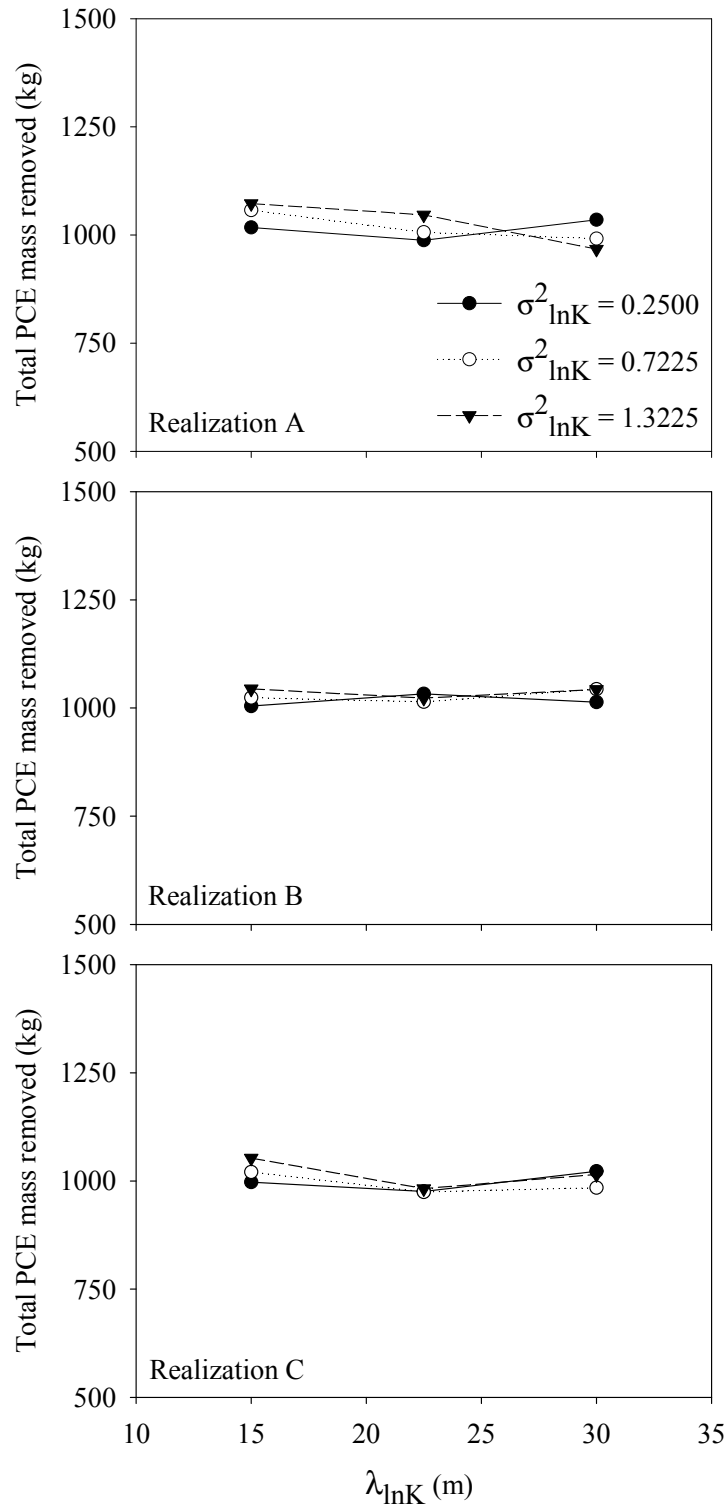


Figure 4.32. Change in total mass of PCE removed from the aquifer with respect to $\lambda_{\ln K}$ for average plume case

gr/m³ to 2.0 gr/m³. The maximum rate of removal was obtained for the fields which had the lowest total pumping rates (K32C and K22C). These fields also had the lowest total remediation costs among the all fields.

Figure 4.33 summarizes the deviation in the optimal remediation costs with respect to $\lambda_{\ln K}$. No regular continuously increasing or decreasing trend was observed as $\lambda_{\ln K}$ increased. Yet, the variation in costs for a given $\lambda_{\ln K}$ was not as significant for different $\sigma^2_{\ln K}$ values and realizations for the average plume case, compared to the original plume case (Figure 4.23). This was due to the same initial mass for cleanup.

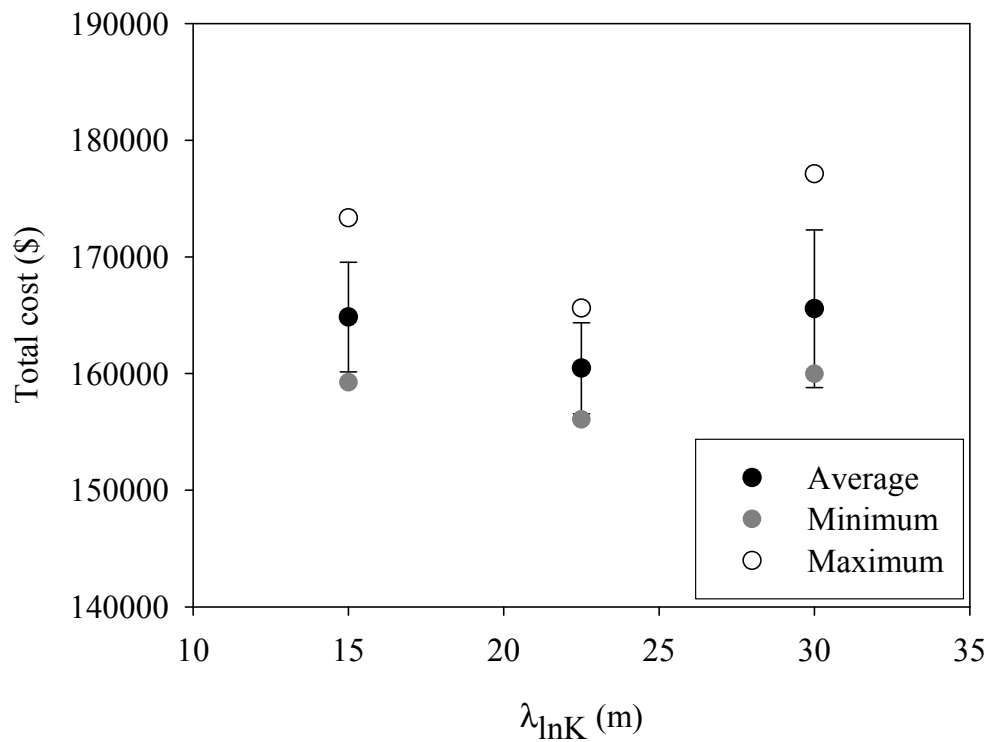


Figure 4.33. Variation in the total remediation costs with respect to $\lambda_{\ln K}$ (error bars represent one standard deviation): average plume case

In Figure 4.33, the trend in the variation in the total remediation costs with respect to $\lambda_{\ln K}$ was not similar to the one observed for the original plume case (Figure 4.23). However, similarly, the highest variation in costs was observed for $\lambda_{\ln K}$ of 30 m for heterogeneous K-fields of different realizations and $\sigma_{\ln K}^2$ values. The difference in the trends observed for the relationship between the total remediation costs and $\lambda_{\ln K}$ of the field was probably due to the distribution of contaminant mass in the aquifer. Unlike original plume case, the initial mass and the area of the PCE plume were constant in average plume case. Yet, the results obtained from the average plume case supported that together with the typical geostatistical parameters used to define a heterogeneous field, the respective locations of high and low K zones and the accumulation or spreading of the contaminant within these zones would be important in fate of the cleanup process and remediation design.

Optimal remediation design and cost were found for the homogenous K-field (i.e. all K values in the aquifer equaled to K_g of the heterogeneous fields) as well that had the average plume as the initial condition. Then optimal remediation designs for heterogeneous fields were compared with the optimum policy for the homogeneous K-field assumption. A single well design (well 13 in Figure 3.10) was adequate for the homogeneous K-field. This active well was chosen as the active well for 13 of the 27 heterogeneous K-fields as well. Therefore, 48% of the heterogeneous fields used the active well of the homogeneous K-field. Yet, the pumping rates at this well for the heterogeneous K-fields varied compared to the homogeneous K-field. For the homogeneous K assumption, the active well pumped at a rate of 432 m³/day. This same well pumped at a rate ranging between 432 and 594 m³/day for heterogeneous aquifer conditions. Only, field K12A had the same pumping rate with the homogeneous K-field assumption. All other K-fields that used well 13 required higher pumping rates that resulted in up to 38% more water withdrawal from the aquifer. The total remediation cost for the homogeneity assumption in K was \$157,700. Providing that the costs for the

heterogeneous aquifers ranged between \$156,100 and \$177,100, heterogeneity resulted in variation in the remediation costs. Heterogeneity generally caused an increase in the remediation cost such that only the remediation costs for 4 K-fields (\$157,600 for K12A, \$157,300 for K12C, \$156,100 for K22C and \$156,100 for K32C) were less than the cost for the homogeneous K-field. The unit cost of remediation of the contaminant plume for the homogeneous K-field was \$160/kg PCE removed while this value ranged between \$156/kg PCE and \$183/kg PCE for heterogeneous fields. Therefore, once again, it was shown that neglecting heterogeneity in K and using the simplifying assumption of homogeneity would result in errors both in the remediation design and prediction of the remediation costs.

4.3.2. Results of the Time-to-Compliance Model

In time-to-compliance optimization model, two different prespecified remediation designs having different pumping schemes were applied to both original and average plume cases. The first design (1-well-policy) included well 13, which was the most frequently selected well in optimal design model for both original and average plume cases under heterogeneous field conditions and the optimum well for homogenous K-field for the average plume case. It pumped at a fixed rate of 175 m³/day, which was relatively low compared to the optimum pumping rates found as a result of optimal design model runs. The second design (7-well-policy) consisted of 7 different wells, wells 3, 7, 9, 13, 17, 19 and 23, pumping at the same rate of 25 m³/day so that the total pumping rate equaled to 175 m³/day. The locations of the wells were shown in Figure 3.18. The aim of selecting two different designs was to find out the effect of different pumping schemes (number of pumping wells, their locations and pumping rates) on time-to-compliance. Maskey et al. (2002) tried to optimize cleanup time on a heterogeneous aquifer by selecting different candidate well locations for the optimization problem. They tried potential well locations outside the plume area and both outside and inside

the plume area. Their results showed that when potential well locations were selected both outside and inside the plume area, well locations inside the plume were selected as active. Shorter cleanup times were achieved for inside wells when compared to potential well locations just outside the plume area. In their modeling study, Bakr et al. (2003) found that selection of the pumping wells inside the plume gave better remediation performance in terms of mass removed from the aquifer with the same total pumping rate and resulted in more reliable remediation for a heterogeneous aquifer. However in none of these studies, the effect of number of wells used for the remediation was investigated. In Section 4.3.1 of this study, where the results of optimal design model were presented, it was seen that the selected optimal wells were always inside the plume area although some of the potential wells were outside the plume area (Figure 3.10 to 3.13). Based on the previous findings of this study and the literature, the selection of pumping well locations inside the plume where the contaminant concentration was higher was an appropriate choice in terms of finding the optimum cleanup times.

As Maskey et al. (2002) expressed well locations were important for finding the optimal system design. It must be stated that the designs used in this part of the study may not be the optimum designs for a given heterogeneous field and the optimal remediation times and their change with respect to different heterogeneity conditions may differ when different pumping well locations are chosen.

4.3.2.1. Results of the Original Plume Case

The results of the optimization runs conducted with original plumes for 1-well-policy on heterogeneous K-fields showed that the optimal remediation times varied between 1920 (for field K23B) and 7142 days (for field K33A). On the other hand, the minimum and maximum time-to-compliance was 2696 days (for field K31C) and 5560 days (for field K32C), respectively, for 7-well-policy. Remediation times for both policies were quite longer than 1260 days, which was

the length of the remediation period in the optimal design model. This was because the location of wells selected for 1-well and 7-well policies might not be the optimum for some of the heterogeneous K-fields. In addition, the total pumping rate ($175 \text{ m}^3/\text{day}$) used in these policies was quite lower than the selected pumping rates found by GA in the optimal design model (in the range of 324 to $680.4 \text{ m}^3/\text{day}$).

Figures 4.34 and 4.35 show the change in time-to-compliance with respect to $\lambda_{\ln K}$ for 1-well and 7-well policies, respectively. As it was the case for the total remediation cost in the optimal design model, there was no regular trend in remediation time with respect to $\lambda_{\ln K}$ for both policies. For 7-well-policy, remediation time seemed fairly constant with respect to $\lambda_{\ln K}$ especially for realization A and B. It varied much more for realization C. For both policies, time-to-compliance generally got higher with increasing $\sigma_{\ln K}^2$ but there were also few fields for which the opposite or the equality among different $\sigma_{\ln K}^2$ was observed.

When time-to-compliance values were compared for 1-well and 7-well policies, it was seen that remediation time was generally higher for 1-well-policy compared to 7-well-policy while the magnitude of the difference changed from field to field. On the other hand, the opposite was observed for fields K23B and K33B for which remediation time for 1-well-policy was well below the time for 7-well-policy. In addition, for fields K13C, K23C and K33C the remediation times were almost the same for both policies.

For 1-well-policy, time-to-compliance changed by up to 272% with respect to minimum remediation period depending on the heterogeneity condition and the respective locations of high and low K zones. When the realizations were investigated individually, the percent change among different heterogeneous cases was 86% for realization A, 156% for realization B and 104% for realization C. For

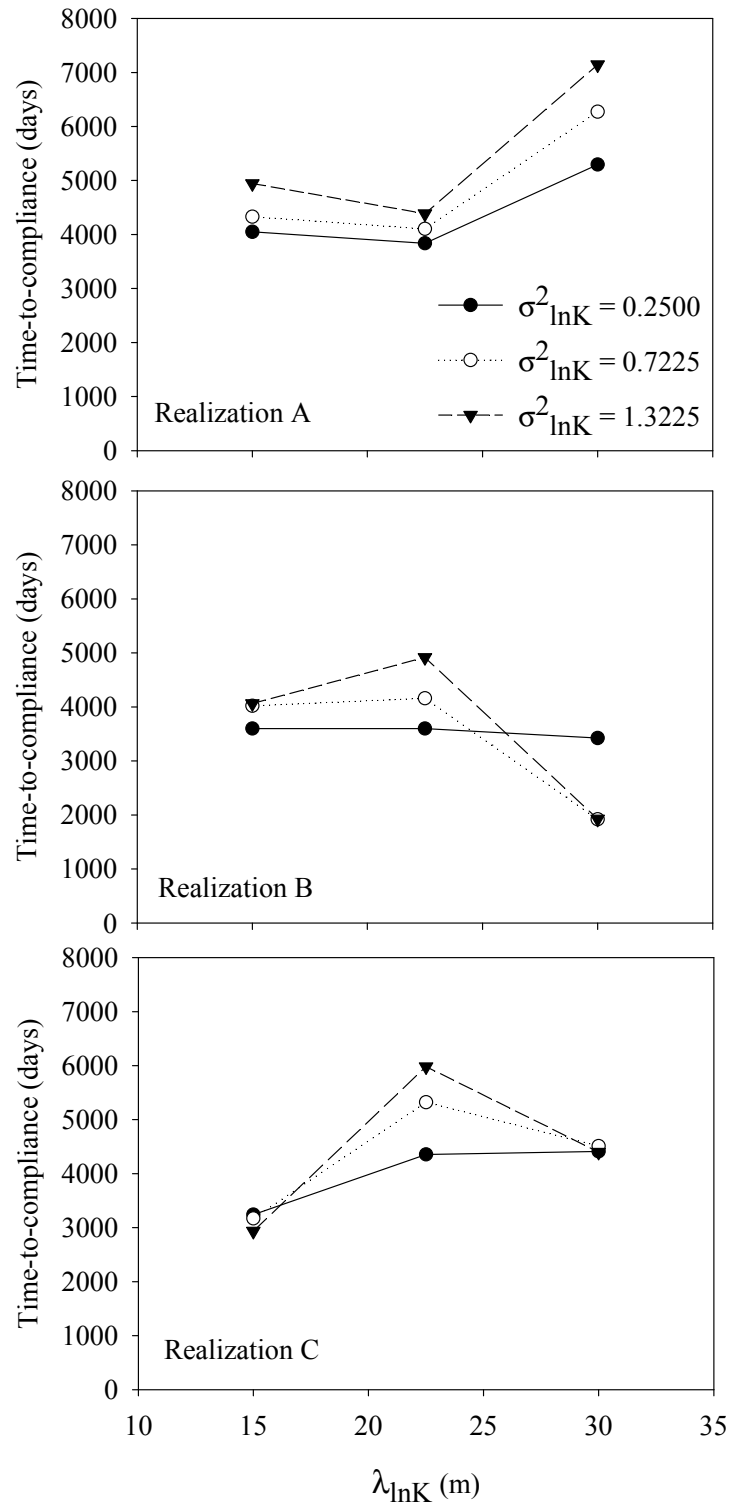


Figure 4.34. Change in the length of remediation periods with respect to $\lambda_{\ln K}$ for 1-well-policy and for original plume

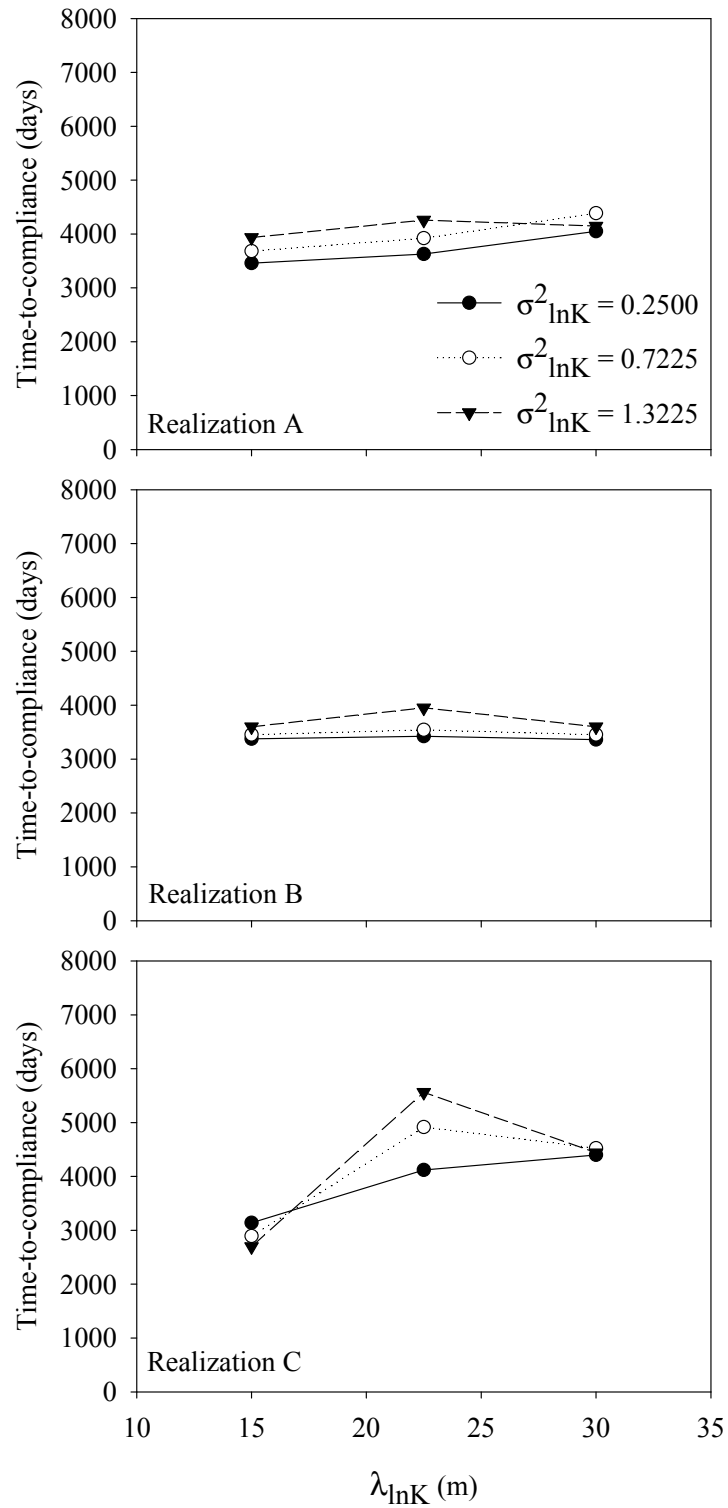


Figure 4.35. Change in the length of remediation periods with respect to $\lambda_{\ln K}$ for 7-well-policy and for original plume

7-well-policy, on the other hand, time-to-compliance changed by up to 106% with respect to minimum time-to-compliance depending on the heterogeneity condition and the respective locations of high and low K zones. When the realizations were investigated individually, the percent change among different heterogeneous cases was 27% for realization A, 17% for realization B and 106% for realization C. Although 106% change in time-to-compliance for 7-well-policy was still very high, it was less than half of the percentage value found for 1-well-policy (272%). These percentage values, which were extremely high especially for 1-well-policy, showed that if a remediation system design was made without considering the heterogeneity conditions and contaminant mass to be cleaned up, the remediation time might show great variations and might be well above the expected length of remediation period.

When Figure 4.34 was compared with Figure 4.16, which shows the change in initial mass of PCE with respect to λ_{lnK} , it was seen that there was not a correlation between initial mass and time-to-compliance, except for realization B, for 1-well design. On the other hand, as explained in Section 4.3.1.1, there was a correlation between initial mass and total remediation cost. The difference for time-to-compliance model might be the use of fixed and possibly non-optimal well location and pumping rate for the remediation. When the optimal designs found in Section 4.3.1.1 were investigated thoroughly, it was seen that well 13 was selected in 5 of the 9 fields for realization B but only 3 and 1 of the 9 fields for realization A and C, respectively. In other words, the use of well 13 was the most appropriate for realization B compared to the other realizations at least in terms of well location. This might be the reason of a correlation between initial mass and time-to-compliance for realization B. Comparison of Figure 4.35 with Figure 4.16 showed that no correlation between initial mass and time-to-compliance existed for any of the realizations for 7-well-policy.

Figure 4.36 presents the variation in time-to-compliance for 27 different fields having different heterogeneity conditions and for 1-well-policy. For each $\lambda_{\ln K}$, the average, standard deviation, minimum and maximum time-to-compliance values obtained for fields of different $\sigma^2_{\ln K}$ and realizations were considered. The trend observed in Figure 4.36 was very similar to that of area of PCE plume and initial mass of PCE in Figures 4.24. There was a slight increase in the average value when $\lambda_{\ln K}$ increased from 15 m to 22.5 m. The average remediation time value showed a very slight decrease between $\lambda_{\ln K}$ of 22.5 m and 30 m. Indeed, this trend was not very different from the trend of total remediation cost (Figure 4.23). The reason of this resemblance might be the dominance of single well designs in optimal design model. The obvious trend in this figure was that when $\lambda_{\ln K}$ increased the spread of remediation time values around average was getting bigger. This was also the same with Figures 4.23 and 4.24. The result of increasing $\lambda_{\ln K}$ was the increase in the distance between high and low velocity regions and the areas of these regions and this might be the reason of increasing variation in time-to-compliance with increasing $\lambda_{\ln K}$.

Similar to 1-well-policy, the change of average, minimum, maximum and standard deviation value of time-to-compliance with respect to $\lambda_{\ln K}$ for 7-well-policy and original plume case is presented in Figure 4.37. The trend in the change of average value of time-to-compliance with respect to $\lambda_{\ln K}$ for 7-well-policy was quite similar to that of 1-well-policy in Figure 4.36. However, the trend in variation of cost values around average was not alike. Unlike 1-well-policy, the variation of remediation time around average value was not the highest when $\lambda_{\ln K}$ was the longest. It increased when $\lambda_{\ln K}$ increased from 15 m to 22.5 m and reached the highest value. With the increase in $\lambda_{\ln K}$ from 22.5 m to 30 m, the variation returned almost the same value of standard deviation with $\lambda_{\ln K}$ of 15 m. In addition, the magnitude of the variation around the average and the standard deviation was not as high as it was in 1-well policy. The result of this change might be the use of

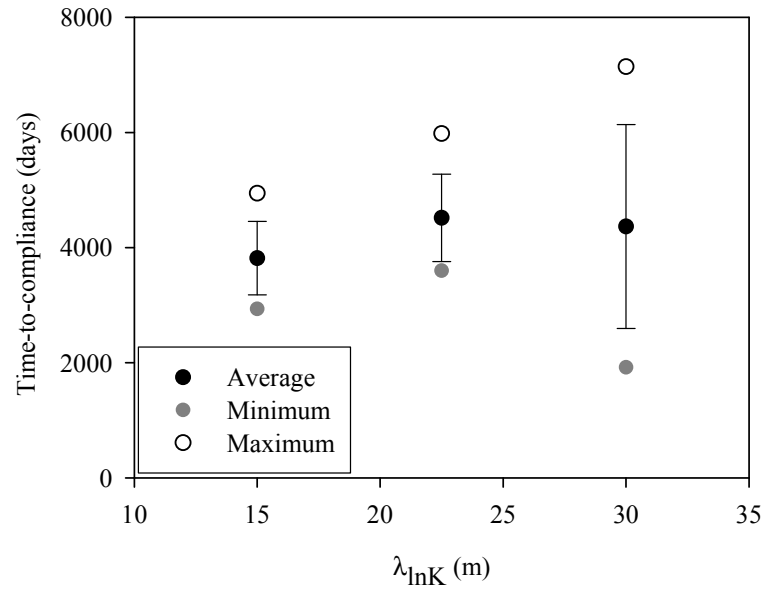


Figure 4.36. Variation in the time-to-compliance with respect to $\lambda_{\ln K}$ (error bars represent one standard deviation): 1-well-policy and for original plume case

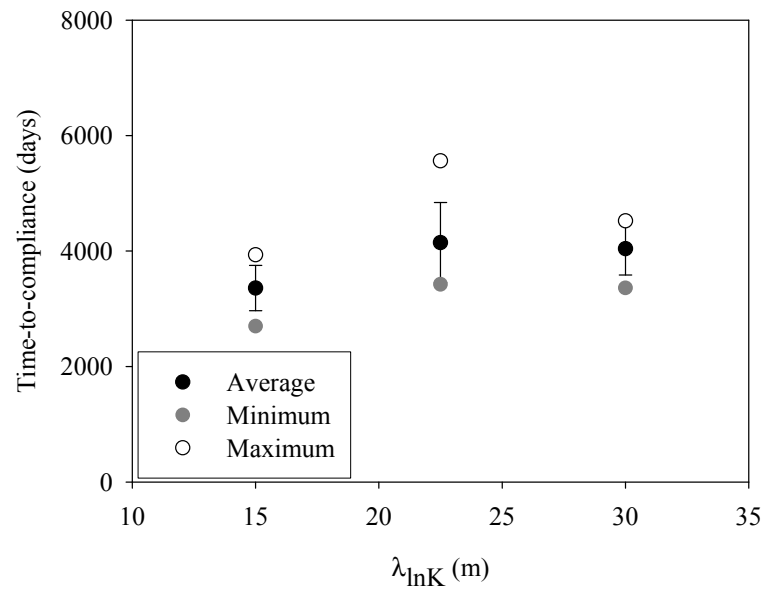


Figure 4.37. Variation in the time-to-compliance with respect to $\lambda_{\ln K}$ (error bars represent one standard deviation): 7-well-policy and for original plume case

seven pumping wells spread over the plume unlike all previous cases (i.e. optimal design model and time-to-compliance model with 1-well-policy). When the wells were spread on the plume over a 90×45 m region they could take PCE mass from very different locations of the aquifer. Enlarging of the active well area might reduce the effect of changing heterogeneity conditions on remediation time.

4.3.2.2. Results of the Average Plume Case

According to the results of the optimization runs conducted with the average plume on heterogeneous K-fields, the maximum and minimum optimal remediation time were 3137 days (for field K12A) and 7422 days (for field K33A), respectively, for the 1-well-policy. Moreover, for 7-well-policy, optimal remediation times varied between 3144 days (for field K31B) and 5168 days (for field K32C). As it was for the original plume case, remediation times for both policies were quite longer than 1260 days. Total pumping rate being much lower than the optimal pumping rates found in optimal design model (between 205.2 and 658.8 m³/day) and the different well locations were the reasons of these long remediation times.

Figures 4.38 and 4.39 show the change in time-to-compliance with respect to $\lambda_{\ln K}$ for 1-well and 7-well policies, respectively. As it was in the original plume case, there was no regular trend in remediation time with changing $\lambda_{\ln K}$ for both policies. Remediation time was generally getting higher with increasing $\sigma^2_{\ln K}$ but there were also few fields for which the opposite or the equality was valid. Aksoy and Culver (2004) employed the simulation-optimization approach in order to explore the change in time-to-compliance with respect to different $\sigma^2_{\ln K}$ values for a given P&T remediation design (7 wells at fixed locations and with fixed pumping rates). They used three different realizations of K-fields and found that time-to-compliance increased with increasing $\sigma^2_{\ln K}$ for one of the realizations. But, it was

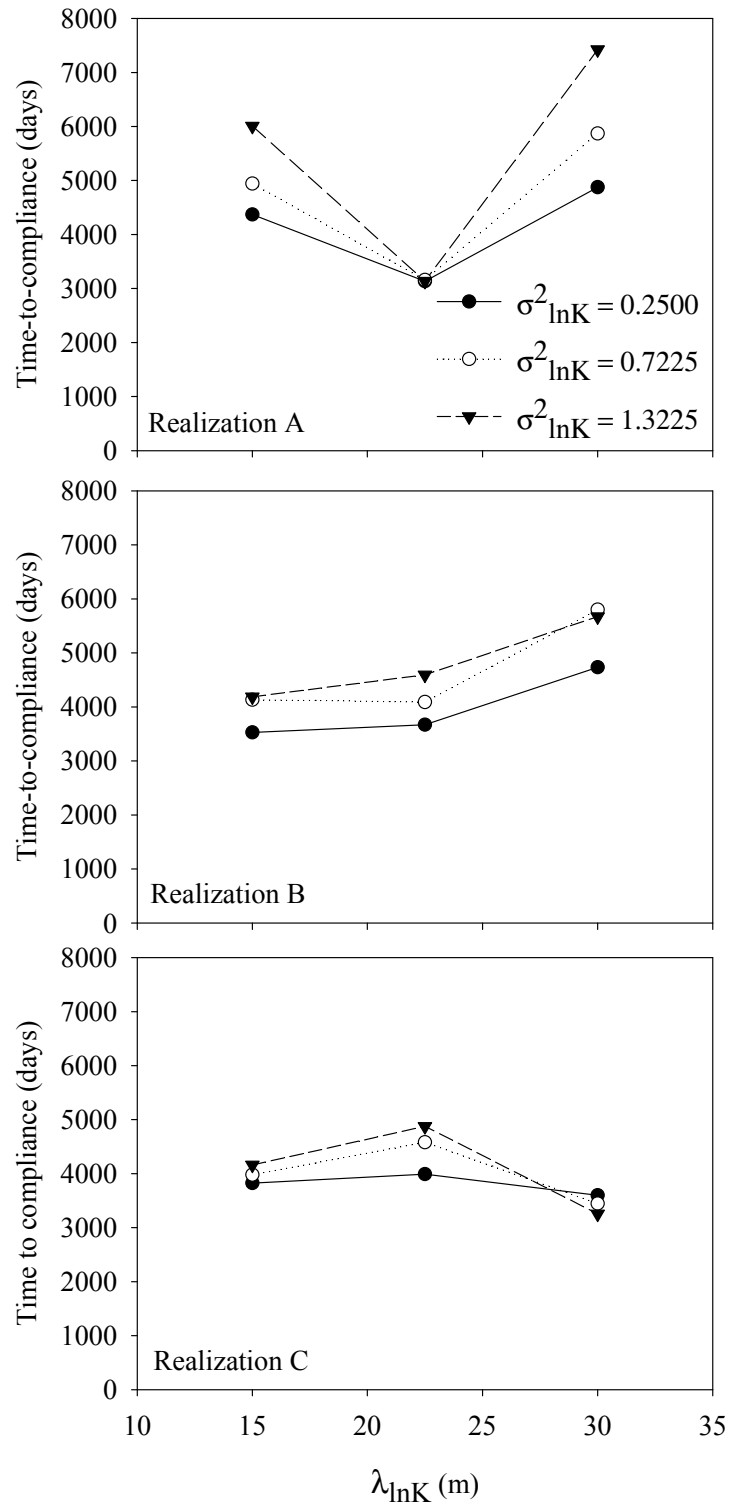


Figure 4.38. Change in the length of remediation periods with respect to $\lambda_{\ln K}$ for 1-well-policy and for average plume

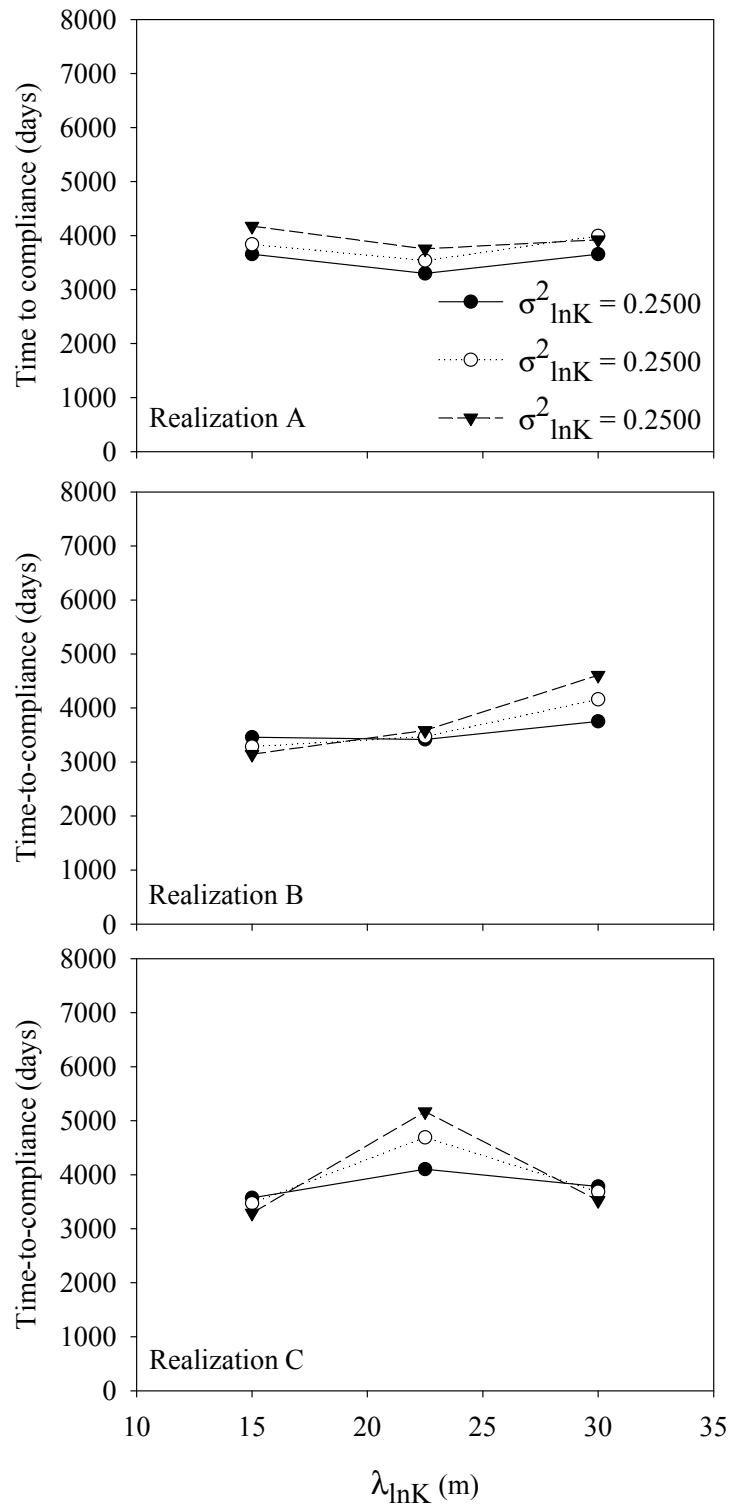


Figure 4.39. Change in the length of remediation periods with respect to $\lambda_{\ln K}$ for 7-well-policy and for average plume

fairly insensitive to K heterogeneity for the others. In general, findings of this study for both 1-well and 7-well policies and original and average plumes were in line with the findings of Aksoy and Culver (2004) such that the trend in the change of time to compliance with respect to $\sigma^2_{\ln K}$ was not constant for different realizations. This study also found that the change of time to compliance with respect to $\lambda_{\ln K}$ was not constant for different realizations, either.

Comparison of time-to-compliance for 1-well and 7-well policies showed that remediation time was generally higher for 1-well-policy compared to 7-well-policy while the magnitude of the difference changed from field to field. On the other hand, the opposite was observed for fields having $\lambda_{\ln K}$ of 22.5 m for realization A (K12A, K22A and K32A) and for fields having $\lambda_{\ln K}$ of 22.5 m and 30 m for realization C (K12C, K22C, K32C, K13C, K23C and K33C). But the differences were not significant.

For 1-well-policy, time-to-compliance changed by up to 136% with respect to the minimum remediation time depending on the heterogeneity condition and the respective locations of high and low K zones. When the realizations were investigated individually, the percent change among different heterogeneous cases was 136% for realization A, 64% for realization B and 50% for realization C. Furthermore, for 7-well-policy, time-to-compliance changed by up to 64% depending on the heterogeneity condition and the respective locations of high and low K zones. When the realizations were investigated individually, the percent change among different heterogeneous cases was 27% for realization A, 47% for realization B and 57% for realization C. Comparison of overall percent changes in time-to-compliance for both original and average plumes is given in Figure 4.40. The percent change in time-to-compliance was greater for 1-well-policy than 7-well-policy for both original and average plumes. It seems that the use of a number of wells instead of a single well and distribution of these wells over a larger area

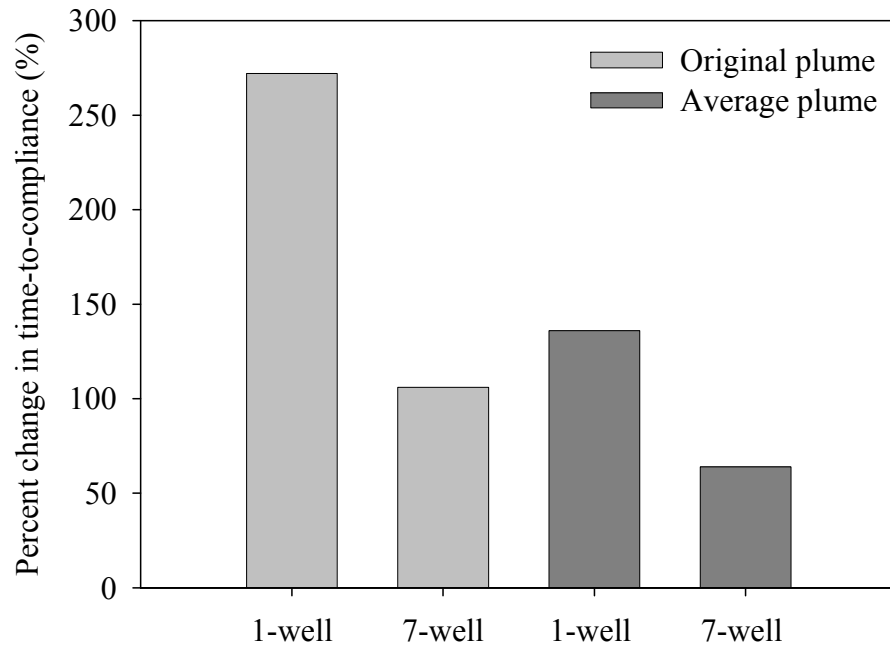


Figure 4.40. Comparison of percent change between minimum and maximum time-to-compliance among all K-fields for the 1-well and 7-well policies with the original and average plumes as the initial conditions (The percentage value was calculated by the division of difference between two values to minimum value)

kept the remediation time in a narrower range for different heterogeneity conditions and stabilized it irrespective of the initial amount and distribution of PCE mass.

Time-to-compliance model was applied to homogenous K-field as well (i.e. all K values in the aquifer equaled to K_g of the heterogeneous fields) with the use of average plume as the initial condition. Remediation times for 1-well and 7-well policies were 3838 and 3614 days for the homogenous K-field. Comparison of the remediation times found for homogenous K-field with the times for heterogeneous K-fields showed that, for the 1-well-policy, remediation times for 9 of the 27 heterogeneous K-fields were smaller than 3838 days. On the other hand, for the 7-

well-policy, 12 of the 27 heterogeneous K-fields gave remediation time smaller than 3614 days. This showed that for a fixed remediation design, heterogeneity in K generally resulted in an increase in the remediation time.

Figure 4.41 demonstrates the change of average, minimum, maximum and standard deviation of time-to-compliance obtained for fields of different $\sigma^2_{\ln K}$ and realizations, with respect to $\lambda_{\ln K}$ for the 1-well-policy. The trend in this figure was very similar to the trend of total remediation cost against $\lambda_{\ln K}$ of the fields for the average plume case (Figure 4.33). The reason of this resemblance was the single well designs being predominant in the optimal design model for the average plume. The trend in the variation was not regular for the average plume but variation was the highest for $\lambda_{\ln K}$ of 30 m as it was in original plume case for the 1-well-policy (Figure 4.36). The change in the trend for average plume compared to original plume might be the result of constant initial mass and area of the PCE plume.

For the 7-well-policy, Figure 4.42 presents the change of average, minimum, maximum and standard deviation of time-to-compliance obtained for all fields of different $\sigma^2_{\ln K}$ and realizations with respect to $\lambda_{\ln K}$. The trend was quite similar to the one for the original plume case shown in Figure 4.37. On the other hand, trends of 1-well and 7-well policies were not similar. Unlike 1-well-policy, for 7-well-policy, the variation of remediation time around the average value was the highest when $\lambda_{\ln K}$ was 22.5 m. As in the case of original plume, the result of this difference may be the enlargement of the remediation area with the use of seven pumping wells.

Results of this study demonstrated that the heterogeneity in K might have a significant impact on time-to-compliance depending on P&T design employed. This impact was not consistent for different spatial distributions of K (i.e. relative

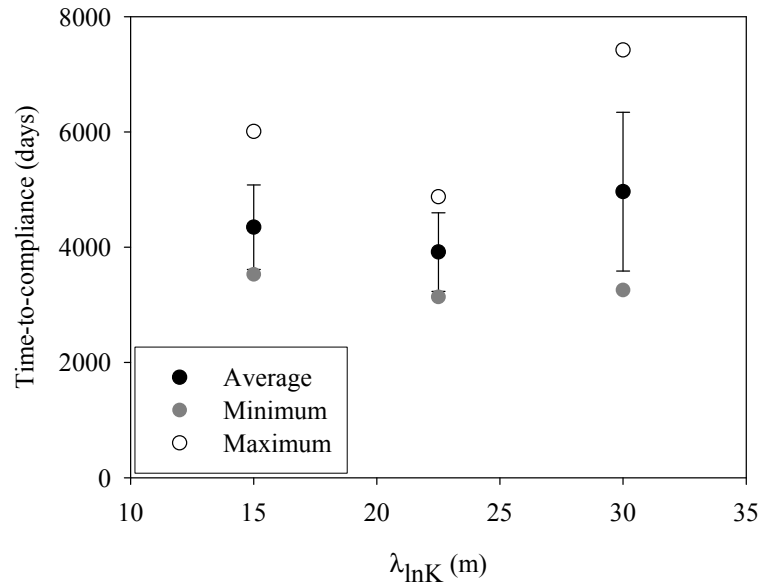


Figure 4.41. Variation in the time-to-compliance with respect to $\lambda_{\ln K}$ (error bars represent one standard deviation): 1-well-policy and for average plume case

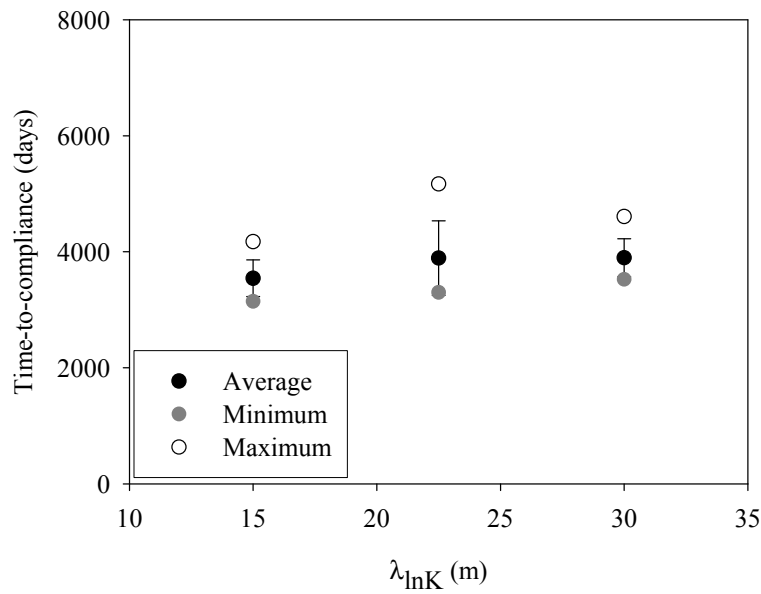


Figure 4.42. Variation in the time-to-compliance with respect to $\lambda_{\ln K}$ (error bars represent one standard deviation): 7-well-policy and for average plume case

locations of high and low K regions). Thus, heterogeneity conditions defined by $\lambda_{\ln K}$ and $\sigma^2_{\ln K}$ and the locations of high and low K zones must be known or predicted by high accuracy for more precise prediction of the performance of the P&T remediation systems. On the other hand, results indicated that when it was not possible to completely define the heterogeneity conditions in the aquifer, P&T designs that employed a number of wells pumping at lower rates instead of a single well might provide a more robust design in terms of time-to-compliance. Smaller number of pumping wells operating at higher pumping rates amplified the impact of heterogeneity. However, at this stage, a trade-off must be made between robustness and costs of P&T designs since the cost of 7-well-policy was higher than that of 1-well-policy due to the well installation cost.

4.4. Effect of Correlation Scale Anisotropy

In this section, the effect of $\lambda_{\ln K}$ anisotropy on P&T remediation system design and cost was investigated with the average plume as the initial condition. For this purpose, two different anisotropy ratios as 1.5:1 ($\lambda_{\ln K,x} = 22.5\text{m}$; $\lambda_{\ln K,y} = 15\text{m}$) and 2:1 ($\lambda_{\ln K,x} = 30\text{m}$; $\lambda_{\ln K,y} = 15\text{m}$) were considered. Two different $\sigma^2_{\ln K}$ (0.2500 and 1.3225) of realization B were used.

The results of the optimization runs performed with the average plume on anisotropic K-fields showed that $\lambda_{\ln K}$ anisotropy resulted in no change in the remediation designs in terms of the number of active wells. Both for isotropic and anisotropic fields, single well designs were chosen as the optimum. However, the location of the wells differed when the fields were anisotropic. This was expected since the locations and the shapes of the low and high K zones differed with changing anisotropy ratio (Figure A.4). In addition, pumping rate changed when fields became anisotropic. For $\sigma^2_{\ln K}$ of 0.2500, pumping rate increased 5% when the anisotropy ratio increased from 1 to 1.5, but decreased 5% below the pumping rate of the isotropic field when anisotropy ratio was 2. On the other hand, for $\sigma^2_{\ln K}$

of 1.3225, pumping rate decreased continuously with increasing anisotropy ratio (down to 21%). Therefore, there existed no unique trend. The relative locations and areas of different K zones determined the trend.

Figure 4.43 shows the total remediation cost on anisotropic K-fields with respect to $\sigma_{\ln K}^2$. The remediation cost was lower for anisotropic K-fields than the isotropic ones, except for field K10B_AN1 ($\lambda_{\ln K, x}$ of 22.5 m, $\lambda_{\ln K, y}$ of 15 m, $\sigma_{\ln K}^2$ of 0.2500). For this field, the remediation cost was almost equal to the cost of isotropic field with $\lambda_{\ln K, x}$ and $\lambda_{\ln K, y}$ of 15 m (i.e. K11B). When the results were investigated with respect to the anisotropy ratio (Figure 4.44), different trends were observed for different $\sigma_{\ln K}^2$ values. For the cases tested in this study, the maximum difference in remediation costs was \$7,620 (5% decrease with respect to isotropic K field) between isotropic and anisotropic fields with an anisotropy ratio of 2 for the high $\sigma_{\ln K}^2$ value. For the low $\sigma_{\ln K}^2$ value, this difference was \$1,630 (1% decrease with respect to isotropic K field).

Similar to the total cost, the amount of PCE removed from the aquifer decreased with increasing anisotropy ratio except for the field K10B_AN1. For this field the amount of removed PCE was almost equal to that on field K11B. These similar trends in the total cost and the amount of PCE removal resulted in a constant unit cost of PCE removal with changing anisotropy such that it was \$159/kg PCE for isotropic fields K11B and K31B but it was \$160/kg PCE for fields K10B_AN1 and K30B_AN1, and \$159/kg PCE for fields K10B_AN2 and K30B_AN2. Therefore, anisotropy did not have any impact on the unit cost of remediation under the conditions considered in this study.

In this study, for the cases studied, the effect of anisotropy ratio on the remediation cost was less significant than the effect of $\sigma_{\ln K}^2$. Hemsí and Shackelford (2006) had the similar outcome for the permeable reactive barrier design. They evaluated the

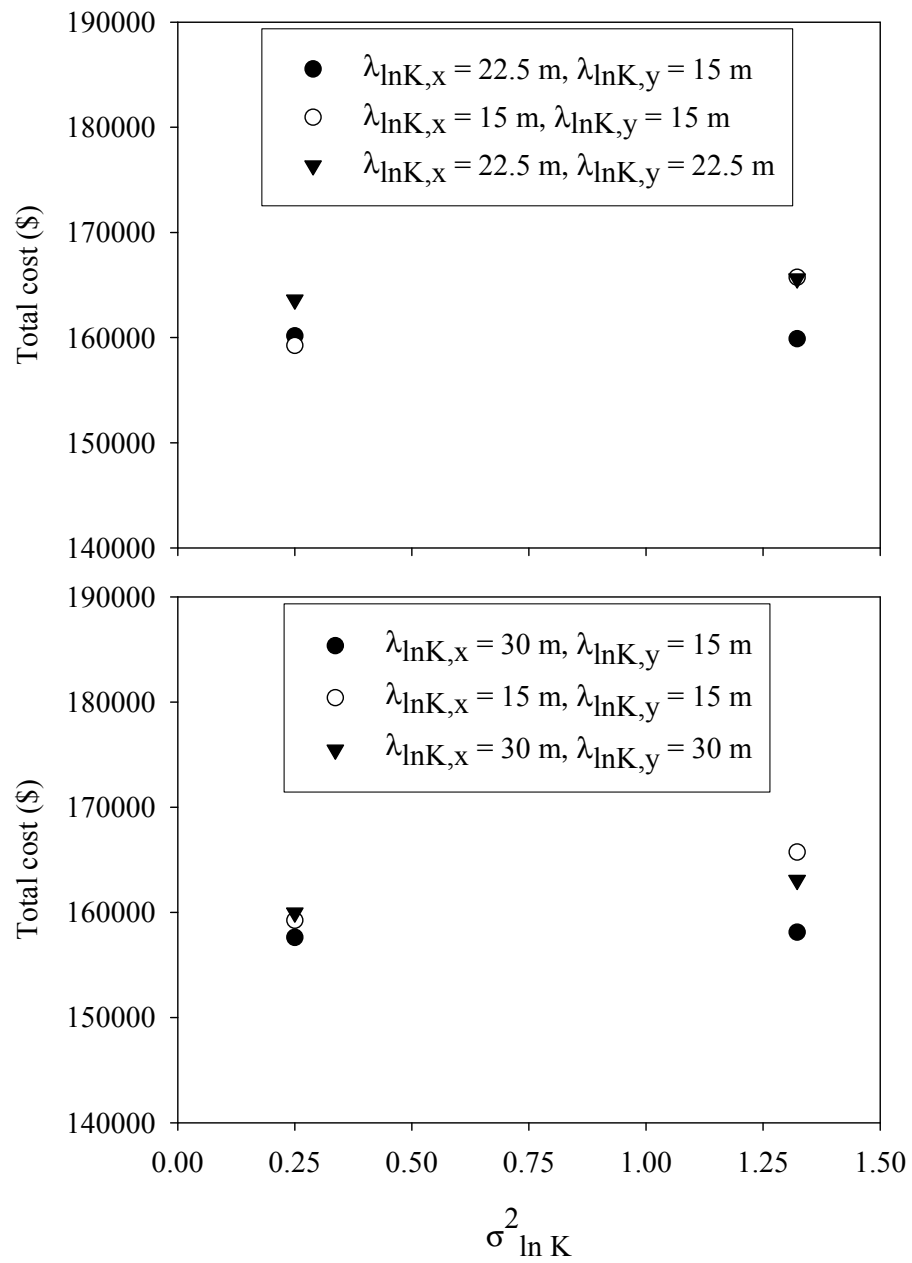


Figure 4.43. Comparison of total remediation cost for isotropic and anisotropic K-fields

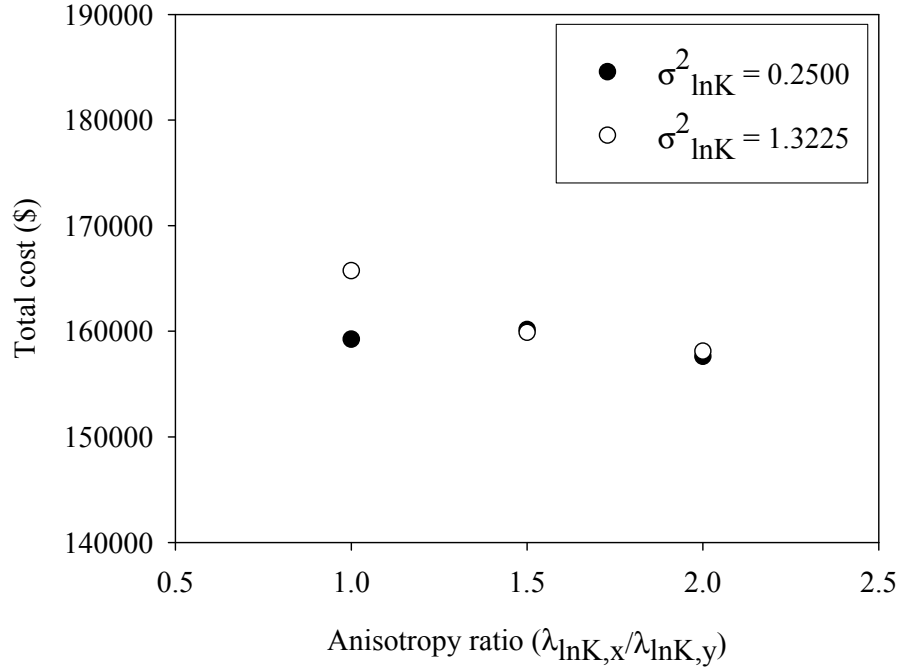


Figure 4.44. Change in total remediation cost with respect to anisotropy ratio ($\lambda_{\ln K, x} / \lambda_{\ln K, y}$). $\lambda_{\ln K, y}$ kept constant as 15 m and $\lambda_{\ln K, x}$ increased from 15 m to 22.5 and 30 m

effect of correlation structure anisotropy of K on permeable reactive barrier design and found that anisotropy had less effect on the design compared to the degree of heterogeneity described by $\sigma_{\ln K}$. Although the remediation methods were different compared to this study, the results were compatible.

4.5. Effect of Correlation Scale and Heterogeneity of K_d

4.5.1. Uncorrelated K_d and K

In this part of the study, the effects of $\lambda_{\ln K_d}$ and heterogeneity in K_d on P&T remediation design and cost were investigated. K_d -fields, details of which were explained in Section 3.1.3, were uncorrelated with the heterogeneous K-fields.

Realizations A and B were chosen as K realizations. Realization C exhibited similar trends with realization A in terms of cost versus $\lambda_{\ln K}$ (Figure 4.28) and was omitted for computational purposes. Simulations were performed for three different K_d realizations, a, b and c. For realization a, fields having three different $\sigma^2_{\ln K_d}$ (0.0256, 0.0740 and 0.1354) were applied on K-fields of three different $\sigma^2_{\ln K}$ (0.2500, 0.7225 and 1.3225) and two different $\lambda_{\ln K}$ (15 and 30 m) values. For the remaining two K_d realizations, namely b and c, two different $\sigma^2_{\ln K_d}$ (0.0256 and 0.1354) and $\sigma^2_{\ln K}$ (0.2500 and 1.3225) and two different $\lambda_{\ln K}$ and $\lambda_{\ln K_d}$ (15 and 30 m) were simulated. It must be stated that, the same λ were used for both K and K_d in the simulations in order to limit the number of simulations and total simulation time.

As it was mentioned in Section 3.1.3, heterogeneous K_d -fields were constructed assuming a constant K_{d_g} (0.36 cm³/g) and certain $\sigma^2_{\ln K_d}$ and $\lambda_{\ln K_d}$ values. In literature, this approach was used by Aksoy and Culver (2004). However, assuming a constant K_{d_g} over the field does not necessarily provide similar contaminant masses for all fields even if the initial contaminant plumes have the same dissolved and kinetically sorbed PCE concentrations. Indeed, even for the heterogeneous K_d -fields which have the same arithmetic mean value, the contaminant mass is not constant. This is due to the fact that sorbed mass on the equilibrium sorption sites is directly related with the K_d and f values at the grid points. Therefore, different K_d values at a specified grid point for different realizations of the K_d -field will lead to different overall initial contaminant masses. Schäfer and Kinzelbach (1992) also called attention to this point and normalized K_{d_g} in order to obtain the same initial contaminant mass for all fields on which they worked. Although this approach results in constant contaminant mass for all fields, it also results in variable K_{d_g} among the heterogeneous K_d -fields.

In order to account for the differentiation in mass of the initial plume in optimal designs, two different approaches, “constant K_d ” and “constant total mass” assumptions were used. These are described below:

- “Constant K_d ” approach has constant K_d , initial dissolved and kinetically sorbed PCE concentrations which are user defined in the model input for all heterogeneous K_d -fields. The fields have three different $\sigma^2_{\ln K_d}$ (0.0256, 0.0740 and 0.1354) and two different $\lambda_{\ln K_d}$ (15 and 30 m) values. However, the initial PCE mass present in the aquifer is different for each heterogeneous K_d -field due to different sorbed masses at the equilibrium sorption sites.
- “Constant total mass” approach has constant total initial PCE mass for all heterogeneous K_d -fields. Initial dissolved PCE masses and the concentration distributions are the same (similar to the average plume case used in the Sections 4.3.1.2 and 4.3.2.2) for all heterogeneous K_d -fields. On the other hand, the total initial sorbed masses on kinetic and equilibrium sites are the same but the concentration distributions are different for each heterogeneous K_d -field. K_d values of each K_d -field were modified to obtain the same overall total PCE mass. In the constant total mass approach, the overall K_d of the fields are different ranging from 0.29 to 0.36. The fields have three different $\sigma^2_{\ln K_d}$ (0.0256, 0.0740 and 0.1354) and two different $\lambda_{\ln K_d}$ (15 and 30 m) values.

For the scope of this study, the Aksoy and Culver’s (2004) constant K_d approach was taken as a basis for the discussion and the simulations were performed for all K and K_d -field combinations mentioned in the first paragraph of this section. On the other hand, the constant total mass approach was applied for 18 different K and K_d -field combinations as well. Constant K_d approach was taken as a basis since it seemed more practical in terms of the real life applications compared to the constant total mass approach since it is more feasible to find K_d and $\sigma^2_{\ln K_d}$ values based on K_d measurements in the field compared to total mass determination.

For the constant Kd_g approach, optimization simulations were performed for the heterogeneous K_d -fields, generated as explained in Section 3.1.3, along with the heterogeneous K -fields as explained in the first paragraph of this section. Then, in order to compare the results of constant Kd_g and constant total mass approaches, optimization simulations were repeated for a number of fields (Kd11a, Kd12a, Kd21a, Kd22a, Kd31a and Kd32a) with modified Kd_g values. The statistical properties of modified heterogeneous K_d -fields are given in Table 4.4. The modified K_d -fields were labeled with the “mod” term added after the original K_d -field name. The statistical properties of heterogeneous K_d -fields used for the constant Kd_g approach are given in Table 3.3. As the background heterogeneous K -field condition for the constant total mass approach, K realization A with three different $\sigma^2_{\ln K}$ (0.2500, 0.7225 and 1.3225), and two different $\lambda_{\ln K}$ (15 and 30 m) were used.

Table 4.4. Summary of the statistical properties of the modified heterogeneous K_d -fields of the constant total mass approach (The unit of K_d is cm^3/g)

Field	$\lambda_{\ln K_d}$ (m)	Kd_g	$\sigma^2_{\ln K_d}$
Kd11a_mod	15	0.36	0.0256
Kd12a_mod	30	0.33	0.0256
Kd21a_mod	15	0.35	0.0740
Kd22a_mod	30	0.31	0.0740
Kd31a_mod	15	0.35	0.1354
Kd32a_mod	30	0.29	0.1354

Firstly, the results for the constant Kd_g approach were evaluated. Before going through the results of the optimization runs, it might be useful to analyze the amount of PCE initially present in the aquifer for each heterogeneous K_d -field. Figure 4.45 shows the change of initial PCE mass with respect to $\lambda_{\ln K_d}$ for different

K_d -fields. The highest amount of PCE mass was observed for K_d -field Kd31c which had 15% higher initial PCE mass compared to homogenous K_d -field. On the other hand, the smallest amount of PCE was present for K_d -field Kd32c which had 5% less initial PCE mass compared to homogenous K_d -field. Figure 4.46 shows the change in Kd_g in the plume area with respect to $\lambda_{\ln Kd}$. The change in Kd_g in the plume area and the initial PCE mass with respect to $\lambda_{\ln Kd}$ were in close agreement. The only difference between the trends of PCE mass and Kd_g in the plume area was for realization a and $\lambda_{\ln Kd}$ of 15 m. However, for these fields, both the mass and the Kd_g values were very close to each other. These results showed that the initial PCE mass was correlated with the Kd_g of the plume area, not the Kd_g of the whole aquifer. Therefore, although all heterogeneous K_d -fields had the same Kd_g in overall, the local K_d values had a significant impact on PCE mass present in the aquifer. Figures 4.45 and 4.46 showed that for the same Kd_g and f values, the initial total mass of the plume would be dependent on the local K_d values. It was seen that, the impact of $\lambda_{\ln Kd}$ is dependent on the realization of the heterogeneous K_d -field for the similar K heterogeneity condition.

When the results of the optimization runs for the constant Kd_g approach were investigated it was seen that ten different wells (wells 3, 8, 9, 13, 14, 18, 19, 22, 23 and 24) were selected in total for all heterogeneous K_d cases. On the other hand, only three different wells (wells 13, 14 and 18) were selected for the same K -fields with homogeneous K_d . Among 68 different K and K_d -field combinations, 32 1-well designs, 31 2-well designs, 3 3-well designs and 2 4-well designs were selected as the optimum design. On the other hand, homogenous K_d assumption resulted in 10 1-well designs and 2 2-well designs for the 12 different heterogeneous K -fields used in this section of the study. Therefore, compared to the homogeneous K_d -fields, heterogeneity in K_d required a larger number of active wells distributed over a wider range.

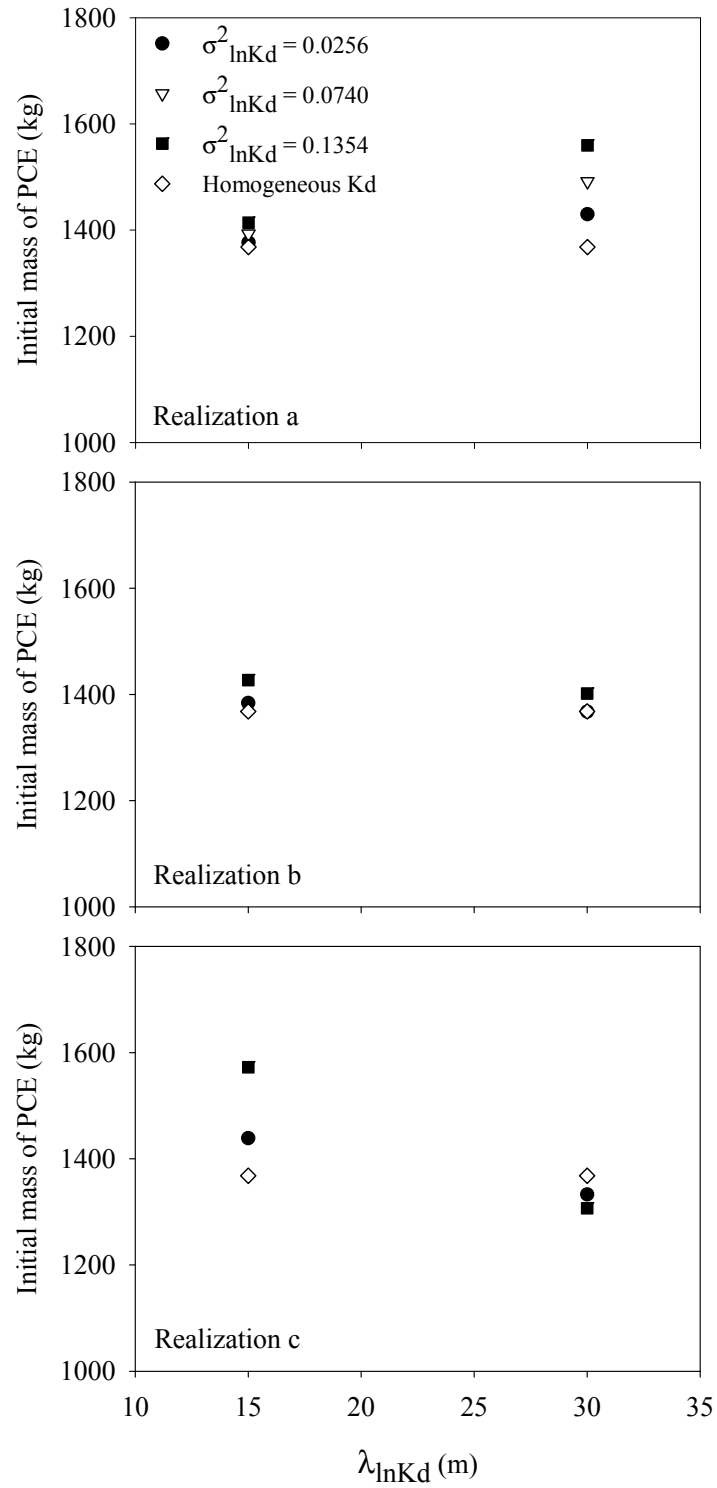


Figure 4.45. Change in the initial total mass of PCE with respect to $\lambda_{\ln Kd}$ for the constant Kd_g approach

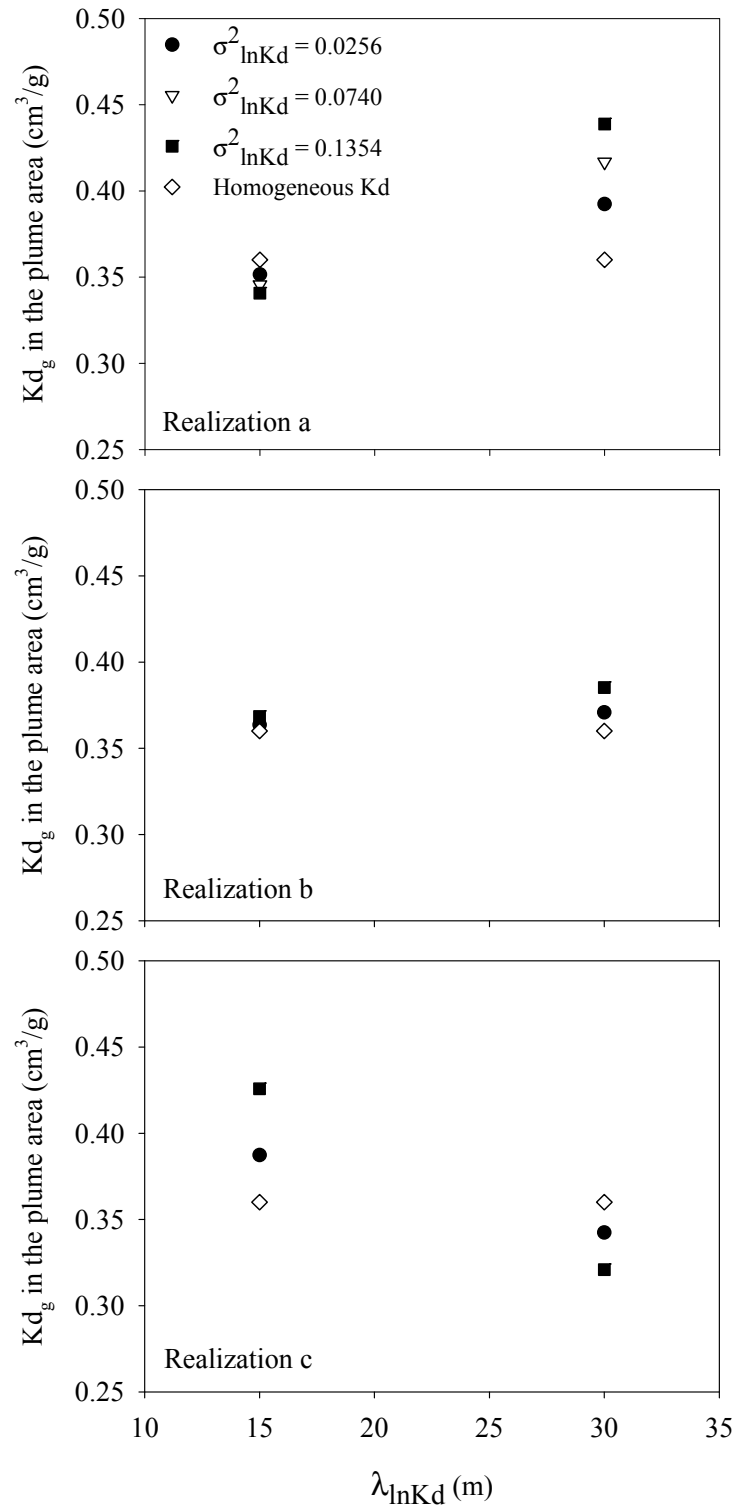


Figure 4.46. Change in Kd_g in the plume area with respect to $\lambda_{\ln Kd}$ for the constant Kd_g approach

When the selected designs were examined individually, it is observed that, for $\lambda_{\ln K_d}$ of 15 m, the same or more wells were required for the remediation on the heterogeneous K_d -fields compared to the homogeneous K_d -field. For the heterogeneous K_d -fields, the total pumping rate was generally higher than the homogenous K_d case but there were few fields which required less pumping. For these fields the designs with higher number of wells with less pumping rates were chosen compared to homogenous K_d case.

For $\lambda_{\ln K_d}$ of 30 m, when the number of wells and the total pumping rate required to cleanup the aquifer were compared with the homogeneous K_d case, it was seen that the same or more number of wells were required for the heterogeneous K_d -fields. The total pumping rate was higher than the homogenous K_d cases for the heterogeneous K_d cases except for few cases. This showed that K_d heterogeneity generally affected the P&T remediation design in a way that either the number of wells or the total pumping rate or both increased.

For $\lambda_{\ln K_d}$ of 30 m, the exceptional heterogeneous K_d -fields for which total pumping rate was less than the homogenous K_d cases were Kd12b/K13B, Kd12b/K33B, Kd12c/K13A, Kd12c/K33A, Kd12c/K13B, Kd12c/K33B, Kd32c/K13A, Kd32c/K33A, Kd32c/K13B and Kd32c/K33B. When Figure 4.45 was investigated for K_d -fields Kd12c and Kd32c it was seen that the amount of initial mass for these fields were less than the mass of the homogeneous K_d -field. For K_d -field Kd12b, the initial mass was the same with the homogeneous K_d -field. Therefore, this might be the reason of less pumping required for these heterogeneous K_d -fields. Here it is worth to note that heterogeneous K_d -field Kd12b resulted in less pumping rate only when it was in combination with K-fields of realization B. For Kd12b/K13A and Kd12b/K33A, higher pumping rate was required for the same number of wells compared to the homogeneous K_d -field. This showed that not only the distribution of K_d and initial mass present in the aquifer, but also the

distribution of K was important in terms of determination of the optimum P&T remediation design.

For the constant K_{dg} approach, the total remediation costs obtained with the combination of selected heterogeneous K and uncorrelated heterogeneous K_d -fields, as described above, are presented in Figures 4.47 and 4.48 for $\lambda_{\ln K_d}$ of 15 and 30 m, respectively. Remediation costs obtained with heterogeneous K but homogenous K_d -fields are also presented on the same figures for comparison purposes.

Results presented for $\lambda_{\ln K_d}$ of 15 m in Figure 4.47 showed that heterogeneity in K_d generally resulted in higher remediation costs compared to homogenous K_d although for some of the cases, where $\sigma^2_{\ln K_d}$ was low, remediation cost might be very close to the cost for the homogenous K_d case. Total remediation cost increased with increasing $\sigma^2_{\ln K_d}$ while the magnitude of this increase changed among different K and K_d realizations as well as different $\sigma^2_{\ln K}$ values. The effect of $\sigma^2_{\ln K_d}$ exhibited up to 9% increase in the total remediation cost (for field combination of Kd11a/K21A) when $\sigma^2_{\ln K_d}$ was 0.0256 for all different K -fields and K_d realizations. However, this value reached to 25% (for field combination of Kd31c/K11B) when $\sigma^2_{\ln K_d}$ was 0.1354. Results obtained for $\lambda_{\ln K_d}$ of 30 m (Figure 4.48) generally showed the similar trends with $\lambda_{\ln K_d}$ of 15 m in terms of change in remediation cost with respect to $\sigma^2_{\ln K}$ and $\sigma^2_{\ln K_d}$. Similar to $\lambda_{\ln K_d}$ of 15 m, for $\lambda_{\ln K_d}$ of 30 m, the effect of $\sigma^2_{\ln K_d}$ indicated a maximum of 17% increase in the total remediation cost (for field combination of Kd12a/K33A) when $\sigma^2_{\ln K_d}$ was 0.0256. However, this value reached to 42% (for field combination of Kd32a/K33A) when $\sigma^2_{\ln K_d}$ was 0.1354. Therefore, the variation in total remediation costs was higher for the higher $\lambda_{\ln K_d}$.

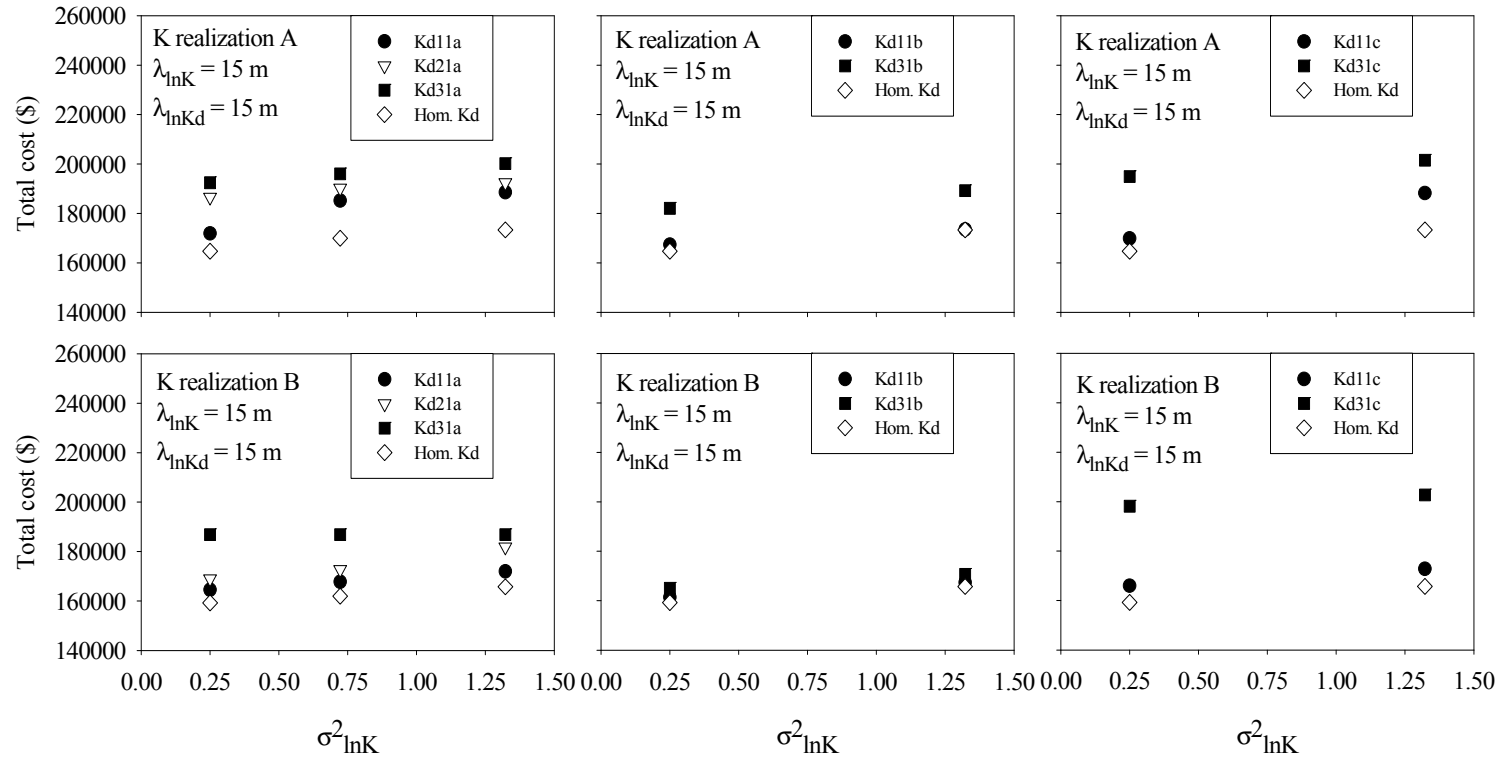


Figure 4.47. Change in the remediation costs with respect to $\sigma^2_{\ln K}$ for Kd realizations a, b and c, K realizations A and B and $\lambda_{\ln Kd}$ of 15 m for the constant Kd_g approach

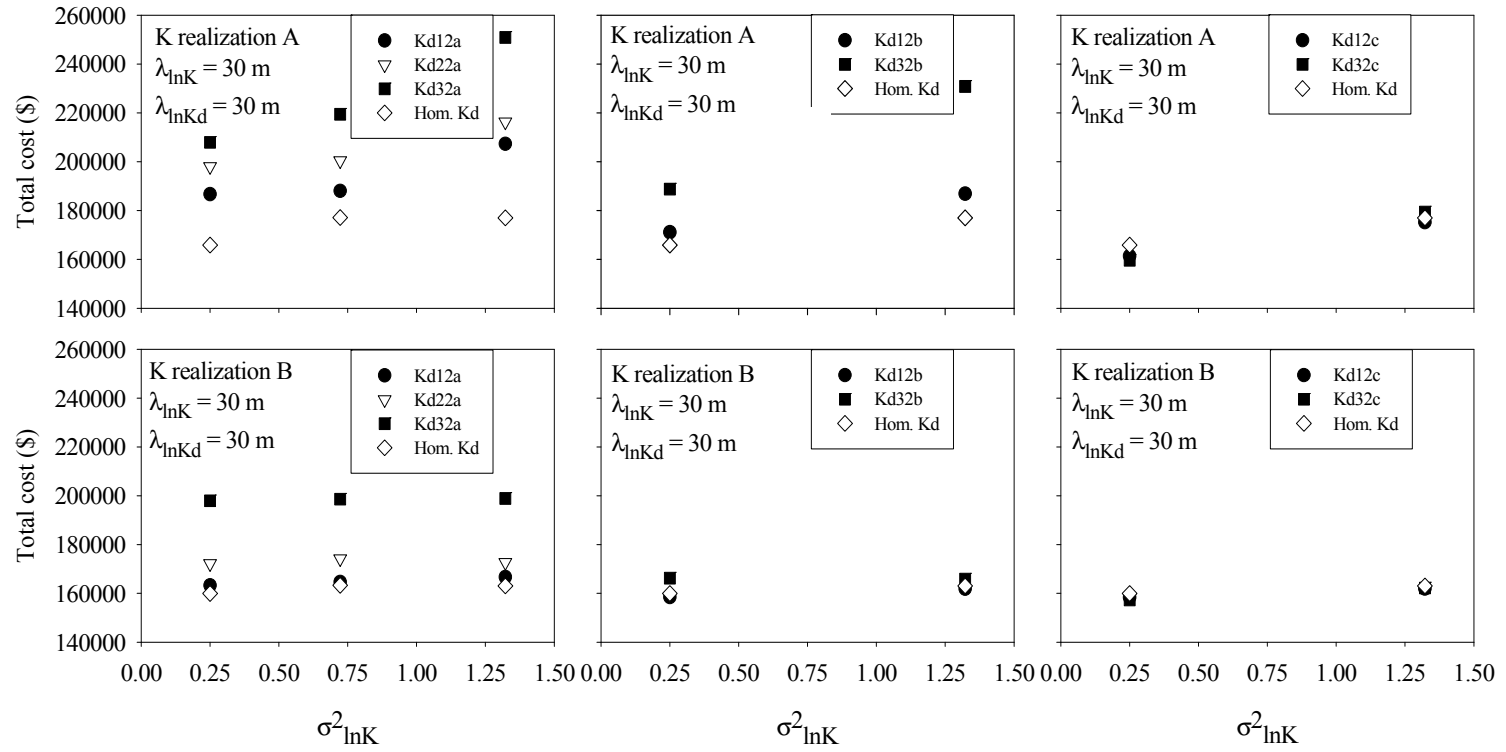


Figure 4.48. Change in the remediation costs with respect to $\sigma^2_{\ln K}$ for K_d realizations a, b and c, K realizations A and B and $\lambda_{\ln Kd}$ of 30 m for the constant K_{dg} approach

When the results presented in Figures 4.47 and 4.48 were compared with Figure 4.45 showing the change in the initial PCE mass with respect to $\lambda_{\ln K_d}$, it was seen that one of the reasons of the generally higher remediation costs for the higher $\lambda_{\ln K_d}$ was the presence of generally the higher amount of mass in the aquifer compared to the homogeneous case. The trends in the remediation costs and the initial masses were quite similar. This showed that amount of contaminant mass initially present in the aquifer was one of the major factors affecting remediation cost. Since the amount of total mass present in the aquifer was originally related with K_d and its heterogeneity, the actual factor was the K_d heterogeneity. However, there are some interesting points in these figures. The first point is that the total cost of remediation is not the highest for the K_d -fields where the highest amount of PCE mass is present. The highest amount of PCE mass was observed for Kd31c (Figure 4.45). However, the highest remediation cost was observed for field combination of Kd32a/K33A, which utilized 4 wells, with the cost of \$250,900 (Figure 4.48). Although the total remediation cost was the highest for this field combination, the unit cost of remediation, \$187/kg PCE, was the second highest. Kd32a was the field for which the second highest amount of mass was present. Presence of higher amount of mass required the removal of higher amount of mass to reach the remediation goal. The unit cost of remediation for field K33A with the homogenous K_d assumption was \$183/kg PCE. Therefore, K_d heterogeneity resulted in 2% increase in the unit remediation cost. The cost of remediation on field Kd31c changed between \$194,940 and \$202,740 depending on the K heterogeneity condition (Figure 4.47). These costs represented 16-24% increase compared to the homogeneous K_d -fields whereas the initial PCE mass in Kd31c was 15% higher than the mass in the homogenous K_d -field. The unit cost of remediation was almost constant for K_d -field Kd31c (varied between \$152/kg PCE and \$154/kg PCE) in spite of the change in K heterogeneity conditions. For the homogenous K_d , this variation was between \$159/kg PCE and \$162/kg PCE for the corresponding K heterogeneity conditions. Therefore, K_d heterogeneity resulted in a decrease up to 6% in the unit remediation cost for only K_d -field

Kd31c when all heterogeneous K conditions were considered. For these cases, both the total cost and the amount of PCE mass removed from the aquifer increased with K_d heterogeneity because of the higher amount of the initial mass. On the other hand, for K_d -field Kd32a remediation cost increased by 22-42% with respect to the cost on the homogeneous K_d -field depending on the K heterogeneity condition. The initial PCE mass for Kd32a was 14% higher compared to homogeneous K_d -field. The change in unit remediation cost was between \$156/kg PCE and \$187/kg PCE for this K_d -field under different K heterogeneity conditions. For homogenous K_d , this variation was between \$156/kg PCE and \$183/kg PCE. The maximum variation in unit cost was observed as 2% increase for Kd32a/K33A. Therefore, the unit cost was not significantly affected by K_d heterogeneity for this case.

When Figure 4.49 relevant to the K_d -field Kd32a and K-field K33A was investigated thoroughly, it could be seen that there was a coincidence of high K_d (red elements in Figure 4.49(a)) and low K (dark blue elements in Figure 4.49(b)) elements on the north of the plume area. In fact, Figure 4.46 showed that Kd32a had the highest K_{dg} in the plume area while Figure 4.18 showed that K_g in the plume area for K-field K33A was lower than 4.5×10^{-5} m/s. These were the evidences of the abundance of high K_d and low K values in the plume area. High K_d regions represented the areas of high sorbed PCE concentrations. Presence of higher sorbed PCE concentrations in the low K regions required more pumping and made the remediation harder which resulted in elevated cost of remediation. Indeed, combination of high K_d and low K values is the worst scenario for a P&T remediation system and the remediation is expected to be costly in such a case.

Another interesting result was obtained for K_d -field Kd32b. The combination of this K_d -field with K-field K33A (i.e. Kd32b/K33A) resulted in the second highest cost of remediation with the cost of \$230,850 (Figure 4.48). This cost was 30%

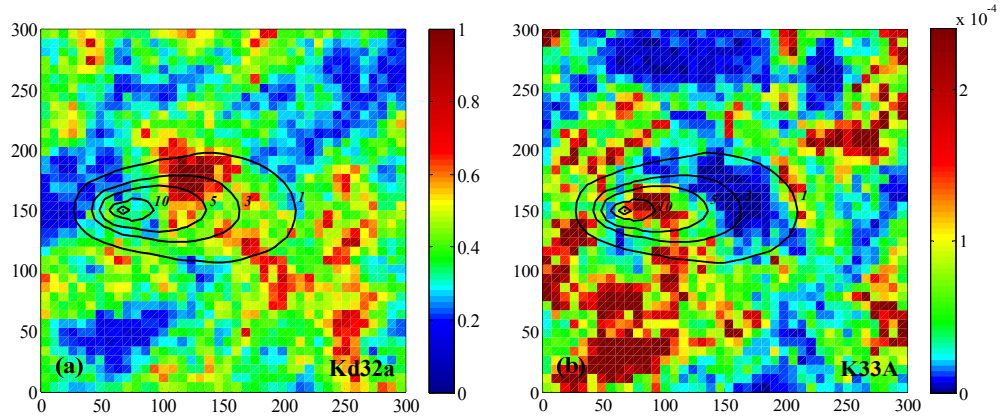


Figure 4.49. Distribution of (a) K_d values on field Kd32a and (b) K values on field K33A along with the average plume

higher than the cost when K_d -field was assumed to be homogeneous. On the other hand, even though the initial mass for Kd32b was higher than the mass in the homogenous K_d -field, the difference was 3%. The unit cost of remediation was the highest among all field cases with a value of \$206/kg PCE for field Kd32b/K33A. When compared to the homogenous K_d -field, 12% increase in the unit cost was observed. According to Figure 4.50, similar to Kd32a/K33A in Figure 4.49, high K_d region (red elements in Figure 4.50(a)) coincided with the low K (dark blue elements in Figure 4.50(b)) region on the east of the plume area and this might be the reason of such a high total and unit remediation cost.

Another eye-catching point in Figure 4.48 was the results obtained for the fields formed with the combinations of K_d realization c (Kd12c and Kd32c) with K realizations A and B. For both K realizations A and B, when $\sigma_{\ln K}^2$ was 0.2500, heterogeneous K_d -field resulted in lower cost (3% decrease for Kd12c/K13A and 1% decrease for Kd12c/K13B) than the homogenous K_d for $\sigma_{\ln K_d}^2$ of 0.0256. The cost decreased more (4% for Kd32c/K13A and 2% for Kd32c/K13B) when $\sigma_{\ln K_d}^2$

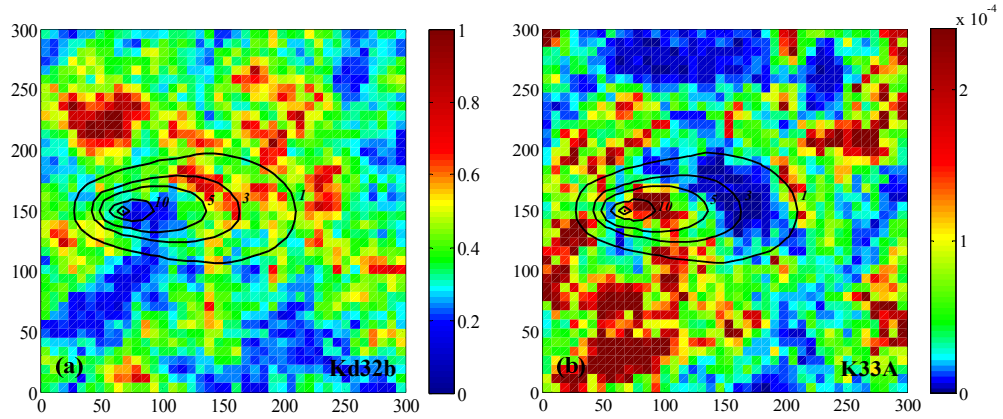


Figure 4.50. Distribution of (a) K_d values on field Kd32b, and (b) K values on field K33A along with the average plume

increased to 0.1354. The reason was that low K_d regions were predominant over the plume area. Low K_d meant lower sorbed concentration in these regions. According to Figure 4.46, showing the change in K_{dg} values in the plume area with respect to $\lambda_{\ln K_d}$, the two of the three lowest K_{dg} were for Kd12c and Kd32c. This showed the predominant characteristics of the low K_d values in these two fields. In addition, Figure 4.45 shows that for K_d -fields Kd12c and Kd32c, the amount of the initial mass was lower than the mass in the homogeneous K_d -field. In this case, presence of low K_d regions and lesser amount of initial mass made the remediation easier and the remediation cost lower. For the higher $\sigma^2_{\ln K_d}$, remediation was even easier since low K_d values and the initial mass became lower with increasing $\sigma^2_{\ln K_d}$. Although K_d was low in the plume area in general, there were also two small high K_d regions, where sorbed PCE concentrations were high, in the plume area (Figure 4.51(a)). Their effect was not visible except for the field Kd32c/K33A which had higher $\sigma^2_{\ln K_d}$. As can be seen in Figure 4.48, the remediation cost for Kd32c/K33A was 1% higher than the homogenous K_d and 2%

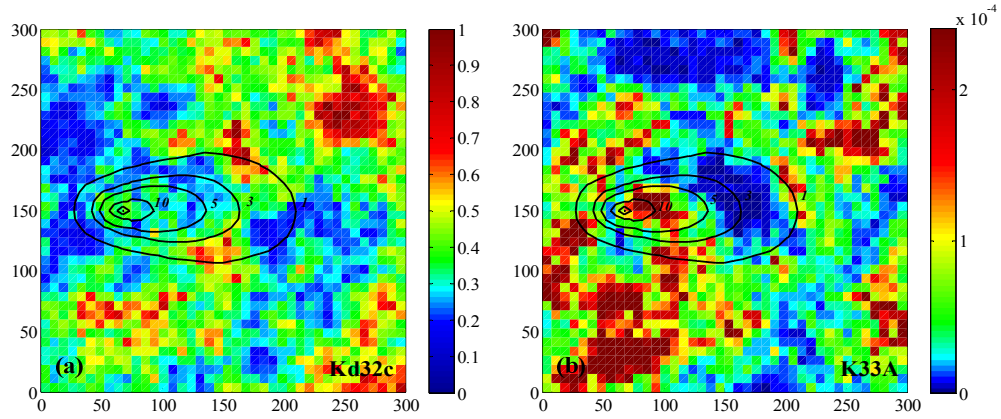


Figure 4.51. Distribution of (a) K_d values on field Kd32c and (b) K values on field K33A along with the average plume

higher than the low $\sigma^2_{\ln K_d}$ (Kd12c/K33A) cases. Although this difference was not very significant, it was due to the coincidence of high K_d (red elements in Figure 4.51(a)) and low K (dark blue elements in Figure 4.51(b)) values on the northeast of the plume area. However, it should be pointed out that even a small region of high K_d could affect the total remediation cost. For the field Kd32c/K33A, the maximum total concentration at the end of the remediation time was observed at the point corresponding to such region. Therefore, even this small region limited the remediation and resulted in an increase in the remediation cost. The change in the unit remediation cost was between \$160/kg PCE and \$187/kg PCE for the mentioned K_d -fields (i.e. combinations of Kd12c and Kd32c with fields of K realizations A and B) above. For the homogenous K_d assumption, the unit remediation cost was \$160/kg PCE, \$158/kg PCE, \$183/kg PCE, and \$156/kg PCE for fields K13A, K13B, K33A, and K33B, respectively. Therefore heterogeneity in K_d resulted in 1 to 4% increase in unit cost for different K and K_d -field combinations, although both the total cost and the amount of PCE mass removed from the aquifer was lower compared to the homogeneous K_d -field.

When the results were analyzed with respect to unit remediation costs for all K and K_d -field combinations used in this study, it was seen that the minimum and the maximum unit remediation costs to reach the water quality standards were \$145/kg PCE and \$187/kg PCE for K_d realization a, \$152/kg PCE and \$206/kg PCE for K_d realization b and \$150/kg PCE and \$187/kg PCE for K_d realization c. Therefore, unit remediation cost changed by up to 42% with respect to minimum (i.e. \$145/kg PCE) among all K and K_d realizations and heterogeneity conditions. Compared to the homogeneous K_d assumption, heterogeneity in K_d resulted in a change in the range of -8% to 12% in unit remediation cost.

All these results showed that besides the initial mass present in the aquifer, the distribution of K and K_d over the aquifer, their heterogeneity characteristics and their relative positions were also important in terms of the determination of optimum P&T remediation cost and design. Therefore, determination of K_d heterogeneity as well as the K heterogeneity in the field is crucial in terms of designing an effective P&T remediation.

For the constant K_{d_g} approach, the change in the average, minimum and maximum remediation costs with respect to $\lambda_{\ln K_d}$ and the standard deviation of the total cost are given in Figure 4.52 for two different K realizations and $\sigma_{\ln K}^2$ separately. In this figure, it was seen that, as was for the K heterogeneity, the standard deviation of the total cost was higher for the longer $\lambda_{\ln K_d}$ for each K realization and $\sigma_{\ln K}^2$. The effect of changing $\lambda_{\ln K_d}$ was more pronounced for K realization A compared to K realization B showing that background K distribution was important, as well, in terms of finding the optimum solution when K_d was heterogeneous.

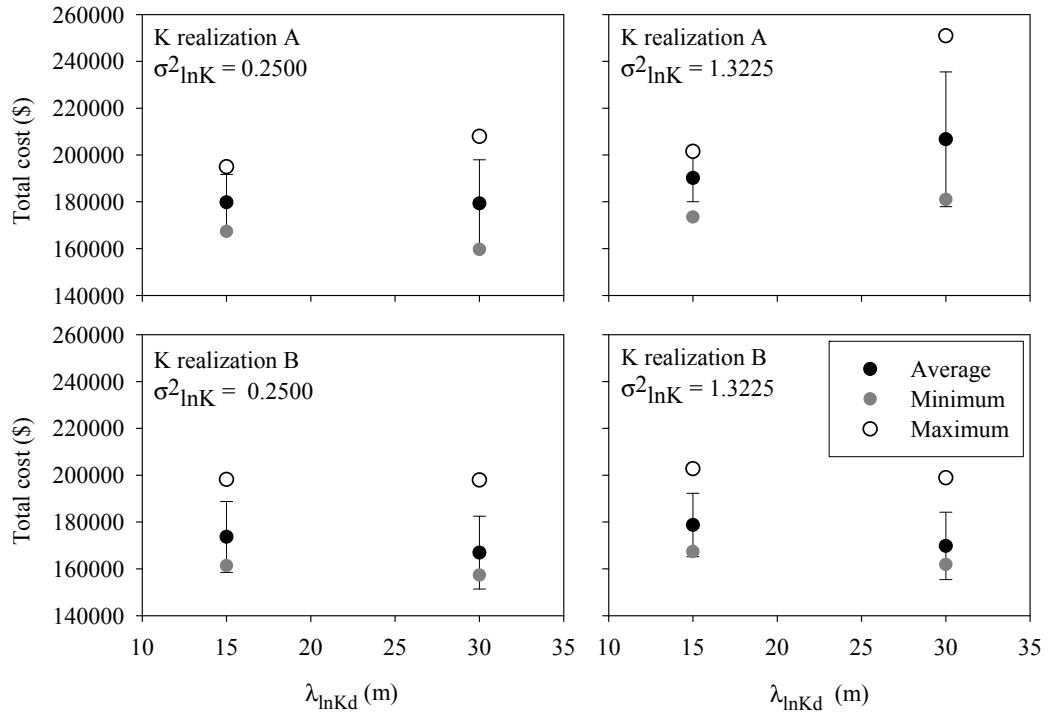


Figure 4.52. Change in average, minimum and maximum remediation cost with respect to $\lambda_{\ln K_d}$ for K_d -fields of the constant K_{d_g} approach for different K cases (Error bars represent one standard deviation)

In literature, Aksoy and Culver (2004) investigated the effect of K_d heterogeneity for two different $\sigma^2_{\ln K_d}$ and three different realizations of K_d but for a single $\lambda_{\ln K}$ and realization of K. They found that lower K_d heterogeneity resulted in similar remediation costs with the homogenous K_d assumption but higher K_d heterogeneity caused significant increase in the remediation cost by up to 50%. The findings of this study are in line with the findings of Aksoy and Culver (2004). However, since they studied on just a single K realization, they were not able to see the effect of changing K distribution on the remediation cost when K_d was heterogeneous. In addition, they did not study the effect of changing $\lambda_{\ln K_d}$ so that this study is unique in terms of studying this effect. Furthermore, they did not analyze their results in terms of initial PCE mass present in the aquifer while this

study considered the effect of initial PCE mass and interpreted the results accordingly. Aksoy and Culver (2004) also found that increasing K heterogeneity might decrease the impact of K_d heterogeneity. This study showed that this may or may not be the case depending on the K distribution and $\lambda_{\ln K_d}$. For example, for K_d -field Kd32b, effect of K_d heterogeneity on remediation cost increased with increasing $\sigma^2_{\ln K}$ for K realization A, but decreased with increasing $\sigma^2_{\ln K}$ for K realization B (Figure 4.48).

In the constant total mass approach, the amount of total PCE mass initially present in the aquifer was constant for all heterogeneous K_d -fields of different K_{d_g} and equal to the mass present in the average plume under the homogenous K_d ($0.36 \text{ cm}^3/\text{g}$) conditions as in Sections 4.3.1.2 and 4.3.2.2. When the components of the total PCE mass, which were dissolved and sorbed PCE mass (kinetically sorbed + sorbed in equilibrium sorption sites), was investigated for modified K_d -fields individually, it was seen that the amount of dissolved mass was constant among all heterogeneous modified K_d -fields. This total dissolved mass and its distribution was also equal to the dissolved mass present in the K_d -fields of the constant K_{d_g} approach. On the other hand, the amount of sorbed mass was constant among the modified K_d -fields but not constant for the K_d -fields of constant K_{d_g} approach. Similarly, kinetically sorbed mass was constant among the modified K_d -fields and the respective fields of the constant K_{d_g} approach. On the other hand, sorbed mass in equilibrium sorption sites was constant for the modified K_d -fields but not constant for the respective K_d -fields of the constant K_{d_g} approach. For constant total mass approach, the amount of sorbed mass in equilibrium sorption sites was 785 kg for all heterogeneous K_d -fields while it changed between 794 to 977 kg for the constant K_{d_g} approach. Therefore, modification of K_d in the constant total mass approach decreased the amount of sorbed mass in equilibrium sorption sites by lowering K_d values over the aquifer. The decrease in K_d values could also be understood from Table 4.4.

When the results were examined in terms of remediation design, it was seen that, for the constant total mass approach, seven different wells (wells 8, 9, 13, 14, 18, 19 and 24) were selected for 18 different K and K_d -field combinations studied. On the other hand, only three different wells (wells 13, 14 and 18) were selected for the same K -fields with homogeneous K_d . Among 18 different K and K_d -field combinations, 4 1-well designs, 12 2-well designs and 2 3-well designs were selected as the optimum designs. On the other hand, respective field combinations of the constant K_{dg} approach resulted in 1 1-well design, 13 2-well designs, 3 3-well designs and 1 4-well design.

For 10 of the 18 studied cases, the number of wells selected was different with an addition of one more active well compared to the homogeneous K_d assumption. For the remaining 8 cases, the number of wells was equal to the homogeneous K_d assumption. Generally, total pumping rate was higher compared to the homogeneous K_d assumption. For 2 cases, the total pumping rate was lower than the pumping rate with homogeneous K_d assumption but for these cases the number of wells was higher. Thus, the results showed that, similar to the constant K_{dg} approach, K_d heterogeneity affected the P&T remediation design in a way that either the number of wells or the total pumping rate or both increased even the initial PCE mass was the same for the homogenous and the heterogeneous K_d -fields. It should also be pointed out that even the K_{dg} values of the heterogeneous fields were lower (down to $0.29 \text{ cm}^3/\text{g}$) compared to the K_{dg} of the homogeneous K_d -fields, the optimal designs required higher number of wells for 56% of the cases. This shows the importance of the K_d heterogeneity and its distribution in the field for remediation.

When the designs obtained with the constant total mass approach was compared with that of the constant K_{dg} approach it was seen that for 12 of the 18 studied cases, the same number of wells was chosen. For the remaining 6 cases, the number of the selected wells was one less than the number of wells selected for the

constant K_{dg} approach. Generally, total pumping rate was less compared to the constant K_{dg} approach. 15 cases required less total pumping rate while 2 had the equal pumping rate with the constant K_{dg} approach. This is expected since K_{dg} s were lower for the constant total mass approach.

For constant total mass approach, the total remediation costs obtained with the combination of selected heterogeneous K-fields (namely K11A, K13A, K21A, K23A, K31A and K33A) and K_d -fields (namely K_{d11a_mod} , K_{d12a_mod} , K_{d21a_mod} , K_{d22a_mod} , K_{d31a_mod} and K_{d32a_mod}) are presented in Figure 4.53 for λ_{lnKd} of 15 and 30 m along with the costs acquired for homogenous K_d -fields. Remediation costs obtained with constant K_{dg} approach for the same fields are also presented on the same figure for comparison.

Figure 4.53 showed that although the initial PCE mass for all studied cases and the homogenous K_d case were the same for the constant total mass approach, the remediation cost for heterogeneous K_d -fields was not the same with the cost for the homogeneous K_d -field. This is expected since K_{dg} of the heterogeneous fields are different and as shown before this has an impact on the remediation design.

Results presented for λ_{lnKd} of 15 m in Figure 4.53 showed that remediation cost increased with increasing σ^2_{lnKd} for all three σ^2_{lnK} studied. However, the magnitude of the increase varied depending on σ^2_{lnK} . Remediation cost increased with increasing σ^2_{lnK} for all three σ^2_{lnKd} studied, too. 9% increase (the maximum value observed for all fields) was observed in the total remediation cost for field combinations of K_{d11a_mod}/K_{21A} and K_{d11a_mod}/K_{31A} in comparison to homogeneous K_d -field when σ^2_{lnKd} was 0.0256. This value increased up to 14% for field combination of K_{d31a_mod}/K_{11A} with respect to the homogeneous K_d -field when σ^2_{lnKd} was 0.1354. Results obtained for λ_{lnKd} of 30 m (Figure 4.53) showed the similar trends with λ_{lnKd} of 15 m in terms of change in remediation cost with

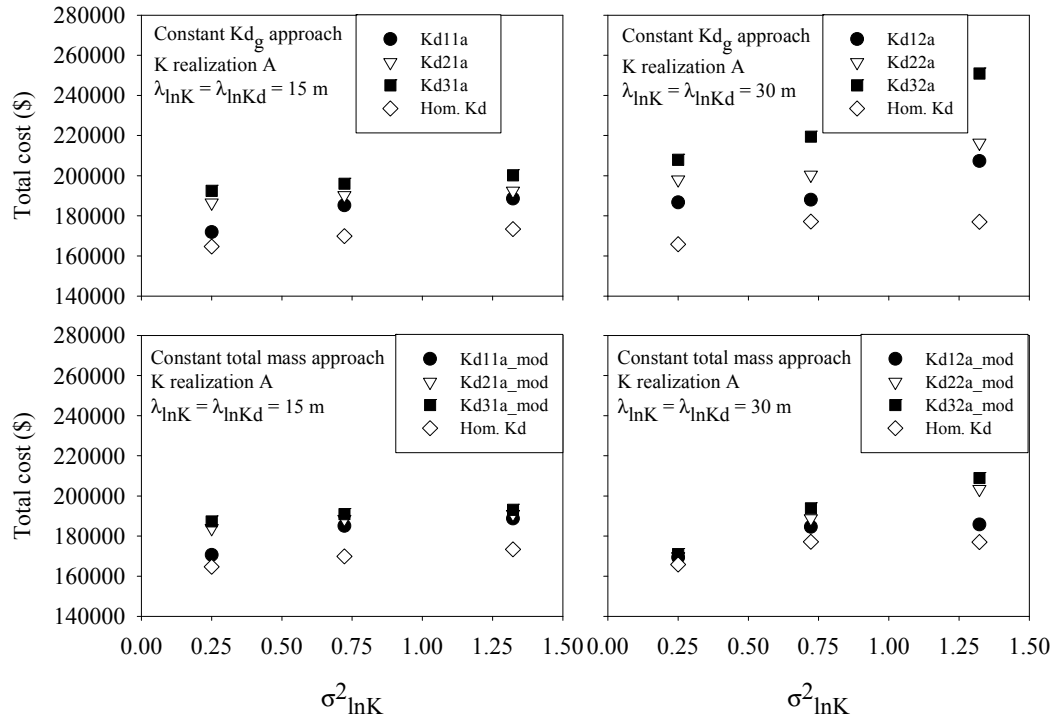


Figure 4.53. Change in remediation cost with respect to $\sigma^2_{\ln K}$ for K_d realization a, K realization A and $\lambda_{\ln K_d}$ of 15 and 30 m for the constant K_{d_g} and the constant total mass approach

respect to $\sigma^2_{\ln K_d}$ and $\sigma^2_{\ln K}$. Similar to $\lambda_{\ln K_d}$ of 15 m, for $\lambda_{\ln K_d}$ of 30 m, maximum 5% increase in the total remediation cost was observed (for field combination of Kd12a_mod/K33A) when $\sigma^2_{\ln K_d}$ was 0.0256. However, this value reached to 18% (for field combination of Kd32a_mod/K33A) when $\sigma^2_{\ln K_d}$ was 0.1354.

Table 4.5 summarizes the all percent changes in the remediation cost for all heterogeneous fields for both the constant K_{d_g} and the constant total mass approaches compared to the respective heterogeneous K-fields with the homogeneous K_d assumption. As can be seen for both approaches, percent increase in remediation cost increased with increasing $\sigma^2_{\ln K_d}$. It is also seen that the range of

Table 4.5. Percent remediation cost increase with respect to the cost on homogeneous K_d -field for the constant total mass and the constant K_{dg} approaches

	Kd11a mod	Kd21a mod	Kd31a mod	Kd11a	Kd21a	Kd31a
K11A	4	12	14	4	13	17
K21A	9	11	12	9	12	15
K31A	9	10	11	9	11	16
	Kd12a mod	Kd22a mod	Kd32a mod	Kd12a	Kd22a	Kd32a
K13A	2	3	3	13	19	25
K23A	4	7	10	6	13	24
K33A	5	15	18	17	22	42

percent change in remediation costs was narrower for the constant total mass (modified K_{dg}) approach. This was as a result of the lower K_{dg} and the total initial mass for the modified K_d -fields.

As mentioned before, when compared to the constant K_{dg} approach, K_d values over the aquifer was lower for the constant total mass approach. This resulted in lower amount of sorbed mass in equilibrium sorption sites initially. However, this situation continued during the remediation and lower K_d resulted in lower amount of sorbed mass in equilibrium sorption sites for the course of remediation. Since the optimization model had a constraint on the maximum total concentration in the aquifer at the end of the remediation time (Equation 3.24), it would be easier to satisfy this constraint for the constant total mass approach compared to the constant K_{dg} approach. Besides the lower overall initial PCE mass, this was the reason of obtaining lower remediation costs for the constant total mass approach.

For the constant total mass approach, the minimum and the maximum unit remediation costs to reach the water quality standards among the all 18 studied cases were \$156/kg PCE and \$191/kg PCE, respectively. For $\lambda_{\ln K_d}$ of 15 m, the minimum and the maximum unit remediation costs were \$160/kg PCE and \$174/kg PCE, respectively, while for $\lambda_{\ln K_d}$ of 30 m, they were \$156/kg PCE and

\$191/kg PCE, respectively. On the other hand, the minimum and the maximum unit remediation costs to reach the water quality standards among the respective K_d -fields of the constant K_{dg} approach were \$159/kg PCE and \$187/kg PCE, respectively. Therefore, the range of unit costs was quite similar for constant K_{dg} and the constant total mass approaches although the change in the unit remediation costs may reach to 8% on a specific K- K_d field combination.

In literature, the constant total mass approach was applied by Schäfer and Kinzelbach (1992) for the investigation of the effect of heterogeneity in K_d on the performance of in-situ bioremediation. Results of Monte Carlo analysis showed that assuming K_d as heterogeneous instead of homogeneous had generally a clear unfavorable effect on the remediation time. An increase in the $\sigma_{\ln K}$ and $\sigma_{\ln K_d}$ had also a significant negative effect by increasing the remediation time. Although results of Schäfer and Kinzelbach's (1992) can not directly be compared with the results of this study (since the remediation methods and the remediation performance measures are different) it is important to show that heterogeneous K_d generally decrease the remediation performance and its effect may increase with increasing $\sigma_{\ln K}^2$ and $\sigma_{\ln K_d}^2$. This study also showed that $\lambda_{\ln K_d}$ and $\lambda_{\ln K}$ may have an additional impact on the remediation performance.

In conclusion, the results obtained in this part of the study showed that assuming K_d as homogenous during the design of P&T remediation systems might cause significant error in both the design and the cost of remediation. The spatial distribution of both K and K_d might change the magnitude of this error since their combinations determine how hard or easy the remediation will be. Determination of $\lambda_{\ln K}$ and $\lambda_{\ln K_d}$ might also be important as well as $\sigma_{\ln K}^2$ and $\sigma_{\ln K_d}^2$ since designs on the fields with lower λ seemed to be on the more safe side while the cost of remediation might show great variation for longer λ .

4.5.2. Correlated K_d and K

In this section, the effects of both negative and positive correlation between K and K_d on P&T remediation designs and costs were investigated. For this purpose, constant K_{dg} approach, described in the previous section, was used. This approach employed a constant K_{dg} ($0.36 \text{ cm}^3/\text{g}$) and certain $\sigma_{\ln K_d}^2$ (0.0256, 0.0740 and 0.1354) and $\lambda_{\ln K_d}$ (15 and 30 m) values while keeping the dissolved and kinetically sorbed PCE concentrations as same (similar to the average plume case) for all cases. However, the total masses were different.

Figure 4.54 shows the initial PCE masses with respect to $\sigma_{\ln K}^2$ and $\sigma_{\ln K_d}^2$ for both negatively and positively correlated K_d -fields. The highest amount of PCE mass was observed for fields K33B-Kd32B and K33C+Kd32C which had 15% higher initial PCE mass compared to the homogenous K_d -field. On the other hand, the smallest amount of PCE was present for fields K33B+Kd32B and K33C-Kd32C which had 9% less initial PCE mass compared to the homogenous K_d -field.

Seven different wells (wells 3, 8, 13, 14, 18, 19 and 23) in total were selected for all negatively correlated K_d -fields. For the positively correlated K_d -fields, again seven but different wells (wells 8, 9, 13, 14, 18, 19 and 24) were chosen. For the negatively correlated K_d -fields, 11 1-well designs, 6 2-well designs and 1 5-well design were selected as the optimum design. On the other hand, for the positively correlated K_d -fields, 13 1-well designs and 5 2-well designs were found as the optimum design. Therefore, in overall, negative correlation between K and K_d resulted in higher effort for remediation.

Examination of individual designs showed that for the negatively correlated K_d -fields, the same or more number of wells were required for the remediation with more total pumping rate compared to the homogeneous K_d -fields except for three

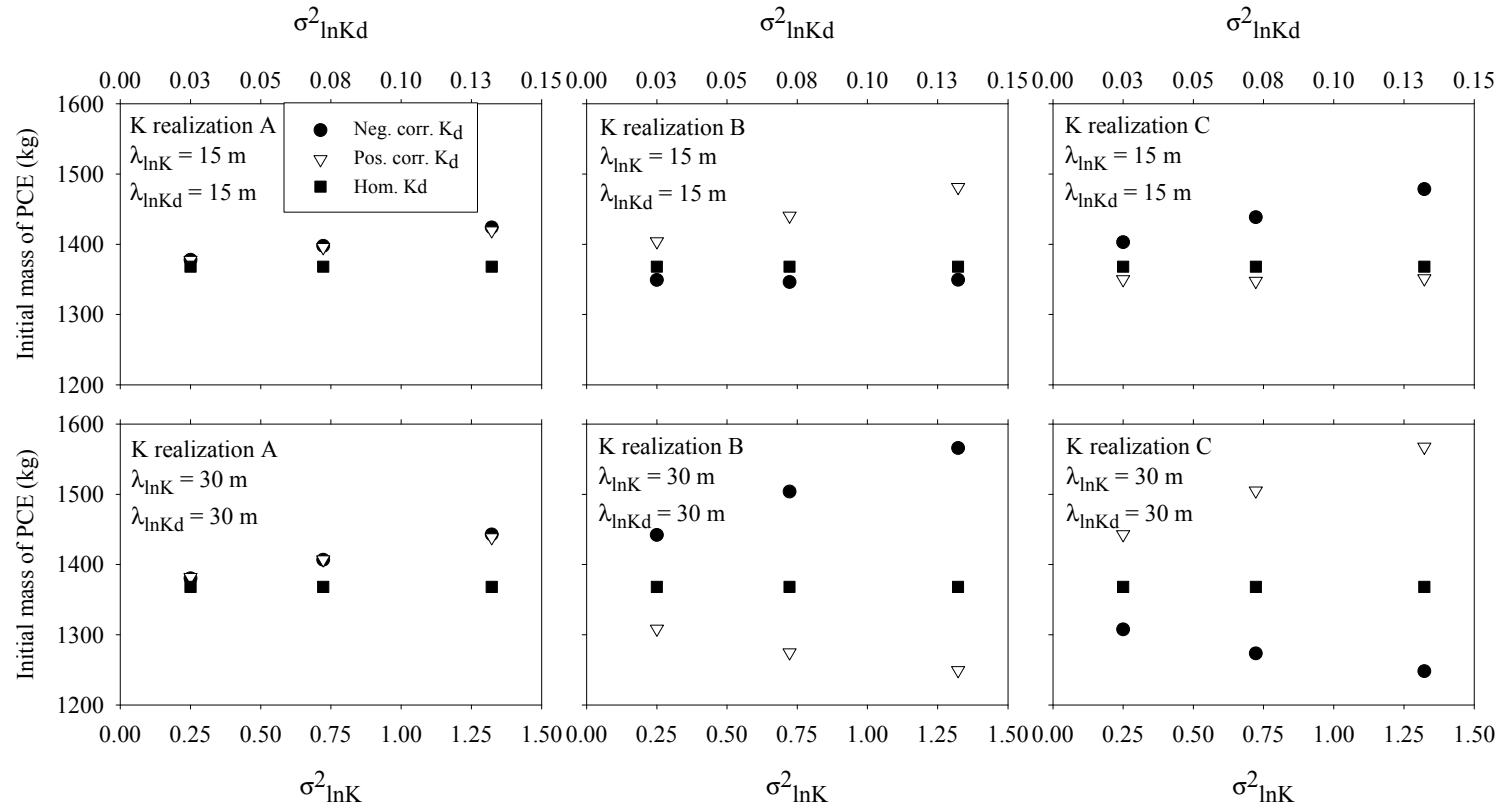


Figure 4.54. Change in the initial mass of PCE with respect to $\sigma^2_{\ln K}$ (bottom axis) and $\sigma^2_{\ln Kd}$ (top axis) for positively and negatively correlated K_d -fields

fields. Therefore, except for three fields, negative correlation generally affected the remediation design in a manner that increased the pumping rates. The exceptional fields that deviated from this behavior were K13C-Kd12C, K23C-Kd22C and K33C-Kd32C. For these fields, total pumping rates were smaller compared to the homogenous K_d -fields while the number of active wells was the same with the homogeneous K_d -fields. Although the detailed discussion about these fields will be given in the following paragraphs of this section, here, it is useful to state that the reason of this exceptional behavior of these fields is the predominance of high K regions in the plume area with low K_d regions together. This makes remediation easier with the requirement of less pumping.

For the positively correlated K_d -fields, 15 K_d -fields ended up with the same number of wells with the corresponding fields with the homogenous K_d assumption, while for the remaining 3 K_d -fields one more well was required. For 11 K_d -fields total pumping rate was less compared to the ones with the homogeneous K_d assumption. The highest percentage decreases were observed for fields K13B+Kd12B, K23B+Kd22B and K33B+Kd32B with 21%, 21% and 12%, respectively. The detailed discussion about these fields will be given in the coming paragraphs of this section but, in shortly, the reason this decrease in total pumping rate is the coincidence of low K regions with low K_d regions in these fields. For the remaining 7 K_d -fields, total pumping rate was more than the pumping rate for the homogeneous K_d assumption. This showed that the effect of positive correlation on the P&T remediation design was not unique such that it could result in both increase or decrease in the total pumping rate depending on the distribution of K and K_d .

The total remediation costs obtained by the positively and negatively correlated K_d -fields are presented in Figure 4.55. Remediation costs obtained with heterogeneous K but homogenous K_d -fields are also presented on the same figures for comparison.

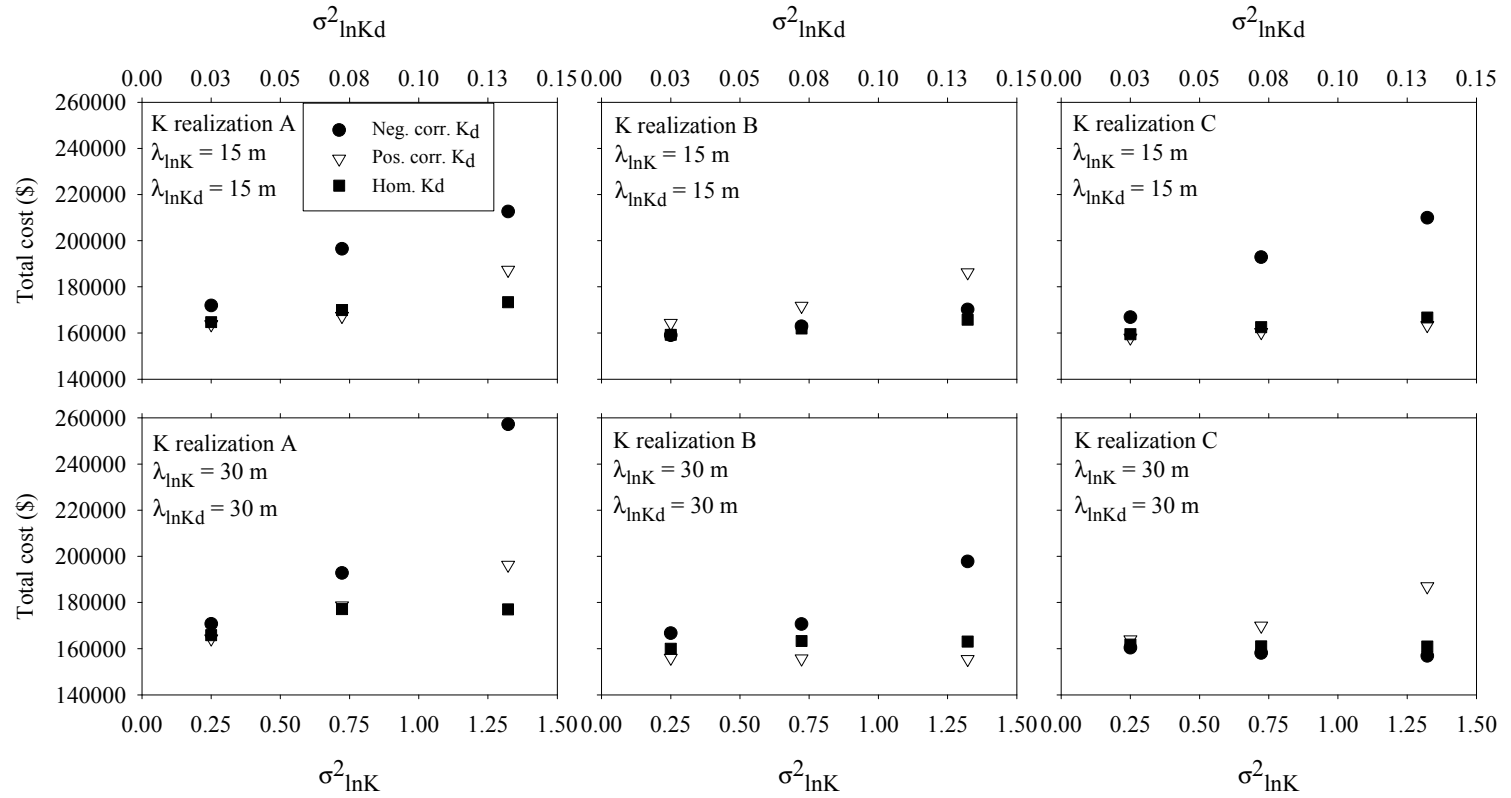


Figure 4.55. Change in remediation cost for correlated K_d -fields with respect to $\sigma^2_{\ln K}$ (bottom axis) and $\sigma^2_{\ln K_d}$ (top axis) for K realizations A, B and C and $\lambda_{\ln K} = \lambda_{\ln K_d}$ of 15 and 30 m

In overall, the effects of changing $\lambda_{\ln K_d}$ and $\sigma_{\ln K_d}^2$ were varying for different realizations of K and K_d . For some of the realizations remediation cost increases with increasing $\sigma_{\ln K_d}^2$ but for some others the opposite might be observed. In addition, for the same realization, the direction of the trend in cost with respect to $\sigma_{\ln K_d}^2$ and $\sigma_{\ln K}^2$ might be different depending on $\lambda_{\ln K_d}$.

The results in Figure 4.55 show that the remediation cost on negatively correlated K_d -fields were higher than the remediation cost on both homogenous and positively correlated K_d -fields except for two K_d distributions which were realization B with $\lambda_{\ln K_d}$ of 15 m and realization C with $\lambda_{\ln K_d}$ of 30 m. When there was a negative correlation between K and K_d , high K_d regions were associated with low K regions and low K_d regions were associated with high K regions. The reason of obtaining higher cost for negatively correlated K_d -fields was the presence of low K and high K_d regions together. Higher K_d meant higher sorbed mass in these regions. Presence of higher sorbed PCE concentrations in the low K regions required more pumping and made the remediation harder which resulted in elevated cost of remediation. On the other hand, if the aquifer on which the contaminant plume spread over had predominantly high K regions, negative correlation with K_d would yield lower sorbed PCE concentrations compared to the homogenous K_d which would ease the contaminant removal and result in lower remediation costs. This explains the low costs observed for some of the heterogeneous K_d -fields that are negatively correlated with K. For the same fields, when there is positive correlation between K and K_d , high K regions are present at high K_d regions. High K_d causes an increase in the sorbed PCE concentration. This may result in an increase the remediation cost despite the favorable flow conditions during pumping as a result of high K.

Fields for realization B with $\lambda_{\ln K_d}$ of 15 m and realization C with $\lambda_{\ln K_d}$ of 30 m were the examples of high K dominant fields. These fields were the only two fields having

a plume area K_g higher than 4.5×10^{-5} m/s which was overall K_g of the aquifer. This showed that high K regions were predominant for these fields. In Figure 4.55, the costs of remediation for the negatively correlated K_d cases were lower than both the homogenous and the positively correlated K_d cases for the fields of realization C with $\lambda_{\ln K_d}$ of 30 m. For these fields (K13C, K23C and K33C) K values were higher than 4.5×10^{-5} m/s for 77% of the plume area. Figure 4.56(a), which presents the field K33C as an example, showed that there was hardly any very low K (represented with dark blue) elements in the plume area. In this case, there was almost no very high K_d element in the plume area, as well, as a result of negative correlation between K and K_d . This could also be seen in Figure 4.54 such that K33C-Kd32C had 9% less initial PCE mass compared to the homogenous K_d -field. Having no very high K_d region and less initial PCE mass made the remediation easier and the remediation cost lower compared to both the homogenous and the positively correlated K_d cases. Remediation cost decreased with increasing $\sigma^2_{\ln K_d}$ on these fields since low K_d values and amount of initial masses became lower with increasing $\sigma^2_{\ln K_d}$. On the other hand, for the same fields, positive correlation resulted in high K_d regions and higher initial mass and this increased the remediation cost. Similar to negative correlation, remediation cost increased with increasing $\sigma^2_{\ln K_d}$ for positive correlation since high K_d values and initial mass became higher with increasing $\sigma^2_{\ln K_d}$.

For realization B with $\lambda_{\ln K_d}$ of 15 m, remediation costs of negatively correlated K_d -fields were lower than the positively correlated K_d -fields. However, remediation costs of negatively correlated K_d -fields were almost the same with the corresponding homogenous K_d -fields when $\sigma^2_{\ln K_d}$ was low and it was %3 higher than the homogenous case when $\sigma^2_{\ln K_d}$ was high. This was because of the presence of small low K regions in the plume area (Figure 4.56(b)). Although 64% of the plume area had a K higher than 4.5×10^{-5} m/s, there were some very low K regions (dark blue

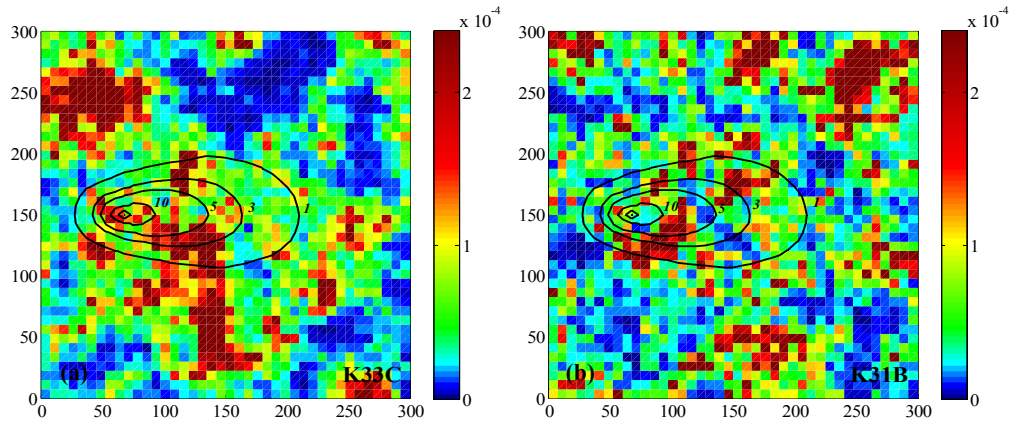


Figure 4.56. K distribution of field (a) K33C and (b) K31B along with the average plume

elements in the Figure 4.56(b)) corresponding to high K_d regions for the negative correlation case. This made remediation harder and increased the costs compared to the fields of realization C with $\lambda_{\ln K_d}$ of 30 m which exhibited a different (decreasing) trend in remediation cost versus $\sigma^2_{\ln K_d}$. Similar to realization C with $\lambda_{\ln K_d}$ of 30 m, percent variations in initial masses and corresponding remediation costs compared to the homogeneous cases did not exhibit a linear relationship. For K31B+Kd31B, 8% more mass resulted in 12% higher cost with respect to homogeneous cases, whereas for K21B+Kd21B, 5% more PCE mass caused 6% higher cost. On the other hand, for K31B-Kd31B, 1% less mass resulted in 3% higher cost with respect to homogeneous cases while for K21B-Kd21B, 2% less PCE mass caused almost the same cost with homogeneous K_d -field. This showed that for some cases having less mass did not result in less remediation cost, but the local K , K_d and sorbed mass affected the removal of the contaminant.

Among all heterogeneous K-fields studied, the fields having the highest number of low K elements were fields of realization B with $\lambda_{\ln K}$ of 30 m and realization C with $\lambda_{\ln K}$ of 15 m. 76% and 60% of the plume areas were covered by K elements of less than 4.5×10^{-5} m/s in fields of realization B with $\lambda_{\ln K}$ of 30 m and realization C with $\lambda_{\ln K}$ of 15 m, respectively, for all $\sigma^2_{\ln K}$. For these fields, positive correlation resulted in lower remediation costs compared to both homogenous and negatively correlated K_d -fields. The cost also decreased with increasing $\sigma^2_{\ln K_d}$. This was because of the coincidence of low K regions with low K_d regions. K_d values in these regions decreased with increasing $\sigma^2_{\ln K_d}$. Furthermore, these positively correlated fields had less initial PCE mass than the homogeneous K_d -field. As a result, the remediation cost decreased. For K33B+Kd32B, 9% less mass resulted in 5% less cost with respect to homogeneous cases whereas for K23B+Kd22B, 7% less PCE mass caused 5% less cost. Oppositely, for the fields of realization B with $\lambda_{\ln K_d}$ of 30 m and realization C with $\lambda_{\ln K_d}$ of 15 m, initial mass was higher for the negatively correlated K_d -fields. This was reflected on the higher total remediation costs. For example, for K33B-Kd32B, 15% more mass resulted in 21% more cost with respect to the homogeneous case whereas for K23B-Kd22B, 10% more PCE mass caused 5% more cost.

The most significant effect of correlation between K and K_d on remediation costs was seen for fields of realization A with $\lambda_{\ln K_d}$ of 30 m for the negative correlation case. Here, the cost of remediation was up to 1.45 times higher than the cost of the homogenous K_d case (for field K33A-Kd32A). For field K33A-Kd32A, not only the cost but also the total pumping rate and the number of active wells were higher. 97% increase in the total pumping rate with respect to the total pumping rate of the homogenous K_d assumption was observed with the use of 5 active wells for this field. This might be because of the presence of higher number of very low K elements in the plume area compared to the other fields. Figures 4.51(b), 4.57(a) and 4.57(b) depict

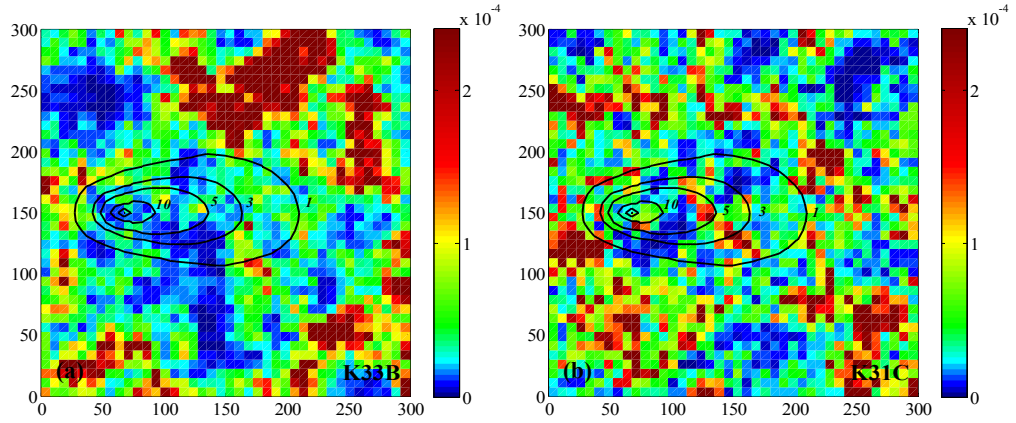


Figure 4.57. K distribution of field (a) K33B and (b) K31C along with the average plume

the distribution of K on fields K33A, K33B and K31C, as examples, along with the average plume. These three fields were the fields having the greatest number of K elements lower than 4.5×10^{-5} m/s. 59% of K elements located in the plume area were lower than 4.5×10^{-5} m/s for field K33A but the number of dark blue elements was higher compared to K33B and K31C. Since there was also a high K region in the highly concentrated contaminant plume areas for field K33A, the trend in remediation cost with respect to $\sigma_{\ln K}^2$ was not similar to realization B with $\lambda_{\ln K_d}$ of 30 m and realization C with $\lambda_{\ln K_d}$ of 15 m for positive correlation case. For realization A with $\lambda_{\ln K_d}$ of 30 m, cost was lower than the homogenous case for the low $\sigma_{\ln K}^2$ but it was higher than the homogenous K_d case for the high $\sigma_{\ln K}^2$. This is due to the fact that high K regions corresponded to high K_d regions for this case and high K_d values became higher with increasing $\sigma_{\ln K}^2$. On the other hand, for realization B with $\lambda_{\ln K_d}$ of 30 m and realization C with $\lambda_{\ln K_d}$ of 15 m, remediation cost was lower than the homogeneous case for all $\sigma_{\ln K}^2$ for the positive correlation case.

For fields of realization A with $\lambda_{\ln K_d}$ of 30 m, initial mass was higher than the mass in the homogenous K_d -field for both positive and negative correlation assumptions. Actually, initial mass was almost the same for the negatively and positively correlated K_d -fields having the same $\sigma^2_{\ln K_d}$. In spite of having almost the same mass, the costs obtained with negatively correlated fields were higher than the costs obtained with the positively correlated fields. Remediation on field K33A-Kd32A cost 31% more compared to K33A+Kd32A while remediation was 8% more costly on field K23A-Kd22A compared to K23A+Kd22A. Similarly, for fields of realization A with $\lambda_{\ln K_d}$ of 15 m, initial mass was almost the same for the negatively and positively correlated fields having the same $\sigma^2_{\ln K_d}$. Again, the costs obtained for the negatively correlated fields were higher than the costs obtained with the positively correlated fields. Remediation cost on field K31A-Kd31A was 14% higher compared to K31A+Kd31A while remediation was 17% more costly on field K21A-Kd21A compared to K21A+Kd21A. This showed that not only the initial mass, but also the distribution of K and K_d and the positions of high or low K/K_d regions relative to the highly concentrated contaminant plume areas were important on the remediation cost and design.

For the negatively correlated K_d -fields, the minimum and the maximum unit remediation costs to reach the water quality standards were \$158/kg PCE and \$214/kg PCE for realization A, \$145/kg PCE and \$160/kg PCE for realization B and \$154/kg PCE and \$172/kg PCE for realization C. Therefore, unit remediation cost changed by up to 48% with respect to the minimum unit cost (\$145/kg PCE) among all negatively correlated K_d realizations and heterogeneity conditions. For the positively correlated K_d -fields, the minimum and the maximum unit remediation costs were \$158/kg PCE and \$170/kg PCE for realization A, \$149/kg PCE and \$172/kg PCE for realization B and \$146/kg PCE and \$162/kg PCE for realization C. Therefore, unit remediation cost

changed by up to 18% with respect to the minimum unit cost among all positively correlated K_d realizations and heterogeneity conditions.

The variation in the total remediation costs under different heterogeneity conditions for the negative and positive correlation assumptions are depicted in Figure 4.58. In this figure, average, minimum and maximum remediation costs, and the standard deviation in the costs with respect to $\lambda_{\ln K_d}$ are given. When the effect of $\lambda_{\ln K_d}$ on P&T remediation cost in case of positive or negative correlation between K and K_d was investigated it was seen that the standard deviation of the results was higher for longer $\lambda_{\ln K_d}$. Figure 4.58 showed that variation of the remediation cost was higher, represented by higher standard deviation, for the negative correlation assumption. The reason of higher standard deviation was that the negative correlation case contained both the best and the worst case scenarios in terms of favorable or unfavorable K and K_d combinations which can improve or impede the remediation. For the negative correlation, high K_d regions corresponded to low K regions, which was the worst case scenario for the remediation and low K_d regions corresponded to high K regions which was the best case scenario for the remediation. This may also explain the range of unit remediation costs observed for the positively and negatively correlated cases discussed in the previous paragraph.

All these analysis showed that the effect of correlation between K and K_d might change depending on the distribution of K and K_d on the contamination area. Negative correlation resulted in higher cost of remediation compared to positive correlation in general because of low K - high K_d (flow-restricted and sorption-limited) regions. However, if the plume spread over an area of high K , positive correlation might also cause higher remediation costs because of high K - high K_d regions. The effect of correlation between K and K_d was more pronounced for the cases where negative

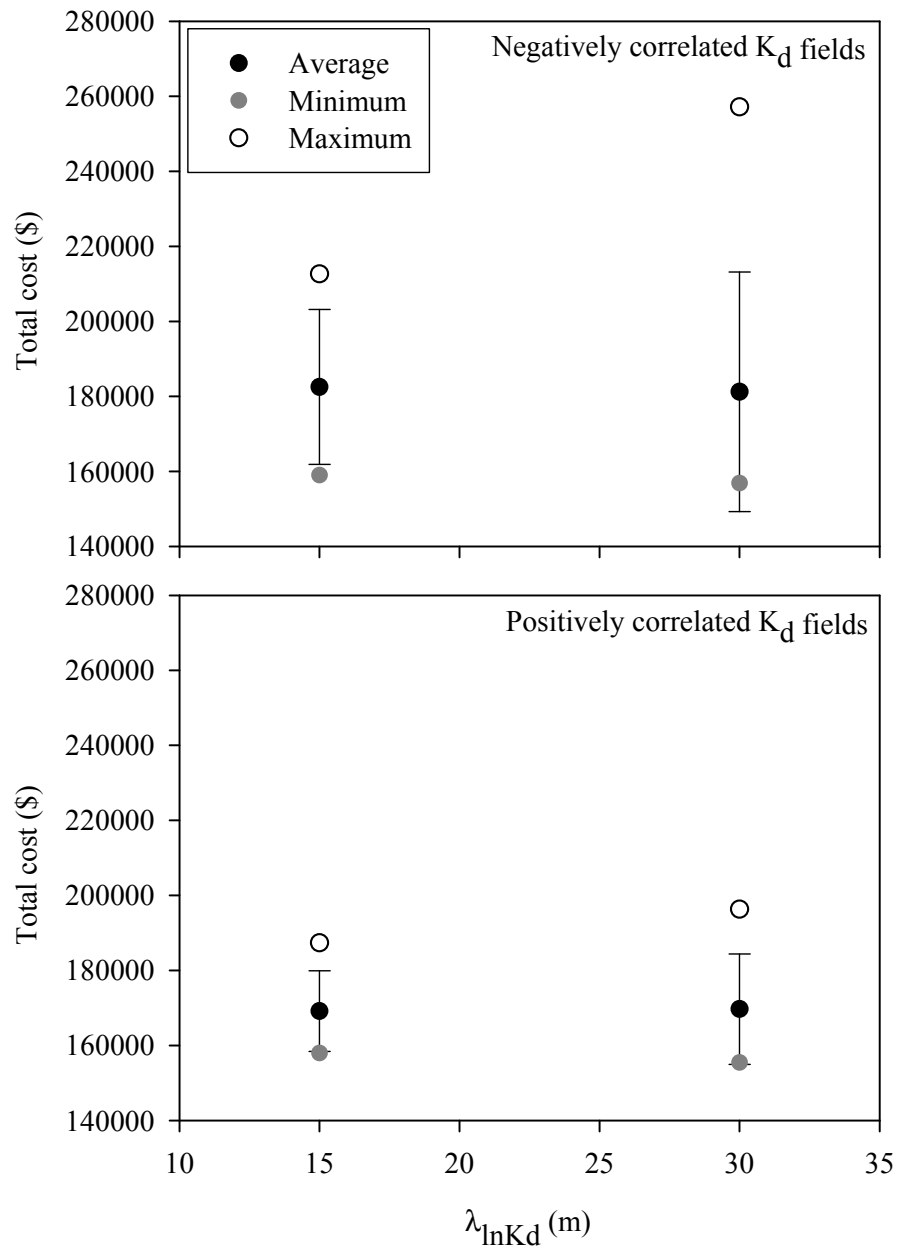


Figure 4.58. Change in average, minimum and maximum remediation cost with respect to $\lambda_{\ln K_d}$ for negatively and positively correlated K_d -fields (Error bars represent one standard deviation)

correlation resulted in higher costs compared to positive correlation. The total remediation cost changed by 0.97 to 1.45 times the cost of the homogenous K_d case for the negative correlated K_d -fields, while 0.95 to 1.16 times for the positively correlated K_d -fields. The results also showed that the presence of high K_d regions in the plume area affected the cost more than the presence of low K_d regions. In other words, when low K_d regions were present, the cost did not decrease at the same ratio at which it increased when high K_d regions were present. Presence of high K_d regions in the plume area might decrease the cost lowering effect of low K_d regions and might even cover this effect up (e.g. field K31A+Kd31A).

In literature, there were studies investigating the effect of correlation between K and K_d on P&T and in-situ bioremediation time (Rabideau and Miller, 1994; Schäfer and Kinzelbach, 1992). However, there was no study examining the effect of correlation between K and K_d on P&T remediation design and cost for horizontally heterogeneous aquifers. Therefore, this study was unique in terms of studying this effect. According to the study of Rabideau and Miller (1994), in which simulations were made for fields which were vertically heterogeneous (perfectly stratified) in both K and K_d , a perfect positive correlation between $\ln K$ and $\ln K_d$ resulted in considerably shorter P&T remediation times while a perfect negative correlation significantly increased it. On the other hand, for an in-situ bioremediation system, Schäfer and Kinzelbach (1992) found that negative correlation between K and K_d resulted in a considerable increase in the remediation time compared to the uncorrelated case. Although results of these two studies were not exactly comparable with the results of this study, they also showed that negative correlation between K and K_d has a negative impact on P&T remediation systems. However, this study also added that the negative impact of negative correlation was not absolutely true for all K - K_d combinations and positive correlation may also have an adverse effect on P&T remediation systems depending on the corresponding distributions of K and K_d and

the amount of the sorbed mass. It should be noted that majority of the studies in literature ignores rate-limited mass transfer and its effect on remediation performance.

4.6. Effect of Correlation Scale and Heterogeneity of α

4.6.1. Uncorrelated α and K_d

In this part of the study, the effects of heterogeneity in α and $\lambda_{\ln\alpha}$ on P&T remediation design and cost was investigated. The average plume was used as the initial plume condition. K and K_d were also assumed to be heterogeneous and various combinations K and K_d -fields selected from the previous phases of the study were used. In this part of the study, K_d -fields used for the constant K_{dg} approach were used. The α -fields used in this section, details of which were explained in Section 3.1.5, were not correlated with either K or K_d -fields. Single K and K_d realizations, realization A and a, respectively, were chosen arbitrarily as K and K_d heterogeneity conditions. Simulations were performed for three different α realizations, i, ii and iii, each having two different $\sigma^2_{\ln\alpha}$ (0.0057 and 0.0299). These heterogeneous α -fields were applied on K and K_d -fields of different $\sigma^2_{\ln K}$ and $\sigma^2_{\ln K_d}$ combinations. As it was the case for the heterogeneous K_d -fields, the same λ were used for K , K_d and α in the simulations.

When the results of the optimization runs for 30 different α , K_d and K -field combinations were investigated, it was seen that 8 different wells (wells 3, 8, 13, 14, 17, 18, 19, and 24) were selected in total. For the corresponding heterogeneous K_d and K -fields with homogeneous α , on the other hand, 5 different wells (wells 3, 13, 14, 18 and 24) had been selected. Among 30 different α , K_d and K -field combinations, 24 2-well designs and 6 3-well designs were selected as the optimum design whereas the homogenous α assumption resulted in 1 1-well design, 3 2-well designs and 1 3-well

design. Therefore, compared to the homogeneous α -fields, heterogeneity in α required a larger number of active wells distributed over a wider area.

When the number of wells and the total pumping rate required to cleanup the aquifer were compared with the corresponding homogeneous α case, it was seen that one more well was required for designs on the fields K11A/Kd11a for all three α distributions (realizations) and two different $\sigma^2_{\ln\alpha}$. For these fields, the total pumping rate was less (up to 28% with respect to homogenous α) or the same with the pumping rate for the homogenous α case. These fields were the ones on which higher remediation costs compared to the homogenous α were obtained. For all other cases, the same number of pumping wells with higher (up to 4%), the same or lower (down to 7%) total pumping rates was required compared to the homogenous α assumption. This showed that heterogeneity in α may or may not affect the design of P&T remediation system depending on all K, K_d and α realizations and heterogeneity conditions.

The total remediation costs obtained with the combinations of selected heterogeneous K, K_d and uncorrelated α -fields (with K and K_d), as described above, are presented in Figures 4.59 and 4.60 along with the costs obtained with the homogenous α and heterogeneous K_d (results of the constant K_{dg} approach), and homogenous α and homogenous K_d -fields for a given $\sigma^2_{\ln K}$ for comparison purposes. Figure 4.59 shows the change in the remediation costs with respect to $\sigma^2_{\ln K}$ for α realizations i, ii and iii and $\lambda_{\ln\alpha}$ of 15 and 30 m. For these simulations $\sigma^2_{\ln K_d}$ was kept constant as 0.0256 in order to see the effect of α heterogeneity while degree of K heterogeneity was changing. Figure 4.60 shows the variation in remediation cost with respect to $\sigma^2_{\ln K_d}$ for α realizations i, ii and iii and $\lambda_{\ln\alpha}$ of 30 m only. For these simulations, $\sigma^2_{\ln K}$ was

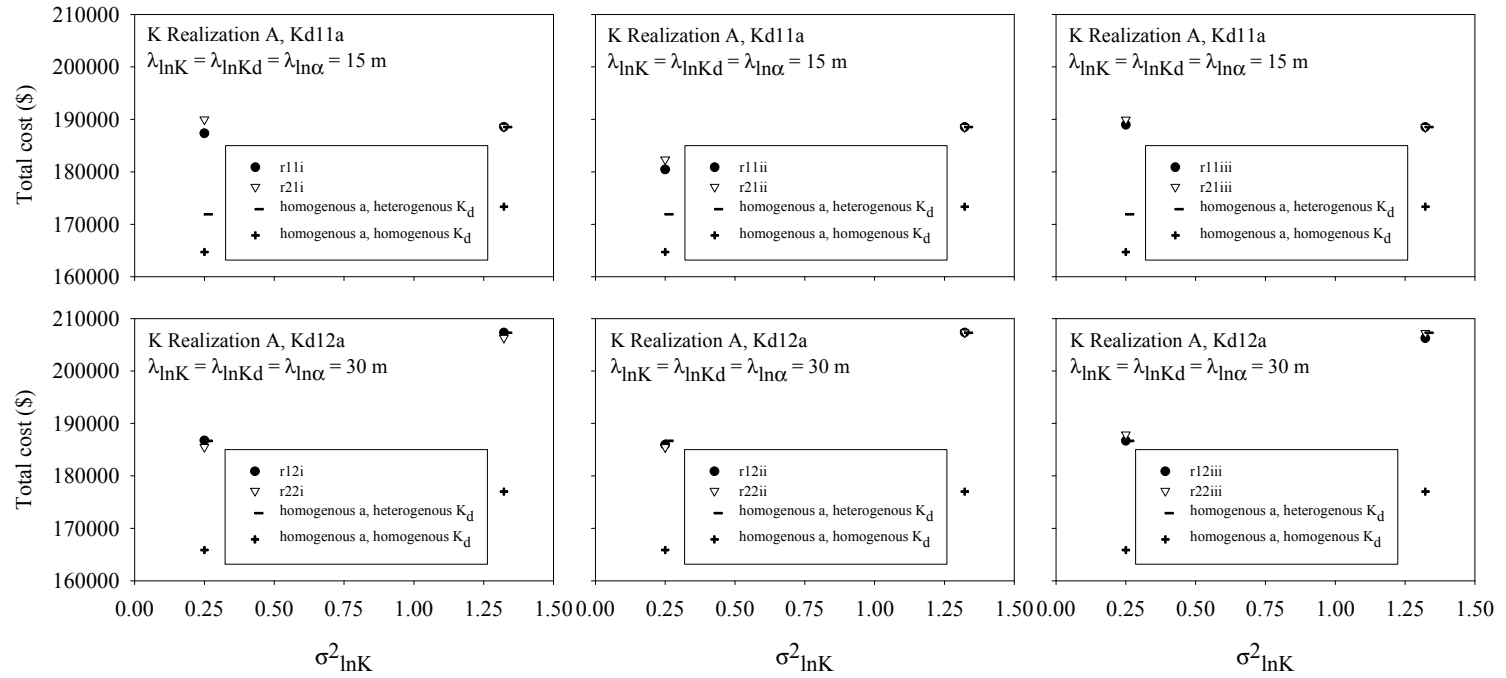


Figure 4.59. Change in remediation cost with respect to $\sigma^2_{\ln K}$ for α realizations i, ii and iii, K realization A and $\lambda_{\ln \alpha}$ of 15 and 30 m

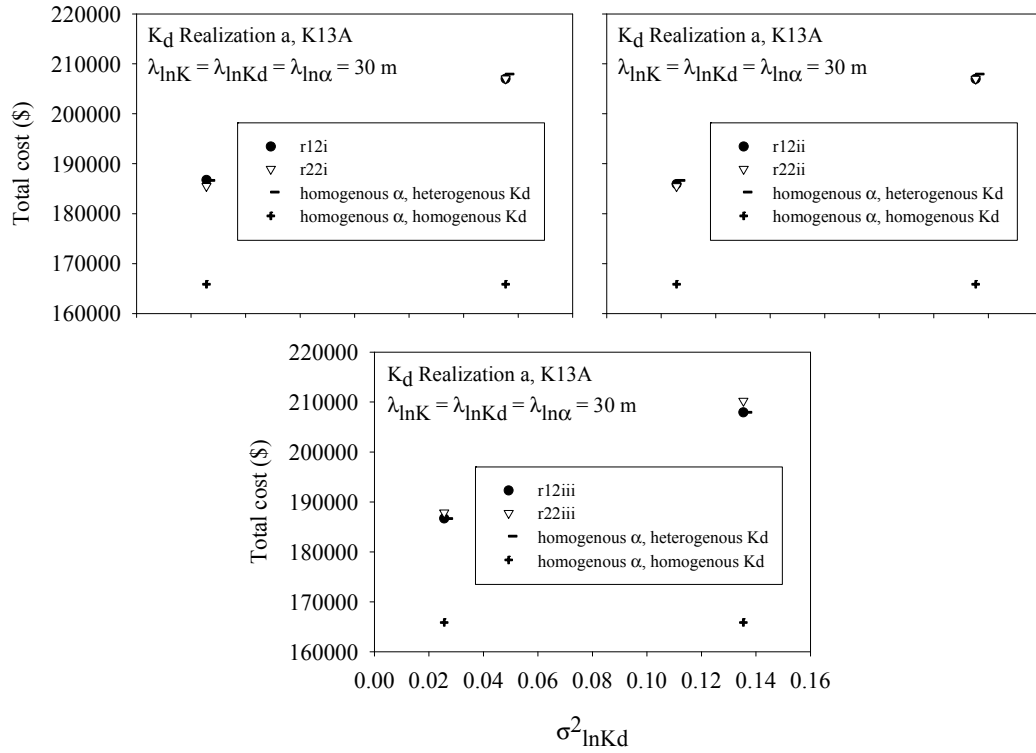


Figure 4.60. Change in remediation cost with respect to $\sigma^2_{\ln K_d}$ for K_d realization a, K-field 13A, $\lambda_{\ln \alpha}$ of 30 m

remained constant as 0.2500, in order to see the effect of α heterogeneity while only the degree of K_d heterogeneity was changing.

Results presented in Figure 4.59 and 4.60 showed that heterogeneity in α generally resulted in higher remediation costs compared to the homogenous α assumption for all three α distributions and two different $\sigma^2_{\ln \alpha}$ for field combination K11A/Kd11a, but for all other cases remediation cost was almost the same with or slightly lower (i.e.

maximum 1% lower) than the cost for the fields with the homogenous α . The increase in remediation cost was mainly because of the one additional active well and its installation cost. When $\sigma^2_{\ln\alpha}$ was considered, it was seen that increase in $\sigma^2_{\ln\alpha}$ may or may not result in increase in the cost of remediation depending on the $\sigma^2_{\ln K}$, $\sigma^2_{\ln K_d}$, $\lambda_{\ln\alpha}$ and distribution of α (i.e. α realization). Since only single realizations for K and K_d have been used for these simulations, effect of changing K and K_d distributions could not be observed. However it is strongly probable that these two factors would also affect the magnitude of change in the remediation cost with changing $\sigma^2_{\ln\alpha}$. Compared to the corresponding homogenous α , the maximum increase in the total remediation cost was 10% when $\sigma^2_{\ln\alpha}$ was low (for field r11iii/Kd11a/K11A) and it was 11% when $\sigma^2_{\ln\alpha}$ was high (for fields r21iii/Kd11a/K11A and r21i/Kd11a/ K11A). On the other hand, when the effect of increasing $\sigma^2_{\ln\alpha}$ from 0.0057 to 0.0299 on the remediation cost was considered, the maximum increase in the remediation cost was observed as 1%. This showed that increasing α heterogeneity did not have a very significant effect on the remediation cost for the studied cases. The α_g value used in this study, 0.0025 d⁻¹, was quite low (see Table 2.2 in Section 2.2). Therefore, α was already a limiting factor for the remediation regardless of its homogeneity or heterogeneity. Different results may be obtained with the use of different α_g value. In addition, $\sigma^2_{\ln\alpha}$ used in this study were 0.0057 and 0.0299 which may be low to see a considerable effect. In terms of the CV values, CVs of the α heterogeneity were the lowest compared to the CVs of the K and K_d heterogeneities. Low CV values were used for α -fields since there was no field scale study reporting α_g or $\sigma^2_{\ln\alpha}$ in the literature which could be used for validation by real life field scale measurements. Actually, if $\sigma^2_{\ln\alpha}$ values were higher, lower α would be observed in the aquifer as well as higher α . Low α means slow transfer of contaminant mass from the sorbed phase to the dissolved phase. If this transfer is too slow, then removal of the contaminant may be dependent on the mobilization of the sorbed mass and remediation becomes harder. This in turn results

in an increase in the remediation cost. Aksoy and Culver (2000) showed that remediation time might exponentially increase while α decreased, especially for slow α in the range of $2.5 \times 10^{-2} - 2.5 \times 10^{-4} \text{ d}^{-1}$ which were published laboratory scale rates for soils contaminated for a long time. Mishra and Gutjahr (1999) found that the variability in K had more significant effect on transverse spreading of the solute than sorption/desorption rate variability for the sorption/desorption rate variance of 0.1. On the other hand Mishra et al. (1999) showed that spatially variable sorption/desorption rate with a σ^2 of 0.5 had a noticeable effect on the breakthrough curve. These studies also strengthened the possibility that using low $\sigma^2_{\ln\alpha}$ might have prevented the observable effect on remediation costs.

Effect of α heterogeneity on remediation costs was more significant for low $\sigma^2_{\ln K}$ compared to high $\sigma^2_{\ln K}$ when $\lambda_{\ln\alpha}$ was 15 m (Figure 4.59). Similar findings were obtained in the study of Aksoy and Culver (2004) where P&T remediation cost were optimized in the presence of α heterogeneity. Aksoy and Culver (2004) utilized three different α realizations with a single $\sigma^2_{\ln\alpha}$ and $\lambda_{\ln\alpha}$ value. The background heterogeneous K -fields had two different $\sigma^2_{\ln K}$ belonging to a single realization while heterogeneous K_d -field was kept constant. Under these conditions they found that α heterogeneity affected the remediation design with an addition of one more well for $\sigma^2_{\ln K}$ of 0.064 but the effect was negligible when $\sigma^2_{\ln K}$ was 0.673. On the other hand, in this study, for $\lambda_{\ln\alpha}$ of 30 m, α heterogeneity exhibited almost no effect on the remediation costs for the two $\sigma^2_{\ln K}$ values considered (Figure 4.59). Therefore, change in $\lambda_{\ln\alpha}$ might result in a change in significance of $\sigma^2_{\ln K}$ on P&T remediation cost.

When the change in the effect of α heterogeneity with respect to $\sigma^2_{\ln K_d}$ was investigated, it was seen that it was not significant (maximum 1% change) for both

low and high $\sigma^2_{\ln K_d}$ (Figure 4.60). However, the simulations were conducted for $\lambda_{\ln \alpha}$ of 30 m only and this picture might change when different $\lambda_{\ln \alpha}$ was used.

When the results were analyzed with respect to the unit remediation costs for all α , K_d and K-field combinations used in this study, it was seen that the minimum and the maximum unit remediation costs to reach the water quality standards were \$156/kg PCE and \$187/kg PCE, respectively. Therefore, unit remediation cost changed by up to 20% with respect to the minimum (i.e. \$156/kg PCE) among all α realizations and α , K and K_d heterogeneity conditions studied. For the respective fields with homogenous α assumption the unit cost ranged between \$159/kg PCE and \$186/kg PCE. Therefore, the ranges of unit costs with or without α heterogeneity were similar. However, when individual α -fields with homogeneous and heterogeneous α assumptions were considered, the maximum percent change in the unit cost was observed for α -fields in combination with K11A/Kd11a as 9-10% depending on the α realizations and heterogeneity conditions. As mentioned before, for these α -fields one additional well was required for the optimal designs. This raised the total cost and the unit remediation cost. For the other α , K_d and K-field combinations, heterogeneity in α resulted in a change in the unit remediation cost in the range of -2% to 1% compared to the homogeneous α assumption.

The averages of the remediation costs obtained for three different α realizations and two different $\sigma^2_{\ln \alpha}$ were taken and the standard deviations were also found. Change in average, minimum and maximum remediation costs and the standard deviation of the costs with respect to $\lambda_{\ln \alpha}$ were given in Figure 4.61 for two different $\sigma^2_{\ln K}$ separately. In this figure, the standard deviation of the results was higher for shorter $\lambda_{\ln \alpha}$ when $\sigma^2_{\ln K}$ was low but the opposite was true when $\sigma^2_{\ln K}$ was high. It is worth to note that

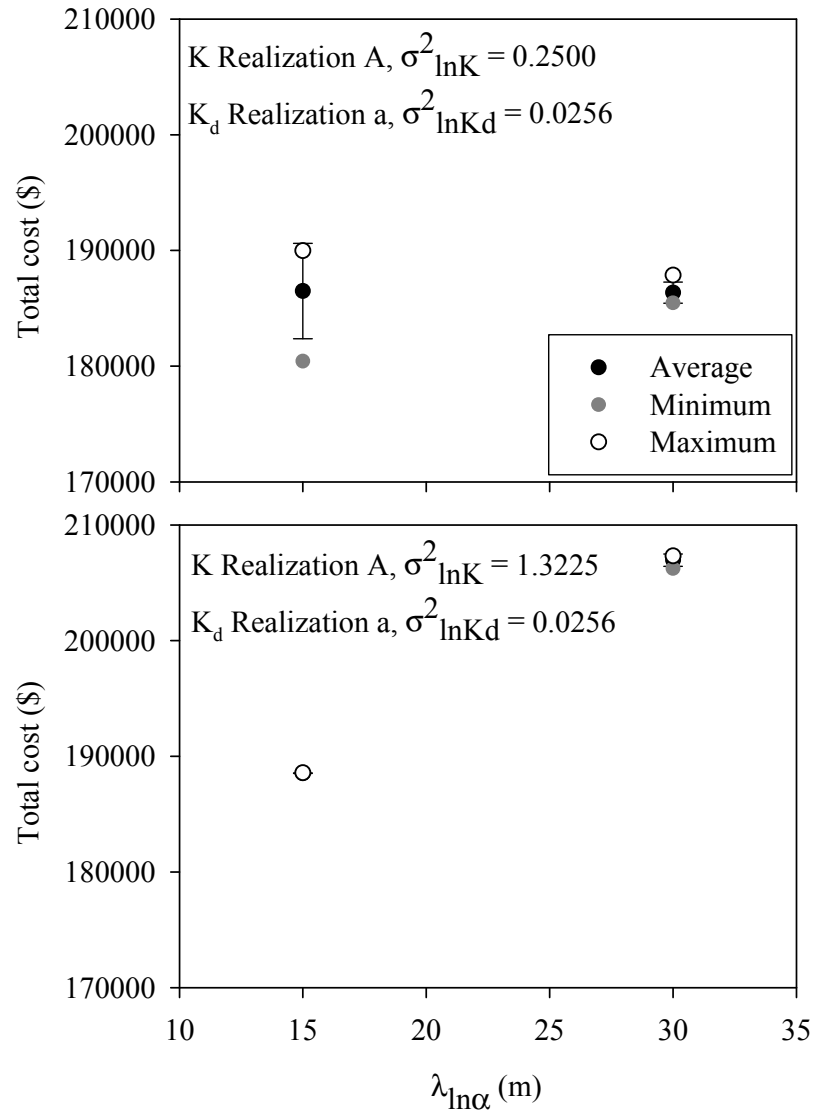


Figure 4.61. Change in average, minimum and maximum remediation cost with respect to $\lambda_{\ln\alpha}$ for uncorrelated α -fields and different K and K_d cases (Error bars represent one standard deviation)

the standard deviations were higher for low $\sigma^2_{\ln K}$ (the top figure in Figure 4.61) compared to high $\sigma^2_{\ln K}$ (the bottom figure in Figure 4.61). Indeed, the standard deviation for higher $\sigma^2_{\ln K}$ was negligibly small (\$17 for $\lambda_{\ln \alpha}$ of 15 m and \$534 for $\lambda_{\ln \alpha}$ of 30 m) showing the insignificant effect of α heterogeneity for more heterogeneous K-fields.

In literature, Rabideau and Miller (1994) modeled P&T remediation in a vertically heterogeneous aquifer assuming nonequilibrium sorption conditions. They found that slow mass transfer rates dramatically increased the projected cleanup time and the cleanup time became longer as the rate of mass transfer happened to be slower. The relative significance of the mass transfer rate effect was slightly decreased as the degree of heterogeneity in K increased. On the other hand, the relative significance of sorption nonequilibrium and K heterogeneity depended on the values of the parameters defining these processes. Either of them dominated over the other in terms of longer cleanup times depending on the values of these parameters. Similar to Rabideau and Miller (1994), Aksoy and Culver (2000) stated that sensitivity of the remediation time to rate-limited sorption was less for heterogeneous aquifers in K compared to the homogenous aquifer. In addition, according to Brusseau (1992c) the effect of rate-limited sorption was less relative to the aquifer heterogeneity in K for the field scale transport. This study focused on remediation costs and designs and results showed that heterogeneity in α may impact the P&T designs and costs depending on the distributions of K, K_d and α , although the relative impact of α heterogeneity was low for the studied cases. It seemed that K and K_d heterogeneities were dominant over α heterogeneity for the parameter ranges used in this study. However, for different values and different combinations of K, K_d and α , different results could be obtained. There is a need for determination of field scale variance and correlation structure for α in order to test whether $\lambda_{\ln \alpha}$ and $\sigma^2_{\ln \alpha}$ values used in this study were in agreement with real life values.

4.6.2. Correlated α and K_d

In this section of the study, the effect of negative correlation between α and K_d on P&T remediation design and cost have been investigated using the average plume as the initial plume condition. Heterogeneous K_d -fields used for these simulations were the positively and negatively correlated K_d -fields with K as generated in Section 3.1.4. The correlation between α and K_d -fields resulted in a correlation between α and K as well. This correlation could be quantified as such. For K_d -fields, which were negatively correlated with K , Equation 3.2 (i.e. $\ln K_d = -4.225 - 0.32 \ln K$) was used for the generation, while the correlation between K_d and α was defined by Equation 3.4 (i.e. $\ln \alpha = -6.47 - 0.47 \ln K_d$). When these two equations were combined, the relationship between α and K , when negatively correlated K_d -fields was used for the simulations, was found as

$$\ln \alpha = -4.48 + 0.1504 \ln K \quad (4.2)$$

When the same procedure was applied to the positively correlated K_d -fields with K , which were generated by the help of Equation 3.3 (i.e. $\ln K_d = 2.181 + 0.32 \ln K$), the equation relating α and K was found as

$$\ln \alpha = -7.495 - 0.1504 \ln K \quad (4.3)$$

Equations 4.2 and 4.3 show that there is a positive correlation between α and K for the simulations performed with the negatively correlated K_d -fields with K , whereas a negative correlation is established between α and K for the simulations performed with the positively correlated K_d -fields with K .

The results of the simulations conducted with the correlated α and negatively and positively correlated K_d -fields with K are presented in Figures 4.62 and 4.63 in terms of the change in total remediation costs with respect to $\sigma^2_{\ln K}$ and $\sigma^2_{\ln \alpha}$. Presence of negative correlation between α and negatively correlated K_d -fields with K was expected to result in either lower or higher remediation costs depending on the K -field conditions. If K was high, then K_d would be low and α would be high. This represents the best situation in terms of contaminant mobilization because of the easy flow of contaminants in low sorption and fast mass transfer zones. On the other hand, if K was low, then K_d would be high and α would be low. This represents the worst situation. One might expect lower remediation cost for the best situation while higher remediation cost for the worst. When the results obtained with three negatively correlated K_d -fields with K were investigated (Figure 4.62), it was seen that the effect of negative correlation with α was not as significant as expected. Among all field cases, the maximum cost increase was obtained as 2% (for the field K33A-Kd32A-r22A). Low K regions were dominant over the fields of K33A (see Section 4.5.2 for details). Therefore, these fields may be the examples where the worst situation was observed. However, even under the worst case condition, the cost increase was not high. On the other hand, fields of realization B with $\lambda_{\ln K}$ of 15 m and realization C with $\lambda_{\ln K}$ of 30 m, where high K regions were governing, may be the examples where the best situation was observed according to the analysis given in Section 4.5.2. According to the results, the costs obtained with the correlated α -fields were almost the same with the cost of the homogenous α cases. Therefore, the expected best situation did not make a significant impact on the remediation cost. When negative correlation between α and positively correlated K_d -fields with K was considered, low K_d and high α regions were associated with low K regions, while high K_d and low α regions were associated with high K regions. Unlike the negatively correlated K_d -field

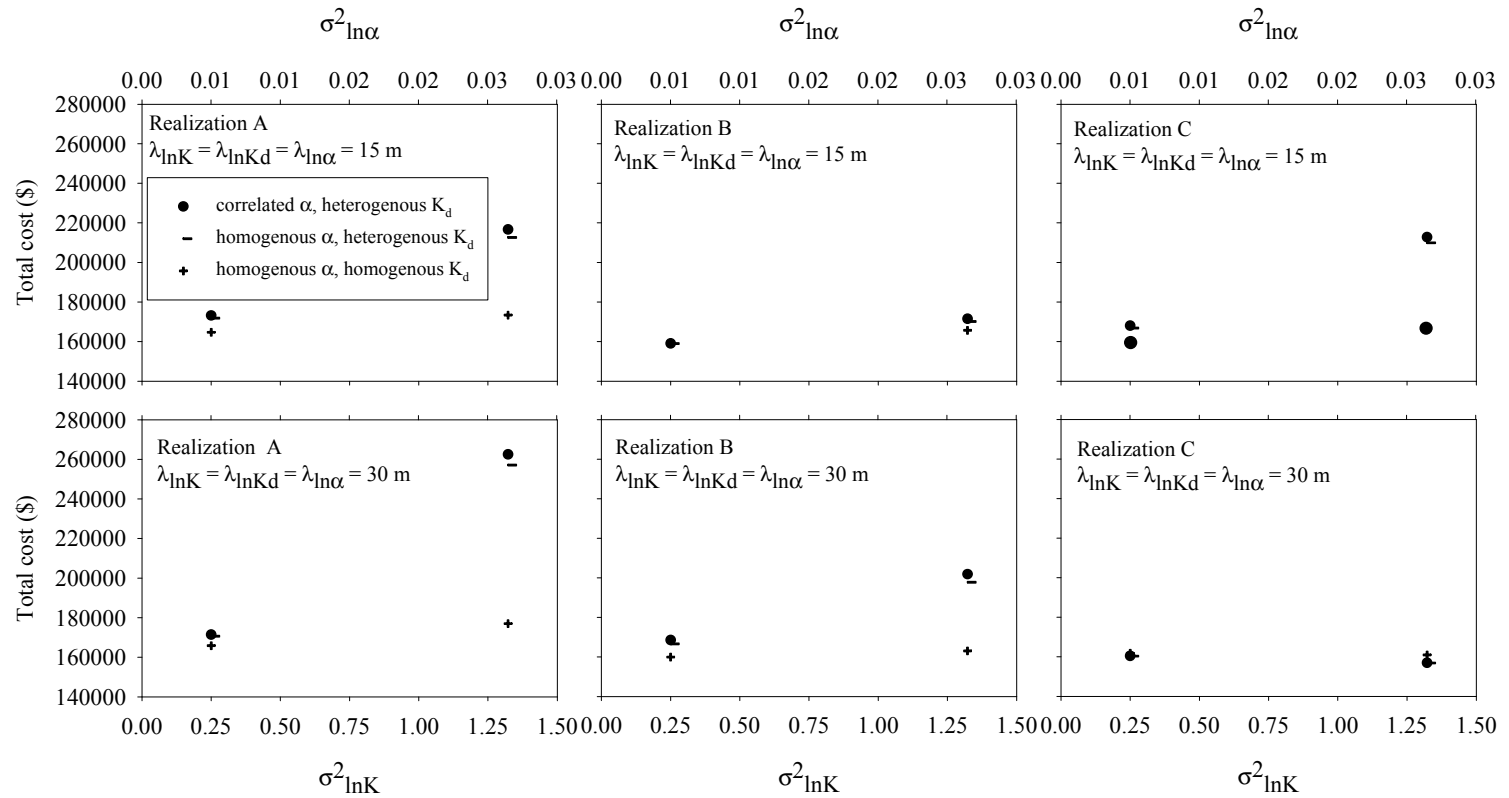


Figure 4.62. Change in remediation cost with respect to $\sigma^2_{\ln K}$ and $\sigma^2_{\ln \alpha}$ for K_d -fields which are negatively correlated with K realizations A, B and C, $\lambda_{\ln \alpha}$ of 15 and 30 m

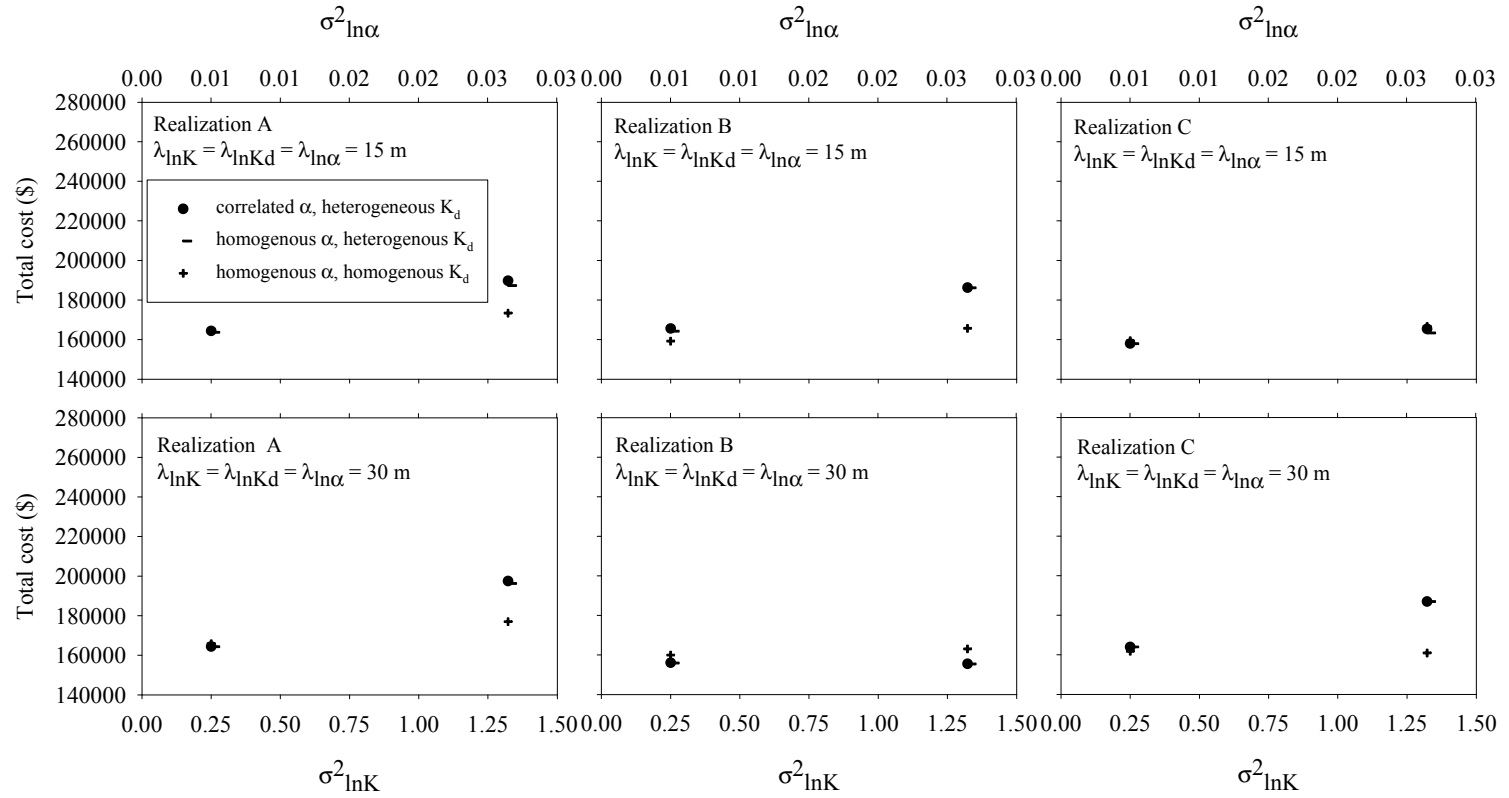


Figure 4.63. Change in remediation cost with respect to $\sigma^2_{\ln K}$ and $\sigma^2_{\ln \alpha}$ for K_d -fields which are positively correlated with K realizations A, B and C, $\lambda_{\ln \alpha}$ of 15 and 30 m

case, now, it was not easy to say which case was better. When the results obtained with positively correlated K_d -fields with K were investigated (Figure 4.63), it was seen that the effect of negative correlation with α was not significant at all such that the maximum cost increase was 1% among all field cases.

When the results of the optimization runs for 24 different α , K_d and K -field combinations were investigated, it was seen that 8 different wells (wells 3, 7, 8, 13, 14, 18, 19 and 23) were selected in total. For the corresponding heterogeneous K_d and K -fields with homogeneous α , on the other hand, 7 different wells (wells 3, 8, 13, 14, 18, 19 and 23) had been selected. Among 24 different α , K_d and K -field combinations, 16 1-well designs, 7 2-well designs and 1 5-well design were selected as the optimum design. The number of wells used for the optimal designs of heterogeneous α fields was always the same with that of corresponding homogeneous α . The locations of the active wells were also the same with the well locations of the corresponding homogeneous α -fields except for 2 cases. This resulted in the different number of selected wells in total (8 versus 7 for heterogeneous and homogeneous α assumptions, respectively). In terms of total pumping rate, it was seen that for 14 α -field cases, total pumping rate was higher than the pumping rate for the corresponding homogeneous α -fields reaching up to a maximum percent increase of 13% for the field K33A-Kd32A-r22A. For this field, the percent cost increase was the maximum among all fields with 2%. For the remaining 10 α -field cases, the total pumping rate was exactly the same with the homogeneous α -fields.

In general, the results showed that the effect of negative correlation between α and K_d (additionally with both positive and negative correlation with K) was not very significant on remediation cost and design. This impact may have either been masked by the heterogeneity in K_d or the reason may be the low α_g and $\sigma_{\ln\alpha}^2$. If α_g

is very small, regardless of the heterogeneity, it may be a governing factor for the design. For higher α_g values with higher $\sigma_{\ln\alpha}^2$, the effect may be more observable.

When the effect of $\lambda_{\ln\alpha}$ on P&T remediation cost obtained with correlated α -fields was investigated, it was seen that the standard deviation of the results was higher for longer $\lambda_{\ln\alpha}$. Change in average, minimum and maximum remediation costs with respect to $\lambda_{\ln\alpha}$ and the standard deviation of the results are given in Figure 4.64. Figure 4.64 very much resembles to Figure 4.58 since the costs obtained with correlated α -fields were almost the same with the cost obtained with the homogenous α -fields as presented in Figure 4.58. Therefore, increasing standard deviation with increasing $\lambda_{\ln\alpha}$ was not due to any effect of correlation between α and K_d but it was due to the effect of correlation between K and K_d as explained in Section 4.5.2.

4.7. Effect of f

In all previous sections of this chapter, optimization runs were performed with an f value of 0.75. In this section, the effect of f value on P&T remediation design and cost was investigated using two more different f values, 0.5 and 0.25. For this purpose, both the original plume and the average plume were used. Changing f value resulted in different amounts of kinetically sorbed masses present as an initial condition at the beginning of the remediation, although the dissolved plumes were exactly the same for all f values. Since the f value only affected the fraction of the sorbed mass which was in the kinetic sorption sites or in equilibrium with the dissolved phase, the total amount of sorbed mass present in the aquifer was the same for all f values tested. Figure 4.65 shows the schematic representation of the final mass distribution resulting from the use of different f values.

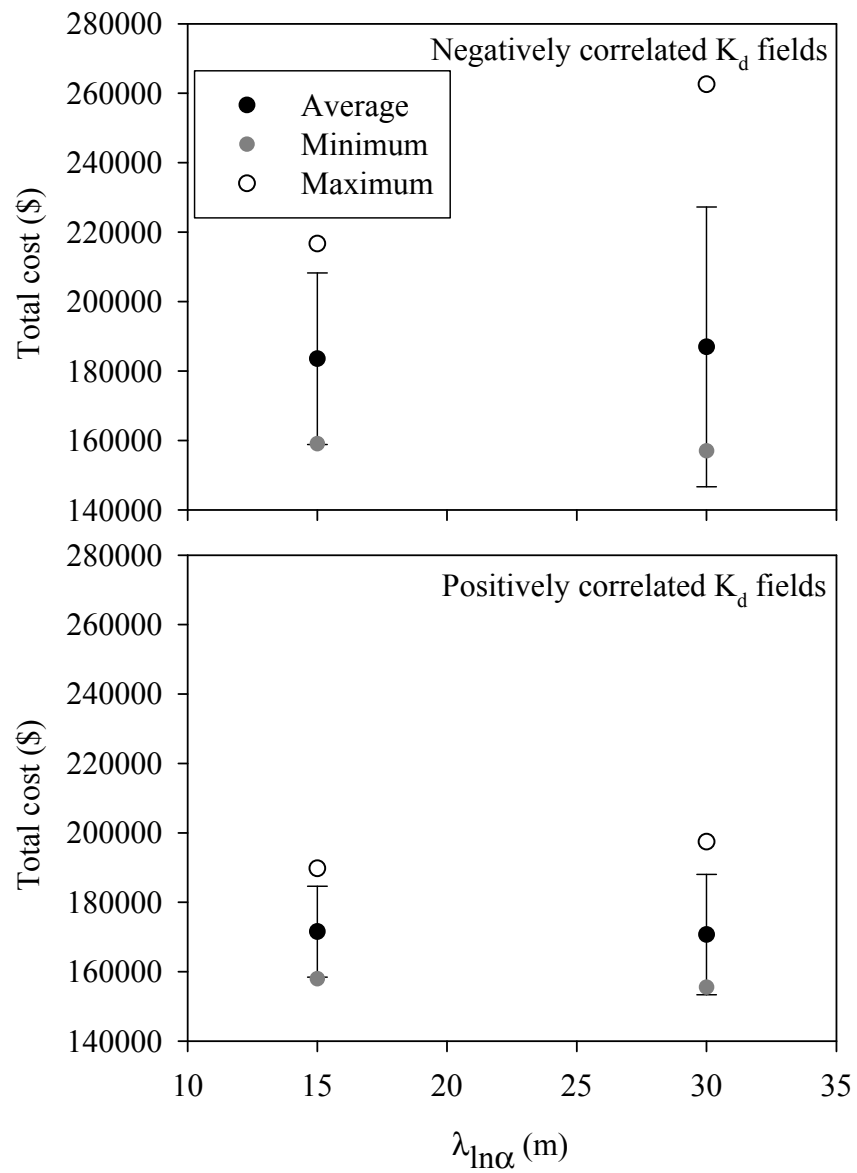


Figure 4.64. Change in average, minimum and maximum remediation cost with respect to $\lambda_{\ln\alpha}$ for correlated α -fields (Error bars represent one standard deviation)

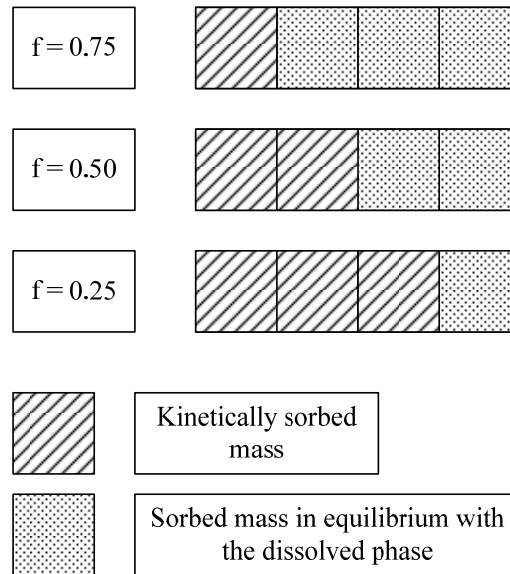


Figure 4.65. Schematic representation of the final mass distribution resulting from the use of different f values

For the original plume case, optimum remediation designs for f value of 0.75 consisted of only 1-well designs. For f value of 0.5, 9 1-well and 9 2-well designs were selected as the optimum. For f value of 0.25, 16 2-well designs and 2 3-well designs were chosen as an optimal design scenario. For 9 K-field cases, the number of active wells was increased from 1 to 2 when f decreased from 0.75 to 0.5. For these 9 cases, the total pumping rate also increased by up to 38% for a given field. For the remaining 9 K-field cases, the active well numbers were the same but the total pumping rates increased by up to 73%. The minimum increase in total pumping rate for all 18 K-field cases was 5%. When f decreased from 0.75 to 0.25, for 16 K-field cases, the number of wells increased from 1 to 2 while for the remaining 2 K-field cases the number of active wells increased from 1 to 3. The increase in total pumping rate was up to 1.9 times when a given field with different f values of 0.25 and 0.75 were compared. The minimum increase for a given field was 60%. When f decreased from 0.5 to 0.25, for 9 K-field cases, the

number of active wells was increased from 1 to 2, for 2 of them active well number rose to 3 from 2 and for the remaining 7 K-field cases, the active well numbers were the same. For all 18 K-field cases, decreasing f from 0.5 to 0.25 resulted in an increase in the total pumping rate by up to 1.2 times. The minimum increase for a given field was 19%.

For the average plume case, optimum remediation designs for f value of 0.75 included only 1-well designs except for a single K-field case. For f value of 0.5, 11 1-well and 7 2-well designs were selected as the optimum. 16 2-well designs and 2 3-well designs were chosen as an optimal design scenario for f value of 0.25. For 6 K-field cases, the number of active wells was increased from 1 to 2 when f decreased from 0.75 to 0.5. For 4 of these 6 cases, the total pumping rate also increased by up to 29% for a given field. For one of these 6 cases, it decreased by 4% and remained the same for the last one. For the remaining 12 K-field cases, the active well numbers were the same but the total pumping rates increased by up to 60%. When f decreased from 0.75 to 0.25, for 15 K-field cases, the number of wells increased from 1 to 2, for 2 K-field cases the number of active wells increased from 1 to 3 and for the last one, it remained the same as 2. The increase in total pumping rate was up to 2.4 times when a given field with different f values of 0.25 and 0.75 were compared. The minimum increase was 67%. When f decreased from 0.5 to 0.25, for 11 K-field cases, the number of active wells was increased from 1 to 2, for 2 of them active well number rose from 2 to 3 and for the remaining 5 K-field cases, the active well numbers were the same. Among all 18 K-field cases, decreasing f from 0.5 to 0.25 resulted in an increase in the total pumping rate by up to 1.3 times. The minimum increase was 38%. Therefore, decreasing f value caused an increase either in the total pumping rate or in the active well number. For most of the fields, both pumping rate and the number of active wells increased even the plume configurations and the initial contaminant masses were variable.

Figure 4.66 shows the variation in the total remediation cost with respect to $\lambda_{\ln K}$ for changing f values for the original plume case. For a given $\sigma_{\ln K}^2$ (0.2500 or 1.3225), the total remediation costs for different f values generally followed the same trends with respect to $\lambda_{\ln K}$ in each realization. The results showed that the total remediation cost increased with decreasing f value for the same $\lambda_{\ln K}$ and $\sigma_{\ln K}^2$. The percent increase was in the range of 1-17% when f decreased from 0.75 to 0.5. The range of percent increase was 22-45% when f decreased from 0.75 to 0.25. This range was 4-29% when f decreased from 0.5 to 0.25.

When the average plume was used as the initial plume condition, the same trends obtained for the average plume conditions were observed such that the total costs increased with decreasing f values (Figure 4.67). The percent increase reached up to 15% when f decreased from 0.75 to 0.5. The minimum increase was 2% for this condition. When the remediation costs for f values of 0.25 and 0.75 were analyzed, it was seen that cost could increase in the range of 22-43%. The range of percent increase was 12-30% when f decreased from 0.5 to 0.25. Similar trends in the total remediation costs with respect to f value for both original and average plume indicated that the total cost increased with decreasing f value independent from the initial plume distributions considered in this study. Therefore, the mass transfer limitations became an important factor in determining the fate of the remediation. Heterogeneity in K impacted the scale of the effect of f value.

When f decreases, the amount of kinetically sorbed mass increases and the sorbed mass on the equilibrium sorption sites decreases. Kinetically sorbed mass represents the slowly desorbing mass where the rate of desorption is determined by α . The sorbed mass on the equilibrium sorption sites, on the other hand, represents the instantaneously sorbed/desorbed fraction of the sorbed mass. When the amount of sorbed mass on kinetic sorption sites increases, slow desorption limits the remediation and satisfying the total concentration constraint becomes harder. In

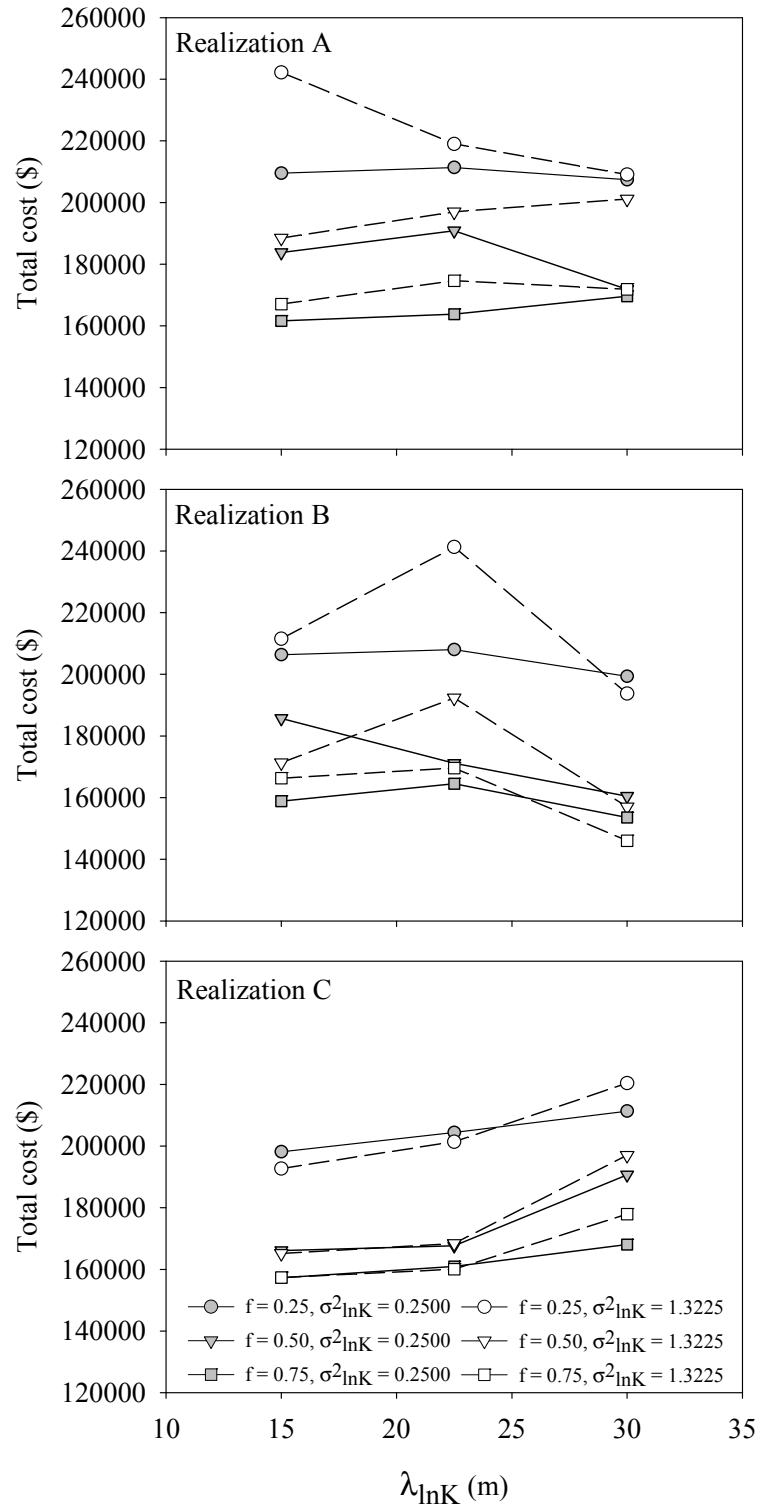


Figure 4.66. Comparison of total remediation costs for the original plume case when $f = 0.25, 0.50$ and 0.75

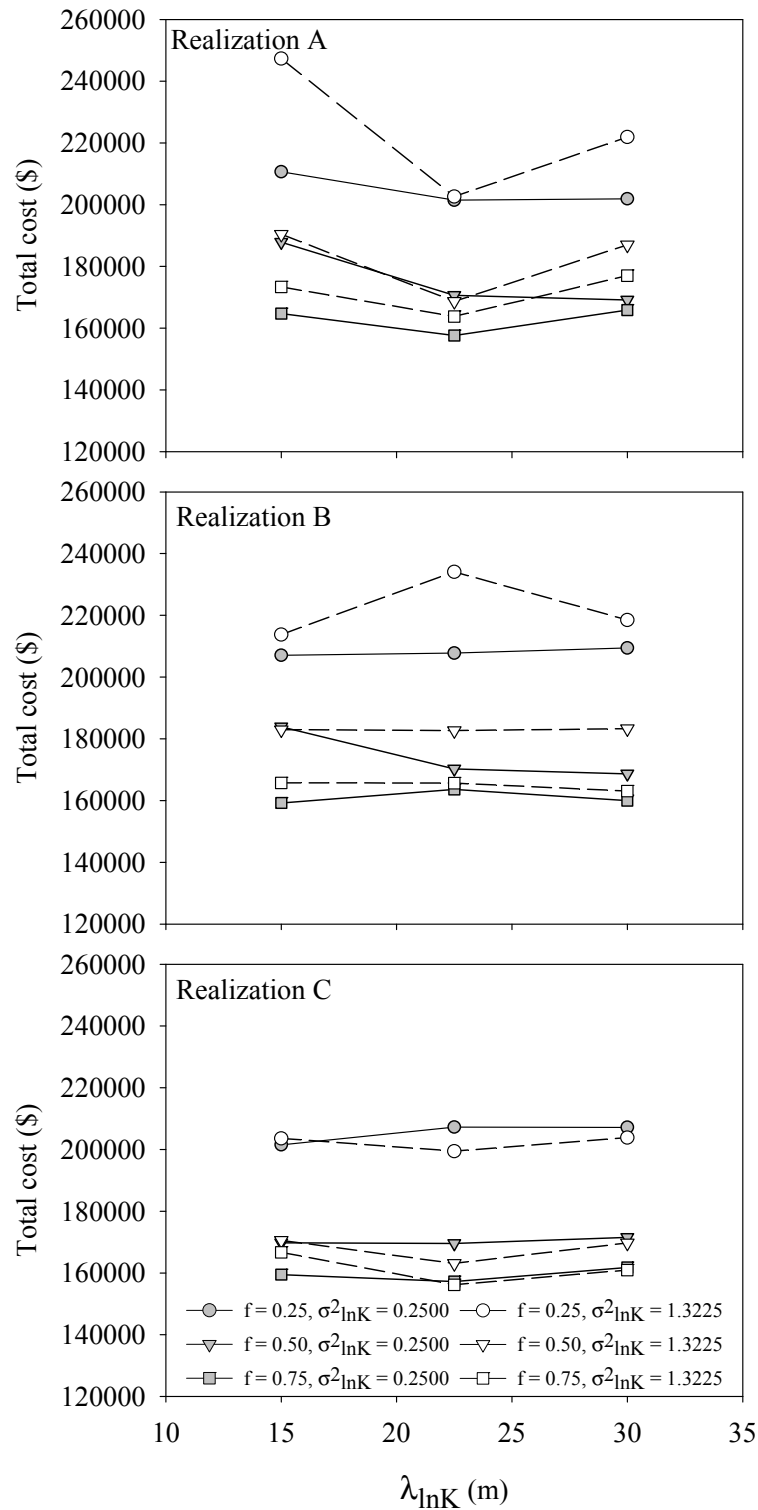


Figure 4.67. Comparison of total remediation costs for the average plume case when $f = 0.25, 0.50$ and 0.75

other words, with a remediation design, which was sufficient to satisfy the total concentration constraint for f value of 0.75, the remediation goal could not be achieved for f values of 0.5 and 0.25. To overcome this problem, either the total pumping rate or the number of active wells and most of the times both need to be increased. This, in turn, results in an increase in the total cost of remediation.

Decrease in f value from 0.75 to 0.25 resulted in 14-30% increase in the unit remediation cost for the original plume case while it caused 9-32% increase for the average plume case. Hence, the increase in the fraction of kinetic sorption sites did not only lead to an increase in the total remediation cost, but also an increase in the unit remediation cost for different plume configurations and initial contaminant masses. This showed the importance of mass transfer limitations.

All these results showed that, selecting the most appropriate f value or determining the sorption characteristics of the contaminant and the subsurface material might be critical for the planning of a P&T remediation system in terms of the prediction of the system design and cost. Mass transfer limitations which are ignored in P&T designs may lead to significant bias in the outcome of remediation.

CHAPTER 5

CONCLUSIONS

5.1. Conclusions

Considering that the heterogeneities in physical and chemical aquifer properties are important factors affecting P&T remediation design and cost, this study evaluated the influence of λ of K, K_d and α on the P&T design and cost for a hypothetical aquifer with different degrees of heterogeneities under rate-limited sorption conditions. Additionally, the study investigated the effect of contaminant mass present in the heterogeneous aquifer and the plume condition on P&T remediation design, cost and management time. In addition, influences of the correlation between different aquifer properties (K and K_d , K_d and α), λ anisotropy of K and the fraction of equilibrium sorption sites (f) on P&T design and cost under different heterogeneity conditions were investigated. For all investigations mentioned above, simulation-optimization approach was used.

First, a sensitivity analysis was made to obtain the best performance of GA (the optimization method used in this study). Different methods of crossover and coding along with different crossover probabilities were tested. The increased GA performance was crucial for P&T system design since even a small percentage of improvement in the result of optimization may lead to significant savings in real life applications. For this study, improved performance of GA in terms of reaching global optimum solutions is important since the analysis is based on comparison of the optimal policies obtained for different heterogeneity conditions. According to

the results, the performance of GA for a certain GA parameter set changes depending on the complexity of the problem, such that solutions of the complex problems are affected more by the GA parameters compared to the relatively simple problems. For the optimal design problem of this study, which was a complex problem, it was shown that uniform crossover and Gray coding exhibited the best performance in terms of reaching the global optimum value compared to the uniform crossover/binary coding, two-point crossover/binary coding and two-point crossover/Gray coding combinations. However, the computational time demanded by uniform crossover was longer compared to two-point crossover regardless of the coding type. On the other hand, for the time-to-compliance model, which was a simpler optimization problem compared to optimal design problem, the distinction between uniform and two-point crossover was insignificant with either binary or Gray coding in terms of reaching the global optimum and the required computational time. Therefore, the use of uniform crossover and Gray coding may be advantageous over two-point crossover and binary coding for complex problems in spite of longer computational time. In conclusion, for complex problems, sensitivity analysis on GA parameters is required to obtain better solutions. However, allocating resources for sensitivity analysis for simple problems may not be that important.

The initial plume generation studies on the heterogeneous K-fields showed that the shape of the head contours and the plume was distorted more with increasing $\sigma_{\ln K}^2$. On the other hand, the effect of $\lambda_{\ln K}$ on head and plume distributions was not as definite as the effect of $\sigma_{\ln K}^2$. A general trend could not be observed with changing $\lambda_{\ln K}$. This study also showed that the effect of $\sigma_{\ln K}^2$ and $\lambda_{\ln K}$ on the shapes and areal extents of the contaminant plumes depended on the K realization, in other words the location of high and low K regions. The areal extents of the contaminant plumes were directly correlated with the total contaminant mass and exhibited similar trends with respect to $\lambda_{\ln K}$. For the same source of continuous contamination in a mass transfer limited and heterogeneous aquifer, the variation

in plume formation, both in terms of mass and area, increased with increasing $\lambda_{\ln K}$. Therefore, the magnitude of $\lambda_{\ln K}$ impacted the transport and mixing of the contaminant together with other heterogeneity parameters. The initial plumes additionally revealed that the total mass and the area of the contaminant plume were in correlation with the K_g of the plume area, not the K_g of the whole aquifer. Therefore, local K values in terms of the distribution of high and low K zones over the aquifer had an important impact on the movement and the distribution of the contaminant plume as well as $\sigma^2_{\ln K}$ and $\lambda_{\ln K}$.

When the impact of K heterogeneity only was considered, it was seen that the respective locations of the high and low K zones and their respective areas defined by $\lambda_{\ln K}$ had a noticeable effect on the active well locations and pumping rates as well as the total remediation costs. The relationships between the total remediation costs and $\lambda_{\ln K}$ did not follow a regular trend for different realizations of the heterogeneous fields. Nevertheless, for the cases that had the same number of active wells, the trends in initial mass of PCE with respect to $\lambda_{\ln K}$ were in close agreement with the trends in total cost of remediation with respect to $\lambda_{\ln K}$. In overall, high $\lambda_{\ln K}$ promoted more variation in the costs. These results were confirmed for the same total initial masses as wells as different masses under different K heterogeneity conditions. In overall, although the amount of PCE mass initially present in the aquifer was important in terms of P&T design and cost, the location and size of the high and low K regions as well as the magnitudes of K were also important. Results obtained on anisotropic K-fields also confirmed that the relative locations and the areas of different K zones mainly affected the P&T remediation design and cost. Therefore, in heterogeneous fields, better definition of the spatial distribution of K can be critical for better remediation design and more accurate prediction of remediation costs.

Heterogeneity in K may also have a significant impact on time-to-compliance depending on P&T design employed. However, this impact is not constant for

different spatial distributions of K . Thus, heterogeneity conditions defined by $\lambda_{\ln K}$ and $\sigma_{\ln K}^2$ and the locations of high and low K zones must be known or predicted by high accuracy for more precise prediction of time-to-compliance. When it is not feasible to completely define the heterogeneity conditions in the aquifer, P&T designs that employ higher numbers of wells pumping at lower rates instead of lower number of wells (i.e. a single well) pumping at higher rates may provide a more robust design in terms of time-to-compliance. Smaller number of pumping wells operating at higher pumping rates magnifies the impact of K heterogeneity. On the other hand, a choice must be made between robustness and costs of P&T designs since the use of higher number of wells may increase the cost of remediation designs.

The results obtained with heterogeneous K_d -fields showed that assuming K_d as homogenous during the design of P&T remediation systems might cause substantial error in both the design and the cost of remediation. The spatial distribution of both K and K_d might change the magnitude of this error since their combinations influence the hardness or easiness of the remediation. Determination of $\lambda_{\ln K}$ and $\lambda_{\ln K_d}$ might also be important as well as $\sigma_{\ln K}^2$ and $\sigma_{\ln K_d}^2$ since designs on the fields with shorter λ appeared to be more risk-free in terms of predicting the remediation costs while the cost of remediation might greatly vary for longer λ . In addition, the correlation between K and K_d can not be disregarded in designing a remediation system, since it may also have significant impact. In this study, a perfect positive or negative correlation between K and K_d was assumed. In real life, it may not be possible to obtain perfect correlations. However, even the moderate correlation between these two parameters may have significant effects on remediation system design and cost since the results of this study indicated the influence of the local parameter values.

The heterogeneity in α may or may not affect the design of P&T remediation system depending on K , K_d and α realizations and heterogeneity conditions ($\lambda_{\ln \alpha}$

and $\sigma^2_{\ln\alpha}$). High K_d heterogeneity can mask the effect of α heterogeneity. The effect of α heterogeneity may show itself as a higher or a lower remediation costs compared to the homogenous α assumption. However, the effect of α heterogeneity was not as significant as the effects of K and K_d heterogeneities. Only single realizations for K and K_d were used in this study and it is probable that for different K and K_d realizations, the effect may change. In general, the effect of negative correlation between α and K_d was also not very significant on remediation cost and design for the conditions considered in this study.

The partition of the sorbed contaminant between equilibrium and kinetic sorption sites is important in fate of the remediation. This is tested by different f values which results in varying amounts of contaminant masses that would desorb slowly. Results showed that increased amount of kinetically sorbed mass resulted in more costly remediation. Therefore, determination of the most appropriate f value by considering the sorption characteristics of the contaminant and the subsurface material may be necessary for the planning of a P&T remediation system.

5.2. Recommendations for the Future Work

This study applied single K_g , Kd_g and α_g values. However, for different values of these parameters, the magnitudes of the variations in remediation costs may be different. In addition, the respective effects of these parameters can change. For example, the reason of not seeing a significant effect of α heterogeneity may be the low $\sigma^2_{\ln\alpha}$ used in this study. Consideration of these parameters in terms of normalized values rather than absolute values may indicate the importance of one parameter over the other in impacting the remediation.

This study accounted for only a single perfect correlation model. The relationship used to correlate K and K_d or other parameter combinations may probably affect the remediation design and cost and this effect may worth to quantify.

The results of this study also supported the idea that the local parameter values and their relative positions to each other are crucial in designing a P&T remediation system for mass transfer limited aquifers. Therefore, better definition of the heterogeneities in the aquifer is essential for better designs. It has been seen that the definition of the heterogeneity by only σ^2 , λ and mean values can introduce bias since in this study the impact of realizations, consequently, the spatial distributions of the local parameters are clearly shown. Thus, more research is needed in determination of this spatial distribution.

Conditioning of parameter fields would reduce the uncertainty in determination of the spatial parameter distribution since it forces the realizations to follow some constraints. This study considered unconditioned K , K_d and α fields but the use of conditioning based on some field measurements may provide more realistic results. The effect of the use of conditioned fields may provide beneficial outcomes for the practical applications. In addition, the effect of the number and the location of conditioning points may be investigated by taking the field characterization cost into account so that the more realistic and stable cost estimate would be obtained with the least cost of field characterization.

REFERENCES

- Abulaban, A., Nieber, J.L., 2000. Modeling the effects of nonlinear equilibrium sorption on the transport of solute plumes in saturated heterogeneous porous media. *Advances in Water Resources* 23 (8), 893-905.
- Air Force Center for Engineering and the Environment (AFCEE), 2007, Groundwater Plume Maps & Information Booklet, Massachusetts Military Reservation, Cape Cod, MA, USA.
- Aksoy, A., 2000. Impact of Kinetic Sorption and Heterogeneities on Aquifer Remediation Design and Costs. PhD Thesis, University of Virginia.
- Aksoy, A., Culver, T.B., 2000. Effect of sorption assumptions on aquifer remediation designs. *Ground Water*, 38 (2), 200-207.
- Aksoy, A., Culver, T.B., 2004. Impact of physical and chemical heterogeneities on aquifer remediation design. *Journal of Water Resources Planning and Management-ASCE* 130 (4), 311-320.
- Allen-King, R.M., Halket, R.M., Gaylord, D.R., Robin, M.J.L., 1998. Characterizing the heterogeneity and correlation of perchloroethene sorption and hydraulic conductivity using a facies-based approach. *Water Resources Research*, 34 (3), 385-396.
- Allen-King, R.M., Divine, D.P., Robin, M.J.L., Alldredge, J.R., Gaylord, D.R., 2006. Spatial distributions of perchloroethylene reactive transport parameters in the Borden Aquifer. *Water Resources Research*, 42 (1), W01413.
- Anderson, M.P., Woessner, W.W., 1992. *Applied Groundwater Modeling: Simulation of Flow and Advective Transport*. Academic Press, San Diego, CA, USA.
- Andersson, C., Destouni, G., 2001. Risk-cost analysis in ground water contaminant transport: the role of random spatial variability and sorption kinetics. *Ground Water*, 39 (1), 35-48.

Andre, J., Siarry, P., Dognon, T., 2001. An improvement of the standard genetic algorithm fighting premature convergence in continuous optimization, *Advances in Engineering Software*, 321, 49-60.

Aral, M.M., Guan, J., 1996. Optimal groundwater remediation design using differential genetic algorithm. *Computational Methods in Water Resources*, 11 (1), 349-357.

Ashlock, D., 2000. *Evolutionary Computation for Modeling and Optimization*. Springer, New York, NY, USA.

Ayvaz, M.T., Karahan, H., 2008. A simulation/optimization model for the identification of unknown groundwater well locations and pumping rates. *Journal of Hydrology* 357 (1-2), 76-92.

Bakr, M.I., te Stroet, C.B.M., Meijerink, A., 2003. Stochastic groundwater quality management: Role of spatial variability and conditioning, *Water Resources Research*, 39 (4), 1078.

Ball, W.P., Roberts, P.V., 1991. Long-term sorption of halogenated organic chemicals by aquifer material. 1. Equilibrium. *Environmental Science and Technology*, 25 (7), 1223-1236.

Barackman, M., Brusseau, M.L., 2004. Groundwater sampling. In *Environmental Monitoring and Characterization*, Eds. Artiola, J.F., Pepper, I.L., Brusseau, M.L., Elsevier Academic Press, pp. 121-139.

Barber, L.B., Thruman, Jr. E.M., Runnells, D.D., 1992. Geochemical heterogeneity in a sand and gravel aquifer: Effect of sediment mineralogy and particle size on the sorption of chlorobenzenes, *Journal of Contaminant Hydrology*, 9 (1-2), 35-54.

Bartow, G., Davenport, C., 1995. Pump-and-treat accomplishments: a review of the effectiveness of ground water remediation in Santa Clara Valley, California, *Ground Water Monitoring and Remediation* 15 (2), 140-146.

Bayer, P., Finkel, M., Teutsch, G., 2004. Combining pump-and-treat and physical barriers for contaminant plume control. *Ground Water* 42 (6), 856-867.

Bellin, A., Rinaldo, A., 1995. Analytical solutions for transport of linearly adsorbing solutes in heterogeneous formations, *Water Resources Research*, 31 (6), 1505-1511.

Berglund, S., 1995. The effect of Langmuir remediation of sorption on pump-and-treat a stratified aquifer. *Journal of Contaminant Hydrology*, 18 (3), 199-220.

- Berglund, S., 1997. Aquifer remediation by pumping: A model for stochastic-advective transport with nonaqueous phase liquid dissolution, *Water Resources Research*, 33 (4), 649-661.
- Berglund, S., Cvetkovic, V., 1995. Pump-and-treat remediation of heterogeneous aquifers: Effects of rate-limited mass transfer. *Ground Water* 33 (4), 675-685
- Bishop, D.J., Rice, D.W., Rogers, L.L., Webster-Scholten, C.P., 1990. Comparison of field-based distribution coefficients (Kds) and retardation factors (Rs) to laboratory and other determinations of Kds, Report No: UCRL-AR-105002, Lawrence Livermore National Laboratory, Livermore, CA, USA.
- Biteman, S.E., 2002. Characterization of Aquifer Heterogeneity and Tracer Test Simulations by Incorporating Geologic Information in the Form of Outcrop Analog and Well Core at a Distal and Medial Outwash Aquifer in Schoolcraft, Michigan. MS Thesis, Michigan State University.
- Bjerg, P.L., Hinsby, K., Christensen, T.H., Gravesen, P., 1992. Spatial variability of hydraulic conductivity of an unconfined sandy aquifer determined by a mini slug test. *Journal of Hydrology*, 136 (1-4), 107-122.
- Boggs, J.M., Rehfeldt, K.R., 1990. Field study of macrodispersion in a heterogeneous aquifer. 2. Observations of hydraulic conductivity variability. Proceedings of the International Conference and Workshop on Transport and Mass Exchange Processes in Sand and Gravel Aquifers Part 1, Oct 1-4 1990, Ottawa, Ontario, Canada.
- Boggs, M.J., Young, S.C., Bontoon, D.J., Shung, Y.C., 1990. Hydrogeologic Characterization of the MADE Site. Report No: EN-6915, Electric Power Research Institute, Palo Alto, CA, USA.
- Bosma, W.J.P., Bellin, A., Van Der Zee, S.A.T.M., Rinaldo, A., 1993. Linear equilibrium adsorbing solute transport in physically and chemically heterogeneous porous formations 2. Numerical Results. *Water Resources Research*, 29 (12), 4031-4043.
- Brogan, S.D., Gailey, R.M., 1995. A method for estimating field-scale mass transfer rate parameters and assessing aquifer cleanup times, *Ground Water*, 33 (6), 997-1009.
- Brusseau, M.L., 1992a. Rate-limited mass transfer and transport of organic solutes in porous media that contain immobile immiscible organic liquid. *Water Resources Research*, 28 (1), 33-45.
- Brusseau, M.L., 1992b. Nonequilibrium transport of organic chemicals: The impact of pore-water velocity. *Journal of Contaminant Hydrology*, 9 (4), 353-368.

Brusseau, M.L., 1992c. Transport of rate-limited sorbing solutes in heterogeneous porous-media - application of a one-dimensional multifactor nonideality model to field data. *Water Resources Research*, 28 (9), 2485-2497.

Brusseau, M.L., Rao, P.S.C., 1989a. Sorption nonideality during organic contaminant transport in porous-media. *CRC Critical Reviews in Environmental Control*, 19 (1), 33-99.

Brusseau, M.L., Rao, P.S.C., 1989b. Influence of sorbate organic matter interactions on sorption nonequilibrium. *Chemosphere*, 18 (9-10), 1691-1706.

Brusseau, M.L., Rao, P.S.C., 1991. Influence of sorbate structure on nonequilibrium sorption of organic compounds. *Environmental Science and Technology*, 25 (8), 1501-1508.

Brusseau, M.L., Reid, M.E., 1991. Nonequilibrium sorption of organic-chemicals by low organic-carbon aquifer materials. *Chemosphere*, 22 (3-4), 341-350.

Brusseau, M.L., Srivastava, R., 1997. Nonideal transport of reactive solutes in heterogeneous porous media 2. Quantitative analysis of the Borden natural-gradient field experiment. *Journal of Contaminant Hydrology*, 28 (1-2), 115-155.

Brusseau, M.L., Srivastava, R., 1999. Nonideal transport of reactive solutes in heterogeneous porous media 4. Analysis of the Cape Cod natural-gradient field experiment. *Water Resources Research*, 35 (4), 1113-1125.

Brusseau, M.L., Jessup, R.E., Rao, P.S.C., 1989. Modeling the transport of solutes influenced by multiprocess nonequilibrium. *Water Resources Research*, 25 (9), 1971-1988.

Brusseau, M.L., Jessup, R.E., Rao, P.S.C., 1990. Sorption kinetics of organic chemicals: Evaluation of gas-purge and miscible-displacement techniques. *Environmental Science and Technology*, 24 (5), 727-735.

Brusseau, M.L., Larsen, T., Christensen, T.H., 1991a. Rate-limited sorption and nonequilibrium transport of organic chemicals in low organic carbon aquifer materials. *Water Resources Research* 27 (6), 1137-1145.

Brusseau, M.L., Jessup, R.E., Rao, P.S.C., 1991b. Nonequilibrium sorption of organic chemicals: Elucidation of rate-limiting processes. *Environmental Science and Technology*, 25 (1), 134-142.

Burr, D.T., Sudicky, E.A., Naff, R.L., 1994. Nonreactive and reactive solute transport in three-dimensional heterogeneous porous-media - mean displacement, plume spreading, and uncertainty. *Water Resources Research*, 30 (3), 791-815.

Byers, E., Stephens, D.B., 1983. Statistical and stochastic analyses of hydraulic conductivity and particle-size in a fluvial sand. *Soil Science Society America Journal*, 47, 1072-1081.

Cameron, D.R., Klute, A., 1977. Convective-dispersive solute transport with a combined equilibrium and kinetic adsorption model. *Water Resources Research*, 13 (1), 183-188.

Campbell, J.E., Longsine, D.E., Reeves, M., 1981. Distributed velocity method of solving the convective-dispersion equation: 1. Introduction, mathematical theory, and numerical implementation. *Advances in Water Resources*, 4, 102-108.

Chakraborty, U.K., Janikow, C.Z., 2003. An analysis of Gray versus binary encoding in genetic search. *Information Sciences: an International Journal*, 156 (3-4), 253-269.

Chan Hilton, A. B., Culver, T. B., 2000. Constraint handling for genetic algorithms in optimal remediation design. *Journal Water Resources Planning Management-ASCE*, 126 (3), 128-137.

Chan Hilton, A.B., Culver, T.B., 2005. Groundwater remediation design under uncertainty using genetic algorithms. *Journal of Water Resources Planning and Management-ASCE*, 131 (1), 25-34.

Chang, L.C., Hsiao, C.T., 2002. Dynamic optimal ground water remediation including fixed and operation costs. *Ground Water*, 40 (5), 481-490.

Chipperfield, A., 1997. Introduction to genetic algorithms. In *Genetic Algorithms in Engineering Systems*. IEE Control Engineering Series 55, Eds. Zalzala, A.M.S., Fleming, P.J., Institution of Electrical Engineers, pp. 1-45.

Coats, K.H., Smith, B.D., 1964. Dead-end pore volume and dispersion in porous media. *Society of Petroleum Engineers Journal*, 4, 73-81.

Connaughton, D.F., Stedinger, J.R., Lion, L.W., Shuler, M.L., 1993. Description of time-varying desorption kinetics: release of naphthalene from contaminated soils, *Environmental Science and Technology*, 27 (12), 2397-2403.

Culver, T.B., Earles, T.A., Gray, J.P., 1996. Numerical Modeling of In Situ Bioremediation with Sorption Kinetics. Report No: DAAL03-91-C-0034; TCN95-066. U.S. Army Research Office, Research Triangle Park, NC, USA.

Culver, T.B., Hallisey, S.P., Sahoo, D., Deitsch, J.J., Smith, J.A., 1997. Modeling the desorption of organic contaminants from long-term contaminated soil using

distributed mass transfer rates. *Environmental Science and Technology*, 31 (6), 1581-1588.

Culver, T. B., Shenk, G. W., 1998. Dynamic optimal ground water remediation by granular activated carbon. *Journal of Water Resources Planning and Management-ASCE*, 124 (1), 59-64.

Cunha, M.D., 2002. Groundwater cleanup: The optimization perspective (A literature review), *Engineering Optimization*, 34 (6), 689-702.

Cushey, M.A., Rubin, Y., 1997. Field scale transport of nonpolar organic solutes in 3-D heterogeneous aquifers. *Environmental Science and Technology*, 31 (5), 1259-1268.

Cvetkovic, V., Dagan, G., Cheng, H., 1998. Contaminant transport in aquifers with spatially variable hydraulic and sorption properties, *Proceedings of the Royal Society of London A*, 454 (1976), 2173-2207.

Cvetkovic, V., Shapiro, A.M., 1990. Mass arrival of sorptive solute in heterogeneous porous media. *Water Resources Research*, 26 (9), 2057-2067.

Deitsch, J.J., Smith, J.A., 1995. Effect of Triton X-100 on the rate of trichloroethene desorption from soil to water, *Environmental Science and Technology*, 29, 1069-1080.

De Jong, K.A., Spears, W.M., 1992. A formal analysis of the role of multi-point crossover in genetic algorithms, *Annals of Mathematics and Artificial Intelligence*, 5 (1), 1-26.

Dekker, T.J., Abriola, L.M., 2000. The influence of field-scale heterogeneity on the infiltration and entrapment of dense nonaqueous phase liquids in saturated formations. *Journal of Contaminant Hydrology*, 42 (2-4), 187-218.

Destouni, G., Cvetkovic, V., 1991. Field scale mass arrival of sorptive solute into the groundwater, *Water Resources Research*, 27 (6), 1315-1325.

Domenico, P.A., Schwartz, F.W., 1990. *Physical and chemical hydrogeology*, Wiley, New York, NY, USA.

Dumitrescu, D., Lazzerini, B., Jain, L.C., Dumitrescu, A., 2000. *International Series of Computational Intelligence, Evolutionary Computation*. CRC Press, Boca Raton, FL, USA.

Dynamac Corporation, 1998. *Characterization of Hydraulic Properties of Potentially Fractured Industrial D Landfill Sites, and A Study of Heterogeneity*

Effects on Fate and Transport in Groundwater, U.S. Environmental Protection Agency, National Risk Management Research Laboratory, Subsurface Protection and Remediation Division, Ada, OK.

Earles, T.A., 1996. Modeling the Effects of Rate Limited Mass Transfer on In-situ Bioremediation. MS Thesis, University of Virginia.

Eastern Research Group, Inc., 1996. Pump-and-treat ground-water remediation: A guide for decision makers and practitioners, Report No: EPA/625/R-95/005, USEPA Center for Environmental Research Information, Cincinnati, OH, USA.

European Environment Agency (EEA), 2009. Progress in management of contaminated sites (CSI 015) - Assessment published Aug 2007, http://themes.eea.europa.eu/IMS/IMS/ISpecs/ISpecification20041007131746/IAssessment1152619898983/view_content, Last accessed March, 2009.

Eggleston, J.R., 1997. Groundwater Flow and Transport in Heterogeneous Aquifers Modeling Spatial Variability Under Limiting Data Conditions. PhD Thesis, Duke University.

Eggleston, J.R., Rojstaczer, S.A., Peirce, J.J., 1996. Identification of hydraulic conductivity structure in sand and gravel aquifers: Cape Cod data set, Water Resources Research, 32 (5), 1209-1222.

Elder, C.R., Benson, C.H., Eykholt, G.R., 2002. Effects of heterogeneity on influent and effluent concentrations from horizontal permeable reactive barriers, Water Resources Research, 38 (8), (27-1)-(27-19).

ENVISAN, 2009. Reference list site remediation, <http://www.envisan.be/index2.html>, Last accessed March, 2009.

Eshelman, L.J., Caruana, R., Schaffer, J.D., 1989. Biases in the crossover landscape. Proceedings of the 3rd International Conference on Genetic Algorithms, pp. 10-19.

Espinoza, F.P., Minsker, B.S., Goldberg, D.E., 2005. Adaptive hybrid genetic algorithm for groundwater remediation design. Journal of Water Resources Planning and Management-ASCE, 131 (1), 14-24.

European Commission, 2005. European Union Risk Assessment Report, Tetrachloroethylene, Part I – Environment, Series: 1st Priority List, Volume: 57, EUR 21680 EN, Eds. Munn, S.J., Allanou, R., Aschberger, K., Berthault, F., Cosgrove, O., Luotamo, M., O'Connor, S., Pakalin, S., Paya-Perez, A., Pellegrini, G., Scheer, S., Schwarz-Schulz, B., Vegro, S., European Commission – Joint

Research Centre, Institute for Health and Consumer Protection European Chemicals Bureau (ECB), p. 38.

Faust, S.D., Aly, O.M., 1987. Adsorption Processes for Water Treatment, Butterworth Publishers, Stoneham, MA, USA.

Fenton, G.A., 1990. Simulation and Analysis of Random Fields, PhD Thesis, Princeton University.

Foster-Reid, G.C., 1994. Variability of Hydraulic Conductivity and Sorption in a Heterogeneous Aquifer. MS Thesis, Massachusetts Institute of Technology.

Freeze, R.A., Cherry, J.A., 1979. Groundwater. Prentice-Hall, Inc., Englewood Cliffs, NJ, USA.

Federal Remediation Technologies Roundtable (FRTR), 2009. Optimization case studies at Federal Remediation Technologies Roundtable (FRTR) member sites, <http://www.frtr.gov/optimization/default.htm>, Last accessed March 2009.

Garabedian, S.P. 1987. Large-scale Dispersive Transport in Aquifers: Field Experiments and Reactive Transport Theory. PhD Thesis, Massachusetts Institute of Technology.

Gelhar, L.W., 1993. Stochastic Subsurface Hydrology, Prentice-Hall Inc., NJ, USA.

Goldberg, D.E., 1989. Genetic Algorithms in Search, Optimization, and Machine Learning. Addison-Wesley, Reading, MA, USA.

Gorelick, S.M., Voss, C.I., Gill, P.E., Murray, W., Saunders, M.A., Wright, M.H., 1984. Aquifer reclamation design: the use of contaminant transport simulation combined with nonlinear programming. Water Resources Research, 20 (4), 415-427.

Guan, J., Aral, M.M., 1999. Optimal remediation with well locations and pumping rates selected as continuous decision variables. Journal of Hydrology, 221 (1-2), 20-42.

Haggerty, R., Gorelick, S.M., 1994. Design of multiple contaminant remediation: Sensitivity to rate-limited mass transfer. Water Resources Research, 30 (2), 435-446.

Harmon, T.C., Roberts, P.V., 1994. Comparison of intraparticle sorption and desorption rates for a halogenated alkene in a sandy aquifer material. Environmental Science and Technology, 28 (9), 1650-1660.

Harter, T., 1994. Unconditional and Conditional Simulation of Flow and Transport in Heterogeneous, Variably Saturated Porous Media, PhD Thesis, University of Arizona.

Harvey, C.F., Haggerty, R., Gorelick S.M., 1994. Aquifer remediation: A method for estimating mass transfer rate coefficients and an evaluation of pulsed pumping. *Water Resources Research*, 30 (7), 1979-1991.

Haupt, R.L., Haupt, S.E., 1998. *Practical Genetic Algorithms*. Wiley, New York, NY, USA.

Hemsi, P.S., Shackelford, C.D., 2006. An evaluation of the influence of aquifer heterogeneity on permeable reactive barrier design. *Water Resources Research*, 42 (3), W03402.

Hess, K.M., Wolf, S.H., Celia, M.A., 1992. Large scale natural gradient tracer test in sand and gravel, Cape Cod, Massachusetts: 3. Hydraulic conductivity and calculated macrodispersivities. *Water Resources Research*, 28 (8), 2011-2027.

Hess, K.M., Davis, J.A., Fuller, C.C., Coston, J.A., 1993. Spatial variability of metal-ion adsorption and hydraulic conductivity in a sand and gravel aquifer, Cape Cod, Massachusetts. U.S. Geological Survey Toxic Substances Hydrology Program-Proceedings of the Technical Meeting, Water-Resources Investigations Report 94-4015, September 20-24, 1993, Colorado Springs, Colorado, pp. 235-242.

Hess, K.M., Davis, J.A., Kent, D.B., Coston, J.A., 2002. Multispecies reactive tracer test in an aquifer with spatially variable chemical conditions, Cape Cod, Massachusetts: Dispersive transport of bromide and nickel. *Water Resources Research*, 38(8), 1161.

Hoffman, F., 1993. Ground-water remediation using smart pump and treat. *Ground Water*, 31 (1), 98-106.

Hoffman, F., 1995. Retardation of volatile organic compounds in ground water in low organic carbon sediments. Interim Report No: UCRL-ID-120471, Lawrence Livermore National Laboratory, Livermore, CA, USA.

Holland, J.H., 1975. *Adaptation in Natural and Artificial Systems: An Introductory Analysis with Applications to Biology, Control, and Artificial Intelligence*. University of Michigan Press, Ann Arbor, MI, USA.

Hollenbeck, K.J., Harvey, C.F., Haggerty, R., Werth, C.J., 1999. A method for estimating distributions of mass transfer rate coefficients with application to

purging and batch experiments *Journal of Contaminant Hydrology* 37 (3-4): 367-388.

Hopgood, A.A., 2001. *Intelligent Systems for Engineers and Scientists*, 2nd Ed., CRC Press, USA.

Hsiao, C.T., Chang, L.C., 2002. Dynamic optimal groundwater management with inclusion of fixed costs. *Journal of Water Resources Planning and Management-ASCE*, 128 (1), 57-65.

Hu, Q., Wang, X., Brusseau, M.L., 1995a. Quantitative structure-activity relationships for evaluating the influence of sorbate structure on sorption of organic compounds by soil. *Environmental Toxicology and Chemistry*, 14(7), 1133-1140.

Hu, B.X., Deng, F.W., Cushman, J.H., 1995b. Nonlocal reactive transport with physical and chemical heterogeneity - linear nonequilibrium sorption with random K_d . *Water Resources Research*, 31 (9), 2239-2252.

Hu, B.X., Wu, J., Zhang, D., 2004. A numerical method of moments for solute transport in physically and chemically nonstationary formations: linear equilibrium sorption with random K_d . *Stochastic Environmental Research and Risk Assessment*, 18 (1), 22-30.

Huang, C.L., Mayer, A.S., 1997. Pump-and-treat optimization using well locations and pumping rates as decision variables. *Water Resources Research*, 33 (5), 1001-1012.

Huyakorn, P.S., Pinder, G.F., 1983. *Computational Methods in Subsurface Flow*. Academic Press, San Diego, CA, USA.

Hyndman, D.W., Dybas, M.J., Wiggert, D., Zhao, X., Wallace, R., Voice, T., Chan, A., Phanikumar, M.S., Criddle, C.S., 2000. Hydraulic characterization and design of a full-scale biocurtain. *Ground Water*, 38 (3), 462-474.

Hyman, M., Dupont, R.R., 2001. *Groundwater and Soil Remediation: Process Design and Cost Estimating of Proven Technologies*, American Society of Civil Engineers Press, Reston, VA, USA.

Indelman, P., Moltyaner, G., Dagan, G., 1999. Determining the hydraulic conductivity spatial structure at the Twin Lake site by grain-size distribution, *Ground Water*, 37 (2), 223-227.

James, B.R., Gorelick S.M., 1994. When enough is enough: The worth of monitoring data in aquifer remediation design. *Water Resources Research*, 30 (12), 3499-3513.

Kinzelbach, W., 1986. *Groundwater Modelling: An Introduction with Sample Programs in BASIC*. Elsevier Science Publishing, New York, NY, USA.

Kitanidis, P.K., 1997. *Introduction to Geostatistics*. Cambridge University Press, New York, NY, USA.

Ko, N.Y., Lee, K.K., Hyun, Y., 2005. Optimal groundwater remediation design of a pump and treat system considering clean-up time, *Geosciences Journal*, 9 (1), 23-31.

Koller, D., Imbrigiotta, T.E., Baehr, A.L., Smith, J.A., 1996. Desorption of trichloroethylene from aquifer sediments at Picatinny Arsenal, New Jersey. U.S. Geological Survey Toxics Substances Hydrology Programs-Proceedings of the Technical Meeting, Water-Resources Investigations Report 94-4015, September 20- 24, 1993, Colorado Springs, Colorado, pp. 329-338.

Lee, M.K., Saunders, J.A., Wolf, L.W., 2000. Effects of geologic heterogeneities on pump-and-treat and in situ bioremediation: A stochastic analysis. *Environmental Engineering Science*, 17 (3), 183-189.

Levine, D., 1996. Users Guide to the PGAPack Parallel Genetic Algorithm Library. ANL-951/18, Mathematics and Computer Science Division at Argonne National Laboratory.

Li, Z., Brusseau, M.L., 2000. Nonideal transport of reactive solutes in heterogeneous porous media 6. Microscopic and macroscopic approaches for incorporating heterogeneous rate-limited mass transfer. *Water Resources Research*, 36 (10), 2853-2867.

Liu, K.H., Enfield, C.G., Mravik, S.C., 1991. Evaluation of sorption models in the simulation of naphthalene transport through saturated soils. *Ground Water*, 29 (5), 685-692.

Liu, W.H., Medina, M.A., Thomann, W., Piver, W.T., Jacobs, T.L., 2000. Optimization of intermittent pumping schedules for aquifer remediation using a genetic algorithm. *Journal of the American Water Resources Association*, 36 (6), 1335-1348.

MacIntyre, W.G., Stauffer, T.B., Antworth, C.P., 1991. A comparison of sorption coefficients determined by batch, column and box methods on a low organic carbon aquifer material. *Ground Water*, 29 (6), 908-913.

- MacIntyre, W.G., Antworth, C.P., Stauffer, T.B., Young, R.G., 1998. Heterogeneity of sorption and transport-related properties in a sand-gravel aquifer at Columbus, Mississippi, *Journal of Contaminant Hydrology*, 31 (3), 257-274.
- Mackay, D.M. 1998. Is cleanup of VOC-contaminated groundwater feasible? In *Contaminated Land and Groundwater: Future Directions*. Eds. Lerner, D.N., Walton, N.R.G., Geological Society, London, Engineering Geology Special Publications, 14, pp. 3-11.
- Mackay, D.M., Cherry, J.A. 1989. Groundwater contamination: Pump-and-treat remediation. *Environmental Science and Technology*, 23 (6), 630-636.
- Mackay, D.M., Ball, W.P., Durant, M.G., 1986. Variability of aquifer sorption properties in a field experiment on groundwater transport of organic solutes: Methods and preliminary results. *Journal of Contaminant Hydrology*, 1 (1-2), 119-132.
- Mantoglou, A., Wilson, J.L., 1982. The turning bands method for simulation of random fields using line generation by a spectral method, *Water Resources Research*, 18 (5), 1379-1394.
- Maraqa, M.A., 2001. Prediction of mass-transfer coefficient for solute transport in porous media. *Journal of Contaminant Hydrology*, 50 (1-2), 1-19.
- Marquis, S.A., Dineen, D., 1994. Comparison between pump and treat, bioremediation, and bioremediation pump and treat combined - lessons from computer modeling ground water monitoring and remediation. *Groundwater Monitoring Review*, 14 (2), 105-119.
- Maskey, S., Jonoski, A., Solomatine, D.P., 2002. Groundwater remediation strategy using global optimization algorithms, *Journal of Water Resources Planning and Management-ASCE*, 128 (6) 431-440.
- Matheron, G., 1973. The intrinsic random functions and their applications, *Advanced Applied Probability*, 5 (3), 439-468.
- Mathias, K.E., Whitley, L.D., 1994. Transforming the search space with Gray coding. *Proceedings of the 1st IEEE International Conference on Evolutionary Computation*, pp. 513-518.
- Maxwell, R.M., Carle, S.F., Tompson, A.F.B., 2008. Contamination, risk, and heterogeneity: on the effectiveness of aquifer remediation. *Environmental Geology*, 54 (8), 1771-1786.

- Mayer, A.S., Kelley, C.T., Miller, C.T., 2002. Optimal design for problems involving flow and transport phenomena in saturated subsurface systems. *Advances in Water Resources*, 25 (8-12), 1233-1256.
- McKinney, D.C., Lin, M.D., 1994. Genetic algorithm solution of groundwater management models. *Water Resources Research*, 30 (6), 1897-1906.
- McKinney, D.C., Lin, M.D., 1996. Pump-and-treat ground-water remediation system optimization. *Journal of Water Resources Planning and Management-ASCE*, 122 (2), 128-136.
- Mishra, A.K., Gutjahr, A., 1999. Transverse dispersion of a kinetically sorbing solute. *Mathematical Geology*, 31 (7), 771-791.
- Mishra, A.K., Gutjahr, A., Rajaram, H., 1999. Transport with spatially variable kinetic sorption: recursion formulation. *Advances in Water Resources*, 22 (5), 549-555.
- Mitchell, M., 1996. *An Introduction to Genetic Algorithms*. The MIT Press, Cambridge, MA, USA.
- Morgan, D.R., Eheart, J.W., Valocchi, A.J., 1993. Aquifer remediation design under uncertainty using a new chance constrained programming technique. *Water Resources Research*, 29 (3), 551-561.
- Mylopoulos, Y.A., Theodosiou, N., Mylopoulos, N.A., 1999. A stochastic optimization approach in the design of an aquifer remediation under hydrogeologic uncertainty. *Water Resources Management*, 13 (5), 335-351.
- NATO/CCMS-Turkey, 2006. Tour de Table: The situation of contaminated sites in Turkey. Country presentation at the NATO/CCMS Pilot Study workshop Prevention and Remediation In Selected Industrial Sectors: Small Sites in Urban Areas, 4-7 June 2006, Athens, Greece, organised by the North Atlantic Treaty Organization Committee on the Challenges of Modern Society, <http://clu-in.org/athens/default.cfm>, Last accessed March, 2009.
- Nkedi-Kizza, P., Biggar, J.W., Selim, H.M., van Genuchten, M.T.H., Wierenga, P.J., Davidson, J.M., Nielsen, D.R., 1984. On the equivalence of two conceptual models for describing ion exchange during transport an aggregated oxisol. *Water Resources Research*, 20 (8), 1123-1130.
- Nkedi-Kizza, P., Brusseau, M.L., Rao, P.S.C., Hornsby, A.G., 1989. Nonequilibrium sorption during displacement of hydrophobic organic chemicals and calcium-45 through soil columns with aqueous and mixed solvents. *Environmental Science and Technology*, 23 (7), 814-820.

Painter, S., Cvetkovic, V., Turner, D., 2001. Effect of heterogeneity on radionuclide transport in the alluvial aquifer near Yucca Mnt., Nevada. *Ground Water*, 39 (3), 326-338.

Pang, L., Close, M., 1999. A field study of nonequilibrium and facilitated transport of Cd in an alluvial gravel aquifer, *Ground Water*, 37 (5) 785-792.

Pfleiderer, S., Moltyaner, G.L., 1993. The use of velocity and conductivity data for the quantification of heterogeneity: A comparison. *Water Resources Research*, 29 (12), 4151-4156.

Piatt, J.J., 1997. Sorption and Biodegradation of Organic Solutes Undergoing Transport in Laboratory-scale and Field-scale Heterogeneous Porous Media. PhD Thesis, University of Arizona.

Piatt, J.J., Backhus, D.A., Capel, P.D., Eisenreich, S.J., 1996. Temperature dependent sorption of naphthalene, phenanthrene, and pyrene to low organic carbon aquifer sediments. *Environmental Science and Technology*, 30 (3), 751-760.

Pickens, J.F., Jackson, R.E., Inch, K.J., 1981. Measurement of distribution coefficients using a radial injection dual-tracer test. *Water Resources Research*, 17 (3), 529-544.

Pignatello, J.J., Xing, B., 1996. Mechanisms of slow sorption of organic chemicals to natural particles, *Environmental Science and Technology*, 30 (1), 1-11.

Pinder, G.F., Dougherty, D.E., Greenwald, R.M., Karatzas, G.P., Kitanidis, P.K., Loaiciga, H.A., Maxwell, R.M., Mayer, A.S., McLaughlin, D.B., Peralta, R.C., Rizzo, D.M., Wagner, B.J., Yager, K.M., and Yeh, W. W-G., 2004. Optimization and modeling for remediation and monitoring. In *Contaminated Ground Water and Sediment: Modeling for Management and Remediation*, Eds. Chien, C.C., Medina M.A., Pinder G.F., Reible D.D., Sleep B.E., Zheng C., CRC Press LLC, pp. 107-178.

Piwoni M.D., Keeley J.W., 1990. Basic concepts of contaminant sorption at hazardous waste sites. United States Environmental Protection Agency Groundwater Issue Report, Report No: EPA/540/4-90/053, USEPA Superfund Technology Support Center for Ground Water, Robert S. Kerr Environmental Research Laboratory, Ada, OK.

Ptacek, C.J., Gillham, R.W., 1992. Laboratory and field measurements of non-equilibrium transport in the Borden aquifer, Ontario, Canada. *Journal of Contaminant Hydrology*, 10 (2), 119-158.

Ptak, T., Teutsch, G., 1994. Forced and natural gradient tests in a highly heterogeneous porous aquifer: instrumentation and measurements. *Journal of Hydrology*, 159 (1-4), 79-104.

Rabideau, A.J., Miller, C.T., 1994. Two dimensional modeling of aquifer remediation influenced by sorption nonequilibrium and hydraulic conductivity heterogeneity. *Water Resources Research*, 30 (5), 1457-1470.

Reeves, C.R., Rowe, J.E., 2003. *Genetic algorithms: Principles and Perspectives, A Guide to GA Theory*. Kluwer Academic Publishers, London, England.

Rehfeldt, K.R., Boggs, J.M., Gelhar, L.W., 1992. Field study of dispersion in a heterogeneous aquifer: 3. Geostatistical analysis of hydraulic conductivity. *Water Resources Research* 28 (12), 3309-3324.

Ricciardi, K.L., Pinder, G.F., Karatzas, G.P., 2007. Efficient groundwater remediation system design subject to uncertainty using robust optimization. *Journal of Water Resources Planning and Management-ASCE*, 133 (3), 253-263.

Roberts, P.V., Goltz, M.N., Mackay, D.M., 1986. A natural gradient experiment on solute transport in a sand aquifer 3. Retardation estimates and mass balances for organic solutes. *Water Resources Research*, 22 (13), 2047-2058.

Robin, M.J.L., Sudicky, E.A., Gilham, R.W., Kachanoski, R.G., 1991. Spatial variability of strontium distribution coefficients and their correlation with hydraulic conductivity in the Canadian Forces Borden Aquifer. *Water Resources Research* 27 (10), 2619-2632.

Rogers, L.L., Dowla, F.U., 1994. Optimization of groundwater remediation using artificial neural networks with parallel solute transport modeling. *Water Resources Research*, 30 (2), 457-481.

Rowe, J., Whitley, D., Barbulescu, L., Watson, J.P., 2004. Properties of Gray and Binary representations, *Evolutionary Computation* 12 (1), 47-76.

Russell, K.T., Rabideau, A.J., 2000. Decision analysis for pump and treat design. *Ground Water Monitoring and Remediation*, 20 (3), 159-168.

Sahoo, D., 1997. Effect of Triton X-100 and pH on the Rate of Desorption of Trichloroethylene (TCE) from Aquifer Material: Laboratory and Field Studies. PhD Thesis, University of Virginia.

Schäfer, W., Kinzelbach, W., 1992. Stochastic modeling of in situ bioremediation in heterogeneous aquifers. *Journal of Contaminant Hydrology*, 10, 47-73.

Schneider, S.H., 1996, Encyclopedia of Climate and Weather, Vol. 2, Water Resources, Oxford University Press, New York, NY, USA.

Selim, H.W., Davidson, J.N., Mansell, R.S., 1976. Evaluation of a two-site adsorption-desorption model for describing solute transport in soils, Proceedings Summer Computer Simulation Conference, Washington D.C. pp. 444-448.

Sharma, S.K., Irwin, G.W., 2003. Fuzzy Coding of Genetic Algorithms. IEEE Transactions on Evolutionary Computation, 7 (4), 344-355.

Simon, F.G., Meggyes, T., Tünnermeier, T., 2002. Groundwater remediation using active and passive processes. In Advanced Groundwater Remediation: Active and Passive Technologies, Eds. Simon, F.G., Meggyes, T., McDonald, C., Thomas Telford, London, pp. 3-34.

Sinha, E., Minsker, B.S., 2007. Multiscale island injection genetic algorithms for groundwater remediation. Advances in Water Resources, 30 (9), 1933-1942.

Storck, P., Eheart, J.W., Valocchi, A.J., 1997. A method for the optimal location of monitoring wells for detection of groundwater contamination in three-dimensional heterogeneous aquifers. Water Resources Research, 33 (9), 2081-2088.

Sudicky, E.A., 1986. A natural gradient experiment on solute transport in a sand aquifer: spatial variability of hydraulic conductivity and its role in the dispersion process. Water Resources Research, 22 (13), 2069-2082.

Tompson, A.F.B., 1990. Flow and transport within the saturated zone beneath Lawrence Livermore National Laboratory: Modeling considerations for heterogeneous media, Report No: UCID-21828, Lawrence Livermore National Lab, Livermore, CA, USA.

Tompson, A.F.B., 1993. Numerical simulation of chemical migration in physically and chemically heterogeneous porous media. Water Resources Research, 29 (11), 3709-3726.

Tompson, A.F.B., Ababou, R., Gelhar, L.W., 1989. Implementation of the three-dimensional turning bands random field generator. Water Resources Research 25 (10), 2227-2243.

Tompson, A.F.B., Falgout, R.D., Smith, S.G., Bosl, W.J., Ashby, S.F., 1998. Analysis of subsurface contaminant migration and remediation using high performance computing. Advances in Water Resources, 22 (3), 203-221.

Travis, C.C., Doty, C.B., 1990. Can contaminated aquifers at superfund sites be remediated? Environmental Science and Technology, 24 (10), 1464-1466.

Turcke, M.A., Kueper, B.H., 1996. Geostatistical analysis of the Borden aquifer hydraulic conductivity field. *Journal of Hydrology*, 178 (1-4), 223-240.

TSI, 2009. Official web site of Turkish Statistical Institute, Environment Statistics. <http://www.turkstat.gov.tr>, Last accessed March, 2009.

Uçankuş, T., Ünlü, K., 2008. The effect of aquifer heterogeneity on natural attenuation rate of BTEX. *Environmental Geology*, 54 (4), 759-776.

U.S. Environmental Protection Agency (USEPA), 1999. Groundwater Cleanup: Overview of Operating Experience at 28 Sites, Report No: EPA-542-R-99-006, Solid Waste and Emergency Response.

USEPA, 2001. Cost Analyses for Selected Groundwater Cleanup Projects: Pump and Treat Systems and Permeable Reactive Barriers, Report No: EPA-542-R-00-013, Solid Waste and Emergency Response.

USEPA, 2004. Treatment Technologies for Site Cleanup: Annual Status Report (Eleventh Edition), Report No: EPA-542-R-03-009, Solid Waste and Emergency Response.

USEPA, 2005(a). Streamlined Remediation System Evaluation (RSE-Lite) for a Ground Water Pump and Treat System, Engelhard Corporation Facility, Plainville, Massachusetts, Report No: EPA 542-R-05-026, Office of Solid Waste and Emergency Response.

USEPA, 2005(b). Streamlined Remediation System Evaluation (RSE-Lite) for a Ground Water Pump and Treat System, the Eaton Corporation Facility Kearney, Nebraska, Report No: EPA 542-R-05-024, Office of Solid Waste and Emergency Response.

USEPA, 2005(c). Streamlined Remediation System Evaluation (RSE-Lite) for a Ground Water Pump and Treat System, Chemko Technical Services, Inc. Facility, Mims, Florida, Report No: EPA 542-R-05-018, Office of Solid Waste and Emergency Response.

USEPA, 2007. Treatment Technologies for site cleanup: Annual Status Report (Twelfth Edition), Report No: EPA-542-R-07-012, Solid Waste and Emergency Response.

USEPA, 2009a. Archived News Articles and Superfund Success Stories, National Priorities List (NPL) Proposed and Final Rules, <http://www.epa.gov/superfund/accomp/>, Last accessed March, 2009.

USEPA, 2009b. Annual Status Report Remediation Database-2003 Update, <http://cfpub.epa.gov/asr/>, Last accessed March, 2009.

Valocchi, A.J., 1985. Validity of the local equilibrium assumption for modeling sorbing solute transport through homogenous soils. *Water Resources Research*, 21 (6), 808-820.

van Genuchten, M.T., Wierenga, P.J., 1976. Mass transfer studies in sorbing porous media. I. Analytical solutions. *Soil Science Society of America Journal*, 40 (4), 473-480.

van Genuchten, M.T., Wagenet, R.J., 1989. Two-Site/two-region models for pesticide transport and degradation: Theoretical development and analytical solutions. *Soil Science Society of America Journal*, 53 (5), 1303-1310.

Vereecken, H., Doring, U., Hardelauf, H., Jaekel, U., Hashagen, U., Neuendorf, O., Schwarze, H., Seidemann, R., 2000. Analysis of solute transport in a heterogeneous aquifer: the Krauthausen field experiment, *Journal of Contaminant Hydrology*, 45 (3-4), 329-358.

Villholth, K.G., Giordano, M., 2007, Groundwater Use in a Global Perspective - Can It Be Managed? In *The Agricultural Groundwater Revolution Opportunities and Threats to Development*, Eds. Giordano, M., Villholth, K.G., Cromwell Press, Trowbridge, UK, pp. 393-402.

Wang, M., Zheng, C., 1997. Optimal remediation policy selection under general conditions. *Ground Water*, 35 (5), 757-764.

Webster, R., Oliver, M.A., 2007. *Geostatistics for Environmental Scientists*, John Wiley and Sons Ltd., West Sussex, England.

Weck, B., Karr, C.L., Freeman, L.M., 1999. Gauss-Legendre integration using genetic algorithms. In *International Series of Computational Intelligence, Industrial Applications of Genetic Algorithms*. Eds. Karr, C.L., Freeman, L.M., CRC Press, pp. 243-256.

Welhan, J.A., Reed, M.F., 1997. Geostatistical analysis of regional hydraulic conductivity variations in the Snake River Plain aquifer, eastern Idaho. *Geological Society of America Bulletin*, 109 (7), 855-868.

Wilf, H.S., 1989. *Combinatorial Algorithms: An Update*, CBMS-NSF Regional Conference Series in Applied Mathematics, 55, Society of Industrial and Applied Mathematics, Philadelphia, PA, USA.

Woodbury, A.D., Sudicky, E.A., 1991. The geostatistical characteristics of the Borden aquifer. *Water Resources Research*, 27 (4), 533-546.

Yan, S., Minsker, B., 2006. Optimal groundwater remediation design using an Adaptive Neural Network Genetic Algorithm, *Water Resources Research*, 42 (5), W05407.

Zhang, Z., Brusseau, M.L., 1999. Nonideal transport of reactive solutes in heterogeneous porous media 5. Simulating regional-scale behavior of a trichloroethene plume during pump-and-treat remediation. *Water Resources Research*, 35 (10), 2921-2935.

Zhao, X., Wallace, R.B., Hyndman, D.W., Dybas, M.J., Voice, T.C., 2005. Heterogeneity of chlorinated hydrocarbon sorption properties in a sandy aquifer. *Journal of Contaminant Hydrology*, 78 (4), 327-342.

Zheng, C.M., Wang, P.P., 2002. A field demonstration of the simulation optimization approach for remediation system design. *Ground Water*, 40 (3), 258-265.

Zimmerman, J.R., 1998. The Impact of Pore Water Velocity on Nonequilibrium Transport. MS Thesis, Michigan State University.

Zinn, B., Harvey, C.F., 2003. When good statistical models of aquifer heterogeneity go bad: A comparison of flow, dispersion, and mass transfer in connected and multivariate Gaussian hydraulic conductivity fields. *Water Resources Research*, 39 (3), 1051.

Zlotnik, V.A., Zurbuchen, B.R., Ptak, T., 2001. The steady-state dipole-flow test for characterization of hydraulic conductivity statistics in a highly permeable aquifer: Horkheimer Insel Site, Germany. *Ground Water*, 39 (4) 504-516.

APPENDIX A

HETEROGENEOUS FIELD REPRESENTATIONS

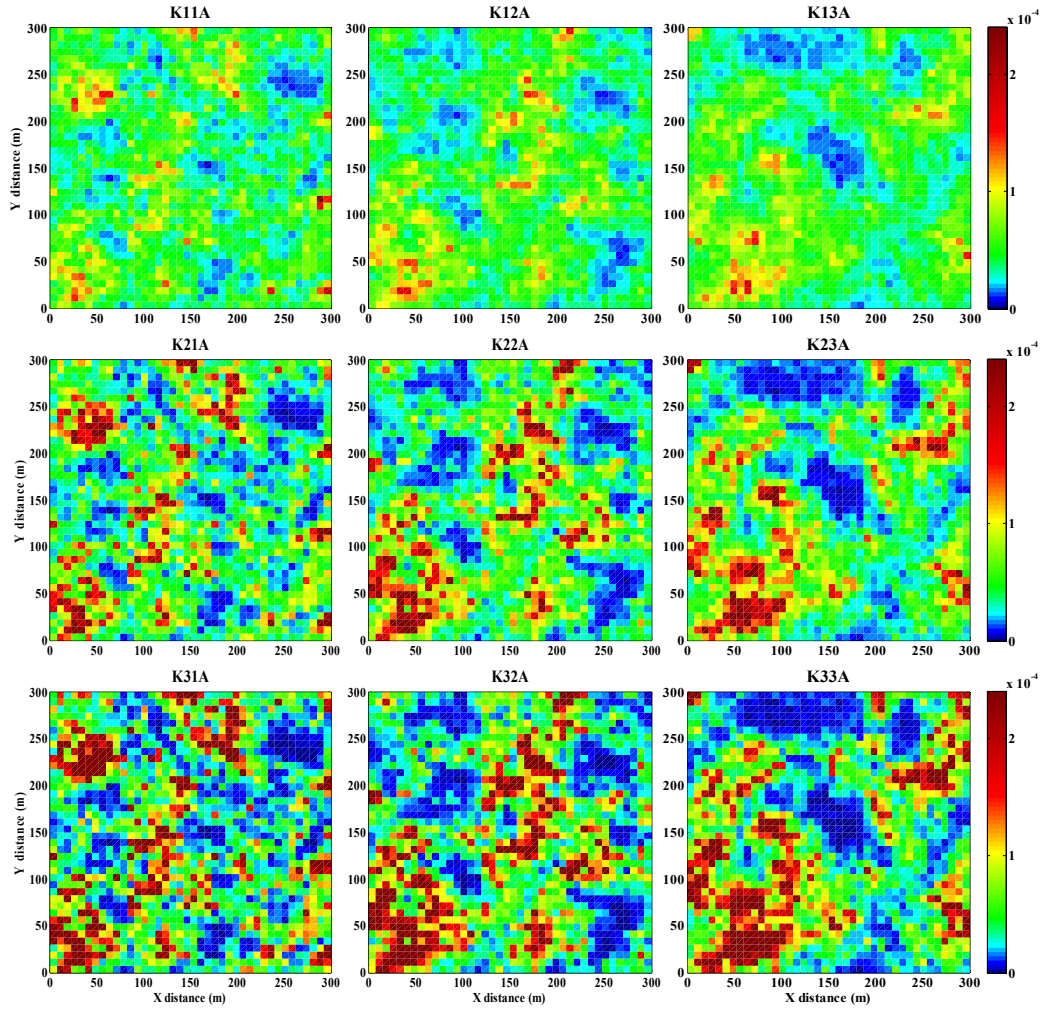


Figure A.1. Heterogeneous K-fields for realization A

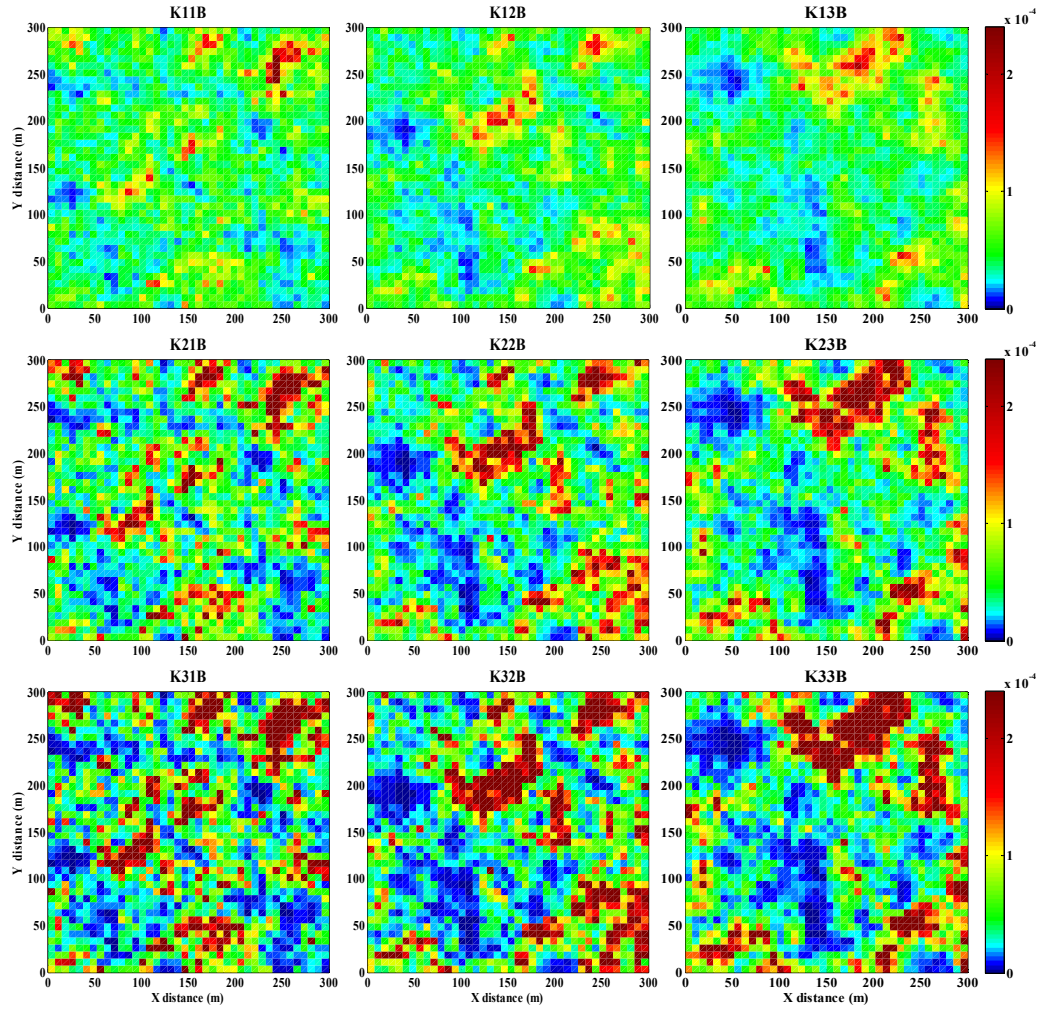


Figure A.2. Heterogeneous K-fields for realization B

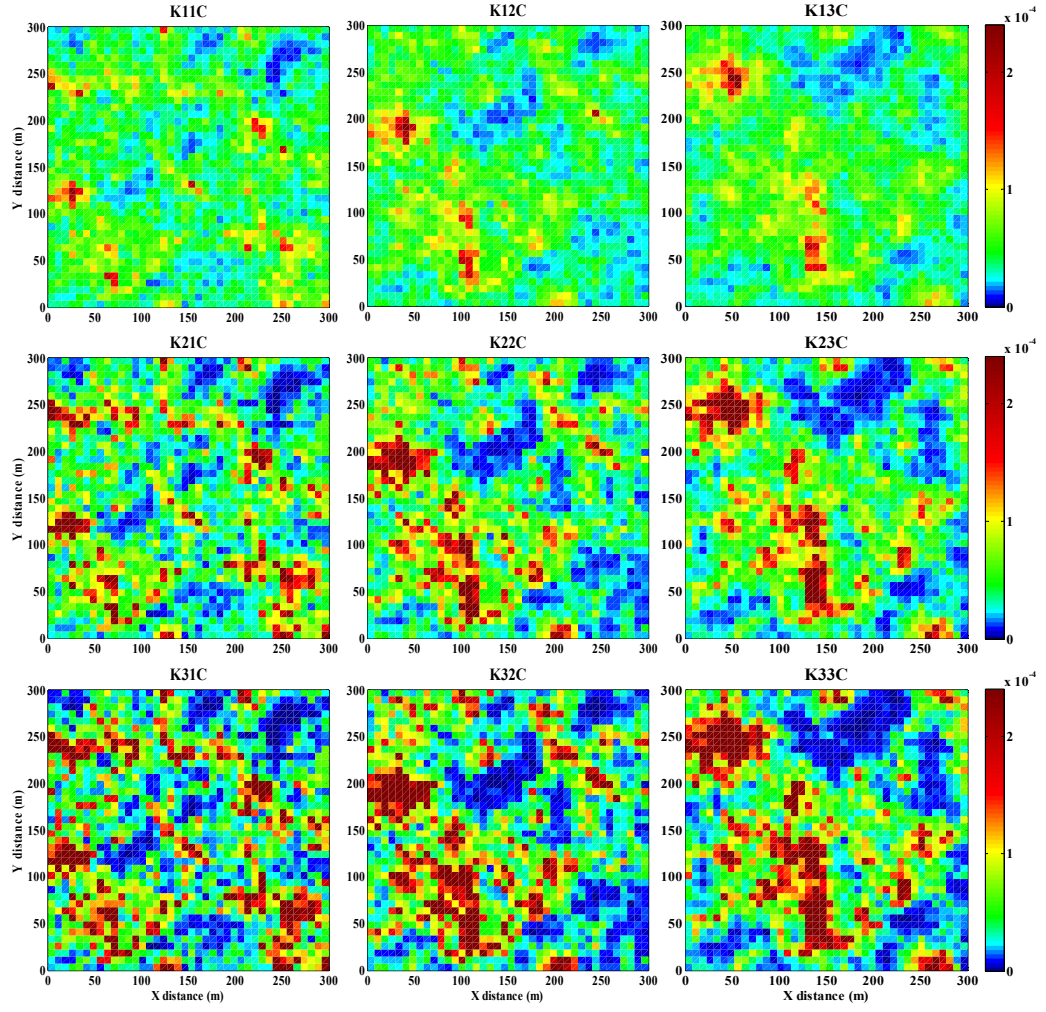


Figure A.3. Heterogeneous K-fields for realization C

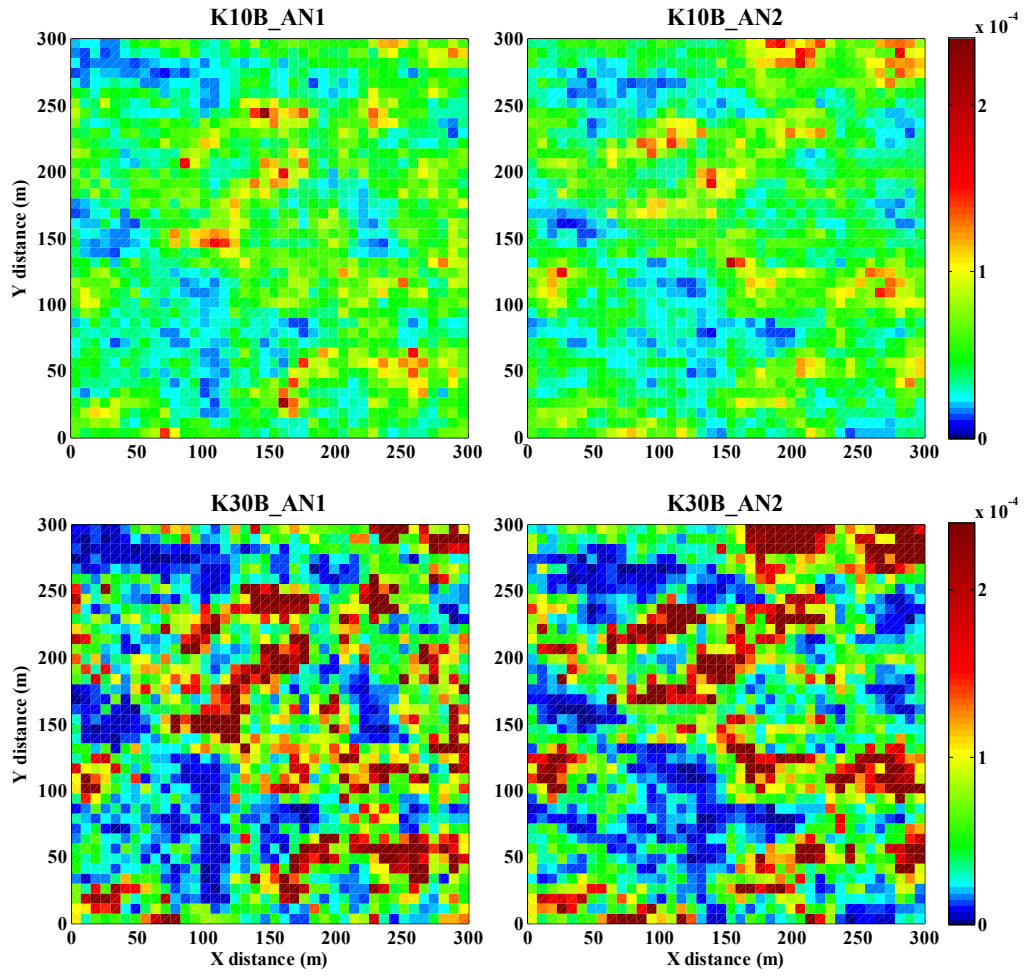


Figure A.4. Anisotropic K-fields

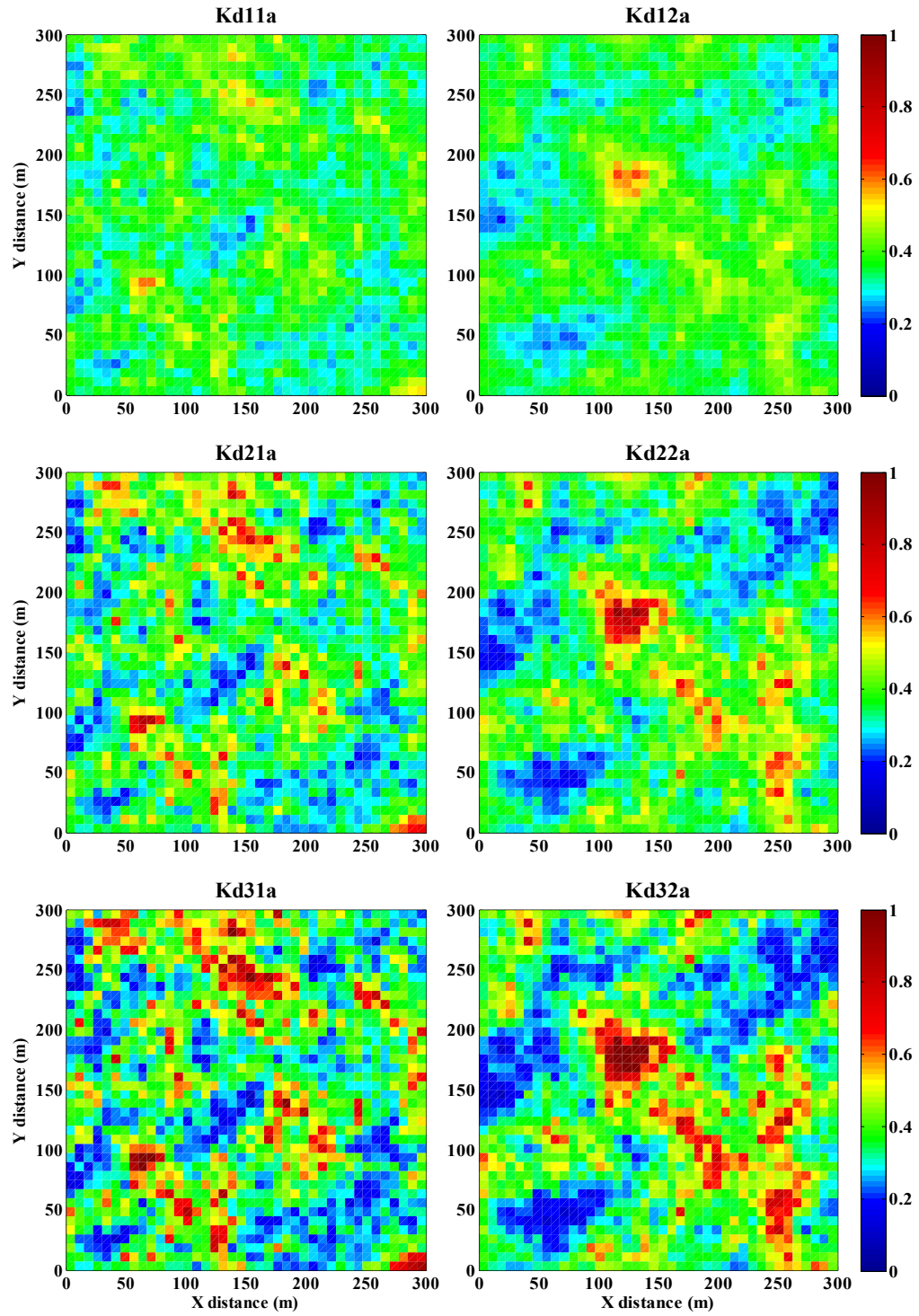


Figure A.5. Heterogeneous K_d -fields for realization a

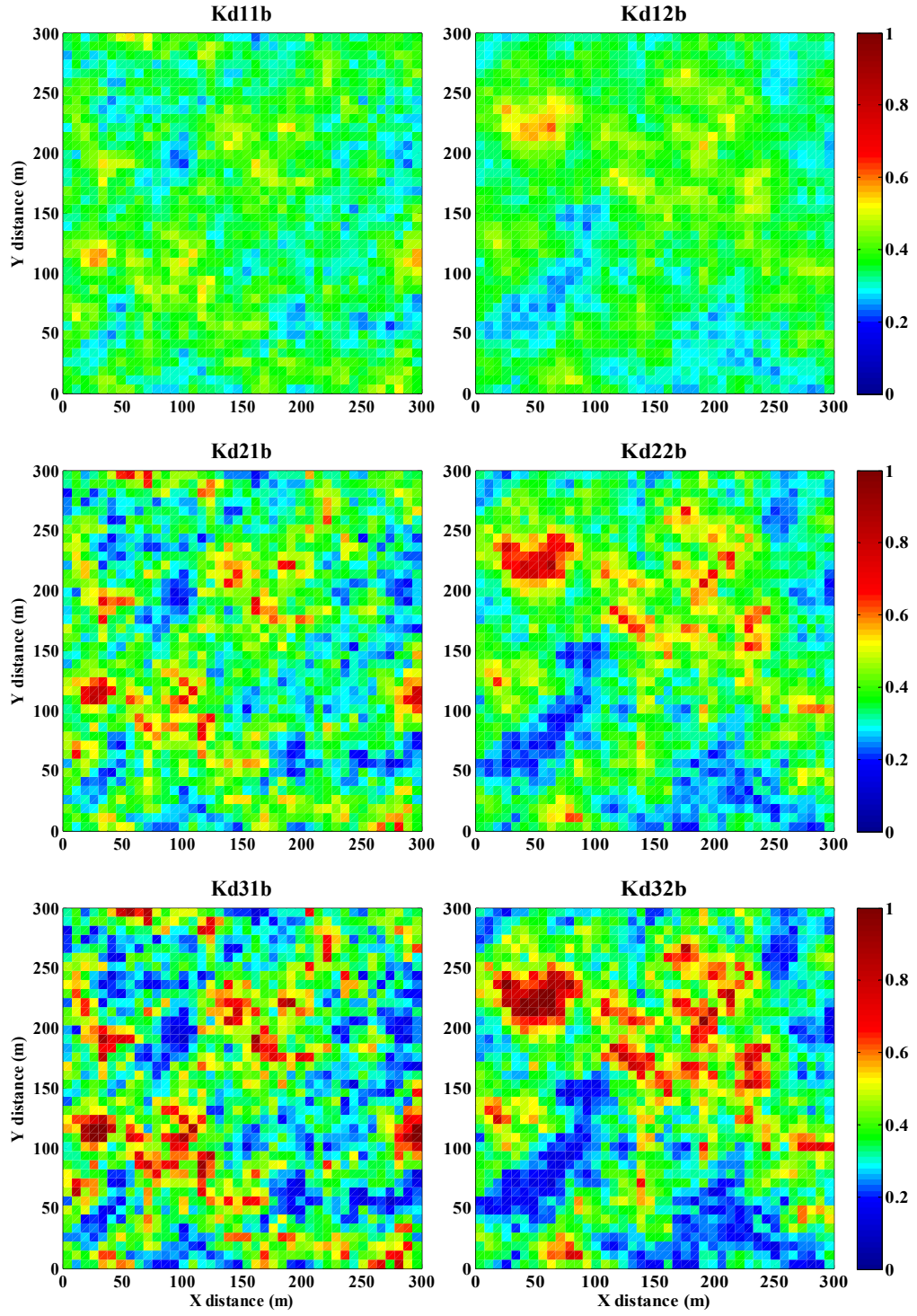


Figure A.6. Heterogeneous K_d -fields for realization b

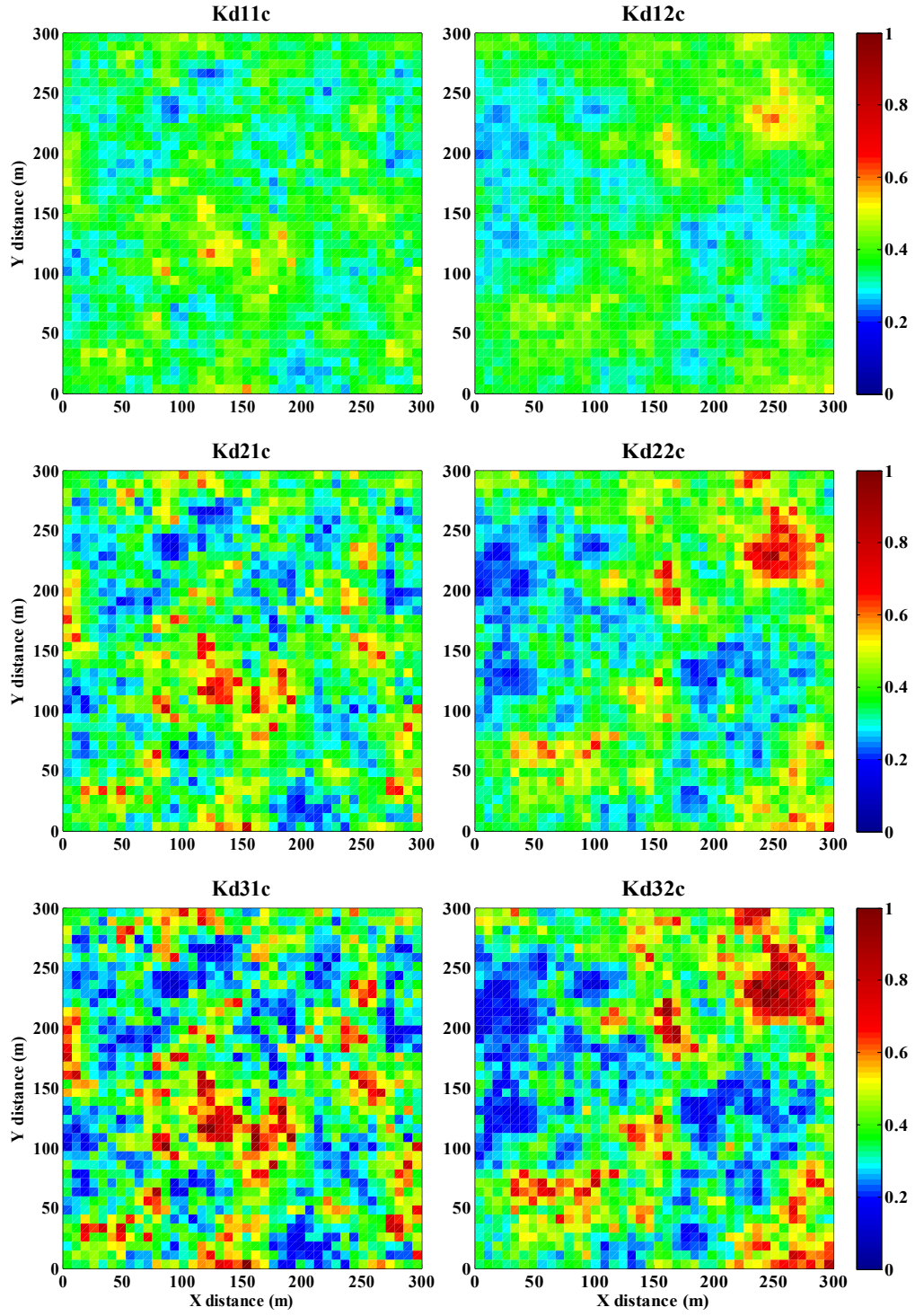


Figure A.7. Heterogeneous K_d -fields for realization c

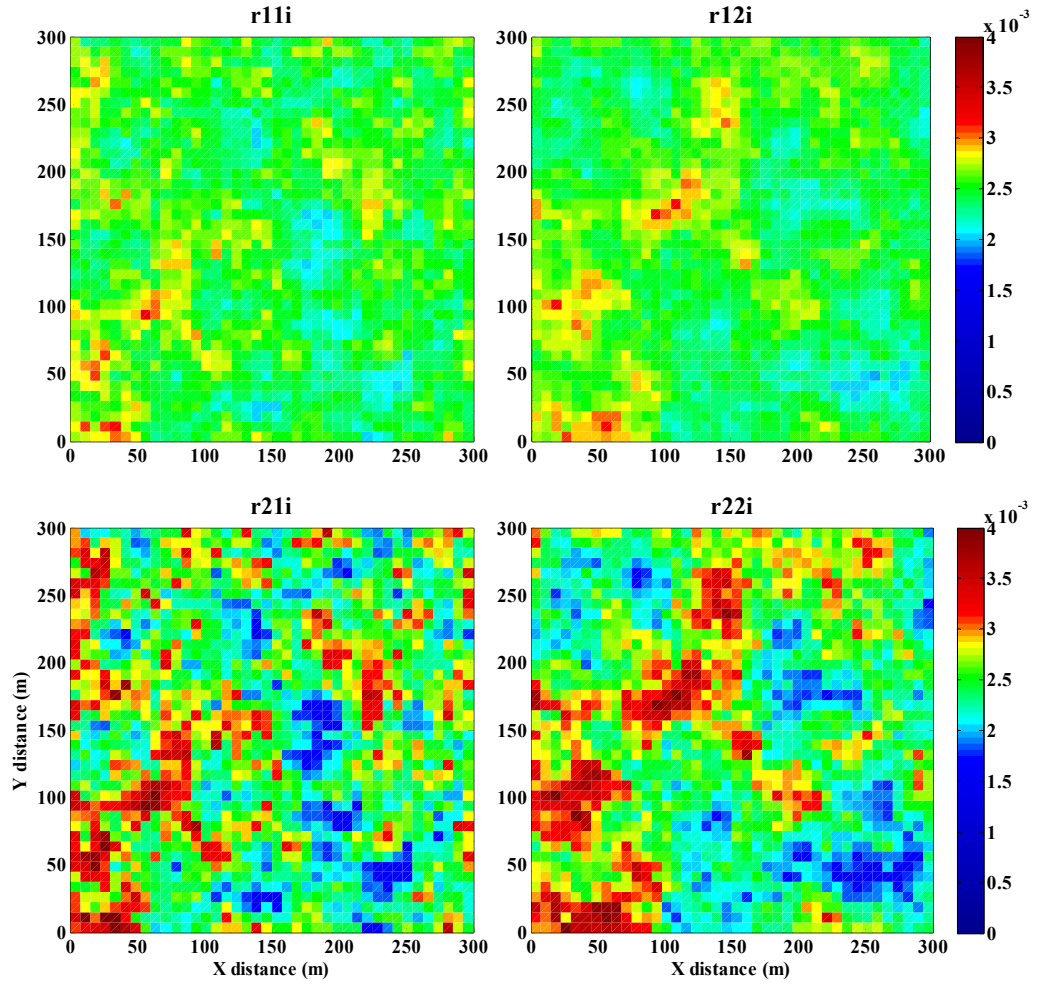


Figure A.8. Heterogeneous α -fields for realization i

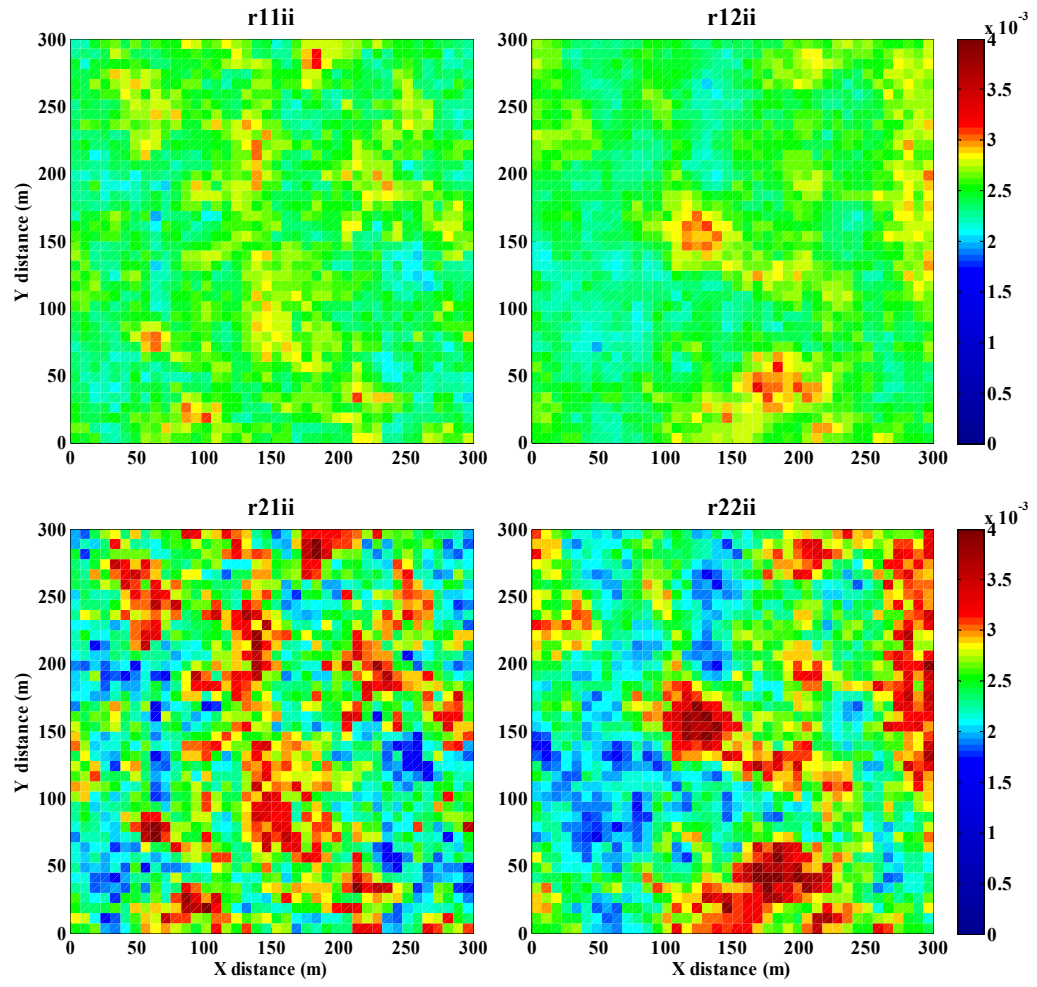


Figure A.9. Heterogeneous α -fields for realization ii

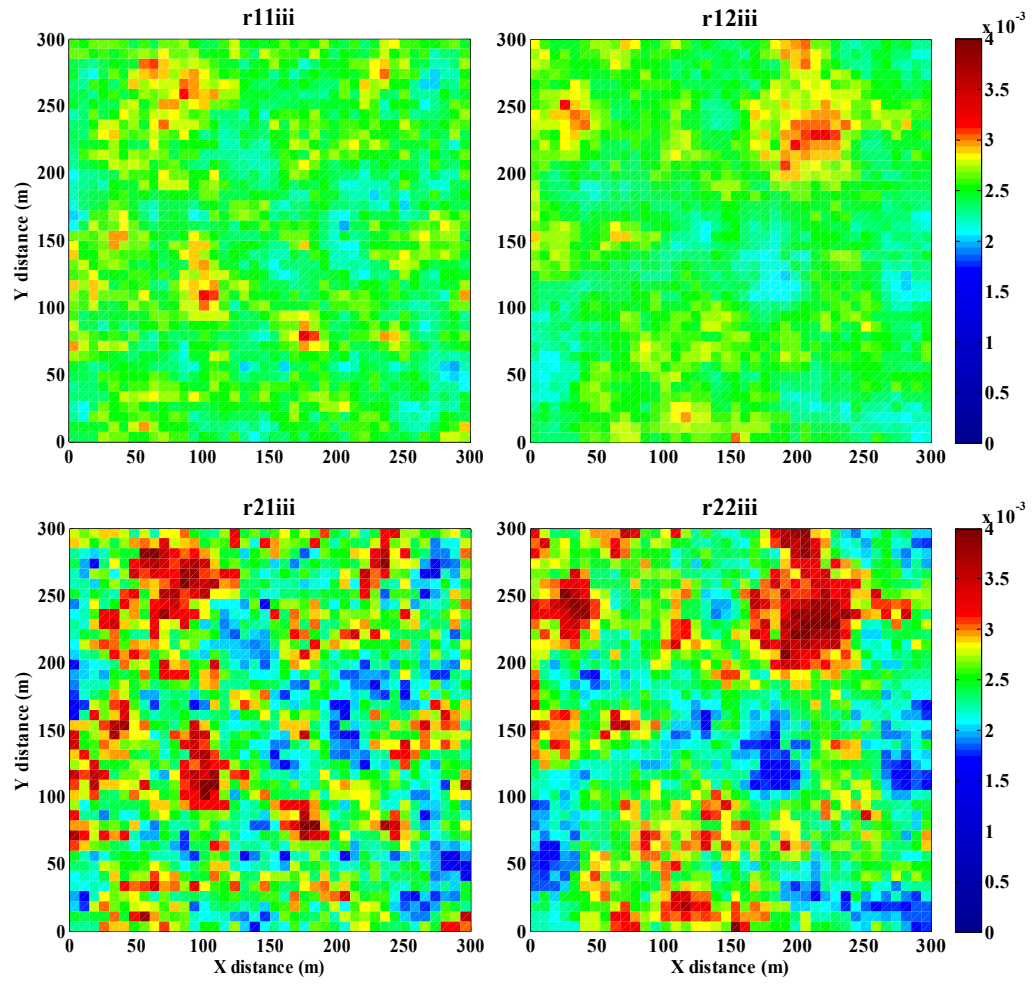


Figure A.10. Heterogeneous α -fields for realization iii

APPENDIX B

COVARIANCE FUNCTION COMPARISONS

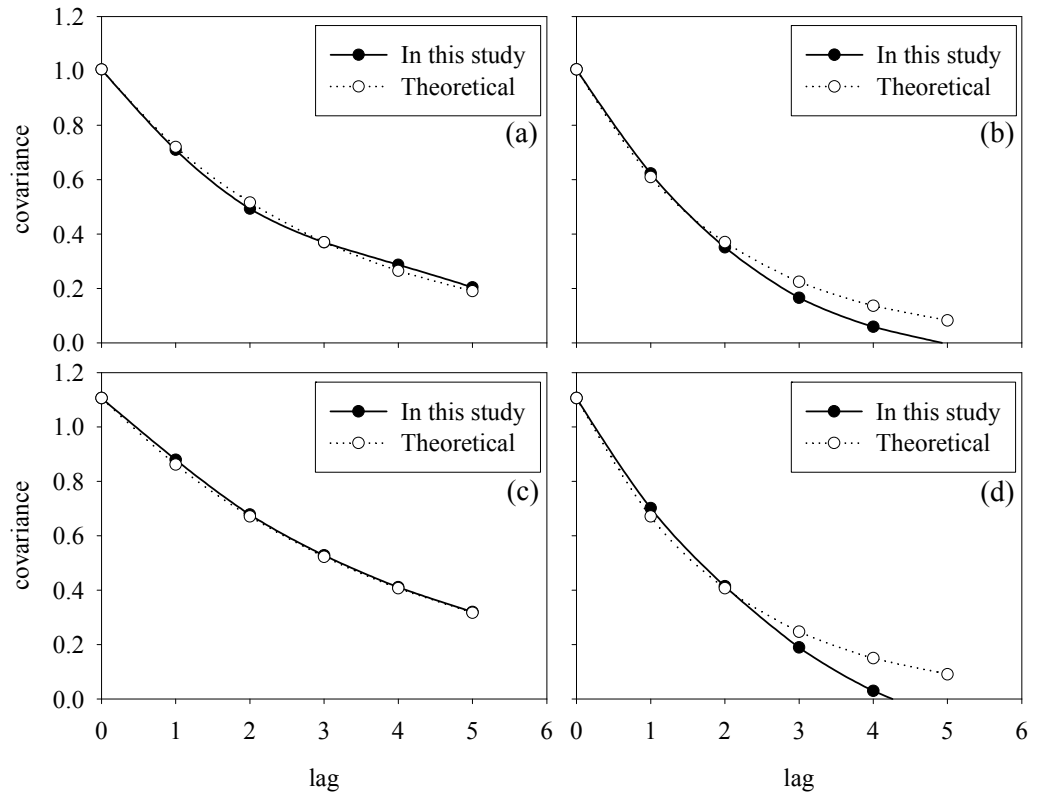


Figure B.1. Comparison of the theoretical covariance function with the covariance function of the anisotropic K-fields generated in this study for realization B (a) $\lambda_{\ln K, x} = 22.5$ m, (b) $\lambda_{\ln K, y} = 15$ m, (c) $\lambda_{\ln K, x} = 30$ m, (d) $\lambda_{\ln K, y} = 15$ m

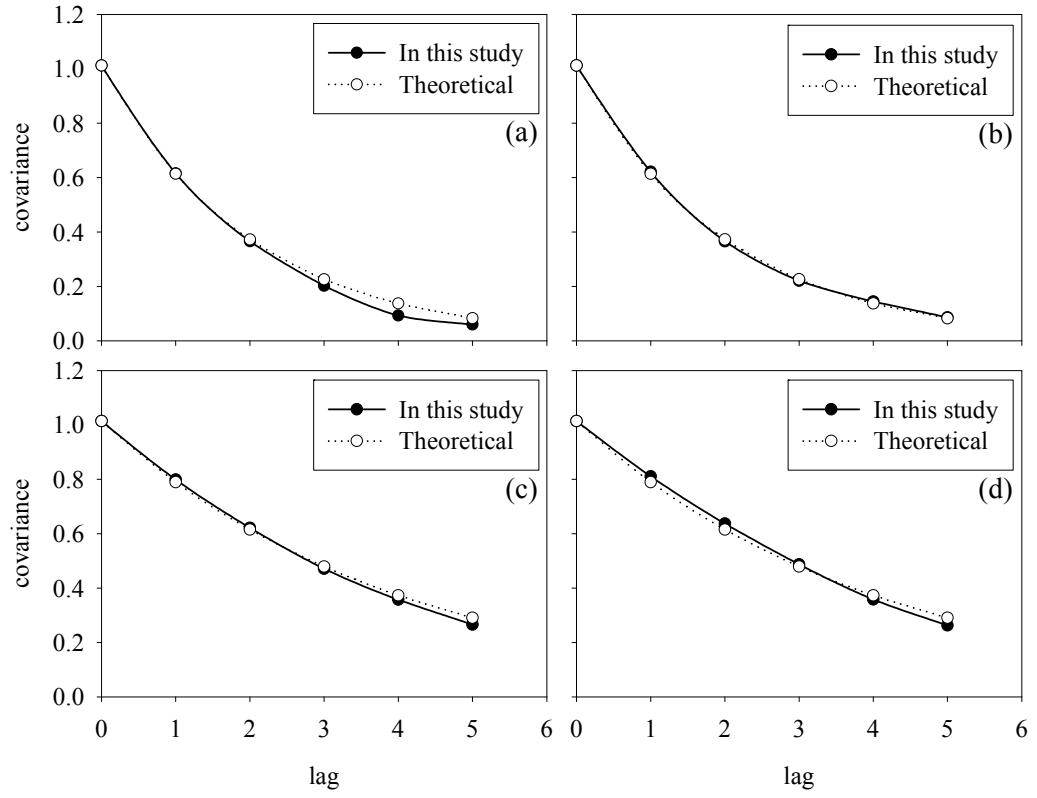


Figure B.2. Comparison of the theoretical covariance function with the covariance function of the K_d -fields generated in this study for realization a. (a) $\lambda_{\ln K_d, x} = 15$ m, (b) $\lambda_{\ln K_d, y} = 15$ m, (c) $\lambda_{\ln K_d, x} = 30$ m, (d) $\lambda_{\ln K_d, y} = 30$ m

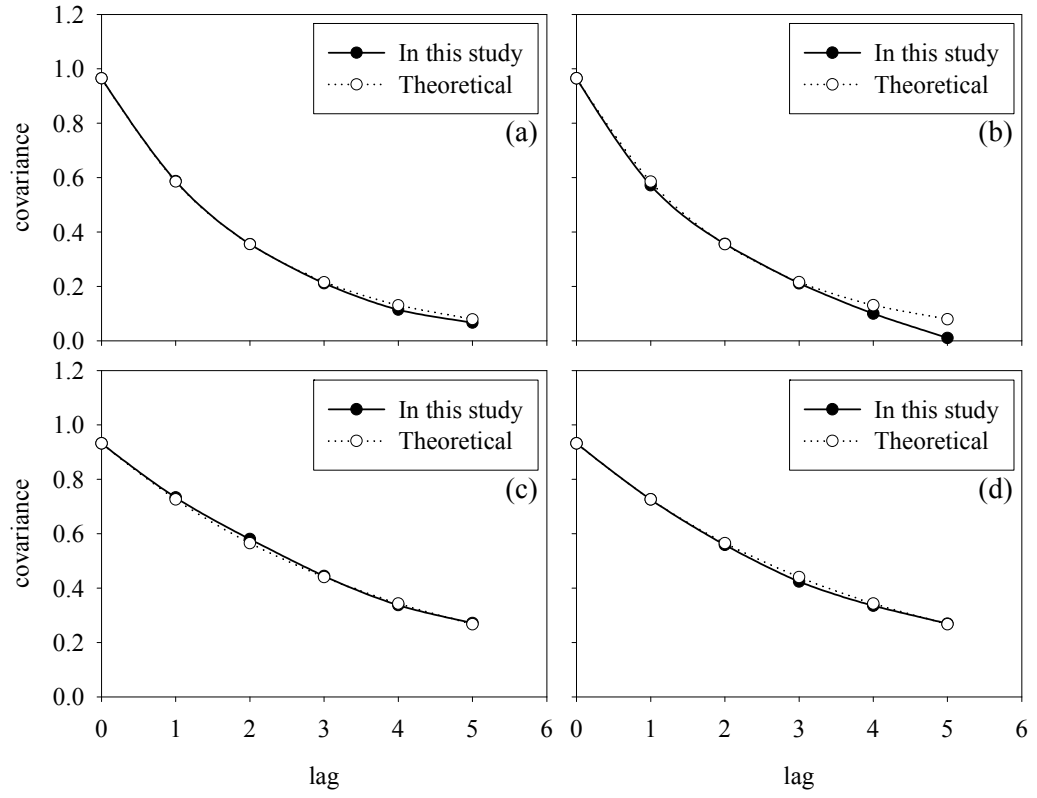


Figure B.3. Comparison of the theoretical covariance function with the covariance function of the K_d -fields generated in this study for realization b. (a) $\lambda_{\ln K_d, x} = 15$ m, (b) $\lambda_{\ln K_d, y} = 15$ m, (c) $\lambda_{\ln K_d, x} = 30$ m, (d) $\lambda_{\ln K_d, y} = 30$ m

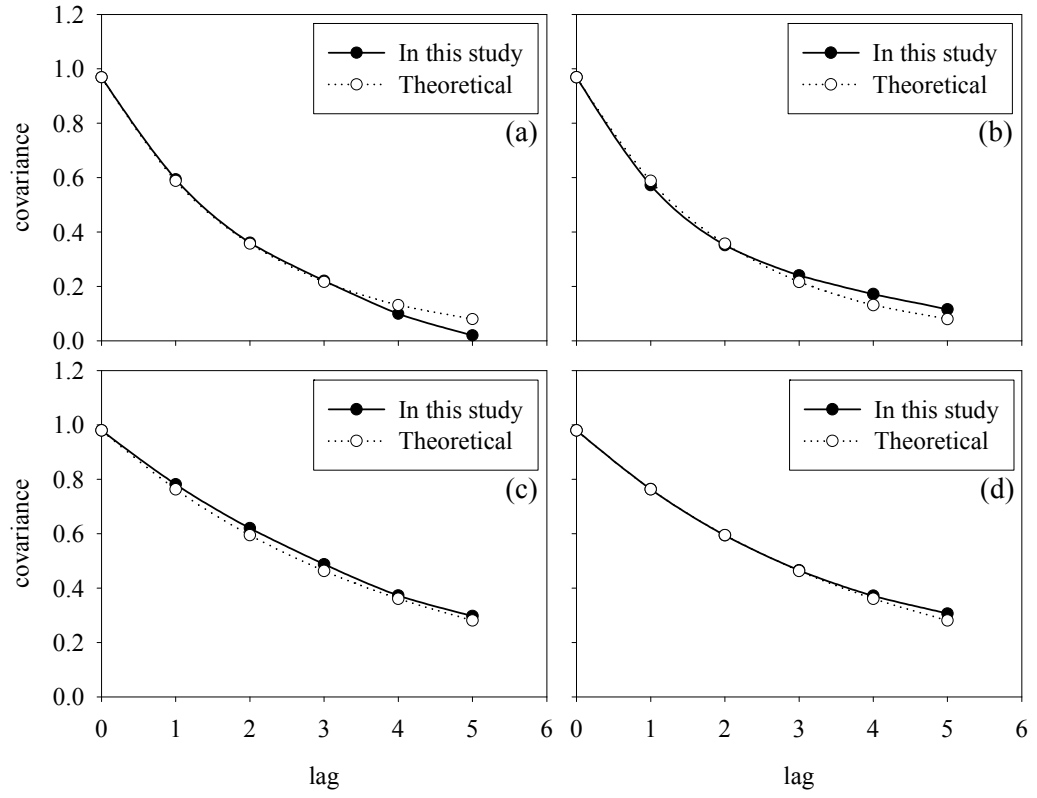


Figure B.4. Comparison of the theoretical covariance function with the covariance function of the K_d -fields generated in this study for realization c. (a) $\lambda_{\ln K_d, x} = 15$ m, (b) $\lambda_{\ln K_d, y} = 15$ m, (c) $\lambda_{\ln K_d, x} = 30$ m, (d) $\lambda_{\ln K_d, y} = 30$ m

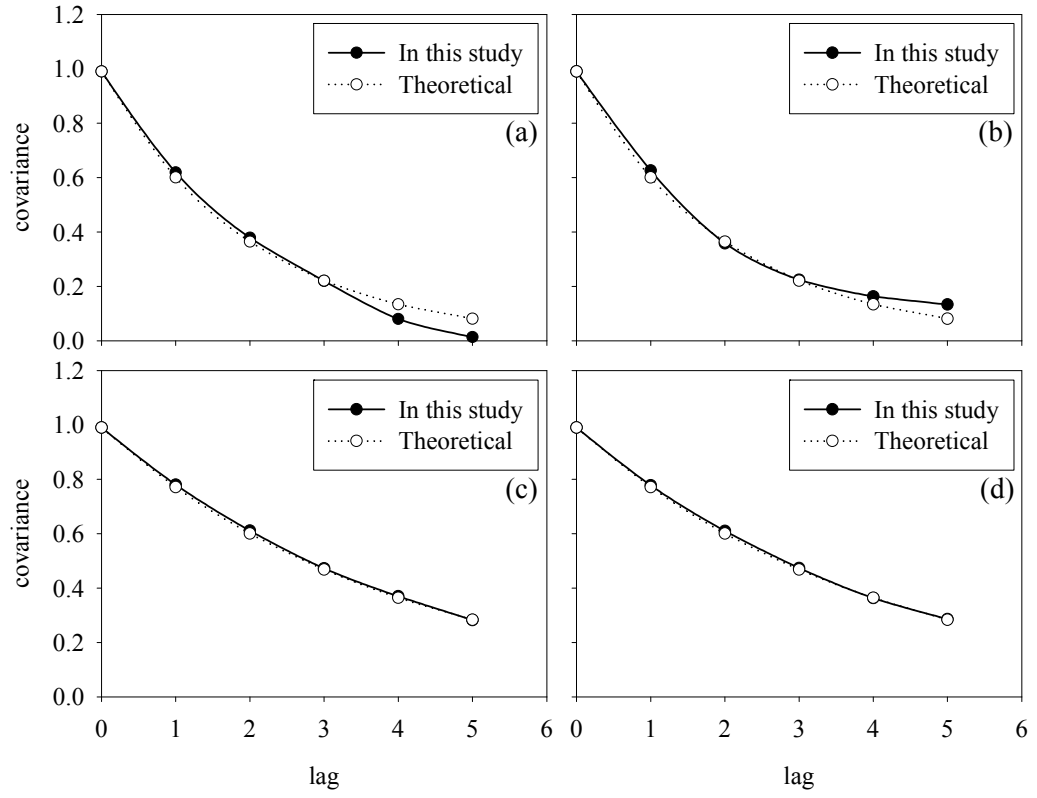


Figure B.5. Comparison of the theoretical covariance function with the covariance function of the α -fields generated in this study for realization i. (a) $\lambda_{\ln\alpha,x} = 15$ m, (b) $\lambda_{\ln\alpha,y} = 15$ m, (c) $\lambda_{\ln\alpha,x} = 30$ m, (d) $\lambda_{\ln\alpha,y} = 30$ m

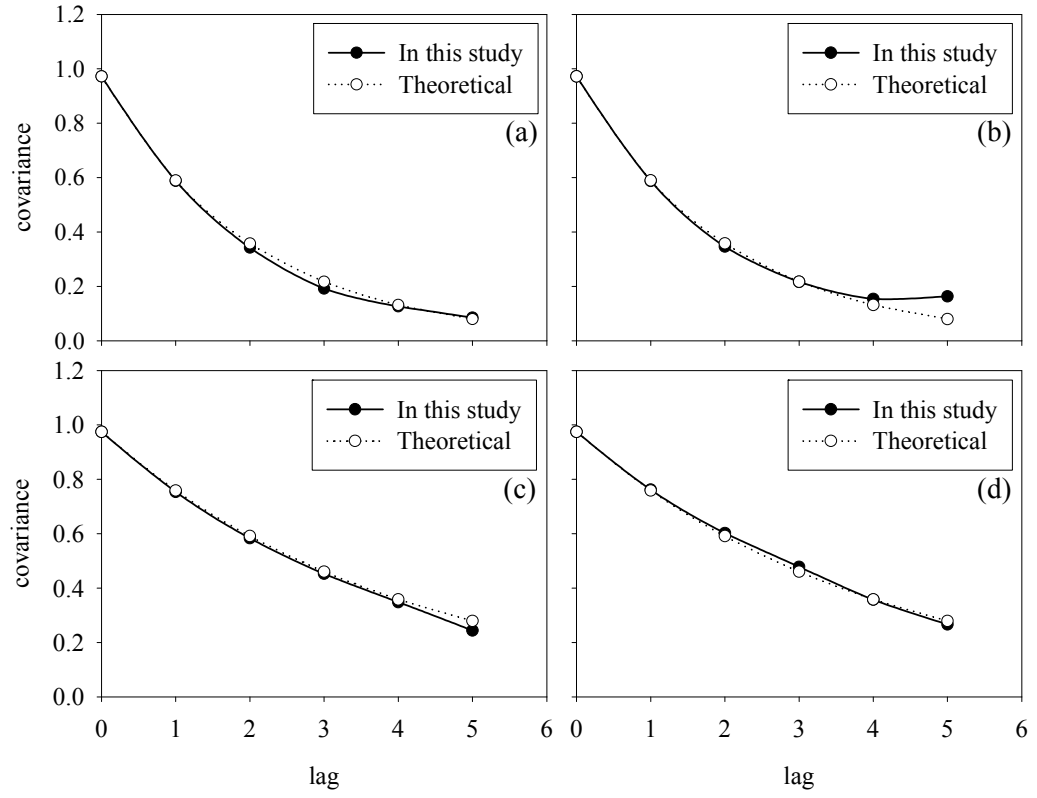


Figure B.6. Comparison of the theoretical covariance function with the covariance function of the α -fields generated in this study for realization ii. (a) $\lambda_{\ln\alpha,x} = 15$ m, (b) $\lambda_{\ln\alpha,y} = 15$ m, (c) $\lambda_{\ln\alpha,x} = 30$ m, (d) $\lambda_{\ln\alpha,y} = 30$ m

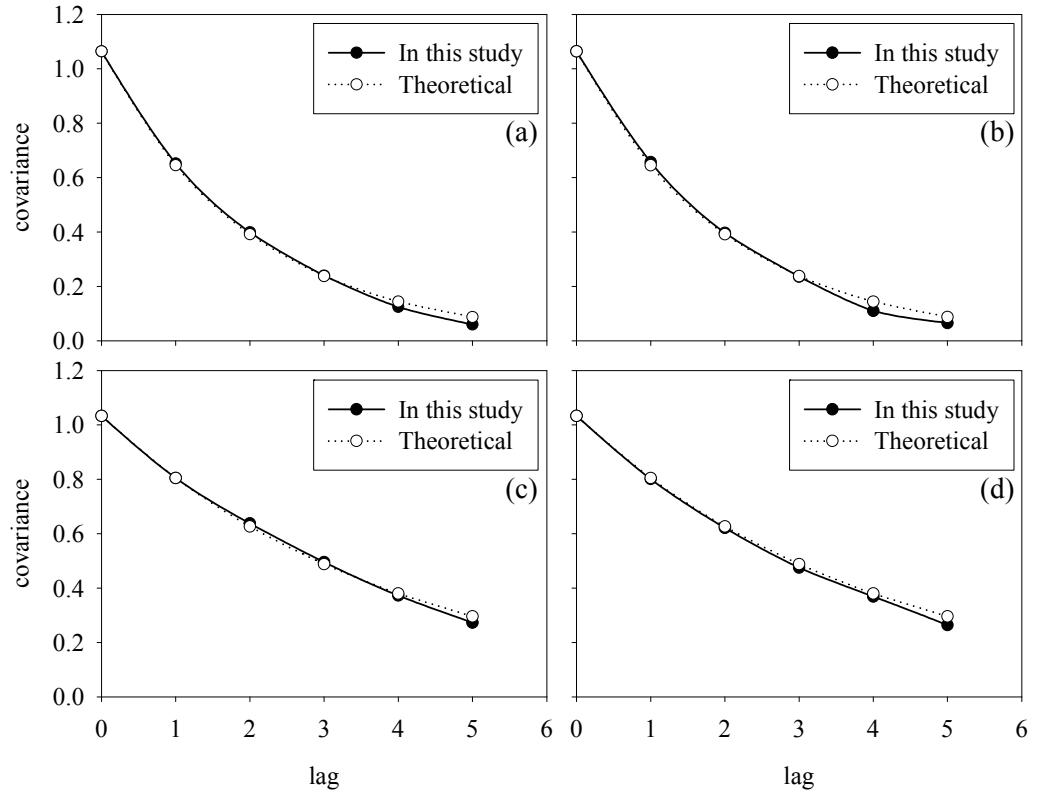


Figure B.7. Comparison of the theoretical covariance function with the covariance function of the α -fields generated in this study for realization iii. (a) $\lambda_{\ln\alpha,x} = 15$ m, (b) $\lambda_{\ln\alpha,y} = 15$ m, (c) $\lambda_{\ln\alpha,x} = 30$ m, (d) $\lambda_{\ln\alpha,y} = 30$ m

CURRICULUM VITAE

PERSONAL INFORMATION

Surname, Name: G ng r Demirci, Gamze
Nationality Republic of Turkey
Contact Information: ggamze@metu.edu.tr, gamzegd@gmail.com

EDUCATION

Ph.D. Middle East Technical University, Department of Environmental Engineering, Ankara, Turkey, 2002 - 2009, CGPA: 4.00/4.00.

M.Sc. Middle East Technical University, Department of Environmental Engineering, Ankara, Turkey, 2000 - 2002, CGPA: 3.79/4.00.

B.Sc. Middle East Technical University, Department of Environmental Engineering, Ankara, Turkey, 1994 - 1999, CGPA: 3.22/4.00.

PROFESSIONAL EXPERIENCE

Teaching Assistant, Middle East Technical University, Department of Environmental Engineering, Ankara, Turkey, Jan 2002 - ongoing.

Visiting Researcher, Massachusetts Institute of Technology, Department of Civil and Environmental Engineering, Cambridge, Massachusetts, USA, Jun 2006 - Jun 2007.

Teaching Assistant, Massachusetts Institute of Technology, Department of Civil and Environmental Engineering, Cambridge, Massachusetts, USA, Feb 2007 - May 2007.

FOREIGN LANGUAGES

Turkish, Native

English, Reading: Very Good, Writing: Very Good, Speaking: Very Good, KPDS score: 92 (November 2008)

Spanish, Reading: Basic, Writing: Basic, Speaking: Basic.

SELECTED PUBLICATIONS

International Peer-Reviewed Journal Publications

- Güngör Demirci G., Demirer G.N., 2004. Effect of initial COD concentration, nutrient addition, temperature and microbial acclimation on anaerobic treatability of broiler and cattle manure. *Bioresource Technology*, 93, 109-117.
- Güngör Demirci G., Aksoy A., ----. Change in optimal pump and treat remediation design with respect to correlation scale of hydraulic conductivity (in review).
- Güngör Demirci G., Aksoy A., ----. Evaluation of the genetic algorithm parameters on the optimization performance: A case study on pump and treat remediation design (in review).

International Conference Publications

- Güngör Demirci G., Aksoy A., 2008. Impact of hydraulic conductivity heterogeneity on time-to-compliance. *Proceedings of IAHR International Groundwater Symposium*, 18-20 June 2008, İstanbul, Turkey, pp. 768-775.
- Güngör Demirci G., Aksoy A., 2008. Impact of Crossover and Decision Variable Coding Forms on the Performance of Genetic Algorithm Optimization: A Case Study on Pump and Treat Remediation Design. *Proceedings of the 20th EURO Mini Conference “Continuous Optimization and Knowledge-Based Technologies”*, EurOPT-2008, 20-23 May 2008, Neringa, Lithuania, pp. 36-41.

- Güngör Demirci G., Aksoy A., 2006. Effect of heterogeneity correlation scale on pump-and-treat remediation design. Proceedings of World Environmental & Water Resources Congress, 21-25 May 2006, Omaha, Nebraska, USA, in CD-ROM.

National Conference Publications

- Güngör Demirci G., Aksoy A., 2008. Clean-up of contaminated aquifers by pump and treat remediation method: Technical obstacles, reasons and solutions. Proceedings of the 11th Industrial Pollution Control Symposium, 11-13 June 2008, İstanbul, Turkey, in CD-ROM.
- Güngör Demirci G., Aksoy A., 2008. Effect of hydraulic conductivity heterogeneity on remediation time for pump-and-treat systems: Simulation-optimization approach. Proceedings of Environmental Problems Symposium Kocaeli-2008, 14-17 May 2008, Kocaeli, Turkey, in CD-ROM.
- Güngör Demirci G., Aslan M., Elahdab T., Aksoy A., 2005. Monitoring and evaluation of water quality of Lake Eymir. Proceedings of the 6th National Environmental Engineering Congress (Volume of Poster Presentations), 24-26 November 2005, İstanbul, Turkey, pp. 72-76.
- Güngör Demirci G., Aksoy A., 2005. Effects of physical heterogeneity on pump-and-treat remediation design. Proceedings of the Modern Methods in Science Symposium, 16-18 November 2005, Kocaeli, Turkey, pp. 636-643.
- Güngör G., Demirer G.N., 2003. Biogas generation potential of broiler and cattle manure. Proceedings of the 2nd Renewable Energy Resources Symposium, 15-18 October 2003, İzmir, Turkey, pp. 355-362.
- Güngör G., Demirer G.N., 2003. Anaerobic treatability of broiler and cattle manure. Proceedings of the 5th National Environmental Engineering Congress, 1-4 October 2003, Ankara, Turkey, pp. 400-410.

Invited Presentations

- Güngör Demirci G., LeBlanc D.R., Harvey C.F., 2007. Estimation of groundwater ages and recharge rates on or near the Massachusetts Military Reservation by tritium method. 25th Cape Cod Toxics Annual Site Meeting organized by United States Geological Survey, 13-15 February 2007, Massachusetts Military Reservation, Cape Cod, Massachusetts, USA.

RESEARCH PROJECTS

As a researcher in:

- Estimation of groundwater ages and recharge rates on or near the Massachusetts Military Reservation by tritium method, joint project of Massachusetts Institute of Technology and United States Geological Survey.
- Analysis of chlorophyll-a distribution in Lake Eymir via lab measurements and remote sensing, funded by Middle East Technical University Scientific Research Fund.
- Analysis of the effects of the heterogeneity scale on pump-and-treat aquifer remediation design, funded by Middle East Technical University Scientific Research Fund.
- Coastal area management in Turkey, funded by Priority Actions Programme Regional Activity Centre of the Mediterranean Action Plan (UNEP).

AWARDS

- International Research Fellowship by Faculty Development Programme of Middle East Technical University, in order to be a visiting researcher at Massachusetts Institute of Technology in USA, Jun 2006 - Jun 2007.
- International Research Fellowship by the Scientific and Technological Research Council of Turkey (TÜBİTAK), in order to be a visiting researcher at Massachusetts Institute of Technology in USA, Jun 2006 - Sep 2006.